STRICTOSIDINE SYNTHASE:

NOVEL 3D-COMPLEX-STRUCTURES AND

RATIONAL RE-ENGINEERING

DISSERTATION

zur Erlangung des Grades

„Doktor der Naturwissenschaften"

im Promotionsfach Pharmazie

am Fachbereich Chemie, Pharmazie und Geowissenschaften
der Johannes Gutenberg-Universität Mainz

Elke Anna-Maria Loris

geb. in Temeswar, Rumänien

Mainz

2008

"Do what you can, with what you have, where you are."

Theodore Roosevelt

Für meine Familie***

Contents

Contents

Contents

Contents

Abbreviations

% (m/V)	Percent by mass (g/100 ml)
% (V/V)	Percent by volume (ml/100ml)
25/50/250	Fractions eluted with 25, 50 and 250 mM imidazole solution
2D/3D	two- and three-dimensional
4-HPAA	p-hydroxyphenylacetaldehyde
5-F	5-fluoro-tryptamine
5-Me	5-methyl-tryptamine
5-MOX	5-methoxy-tryptamin
5-OH	5-hydroxy-tryptamine
6-F	6-fluoro-tryptamine
6-Me	6-methyl-tryptamine
11-Me	11-methyl-strictosidine
Å	Ångström; unit of length equal to 0.1 nanometer or 1×10^{-10} meters
AAE	Acetylajmalan esterase
AE	Arctic Express™ competent cells
bp	Base pair
BSA	Bovine Serum Albumine
$CDCl_3$	Deuterated chloroform
CD_3OD	Deuterated methanol
CE	Crude extract
CITES	Convention on International Trade in Endangered Species of wild Fauna and Flora
$CHCl_3$	Chloroform
^{13}C- NMR	Carbon-13 Nuclear magnetic resonance spectroscopy
CPR	Cytochrome P450 reductase
C. roseus	*Catharanthus roseus*
d	Day
Da	Dalton
DAB	The German Pharmacopoeia (Das Deutsche Arzneibuch)
DHVR	1,2-Dihydrovomilenine reductase
DIIS	Deacetylisoipecoside synthase
DIS	Deacetylipecoside synthase
DNA	Deoxyribonucleic acid
dNTPs	Deoxynucleoside triphosphates
EC number	Enzyme Commission numbers (used for the numerical classification of enzymes)
E. coli	*Escherichia coli*
EDTA	Ethylenediaminetetraacetic acid
eV	electronvolt
EIC	Extracted ion current
EMBL	European Molecular Biology Laboratory
FPLC	Fast protein liquid chromatography
GDH	Geissoschizine dehydrogenase
h	Hour
HEPES	4-(2-hydroxyethyl)-1-piperazineethanesulfonic acid
Hz	Hertz
His_6-tag	Hexa-histidine tag
^{1}H-NMR	Hydrogen-1 Nuclear magnetic resonance spectroscopy
HPLC	High Performance Liquid Chromatography

HSQC	Heteronuclear Single Quantum Coherence
I	Inhibitor concentration.
I/σ(I)	Signal to noise ratio
IC_{50}	The concentration of a compound that is required for 50% inhibition *in vitro*
IMAC	Immobilized-Metal-Affinity-Chromatography
IPTG	Isopropyl β-D-1-thiogalactopyranoside
IUCN	International Union for Conservation of Nature and Natural Resources
KAc	Potassium acetate
k_{cat}	Turnover number (maximum number of enzymatic reactions catalyzed per second)
k_{cat}/K_M	Specificity constant (measure of the enzyme's conversion efficiency)
K_i	Inhibitor constant
K_M	Michaelis constant
K_M'	K_M value in the presence of inhibitor
KPi	Potassium phosphate buffer
LC-MS	Liquid chromatography-mass spectrometry analysis
LB	Lysogeny Broth medium
LBS	LB medium containing 1 M sorbitol and 1 % (V/V) glycerol
M	Marker (proteins or DNA)
MeOH	Methanol
MIA	monoterpenoid indole alkaloids
min	Minute
MIT	Massachusetts Institute of Technology
MOPS	3-(N-morpholino)propanesulfonic acid
M_r	Molecular Weight
m/z	Mass-to-charge
NADPH	Nicotinamide adenine dinucleotide phosphate
NAMT	Norajmalan methyltransferase
NCS	Norcoclaurine synthase
Ni-NTA	Nickel-Nitrilotriacetic acid
OD	Optical density
OD_X	Optical density at a given wavelength x
O. pumila	*Ophiorrhiza pumila*
PAGE	Polyacrylamide gel electrophores
PCR	Polymerase Chain Reaction
PDB	Protein Data Bank
P	Pellet
PNAE	Polyneuridine aldehyde esterase
PR	Perakine reductase
RG	Raucaffricine glucosidase
RMS deviation	Root mean square deviation
RNA	Ribonucleic acid
rpm	Rounds per minute
R. serpentina	*Rauvolfia serpentina*
RT	Room temperature
s	Second
SD	Standard deviation
SDS	Sodium dodecyl sulfate
SDS-PAGE	Sodium dodecyl sulphate polyacrylamide gel electrophoresis
SG	Strictosidine glucosidase
STR	Strictosidine synthase

STR1	Strictosidine synthase deriving from the Indian medicinal plant *R. serpentina*
STR1-His$_6$	His$_6$-tagged STR1
STR_CR	Strictosidine synthase deriving from *Catharanthus roseus*
STR_OP	Strictosidine synthase deriving from *Ophiorrhiza pumila*
str1-pQE2	Expression vector STR1 wild-type
str1_V208A-pQE2	Expression vector mutant V208A (example)
TAE	Buffer containing 40 mM Tris-acetate, 0.2 M acetic acid, 1 mM EDTA
TCM	Traditional Chinese medicine
TE	Buffer containing 10 mM Tris-HCl, 1 mM EDTA
TIC	Total ion current
TLC	Thin layer chromatography
T_m	Primer melting temperatures
Tris	Tris(hydroxymethyl)aminomethane
U	Unit (1U =1 6.67 nkat)
UV	Ultraviolet
V	Voltage
v	Velocity/reaction rate
V208A (example)	point mutation at residue 208, amino acids 1-letter
Val208 (example)	residue, amino acids 3-letter
VH	Vinorine hydroxylase
v_{max}	Maximum reaction rate (velocity)
VR	Vomilenine reductase
VS	Vinorine synthase
W	Watt
x g	x-fold gravitation

Table of Standard Amino Acid Abbreviations

Amino Acid	3-letter	1-letter
Alanine	Ala	A
Arginine	Arg	R
Asparagine	Asn	N
Aspartic acid	Asp	D
Cysteine	Cys	C
Glutamic acid	Glu	E
Glutamine	Gln	Q
Glycine	Gly	G
Histidine	His	H
Isoleucine	Ile	I
Leucine	Leu	L
Lysine	Lys	K
Methionine	Met	M
Phenylalanine	Phe	F
Proline	Pro	P
Serine	Ser	S
Threonine	Thr	T
Tryptophan	Trp	W
Tyrosine	Tyr	Y
Valine	Val	V

I. Introduction

I.1 *Rauvolfia serpentina* – current relevance of an old medicinal plant

Rauvolfia serpentina (L.) Benth. ex Kurz[1] (Indian snake root) is a white flowering, evergreen, small shrub (30 – 100 cm), originating in the tropical Himalayan and Indian regions, in Ceylon and Java (WICHTL, 2002; Figure 1). It belongs to the family of Apocynaceae. Aside from *R. serpentina*, three further *Rauvolfia* species achieved medicinal significance in the past: *R. vomitoria* Afzel. (syn. *R. congolana*; Africa), *R. verticillata* (Lour.) Baill. (Chinese snake root) and *R. tetraphylla* L. (syn. *R. canescens* L.; America, Caribbean)[1].

R. serpentina is one of the so called 50 fundamental herbs used in traditional Chinese medicine (TCM; WONG, 1976). The plant has also been used therapeutically for millennia in Indian Ayurvedic medicine ("Sarphagandha root") for the treatment of insanity as well as snake bites and fever (SAHU, 1979). The German Pharmacopoeia "Das Deutsche Arzneibuch" edition 9 (DAB 9) includes the plant roots as the herbal drug "*Rauvolfiae* Radix". It demands a minimum alkaloid yield of 1 % calculated as reserpine. The roots are used as standardized extract for the treatment of hypertonia.

Figure 1. *Rauvolfia serpentina*. Approximately 2 year old plant, which is cultivated in the laboratory of Prof. Dr. J. Stöckigt, Johannes Gutenberg-University Mainz, Germany. The picture depicts the small white blossoms characteristic of this species.

The plant contains more than 50 different alkaloids, commonly known as *Rauvolfia*-alkaloids which belong to the family of monoterpenoid indole alkaloids[2]. The highest alkaloid concentration (1 – 3 %) occurs in the roots (calculated as reserpine, the quantitatively main compound) and 90 % of which is located in the cortex whereas 10 % in the wooden portion

---

[1] Accepted scientific names retrieved (July, 10th, 2008) from "The Integrated Taxonomic Information System" (ITIS) and "The International Plant Names Index" (IPNI). Available online: http://www.itis.gov and http://www.ipni.org.
[2] "Hunnius Pharmazeutisches Wörterbuch" 7th edition (1993). BURGER, A., WACHTER, H. (eds.) Walter de Gruyter Berlin, New York, 1196-1197

of the root. The most important *Rauvolfia*-alkaloids are reserpine, ajmaline, ajmalicine (synonym raubasine) and yohimbine. All of the aforementioned members are therapeutically used as isolated compounds as illustrated in Figure 2. The extract of *Rauvolfiae* Radix shows three effects which correlate to the specific activity profiles of these compounds: central sedative effect (reserpine), peripheral vascular dilatation (hypotensive effect of reserpine and ajmalicine) and heart rate deceleration (ajmaline). The standardized total extract is implemented as anti-hypertensive, sedative and spasmolytic agent. FINTELMANN et al. (1989) report increased tolerability of the extract compared to reserpine, however, adverse effects of both the extract and the single *Rauvolfia*-alkaloids are considerable. They are mainly characterized by the inhibition of the sympathetic nervous system. Today extracts represent an antiquated dosage form and the extract from *Rauvolfia* Radix is not the state of the art treatment of hypertension. Yohimbine is a sought after aphrodisiac (observable on the active internet trade), whereas the usage of reserpine and ajmalicine in the treatment of hypertension as well as the usage of ajmaline as an anti-arrhythmic drug has decreased. Today more effective, synthetic compounds with better side effect profiles are available and have replaced the *Rauvolfia*-alkaloids.

Reserpine
➢ hypertension, sedative

Ajmaline
➢ cardiac arrhythmia

Ajmalicine (Raubasine)
➢ hypertension

Yohimbine
➢ adrenic receptor blocker
➢ aphrodisiac
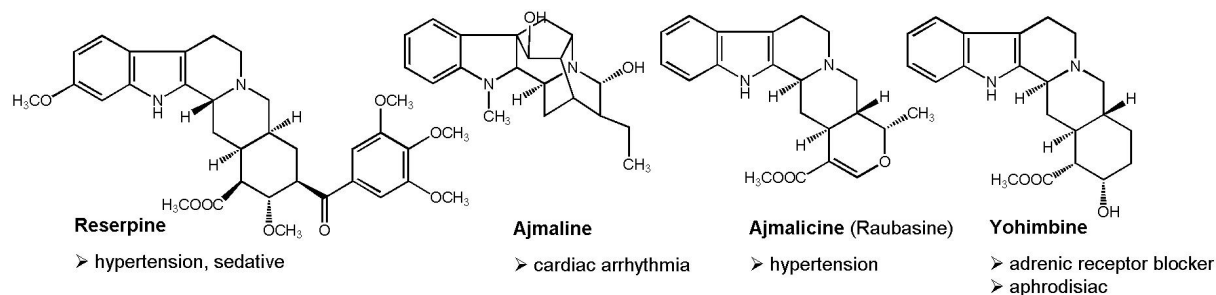
Figure 2. Prominent examples of *Rauvolfia*-alkaloids and their therapeutical application. References: BURGER and WACHTER (1993)[3], MUTSCHLER et al. (2008) and HÄNSEL (2004).

R. serpentina is a rich source of pharmacologically interesting compounds, however, due to poor yields most of the *Rauvolfia*-alkaloids have not been investigated in detail. Determining a method for increasing the amount of material available for experimental usage can advance this field rapidly. In this context, the current work represents a basic investigation of a new production strategy for the recovery of monoterpenoid indole alkaloids. It demonstrates the enzymatic synthesis of the biosynthetic key intermediate strictosidine and derivatives of this compound by use of re-engineered enzymes and provides the opportunity to introduce chemical modifications into the indole-skeleton, which can influence the potency and adverse effect profiles of the compounds. Understanding the structure-activity

---

[3] "Hunnius Pharmazeutisches Wörterbuch" 7th edition (1993). BURGER, A., WACHTER, H. (eds.) Walter de Gruyter Berlin, New York, 1196-1197

relationship (SAR) can help to improve the properties of (natural) compounds. Several examples show that even minor changes in structure can greatly influence the pharmacological properties of natural products and change them into modern, potent therapeutic agents (e. g. the camptothecin derivatives topotecan and irinotecan; LORENCE and NESSLER, 2004; LI et al., 2006).

Currently the scientific importance of the Indian medicinal plant *R. serpentina* is found in the investigation of its biosynthetic network, which is an extraordinary example in the field of natural product biosynthesis. It represents one of the most detailed investigated medicinal plants in the entire alkaloid field. After the investigation of the pharmacological properties of the isolated alkaloids, research later focused on biosynthesis and regulation aspects. The pathways leading to monoterpenoid indole alkaloids of the ajmalan- and sarpagan-type are extensively investigated at the molecular and enzymatic levels (STÖCKIGT, 1995; STÖCKIGT and PANJIKAR, 2007). Furthermore the three-dimensional structures of several enzymes involved in the biosynthetic network of *R. serpentina* have been structurally determined (STÖCKIGT et al., 2007; STÖCKIGT and PANJIKAR, 2007).

I.2   The monoterpenoid indole alkaloid family

The monoterpenoid indole alkaloids form one of the structurally and pharmacologically most diverse alkaloid families occurring in higher plants. Approximately 2000 members are known until now. Several of them achieved medical applications and are long standing, commonly used therapeutic agents (STÖCKIGT and RUPPERT, 1999; HÄNSEL, 2004). Prominent examples of developed therapeutics are shown in Figure 3. They are used in the treatment of cancer (vincristine and vinblastine, derivatives of camptothecin), malaria (quinine), arrhythmic heart disorders (quinidine, ajmaline), hypertension (ajmalicine, reserpine) and disturbed cerebral blood flow (vincamine; STÖCKIGT and RUPPERT, 1999).

Structurally this alkaloid family is characterized by an indole skeletal structure originating from the amino acid tryptophan. The glucosylated seco-iridoid aldehyde secologanin represents the monoterpenoid component. After decarboxylation of tryptophan, yielding tryptamine (by tryptophan decarboxylase; LEETE, 1961), the condensation of both precursors yields strictosidine. The enzyme involved, namely strictosidine synthase (STR, EC 4.3.3.2), deriving from the Indian medicinal plant *R. serpentina*, is the object of the current work. Several *in vivo* feeding experiments clearly demonstrated strictosidine as the sole biogenetic precursor of various indole alkaloid types (STÖCKIGT and ZENK, 1977a and 1977b; RUEFFER et al., 1978; BROWN et al., 1977a, 1977b; BROWN and LEONARD, 1978; BATTERSBY et al., 1978; NAGAKURA et al., 1979; STÖCKIGT and RUPPERT, 1999). The STR reaction potentially

represents the biosynthetic entry to probably all monoterpenoid indole alkaloids occurring in higher plants and STR occupies an outstanding role in nature's strategies to generate the entire alkaloid family. In the current work STR is used as the general abbreviation for strictosidine synthase of all species, whereas STR1 refers specifically to the enzyme originating from *R. serpentina*.
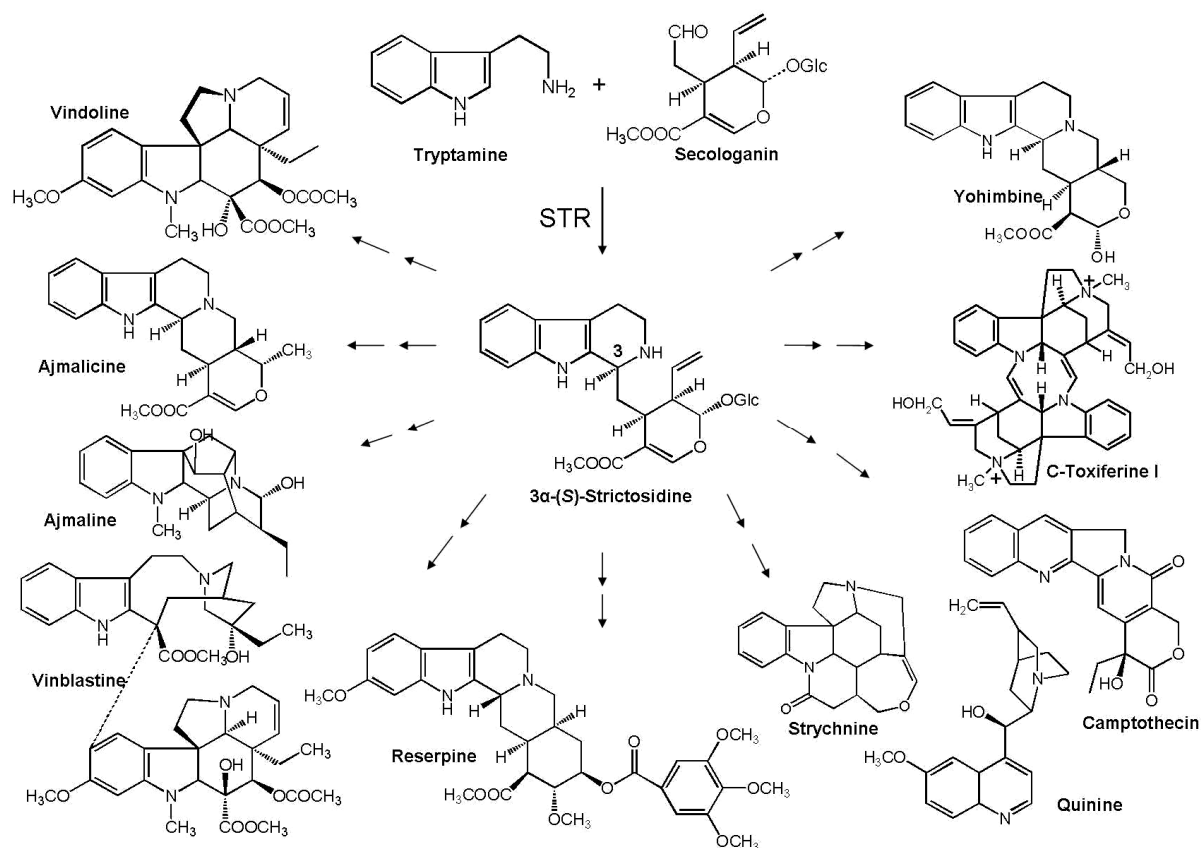
Figure 3. The strictosidine synthase (STR) reaction and the central biosynthetic role of strictosidine for the biosynthesis of monoterpenoid indole alkaloids. STR is the key enzyme in the biosynthesis of the monoterpenoid indole alkaloids - one of the largest and structurally most diverse alkaloid families in higher plants. Prominent examples with pharmacologically interesting properties are presented.

After the strictosidine formation, the pathway branches out and many rearrangements cause the eminent structural diversity in this large alkaloid family. In some cases the biosynthetic pathways are well investigated even at the enzymatic level (such as the ajmaline biosynthesis in *R. serpentina* reviewed in STÖCKIGT and PANJIKAR, 2007; or the ajmalicine biosynthesis in *C. roseus*: ZENK, 1980; ZENK and JÜNGER, 2007).

Natural reserves of medicinal plants are declining, which is in the case of *Rauvolfia* mainly a result of over-harvesting (MISHRA, 2000). The IUCN (**I**nternational **U**nion for **C**onservation of

Nature and Natural Resources) has kept it under endangered status[4]. Trade with wild plants is strictly regulated and CITES (Convention on International Trade in Endangered Species of wild Fauna and Flora) lists *Rauvolfia* as a plant not necessarily threatened with extinction, but which may become one (Appendix II species)[5].

The main practical source of monoterpenoid indole alkaloids is the extraction from plant material from agriculturally cultivated medicinal plants (PASQUALI et al., 2006). Though the cultivation of medicinal plants for alkaloid extraction faces some disadvantages such as the poor yield of secondary metabolites in differentiated plants, dependence on environmental conditions and long maturation periods, it is the main source due to the lack of efficient alternatives (VERPOORTE et al., 1993). *R. serpentina* for instance is under cultivation in India, Sri-Lanka and Nepal (DUTTA et al., 1962; CHAPMAN and CHOMCHALOW, 1996[6]). It takes several years for maturation and the average yield amounts to 2 – 4 t/ha of dried roots per year after the third year[7]. The total alkaloid yield from *Rauvolfia* roots is 0.8 – 2 % (HÄNSEL, 2004). An even lower amount of two valuable monoterpenoid indole alkaloids used in chemotherapy is isolated from *C. roseus*: vinblastine and vincristine are produced at extremely low levels (0.0003 %, SVOBODA and BLAKE 1975; HÄNSEL, 2004). They represent only trace compounds in this plant (SEVESTRE-RIGOUZZO et al., 1993). The worldwide production volume is therefore limited to a few kilograms only (VERPOORTE et al., 1993). The market-prices of the two anti-cancer agents from *C. roseus* amount to > 100,000 US $ per gram (ZENK and JÜNGER, 2007).

The search for alternative production strategies is multifaceted. The optimization of agriculture is still an object of research. Recently JALEEL and co-workers published several studies on *C. roseus* plants (JALEEL et al., 2007a, 2007b, 2008). They investigated the effect of water deficit stress and found that the economically important alkaloid ajmalicine accumulated in the plants under drought stress. They concluded that water deficit areas might be suitable for the cultivation of medicinal plants. Due to the high economic value of compounds such as vincristine, vinblastine etc., the extraction of indole alkaloids from plant

---

[4] IUCN Red Data Book (1978) and IUCN Guidelines on the conservation of medicinal plants (1994).
[5] Earth Negotiation Bulletin, Vol. 21, No. 62, April 28th 2008, page 3 – 4; available online at http://www.iisd.ca/vol21/enb2162e.html.
[6] CHAPMAN K. R., CHOMCHALOW, N. (1996). Production of Medicinal Plants in Asia. First Asian Symposium on Industrial Utilization of Medicinal and Aromatic Plants in FAO/RAP, Bangkok, November 1996.
[7] Ecocrop: The crop environmental requirements database, provided by the Food and Agriculture Organization of the United Nations (FAO); available online at http://ecocrop.fao.org/ecocrop/srv/en/cropView?id=9185

material is constantly being optimized. Hereby several extraction methods have been developed (VERMA et al., 2008).

Furthermore, the total synthesis of monoterpenoid indole alkaloids has been the object of intensive research in the last century. The interest in the total synthesis of indole alkaloid natural products stems from their complex structures and their diverse medicinal properties mentioned above (COX and COOK 1995; STORK et al., 2005). The development of an stereo-selective route, based on a common intermediate would not only increase the amount of material available for industrial and research purposes it would also provide the opportunity for derivatization in order to obtain greater potency and a better adverse effect profile (COX and COOK 1995). However, due to their complex structure, which often includes several stereo centers (e.g. 9 chiral C-atoms for ajmaline), the total synthesis of monoterpenoid indole alkaloids is lengthy and expensive, and thus representing a challenging aim (GRÄTHER and SCHNEIDER, 2001). Despite the endeavors throughout the past century, only few syntheses have been reported until date (reviewed by LEWIS, 2006). Successful approaches are long winded and mostly not attractive for the industrial production of monoterpenoid indole alkaloids (PASQUALI et al., 2006).

The total synthesis of the bis-indoles vincristine and vinblastine from *C. roseus* was not achieved until recently (HUGHES and SHANKS, 2002). In all cases, the supply of the vindoline moiety relied on natural sources. Moreover the coupling of the two indole units was a major hurdle to overcome. In 2002, YOKOSHIMA et al. presented for the first time a total synthesis of both indole units (catharanthine and vindoline) and their stereo-selective coupling (incorporating far more than 20 individual reaction steps).

The quinine total synthesis of WOODWARD and DOERING (1944, 1945) has never been utilized for industrial production of a substitute of naturally occurring quinine, although there had been a great public interest during World War II, because of its importance in the treatment of malaria. Several more efficient quinine total syntheses have been achieved (STORK et al., 2001) but none of them can in economic terms compete with the isolation of the alkaloid from natural sources. *Cinchona* trees remain the only practical source of quinine (WEINREB, 2001).

Since higher plants are difficult to work with, most approaches focused on plant suspension cultures and attempted to enhance their production of secondary metabolites. Progress was achieved by further development of cultivation media and bioreactor systems, screening and selection of high production cell lines and cultivation of differentiated cells, so called organ cultures (DEUS-NEUMANN and ZENK, 1984; VERPOORTE et al., 1999 and 2000). Several studies on the production of ajmalicine were performed (FULZELE and HEBLE, 1994; NAMDEO

et al., 2002; SATDIVE et al., 2003) and reportedly an experiment yielded > 300 µg ajmalicine per gram dry weight (14 d) with the large-scale cultivation of *C. roseus* in a bioreactor system using tryptophan enriched medium. Similar achievements for the production of catharanthine were reported by PARK et al. (1990). The addition of chemical growth regulators has also been re-investigated in recent years in order to influence the production of secondary metabolites in cell suspension cultures and hairy root cultures (MORENO-VALENZUELA et al., 2003; SIATKA and KASPAROVÁ, 2008).

The metabolic engineering of plants (in plant cell cultures, plant tissue cultures or intact plants) represents a promising technology and the utilization of plants and plant cells as "factories for the production of pharmaceuticals and specialty chemicals" (KUTCHAN, 2000) seems to be practicable (Verpoorte et al., 2000). The biotechnological approaches consider also transgenic microorganisms and isolated enzymes (KUTCHAN, 2000, 2005; HUGHES and SHANKS, 2002). All these methods require the knowledge of the respective biosynthetic pathways on genetic and enzymatic level and in many cases this remains the major constraint (VERPOORTE et al., 1999, 2000). For certain compounds, such as taxol (JAZIRI et al., 1996), a plant cell culture production is feasible. Another successful example is represented by the over-expression of STR and tryptophan decarboxylase in transgenic *C. roseus* cells, which resulted in a 10-fold enhanced strictosidine yield (CANEL et al., 1998). However, in most cases the secondary metabolites, in particular the economically important compounds quinine, vincristine and vinblastine, are produced at very low levels or not at all (VERPOORTE, 1999).

The current work should be considered in this context as another strategy for the production of monoterpenoid indole alkaloids by enzymatic synthesis using STR1 and its engineered mutants.

I.3   The biosynthetic network of *Rauvolfia serpentina*

The achievements in the investigation of the biosynthetic network of *Rauvolfia serpentina* is an extraordinary example in the field of natural product biosynthesis. During the last decades it has resulted in cloning, expression, crystallization and structure elucidation of several enzymes involved (STÖCKIGT et al., 2007; STÖCKIGT and PANJIKAR, 2007). In the field of alkaloid biosynthesis, the pathway leading to the monoterpenoid indole alkaloid ajmaline (including several sideways) in *Rauvolfia serpentina* is one of the most detailed investigated in the field of alkaloid biosynthesis (SUN et al., 2008). It is one of the very few examples from the alkaloid field, which at present delivers a coherent knowledge of the biosynthetic routes

at the enzyme level (STÖCKIGT and PANJIKAR, 2007). The pathway (including the three-dimensional enzyme structures which are thus far elucidated) is outlined in Figure 4.

By condensation of the two biosynthetic precursors of the monoterpenoid indoles, namely tryptamine and the glucosylated seco-iridoid secologanin, STR1 initiates the biosynthetic pathway to ajmaline by a Pictet-Spengler type condensation (PICTET and SPENGLER, 1911; STÖCKIGT et al., 2008). The enzymatic reaction is completely stereo-selective, leading to 3α-(S)-strictosidine. As mentioned above, strictosidine represents the common precursor of probably all monoterpenoid indole alkaloids occurring in higher plants and it is subsequently deglycosilated by strictosidine glucosidase (SG, EC 3.2.1.105; GERASIMENKO et al., 2002). The resulting strictosidine-aglycon is highly reactive and in the biosynthesis of ajmaline in *R. serpentina* it rearranges into the Corynanthean-skeleton yielding 4, 21- dehydro-geissoschizine. The subsequent steps include the reduction of this intermediate in a NADPH depending reaction catalyzed by geissoschizine dehydrogenase (GDH; EC 1.3.1.36) yielding geissoschizine (PFITZNER and STÖCKIGT, 1982) and the formation of the sarpagan skeleton by the sarpagan bridge enzyme (SCHMIDT and STÖCKIGT, 1994). For the purpose of clarity, both steps are not included in Figure 4.

The conversion of polyneuridine aldehyde into 16-epi-vellosimine is catalyzed by polyneuridine aldehyde esterase (PNAE, EC 3.1.1.78, PFITZNER and STÖCKIGT, 1983a and 1983b), an enzyme functionally expressed for the first time by DOGRU et al. (2000) and recently crystallized in the laboratory of Prof. Dr. J. Stöckigt, Johannes-Gutenberg University Mainz (unpublished data).

The structure of acetyl-CoA dependent vinorine synthase (VS; EC 2.3.1.160; PFITZNER et al., 1986) was likewise determined by MA et al. (2005a, 2005b). VS catalyzes the formation of vinorine, which is subsequently hydroxylated by vinorine hydroxylase (VH, EC 1.14.13.75; FALKENHAGEN et al., 1995; FALKENHAGEN and STÖCKIGT, 1995; synonym vinorine 21-monooxygenase) and cytochrome P450 reductase (CPR; heterologously expressed in yeast; RUPPERT et al., unpublished data) yielding vomilenine. Based on vomilenine, it requires only four steps to yield ajmaline (not shown in Figure 4). The enzymes involved are vomilenine reductase (VR; EC 1.5.1.32; VON SCHUMANN et al., 2002), 1,2-Dihydrovomilenine reductase (DHVR; EC 1.3.1.73; GAO et al., 2002), acetylajmalan esterase (AAE; RUPPERT et al., 2005) and norajmalan methyltransferase (NAMT). AAE has been heterologously expressed. The late stage of the route to ajmaline remains vague at the enzymatic level.
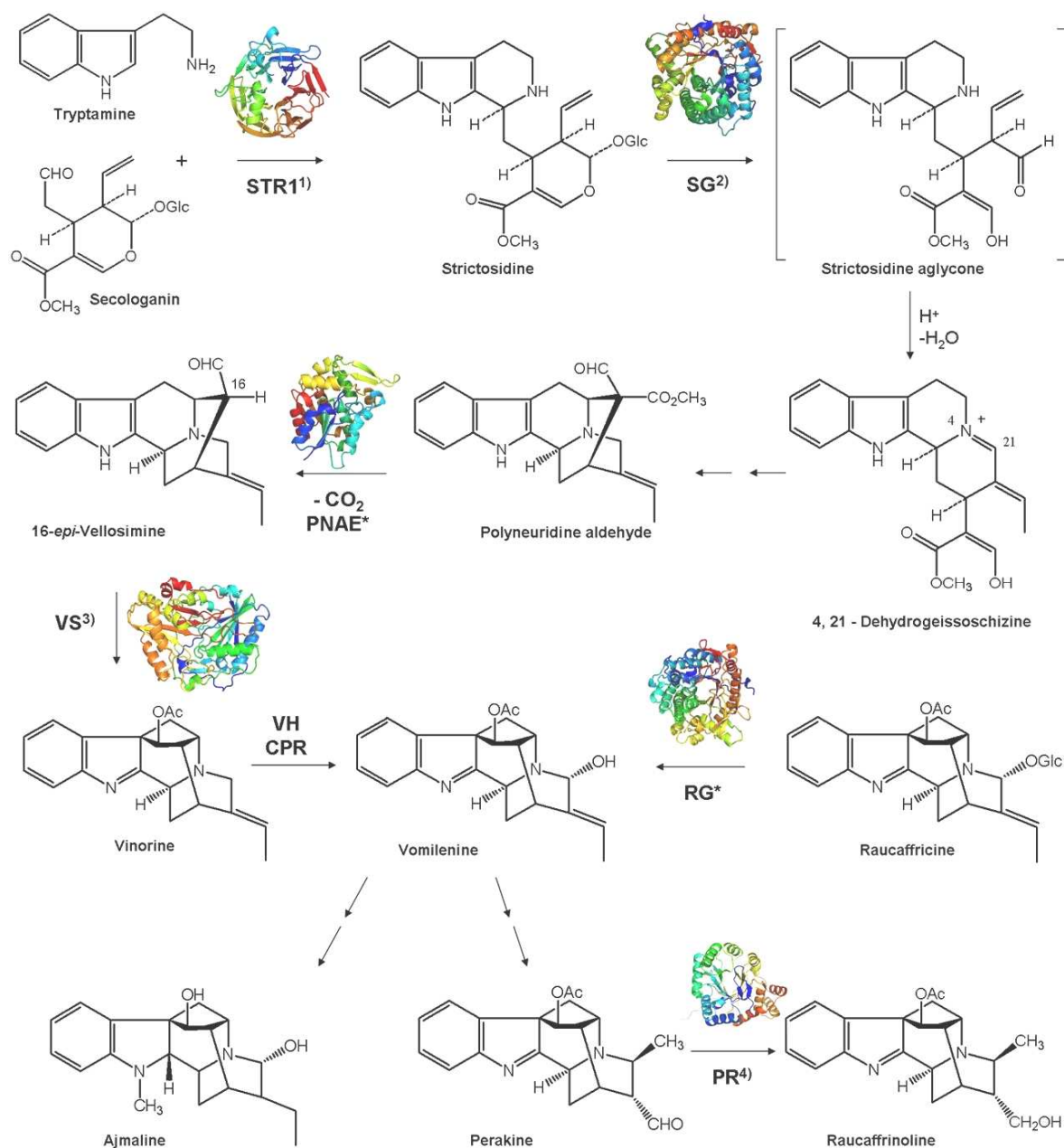
Figure 4. The biosynthetic network of the alkaloids of *R. serpentina*. Sequences of the biosynthesis of ajmaline in *R. serpentina* including sideways. STR1 strictosidine synthase; SG strictosidine glucosidase; PNAE polyneuridine aldehyde esterase; VS vinorine synthase; VH vinorine hydroxylase; CPR cytochrome P 450 reductase; RG raucaffricine glucosidase; PR perakine reductase. References for the published X-ray structures: 1) MA et al., 2006 2) BARLEBEN et al., 2007 3) MA et al., 2005b 4) ROSENTHAL et al., 2006 ; SUN et al., 2008. * labels unpublished data.

The metabolic network of *R. serpentina* includes several intermediate stage side routes of the ajmaline pathway. The formation of raucaffricine is one of the most important, because this alkaloid has been detected as the main alkaloid of *Rauvolfia* cell cultures (SCHÜBEL and STÖCKIGT, 1984). The enzyme raucaffricine glucosidase (RG, EC 3.2.1.125) removes the glucose and it hereby converts the glucoside back to vomilenine. RG was identified, characterized and its cDNA was cloned in *E. coli* by WARZECHA et al., (1999, 2000). Recently

the successful crystallization was achieved and the three-dimensional structure determined (RUPPERT et al., unpublished). Another branch in the metabolic pathway to ajmaline, which has been investigated at the molecular level, is the NADPH-dependent formation of raucaffrinoline by the reduction of perakine. The reaction is performed by perakine reductase (PR). Expression, purification, crystallization and preliminary X-ray analysis of PR were recently completed (ROSENTHAL et al., 2006; SUN et al., 2008).

Cell suspension cultures of the medicinal plant *R. serpentina* were the source for the elucidation of the pathway to the anti-arrhythmic ajmaline and structurally related alkaloids of the sarpagan- and ajmalan-type. The progress is mainly based on the systematic application of this efficient biological system together with methodologies of phytochemistry, biochemistry and molecular biology. This includes enzyme isolation and characterization as well as the isolation and functional expression of cDNAs coding for enzymes involved. The so called "reverse genetic approach" was employed (starting with partial amino acid sequences obtained from purified *Rauvolfia* enzymes after partial digestion and sequencing of the resulting peptides; STÖCKIGT and PANJIKAR, 2007). Over-expression enables the production of highly purified enzyme in mg amounts suitable for characterization studies and crystallization experiments. So far, more than 15 enzyme-catalyzed reactions are characterized in the biosynthetic network of *R. serpentina* and for 6 of them, the respective enzyme could be structurally determined (STÖCKIGT and PANJIKAR, 2007). This gives an almost coherent molecular overall picture of the biosynthetic network of *R. serpentina*, in particular of the ajmaline route at the enzymatic level. The ambitious aim is to determine the three-dimensional structures of all enzymes involved in the 10-step biosynthetic pathway of the alkaloid ajmaline. To the author's knowledge, it will provide for the first time a complete atomic insight into the biosynthesis of a natural product as complex as ajmaline. The only comparable investigation is the shikimate pathway which involves seven enzymes. To date, crystal structures for all of the pathway enzymes have been determined (BAGAUTDINOV and KUNISHIMA, 2007).

I.4   The previous status of research on STR1 from *R. serpentina*

Due to its outstanding role in the biosynthesis of the monoterpenoid indole alkaloids, STR is one of the most extensively investigated enzymes in alkaloid biosynthesis. Although the enzyme activity of STR has been detected in several plant cell cultures (TREIMER and ZENK, 1979a; PENNINGS et al., 1989), it has been investigated to a varying degree of detail. The enzyme from *Rauvolfia serpentina* (STR1) became broadly characterized and first sequence analyses were made after its cDNA was isolated and functionally expressed, representing the first example in alkaloid research (KUTCHAN et al., 1988; KUTCHAN, 1989, 1993).

Therefore STR1 became one of the best investigated enzymes in the field of alkaloid biosynthesis.

STR has been isolated and cloned from cell suspension cultures of *R. serpentina* Benth. ex Kurz, Apocynaceae (TREIMER and ZENK, 1979a, 1979b; PFITZNER and ZENK 1989; KUTCHAN et al., 1988; KUTCHAN 1989, 1993; PENNINGS et al., 1989; BRACHER and KUTCHAN 1992), *Catharanthus roseus* G. Don., Apocynaceae (MIZUKAMI et al., 1979; PFITZNER and ZENK 1989; MCKNIGHT et al., 1990; DE WAAL et al. 1995; ROESSNER et al., 1992; GEERLINGS et al., 2001) and *Ophiorrhiza pumila* Cham. ex Benth., Rubiaceae (YAMAZAKI et al., 2003a and 2003b). The enzyme was also detected in *Cinchona robusta* Howard, Rubiaceae (STEVENS et al. 1993) but it has not been further characterized in this plant.

Until now, five STR enzymes have been heterologously expressed and their activity has been demonstrated. Three of these originate from different species of the genus *Rauvolfia*, namely *R. serpentina* (STR1; KUTCHAN et al., 1988), *R. mannii* (BRACHER and KUTCHAN, 1992) and *R. verticillata* (WANG-HONG et al., 2006). They exhibit 100 % sequence identity. The other two enzymes deriving from *C. roseus* (STR_CR; TREIMER and ZENK, 1979b) and from *O. pumila* (STR_OP; YAMAZAKI et al., 2003a) show respectively 79 % (STR_CR) and 58 % (STR_OP) sequence identity to STR1. While the current work presents a systematic substrate specificity study of STR1, a detailed summary of accepted substrates of STR_CA has been reported recently (MCCOY et al., 2006). The experimental evidence on STR_OP is rudimentary in comparison to STR1 (YAMAZAKI et al., 2003b).

In 2004 protocols for the crystallization of STR1 were developed (MA et al., 2004, KOEPKE et al., 2005), which represented another milestone in the investigation of this enzyme. The three-dimensional structure of the *R. serpentina* STR1 was determined shortly after (MA et al., 2006). These experiments allowed the first molecular insight into the enzymes structure and function. It is the only STR enzyme which has been structurally elucidated today. The current knowledge, pertaining to the structure and function of STR1 (reviewed by STÖCKIGT et al., 2008), will be briefly summarized in the following section.

I.4.1 Overall architecture

The crystal structure of *R. serpentina* STR1 has been determined for the native protein, and furthermore in complex with the two substrates tryptamine and secologanin at resolutions ranging from 2.3 to 3.0 Å (MA et al., 2006; Figure 5). The resolved structures provided a first insight into the STR1 architecture, including distinct information on its active site and catalytic mechanism.
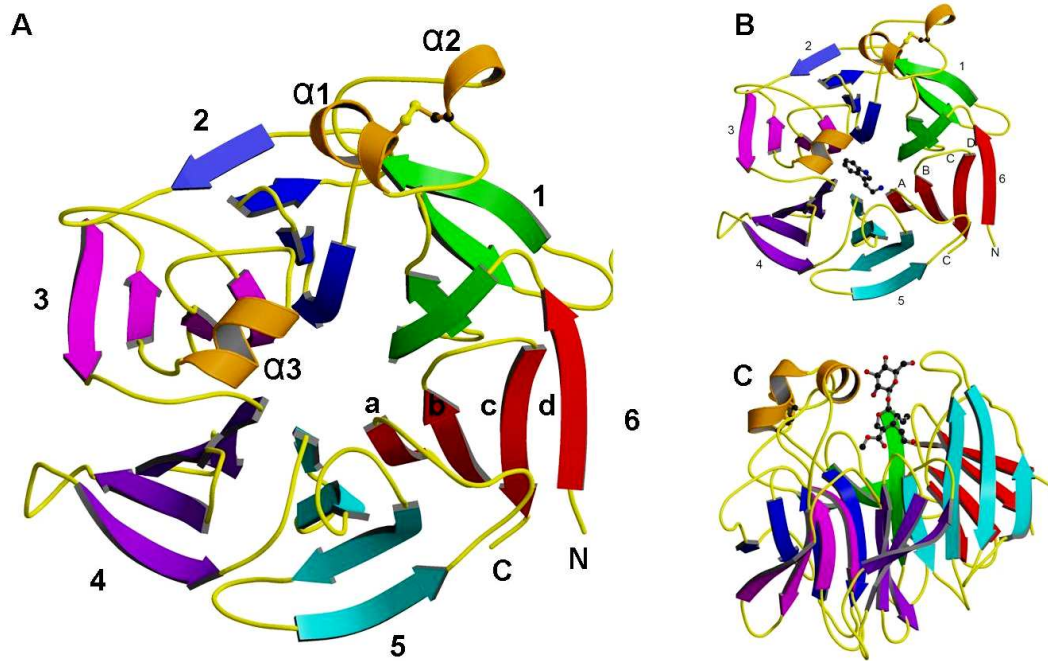
Figure 5. Six-bladed β-propeller structure *of R. serpentina* **STR1 as displayed in** Mᴀ **et al. (2006).** The crystal structures were solved by multiple wavelength anomalous dispersion method at resolutions from 2.3 Å to 3.0 Å. (A) View of the six-bladed β- propeller fold as cartoon representation from above. (B) Front view of STR1 in complex with tryptamine. The active site is located near the six-fold pseudo-symmetry axis. (C) A side view of the propeller in complex with secologanin.

The overall enzyme structure of STR1 represents a β-propeller comprising 6 blades (labeled from 1 to 6 in Figure 5 A), which are radially arranged around a central six-fold pseudo-symmetry axis. Each propeller blade contains four β-strands (labeled from a - d) which form a twisted, anti-parallel β-sheet. The substrate binding pocket of the enzyme is located on top of the propeller, near the pseudo six-fold symmetry axis. STR1 is the first protein from the plant kingdom that shows this particular fold. Enzymes belonging to the six-bladed β-propeller fold display an extreme diversity of sequence and function and they feature wide-spread occurrence (Jᴀᴡᴀᴅ and Pᴀᴏʟɪ, 2002). STR1 does not show sequence similarities with other six-bladed β-propeller structures and it does not share any functional homologies (Mᴀ et al., 2006).

There are three helices in the STR1 structure (α1, α2 and α3, Figure 5). Two of them are connected by a disulfide bridge, which pulls the two helices closer together and which might be essential for the integrity of the substrate binding site and for the overall structure of the enzyme. The third helix (α3) forms a cap over the active site. Together with a loop of blade 5, it shapes the substrate binding pocket and provides STR1 with a closed active site, in which a highly hydrophobic environment is created. Both tryptamine and secologanin are bound in the same substrate binding pocket in close proximity to each other. The main amino acid

residues involved in forming the surrounding active centre are Tyr105, Trp149, Val167, Met180, Val208, Phe226, Ser269, Met276, His277, His307, Phe308, Glu309, Leu323, and Phe324. Tryptamine is located at the bottom of the pocket where its primary amine group is connected with residue Glu309 by a hydrogen bond. This residue was assumed to act as a catalytic residue and mutagenesis studies confirmed its essential role in the reaction mechanism (Ma et al., 2006). Additional key residues involved in the binding of tryptamine are Phe226 and Tyr151, which lie parallel to the aromatic indole ring system, where they appear to act as scaffolds and fix it by π-π interactions. Secologanin does not occupy the tryptamine position, but it is in close proximity, with the aldehyde group facing towards the primary amine of tryptamine. The hydrophilic glucose unit points away from the pocket and is accessible to the solvent.

I.4.2 Mechanistic aspects of the STR1 reaction and related Pictet-Spengler-type reactions

The reaction catalyzed by STR is a stereo-selective Pictet-Spengler condensation between tryptamine and secologanin, and yields 3α-(S)-strictosidine (S stereochemistry at carbon 3, Figure 6 A). Discovered almost 100 years ago (Pictet and Spengler, 1911), the Pictet-Spengler condensation has been an important reaction for the synthesis of indole and isoquinoline alkaloids. It is often applied in organic chemistry in order to chemically synthesize tetrahydro-isoquinoline skeletons (Cox and Cook, 1995; Larghi et al., 2005). In higher plants, the Pictet-Spengler reaction plays a central role in the biosynthesis of a large number of structurally diverse alkaloids; many of them are of substantial pharmaceutical importance (Stöckigt et al., 2008). Beside the alkaloids of the monoterpenoid indole alkaloid family, two more alkaloid families derive from so called "Pictet-Spenglerases" (O'Connor and Maresh, 2006): the benzylisoquinoline alkaloid family and the monoterpenoid isoquinoline family. The individual enzymes, initiating the biosynthesis by this particular reaction have been characterized to differing extents.

The Pictet-Spengler type condensation of dopamine and secologanin is catalyzed by deacetylipecoside synthase (DIS; EC 4.3.3.4) and deacetylisoipecoside synthase (DIIS; EC 4.3.3.3) and yields 1-(R)-deacetylipecoside (likely the biosynthetic precursor of nitrogenous glycosides; De-Eknamkul et al., 2000) and 1-(S)-deacetylisoipecoside respectively. The latter represents the initial step in the biosynthesis of tetrahydroisoquinoline monoterpenoid alkaloids (e.g. the emetic drugs emetine and cephaeline). Both enzymes have been detected in cell-free extracts of *Alangium lamarckii* Thw. (Alangiaceae) (De-Eknamkul et al., 1997 and 2000). Due to the instability of DIIS, DIS alone has been purified and analyzed. DIS features similar properties to STR1 in terms of molecular size, reaction mechanism, temperature- and

pH-optimum. Both enzymes involve secologanin as the non-amine compound and they exhibit a limited substrate spectrum. On the other hand they differ in origin, absolute product configuration and substrate acceptance. Dopamine, the native substrate of DIS, is not converted by STR1, and this also applies vice versa in the case of the interaction of tryptamine with DIS. It was hypothesized that an evolutionary relationship between these two enzymes may exist, however, to confirm this assumption the determination of the amino acid sequence of DIS is required.

Norcoclaurine synthase (NCS; EC 4.2.1.78) the Pictet-Spenglerase initiating the biosynthesis of benzylisoquinoline alkaloids (which includes therapeutically valuable compounds such as the analgesic morphine and the antitussive codeine) was detected in 1981 (RUEFFER et al., 1981), then cloned and over-expressed (SAMANANI et al., 2004; MINAMI et al., 2007; LUK et al., 2007). The enzyme catalyzes the condensation of dopamine and p-hydroxyphenylacetaldehyde (4-HPAA) leading to (S)-norcoclaurine (Figure 6 C). The reaction mechanism seems to be analogous to STR1 (LUK et al., 2007), but the amino acid sequence alignment showed no sequence identity of NCS with STR1. MA et al. (2006) suggested that the related reaction types catalyzed by STR1 and NCS may have been the result of convergent evolution of distinct ancestry. Recently, the first structural information on NCS from *Thalictrum flavum* L. was reported: a semi-experimental homology model of NCS (without a signal peptide) confirmed the authenticity of NCS as a real "Pictet-Spenglerase" (BERKNER et al., 2008). It allowed for conclusions on the conformation, catalytic site and the reaction mechanism of NCS. Furthermore, PASQUO et al. (2008) published a crystallization protocol and preliminary X-ray data analysis of NCS from *T. flavum.* The final determination of the three-dimensional structure is expected and will provide molecular insight and the evaluation of the model.

The classical Pictet-Spengler-reaction is a two-part reaction which involves an aromatic amine and an aldehyde under acidic conditions. It is considered as a type of Mannich reaction and represents an intra-molecular addition of a CH-acidic substrate to a Schiff base formed between an aldehyde group and a primary amine component. In contrast to the biological Pictet-Spengler reaction catalyzed by STR1 (which leads exclusively to 3α-(S)-strictosidine), the chemical Pictet-Spengler synthesis yields strictosidine as well as vincoside, the 3β-(R) epimer (STÖCKIGT et al., 2008). The mechanistic knowledge of the enzymatic reaction is very limited. The structure elucidation of STR1 by MA et al. (2006) allowed for a hypothesis, which was initially confirmed by site-directed mutagenesis: the amino acid residue Glu309 in the active site was identified as the catalytic residue, which was involved in the strictosidine formation.
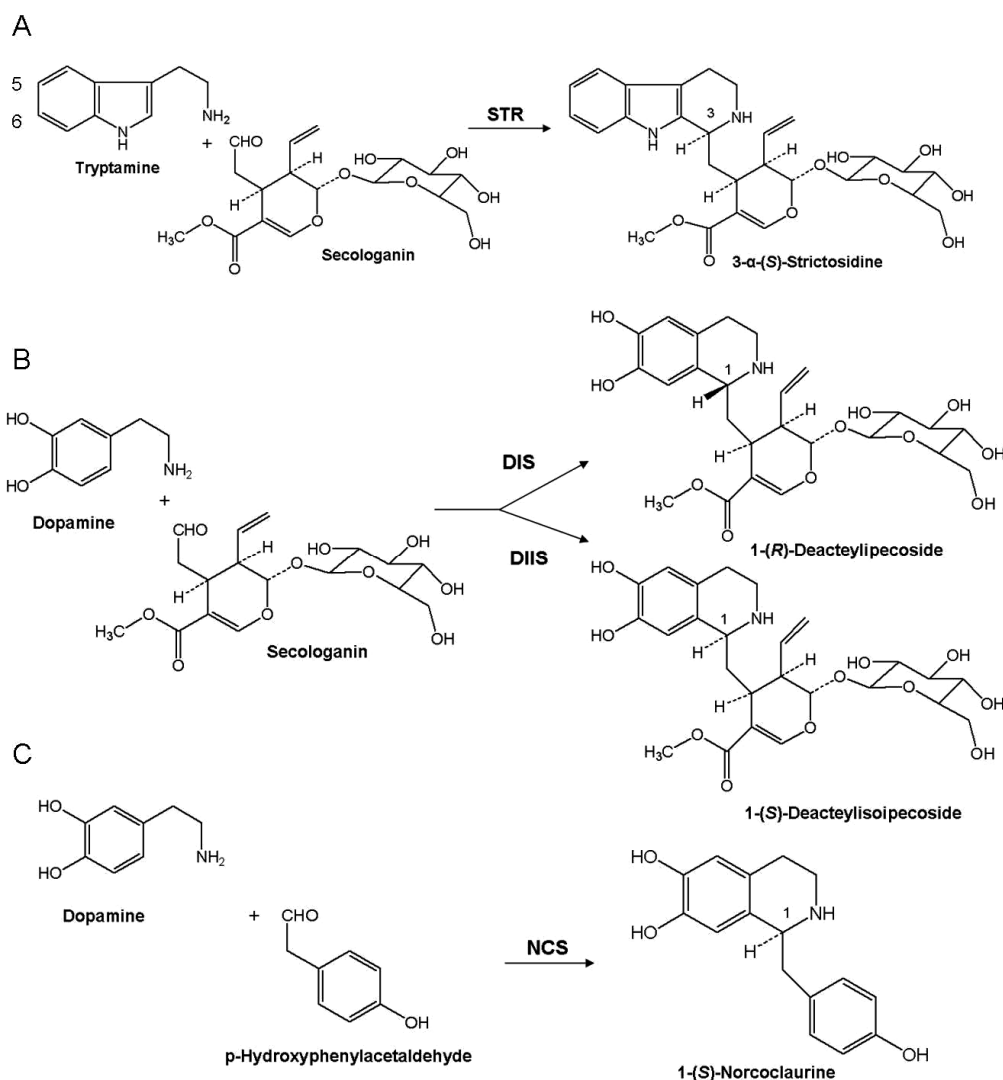
Figure 6. STR reaction (A) and the two other two examples of potential Pictet-Spenglerases (B and C). Biological Pictet-Spengler reactions catalyzed by strictosidine synthase (STR), deacetylipecoside synthase (DIS), deacetylisoipecoside synthase (DIIS) and norcoclaurine synthase (NCS).

I.5 The importance of three-dimensional structure determination and the aim of the current study

The structural determination of proteins plays a highly important part in biology today due to its essential contribution: the understanding of life processes at the molecular level. Structural biology is a rapidly expanding research field with various opportunities and applications. For E. N. Baker and G. G. Dodson it "brings the excitement of discovery" and "illustrates at the same time the beauty and the importance of detail in understanding biological processes" (BAKER and DODSON, 2005).

The analysis of basic physical and biochemical properties (such as molecular mass, pH- and temperature-optimum, kinetic data, substrate specificity, inhibition studies and random site-directed mutagenesis) is an important part of the functional investigation of an enzyme. However, it is mainly the three-dimensional structure, which allows direct investigation in atomic detail. Structural biology and crystallography in particular elucidate the overall architecture of enzymes and contribute to the molecular characterization of catalytically and structurally important amino acid residues (STÖCKIGT et al., 2008). The opportunity to provide molecular insight into mechanisms of action of a particular protein enables the correlation of structure and (re-)activity. Structural determination is highly required for rational re-design and for structure-based drug development in order to customize ligands for individual target proteins.

The research field of structural biology is expanding rapidly and the increasing number of protein structures implicates the possibility of discovering unexpected evolutionary relationships by comparing large numbers of protein structures. Furthermore, with increasing structural information, sequence derived predictions deduced from structural alignments are becoming increasingly reliable. Until now such information cannot be accurately obtained from primary structure or cDNA sequence alignment studies (ROST and O'DONOGHUE 1997; ROST 1998, 2001). Genome sequence project based conclusions relating to the protein structure and function still remain speculative. Structural determination helps to evaluate theoretical methods (*ab initio* calculations, modeling, alignment studies). In the case of known function and three-dimensional structures, conclusions can be drawn more easily for related enzymes and new functional hypotheses can be generated.

The structural investigation of enzymes allows non-random site-directed mutagenesis experiments in order to investigate the mechanism of the enzyme on the molecular level or perform structure-based evolution studies. It enables a rational re-design and engineering of enzymes with new or improved properties such as substrate specificity, stability, kinetic properties, and turnover number – also for commercial applications (ZENK and JÜNGER, 2007). The generation of a faster superoxide dismutase exemplifies the power of rational re-design (CHEN, 2001). GETZOFF et al. (1992) succeeded in optimizing the velocity of this enzyme, which already is one of the fastest enzymes known.

The three-dimensional structures presented in this work completed the molecular image of STR1 and provided for the first time the prerequisite for its rational engineering. In the current work a successful engineering strategy, based on the novel crystal structures was presented. The structural determination of STR1 rapidly advanced the research on this unique enzyme. The initial phase of the enzyme reaction was structurally well determined. Achieving a

molecular insight into the later stages was a major aim of the present work. It focused on expanding the current knowledge on the three-dimensional structure of STR1 via investigations on further enzyme-ligand complex structures in order to complete the three-dimensional image of STR1 and to acquire more details on the reaction mechanism.

The successful synthesis of a compound approximating the conformation of an assumed iminium intermediate occurring during the enzymatic reaction, which acted as a potent inhibitor of the STR enzyme from *C. roseus*, was achieved by Anne Friedrich in 2006 (MARESH et al., 2008). It represented the starting point for the further investigation of this compound with the enzyme from *R. serpentina*. It was necessary to elucidate the structure of STR1-inhibitor complex in order to obtain further information on the reaction mechanism. In particular, the structure was expected to give insight into the transition states passed during the catalyzed Pictet-Spengler reaction.

The ability of strictosidine to interact with the enzyme structure was investigated and the resulting structure illustrated the late phase of the enzymatic reaction. It allowed for understanding the structural interaction between enzyme and product and represented the basis for the investigation of the active site. The analysis of this complex structure was necessarily focused on the identification of crucial residues with influence on both the substrate acceptance and the catalytic function of the enzyme. As mentioned above, the major goal was the development of an engineering strategy for the rational re-design of STR1. Site-directed mutagenesis experiments were then performed with the aim to broaden the substrate specificity of STR1 and herewith the amount of enzymatically accessible strictosidine derivatives. The question whether re-engineering of STR1 can benefit the production of strictosidine and enhance the number of available strictosidine derivatives was related to a so called biomimetic approach developed by H. Schübel and J. Stöckigt (LORIS et al., 2007). It combined enzymatic and chemical reactions in a "one pot" reaction in order to synthesize N-analogous heteroyohimbine derivatives. The successful synthesis of novel strictosidine derivatives with high yields and the possibility for further chemical modifications, would allow the generation of large libraries of new alkaloid compounds via this chemo-enzymatic approach.

II. Materials

II.1 Bacterial strains

The *Escherichia coli* (*E. coli*) strains used for expression of recombinant STR1 and mutants in this work are listed in Table 1. They were maintained and cultivated according to the recommendations and standard protocols of the suppliers. For heterologous expression of STR1-His$_6$ and its engineered variants, *E. coli* strain M15 [pREP4] was routinely used. In the course of optimization efforts Arctic Express™ and XL1-Blue MRF' were applied: the first for STR-His$_6$ and its mutant W149A, the latter for the mutant only.

Table 1. Bacterial strains used in this work. For cultivation conditions see III.1.

Strain	Company	Description	Usage
Top10F´	Invitrogen (Karlsruhe, Germany)	F´{*lac*I^q, Tn*10*(Tet^R)} *mcr*A Δ(*mrr-hsd*RMS-*mcr*BC) Φ80*lac*ZΔM15 Δ*lac*X74 *rec*A1 *ara*D139 Δ(*ara-leu*)7697 *gal*U *gal*K *rps*L (Str^R) *end*A1 *nup*G	In vivo reproduction of plasmids and sequencing
XL1-Blue MRF´	Stratagene (Heidelberg, Germany)	*Δ(mcrA)183 Δ(mcrCB-hsdSMR-mrr)173 endA1 supE44 thi-1 recA1 gyrA96 relA1 lac* [F'*proAB lacI^{q}ZΔM15 Tn10* (Tet^r)]	In vivo reproduction of plasmid *str1_W149A*-pQE2
M15 [pREP4]	Qiagen (Hilden, Germany)	*E. coli* K12 (Nal^S, Str^S, Rif^S, Lac$^-$, Ara$^-$, Gal$^-$, Mtl$^-$, F$^-$, RecA$^+$, Uvr$^+$, Lon$^+$)	Standard expression host
Arctic Express™	Stratagene (Heidelberg, Germany)	*E. coli* B F$^-$ *ompT hsdS*(r$_B^-$ m$_B^-$) *dcm*$^+$ Tet^R *gal endA* Hte [cpn10 cpn60 Gent^R]	Expression of *str1*_pQE2 and *str1_W149A*-pQE2

II.2 Vector

Stable expression of the STR1 gene in *E. coli*, was achieved via pQE-2 vector (Figure 7) purchased from Qiagen. This is a vector for N-terminal His$_6$-tag constructs with a strong T5 promoter (PT5), which permits high-level expression of His$_6$-tagged proteins. It features β-lactamase gene (*bla*) allowing for ampicillin selection. The N-terminal His$_6$-tag encoded by pQE-2 vector possesses a sequence optimized for TAGZyme enzyme digestion. This facilitates the removal of the His$_6$-tag and herewith the production of His$_6$-tag-free protein.
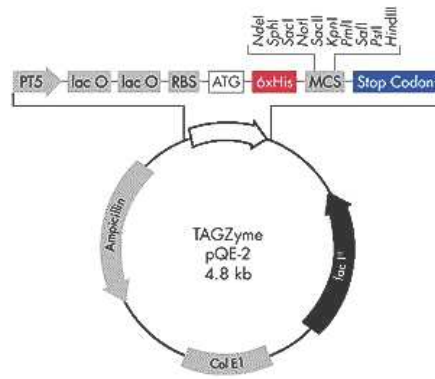
Figure 7. pQE-2 vector. PT5: T5 promoter; lac O: lac operator; RBS: Ribosome-binding site; ATG: Start codon; 6xHis: 6xHis tag sequence; MCS: Multiple cloning site; Col E1: Col E1 origin of replication; Ampicillin: Ampicillin resistance gene; laclq: laclq repressor gene. The picture is taken from the Qiagen web page.[8]

II.3 Bacterial media and solutions

Sterilization was completed under standard conditions by autoclaving at 121 °C for 20 min. Compounds sensitive to high temperatures were sterile filtered (pore size 0.2 µm) with subsequent addition to the medium after cooling.

LB Medium (lysogeny broth), BERTANI (1951 and 2004): Yeast extract 5 g/l, Tryptone 10 g/l, NaCl 10 g/l, pH 7.0. For plate preparation 15 g/l agar was added to the mixture.

LBS Medium: LB medium containing 1 M sorbitol and 1 % (V/V) glycerol. Double concentrated LB-medium and a stock solution with 2 M sorbitol and 2 % glycerol were prepared separately and autoclaved under standard conditions. Prior to usage the solutions were mixed 1:1.

Antibiotic stock solutions: The antibiotics were solved in autoclaved, distilled water and sterile filtered. The stock solutions were diluted 1:1000 with the medium after sterilization and cooling.

Ampicillin   50 and 100 mg/ml
Kanamycin   25 mg/ml
Gentamicin   20 mg/ml

IPTG 1 M stock solution: 238 mg/ml isopropyl-β-thiogalactoside in water, sterile filtered and stored in aliquots at -20 °C.

---

[8]http://www1.qiagen.com/Products/Protein/Purification/TAGZymeSystem/TAGZymepQEvector.aspx?ShowInfo

II.4 Buffer solutions

II.4.1 Buffers for Protein purification with Ni-NTA

Lysis buffer: 50 mM NaH_2PO_4, 300 mM NaCl, 10 mM imidazole, pH 8;
                           1 mg/ml lysozyme

Wash buffer: 50 mM NaH_2PO_4, 300 mM NaCl,
                           10, 25, 40 or 50 mM imidazole, pH 8

Elution buffer: 50 mM NaH_2PO_4, 300 mM NaCl, 250 or 500 mM imidazole, pH 8

II.4.2 Buffers for DAPase digestion

10xTAGzyme buffer: 200 mM NaH_2PO_4, 1.5 M NaCl; pH adjusted to 6.3 with NaOH;
                    after sterile filtration it was stored at 2 – 8 °C; upon dilution pH
                    shifted to 7.0.

II.4.3 SDS PAGE buffers

Sample buffer: 0.2 M Tris-HCl, pH 6.8, 40 % (V/V) glycerol, 20 % (V/V) MSH,
                      8 % (m/V) SDS, 0.02 % (m/V) Bromophenol-Blue

Running buffer: 50 mM Tris, 0.2 M glycine, 0.15 % (m/V) SDS

Stacking gel buffer: 5 % acrylamide, 125 mM Tris-HCl pH 6.8, 0.1 % (m/V) SDS

Separation buffer: 11 – 15 % acrylamide, 375 mM Tris-HCl pH 8.8,
                      0.1 % (m/V) SDS

Staining solution: 0.25 % (m/V) Coomassie Brilliant Blue R-250,
                      45 % (V/V) methanol, 9 % (V/V) acetic acid

De-staining solution: 30 % (V/V) methanol, 10 % (V/V) acetic acid

II.4.4 Agarose gel electrophoresis buffers

TAE buffer: 40 mM Tris-acetate, 0.2 M acetic acid, 1 mM EDTA, pH 8.0

Sample buffer: 0.25 % Bromophenol-Blue, 30 % glycerol in water

II.4.5 Buffer for enzyme assay/activity tests

Standard assay buffer: 50 mM potassium phosphate (KPi) buffer, pH 7.0

II.4.6 Buffers for preparing competent *E. coli*

TFB1:   100 mM RbCl, 50 mM $MnCl_2$, 30 mM potassium acetate, 10 mM $CaCl_2$, 15 % glycerol, pH 5.8, sterile filtered

TFB2:   10 mM MOPS, 10 mM RbCl, 75 mM $CaCl_2$, 15 % glycerol, pH 6.8, sterile filtered

II.4.7 Buffers for alkaline lysis mini-preparation

Resuspension buffer: 50 mM glucose, 25 mM Tris, 10 mM EDTA, 10 mg/ml RNAse

Alkaline lyses buffer: 0.2 M NaOH and 1 % (m/V) SDS

KAc buffer: 3 M potassium acetate, pH 5.2

TE buffer: 10 mM Tris-HCl, 1 mM EDTA, pH 7.5

II.5 Column material and columns

Table 2. Column material applied in the current work.

Product	Company
HR 10 chromatography column	GE Healthcare Europe (Munich, Germany) Former Amersham Pharmacia Biotech (Freiburg, Germany)
Ni-NTA Superflow	Qiagen (Hilden, Germany)

▼

Table 2. Continued

LiChrospher© 60 RP select B HPLC-column (125 x 4 mm; 5 µm) Pre-column LiChrospher© 60 RP select B (4 x 4 mm; 5 µm)	Merck (Darmstadt, Germany)

II.6 Molecular biology material

II.6.1 Oligonucleotides

The oligonucleotides, designed for site-directed mutagenesis, were ordered from MWG Biotech GmbH (Ebersberg, Germany). They were delivered in lyophilized state and solved with Ampuwa water to a final concentration of 100 pmol/µL. For PCR cycles, a 10-fold dilution (10 pmol/µl) was used. The stock solutions were stored at -20 °C.

II.6.2 Kits, enzymes and nucleotides

Table 3. Alphabetical list of molecular biology equipment used in the current work.

Product	Company
Agarose for molecular biology	AppliChem (Darmstadt, Germany)
DAPase	Qiagen (Hilden, Germany)
dNTPs	Promega (Madison, USA)
λ-DNA – *HindIII* digest	New England Biolabs (Ipswich, USA)
LMW SDS marker kit	GE Healthcare Europe (Munich, Germany)
Lysozyme	Sigma (Deisenhofen, Germany)
NucleoSpin© Plasmid Kit and Nucleospin© Extract Kit II	Macherey and Nagel (Düren, Germany)
Phusion DNA polymerase	New England Biolabs (Ipswich, USA)
Pfu Turbo polymerase	Stratagene (La Jolla, CA, USA)
PfuPlus! DNA-Polymerase	Roboklon (Berlin, Germany)
Primer	MWG Biotech (Ebersberg, Germany)
Restriction Enzymes and buffers for restriction digest	New England Biolabs (Ipswich, USA)
Smart Ladder	Eurogentec (Seraing, Belgium)

II.7 Material for crystallization

II.7.1 Buffers

Crystallization buffer: 10 mM Tris-HCl, pH 8.0

Precipitant buffers: 0.7 – 0.9 mM Potassium sodium tartrate x 4 H_2O, 100 mM
HEPES-Na, pH 7.0, 7.3, 7.5 or 7.7; sterile filtered

II.7.2 Equipment

Table 4. Crystallization material.

Product	Company	Usage
VDX™ plate	Hampton Research (Aliso Viejo, USA)	24 well crystallization plate for crystallization with hanging drop method
Plain square cover slides 22 mm x 0.22 mm	Hampton Research (Aliso Viejo, USA)	Siliconized cover slides for crystallization
Silicone oil Medium viscosity	Bayer (Leverkusen, Germany)	Immersion oil (silicone) for sealing cover slides to crystallization plates, medium viscosity
Syringe 1 ml	B. Braun (Melsungen, Germany)	Dispenser for manually applying silicone oil to the plate
Cryo loops (consisting of magnetic base, metal pin and fiber loop secured to each other by epoxy glue)	Hampton Research (Aliso Viejo, USA)	Fishing, soaking and mounting of crystals; attachment to goniometer head for data collection

II.8 Tryptamine, tryptamine analogues and secologanin

Compounds used for enzyme assay were purchased in the highest available purity from Fluka (Seelze, Germany), Roth (Karlsruhe, Germany) or Sigma-Aldrich (Seelze, Germany). They were used without further purification. 6-Methyl-tryptamine was a gift of Prof. Sarah O'Connor (MIT, Cambridge, MA, USA). Secologanin was obtained from Dr. Hongbin Zou by extraction from leaves of *Lonicera xylosteum* (KINAST and TIETZE, 1976).

II.9 Chemicals, solutions and lab equipment

Table 5. Chemicals, solutions and lab equipment. List of chemicals, solutions and lab equipment according to the alphabetical order of manufacturers (left).

Company/Producer	Products
Amicon (Witten, Germany)	Centriprep YM-10 10 kDa centrifugal filter units
AppliChem (Darmstadt, Germany)	- Antibiotics - Fine chemicals (IPTG, SDS, Coomassie Brilliant Blue R-250 etc.) - Agarose for molecular biology - Acrylamide solution (30:29:1)
Biozym (Hess. Oldendorf, Germany)	PCR- and reaction-tubes, pipette tips
Eppendorf (Hamburg, Germany)	Pipettes
Fresenius (Bad Homburg, Germany)	Ampuwa (sterile water for molecular biology)
Fischer Scientific (Schwerte, Germany)	- Graduated Tubes - Erlenmeyer flasks (1 l) - Acetonitrile HPLC grade
Fluka (Seelze, Germany)	Fine chemicals (secologanin, tryptamine and most of its derivatives)
Intermedica (Klein-Winternheim, Germany)	Semi-micro cuvettes, protective gloves
Life Technologies (Eggenstein, Germany)	Yeast extract, tryptone, agar
Macherey and Nagel (Düren, Germany)	Circles filter papers (Ø 15 cm)
Marienfeld Laboratory glassware (Lauda-Königshofen, Germany)	Capillary tubes (100 x 0.1 mm)
Merck KGaA (Darmstadt, Germany)	- Methanol HPLC grade CD_4OD for ^{1}H- and ^{13}C-NMR analysis - Fine chemicals - TLC plates (20 x 20 cm, 1.0 mm, silica gel 60 F_{254})
Sarstedt (Nürmbrecht, Germany)	Pipette tips
Schleicher and Schnell (Dassel, Germany)	- Whatman[©] syringe sterile filter (pore size 0.2 µm) - Whatman[©] celluloseacteate membrane filters (Ø 50 mm, pore size 0.45 µm)
Serva (Heidelberg, Germany)	Servapor dialysis tubes (Ø 9, 16 and 29 mm, MWCO 12000 - 14000)
Schott (Mainz, Germany)	Laboratory glassware (flasks, NMR tubes)
VWR (Darmstadt, Germany)	Laboratory glassware and equipment (Pasteur pipettes, flasks)

II.10 Instruments

Table 6. List of instruments. Instruments applied in this work are listed according to their purpose of usage.

Instrument / Purpose of Usage	Type of Instrument and manufacturer
Agarose gel documentation	▪ UV-Transilluminator, 302 nm (Bachofer, Reutlingen, Germany) ▪ Canon Powershot G5 digital camera
Analytical (precision) balance	▪ Satorius Research R-160 P (Satorius Göttingen, Germany) ▪ Precision balance Satorius 1219 MP (Satorius Göttingen, Germany)
Autoclave	Technoclav 120 steam sterilization (Fedegari Autoclavi, Spa, Italy)
Centrifuges	▪ Refrigerated floor centrifuges: Beckmann Avanti™ J-30I and J-25 with rotors JA10, JA20 and JA 30.50 Ti (Beckmann Coulter, Munich, Germany) ▪ Refrigerated bench centrifuge Universal 32R (Hettich, Tuttlingen, Germany) ▪ Small bench centrifuges Biofuge A and Biofuge 15 (Heraeus, Sepatech, Osterode, Germany)
Electrophoresis	▪ BlueMarine 100 and 200 horizontal electrophoresis instrument (Serva, Heidelberg, Germany) ▪ SE 600 Hoefer vertical electrophoresis instrument (Amersham Pharmacia Biotech, Freiburg, Germany) ▪ COMPHOR Midi electrophoresis system (Biozym, Hess. Oldendorf, Germany) ▪ Power supply units: PowerPac 3000 (BioRad, Munich, Germany), E835 and E844 (Consort, Turnhout/Belgium) ▪ The system was operated in a Liebherr refrigerator (glass line)
Electroporation	Easyject optima (Equibio, Ashford, UK)
Freeze drying equipment	Freeze dryer unit Alpha I-6 (Christ, Osterode, Germany) and vacuum pump ADEB71N4R3 (AEG/Electrolux, Stockholm, Sweden)
Instruments for maintaining temperature	▪ Ecocell 55 (MMM Medcenter, Gräfelding, Germany) ▪ Incubator (Memmert, Schwabach, Germany) ▪ Water bath F20 HC (Julabo, Seelbach, Germany) ▪ Thermomixer 5437 (Eppendorf, Hamburg, Germany) ▪ Thermoshake (Gerhardt, Bonn, Germany) ▪ GFL shaking incubators 1083 and 3032 (GFL Burgwedel, Germany)

▼

Table 6. Continued.

HPLC Analysis	Merck-Hitachi (Darmstadt, Germany): ▪ Integrator D-2500 ▪ Autosampler AS-2500 ▪ UV/VIS-Detector L-4250 ▪ Pump L-6500
Microscopy and documentation of crystals	▪ Laborlux S (Leitz, Wetzlar, Germany) ▪ Stereo microscope SM22-GT-14OF with polarization equipment and photo adapter ▪ Nikon Coolpix 4500 Set SM22 (Nikon)
Mixing	Vortex REAX 2000 (Heidolph, Kehlheim, Germany)
NMR Analysis (see III.4.3.3)	▪ Bruker DRX Avance 400 MHz ▪ Bruker Avance 700 MHz ▪ Bruker 300 MHz ▪ Bruker cryo 600 MHz
PCR cycler	▪ Genius Techne (Jepson Bolton, Watford, UK) ▪ Mastercycler personal (Eppendorf, Hamburg, Germany)
pH meter	InoLab© pH 720 (WTW, Weilheim, Germany)
Protein Purification (cold room)	▪ Peristaltic pump IPC-pump (ISMATEC, Basel, Switzerland) ▪ UV-detector 2158 UVICORD SD (LKB Bromma, Sweden) ▪ Chart recorder REC 102 (Pharmacia LKB Freiburg, Germany)
Protein Purification (FPLC)	ÄKTA Explorer System consisting of ▪ 2 pumps P-900 ▪ Flow cells with volumes 22 µl and 88 µl for measurement of temperature, pH and conductivity ▪ UV/VIS monitor UV-900 ▪ Fraction collector ▪ System was operated in MaxiColdLab-refrigerator (LKB, Sweden) ▪ Results were evaluated with Pentium 133-MHz PC Compac, software UNICORN Control system; operator system OS/2 Warp (IBM)
Rotary evaporator ▪ volume reduction ▪ separation of a solvent	▪ Rotavapor RE 111 (Büchi Labortechnik, Flawil, Switzerland) ▪ Membrane vacuum pump (Vacuubrand, Wertheim, Germany) ▪ Heating apparatus type 51701 (Heidolph, Schwabach, Germany)

▼

Table 6. Continued.

Shaker	▪ HTRIEB type GV1K15M4 (Heynau, Munich, Germany) ▪ Pilot shake (B. Braun, Melsungen)
Ultrasonic homogenizer for disruption of bacteria cells	▪ Sonoplus HD 2070 (Bandelin electronics, Berlin, Germany)
Ultrasonic water bath (HPLC eluent degasser)	Sonorex RK 5105 (Bandelin electronics, Berlin, Germany)
UV spectroscopy ▪ protein concentration ▪ OD determination	▪ Lambda 2-spectrometer (Perkin-Elmer, Überlingen, Germany) ▪ Biophotometer (Eppendorf, Hamburg, Germany)

III. Methods

III.1 Expression, purification and chemical analysis of recombinant proteins

III.1.1 Preparative expression of STR1 and its mutants in *E. coli*

To obtain homogeneous STR1 suitable for crystallization experiments, activity tests and kinetics, the *str1*-pQE2 plasmid, constructed by Xueyan Ma (MA et al., 2004) was transformed into the *E. coli* strain M15[pREP4]. For expression of STR1-mutants *str1*-pQE2 plasmid was completely re-engineered by PCR with primers, which respectively contain the point mutation. The re-engineered plasmids (*str1_V208A*-pQE2, *str1_V208G*-pQE2, *str1_E205V/V208A*-pQE2, *str1_V167A*-pQE2, *str1_V167G*-pQE2, *str1_E309D*-pQE2, and *str1_W149A*-pQE2) were transformed into the *E. coli* strain M15 [pREP4] (Qiagen, Hilden, Germany).

III.1.1.1 Standard expression protocol

A single colony of freshly transformed cells was grown in 20 ml LB-medium, containing 100 µg/ml ampicillin and 25 µg/ml kanamycin with shaking (160 rpm) at 37 ° C overnight. Alternatively inoculums of 20 µl overnight-grown culture were used. The culture was scaled up by adding 500 µl of the suspension to a 1l-Erlenmeyer flask, containing 500 ml LB-medium (including antibiotics) with further shaking at 37 °C for 12 to 15 h.

For the expression of STR1 and its engineered variants, 20 ml of this bacterial culture were inoculated to 20 1l-Erlenmeyer flasks containing 500 ml LB-medium each, 50 µg/ml ampicillin and 25 µg/ml kanamycin. This "production-culture" was grown for 4 to 5 h (OD_{600} 0.5 – 0.7) with shaking (100 rpm) at room temperature (RT; 22 – 24 ° C) before expression was induced by adding IPTG to a final concentration of 0.5 mM.

After 24 h, the cells were harvested by centrifugation (10 min, 8000 rpm), the pellet was immediately resuspended in lysis buffer or stored in portions of 20 g at –20 ° C until further use.

In order to increase solubility and optimize the yield of protein, different IPTG concentrations (0.1 – 0.5 mM), and times of induction (0 – 12 h after inoculation), growing temperatures (10 – 24 °C) and growing intervals (20 – 48 h) wer e used.

III.1.1.2 Expression at low temperatures

For expression at low temperatures (10 – 12 ° C), *str1*-pQE2 and *str1_W149A*-pQE2 plasmids were transformed to Arctic Express™ competent cells (Stratagene, Heidelberg, Germany), which expressed cold-adapted chaperones (cpn60 and cpn10).

Starting from a non-induced Arctic Express™ culture (in LB-medium containing 20 µg/ml gentamicin and 50 µg/ml ampicillin), which was grown overnight continuously shaking (160 rpm) at 37 °C, 4 Erlenmeyer flasks containing 500 ml LB-medium (without antibiotics) were inoculated with 50 ml respectively and grown for 4 h at 30 ° C. Then the flasks were transferred to a thermoshaker in the cold-room. For acclimatization to a growing temperature of 10 – 12 °C the cultures were shaken for 30 min under these conditions. Then expression was induced by adding IPTG to a final concentration of 0.5 mM and grew overnight with shaking at 10 – 12 °C.

III.1.1.3 Expression under osmotic stress

With a small-scale experiment the expression under osmotic stress was tested for STR1 mutant W149A in M15 [pREP4] cells. For this purpose, 4 Erlenmeyer flasks containing 500 ml LBS medium (see II.3) were inoculated respectively with 25 ml of an overnight grown culture and incubated with shaking at RT. When OD_{600} was 0.4, the culture was induced by adding IPTG to a final concentration of 0.4 mM. Cells were harvested after 72 h by centrifugation (8 min, 11000 – 14000 x g, rotor JA-10).

III.1.2 Small-scale expression cultures

Small scale pilot experiments allowed the selection of clones featuring best expression rates and were performed for the STR1 mutants before proceeding with a large scale preparation. Aliquots of the cells were lysed in a small volume of sample buffer and analyzed directly by SDS PAGE (III.1.8). Additionally, lysates from small expression cultures (3 – 5 l) were purified by Nickel-Nitrilotriacetic acid (Ni-NTA) affinity chromatography (III.1.3), to measure the amount of soluble enzyme (III.1.6).

III.1.2.1 Small-scale expression cultures of M15 cells

Colonies of freshly transformed cells were grown in 20 ml LB-medium containing 50 µg/ml ampicillin and 25 µg/ml kanamycin under shaking (160 rpm) at 37 ° C for 8 h. Subsequently the culture was divided into two: one part was induced by adding IPTG to a final concentration of 1 mM and the other remained non-induced. Both were grown overnight at RT under shaking. Then aliquots of the cells were analyzed by SDS PAGE (III.1.8).

For quantification, non-induced cultures were scaled up to 5 l LB-medium as described in the standard expression protocol (III.1.1.1). After harvest, a crude extract was prepared and purified by Ni-NTA affinity chromatography. The concentration of the eluted protein was determined by Bradford assay and the purity estimated by SDS PAGE (III.1.6 and III.1.8).

III.1.2.2 Small scale expression cultures of Arctic Express™ cells

For pilot experiments, single colonies of freshly transformed cells were grown in 5 ml LB-medium containing gentamicin (20 μg/ml) and ampicillin (50 μg/ml) at 37 °C for 7 h. Then 3 ml LB-medium (without any antibiotics) was inoculated with 200 μl of these cultures respectively and grown for another 4 h at 30 °C, before it was transferred to a shaker in the cold-room for acclimatization to the growing temperature of 10 – 12 °C. After 10 min under these conditions, the cultures were induced by adding IPTG to a final concentration of 1 mM and grew overnight with shaking at 10 – 12 °C. Aliquots of the culture were monitored by SDS PAGE.

To quantify the amount of soluble enzyme expressed 500 ml LB medium containing gentamicin (20 μg/ml) and ampicillin (50 μg/ml) were inoculated with 500 μl of non-induced bacteria culture and grown at 37 °C overnight under shaking. Five 1l Erlenmeyer flasks containing 500 ml LB-medium (without antibiotics) were inoculated with 50 ml of this overnight culture and shaken for 3 h at 30 °C. Then, the flasks were transferred to the cold room for shaking at 10 – 12 °C. After 30 min at 10 – 12 °C, the cultures were induced by adding IPTG to the flasks (final concentration 0.5 mM) and were grown for 24 h under these conditions. The cells were harvested by centrifugation (8000 rpm, 10 min). After preparation of lysates and purification by Ni-NTA affinity chromatography, the amount of soluble enzyme was determined by Bradford assay (III.1.8) and the purity estimated by SDS PAGE (III.1.6).

III.1.3 Purification procedure

The purification procedure was based on the protocol published by MA et al. (2004). The *str1*-pQE2 expression vector, constructed by Dr. Xueyan Ma, did not contain the signal peptide (residues 1 – 27), which is not necessary to promote proper folding of the protein and seems to be important only for compartmentalization of the enzyme. Additionally it introduced a hexa-histidine-tag (His$_6$-tag) at the N-terminus of the enzyme, enabling the purification by affinity chromatography on Ni-NTA Superflow column material.

III.1.3.1 Preparation of crude extracts of *E. coli* cells

The cell pellet was thawed on ice for 30 min if necessary. The cells were resuspended in lysis buffer (II.4.1) at 2-5 ml per gram wet weight. After homogenization by 10 s bursts of the ultrasonic homogenizer Sonoplus HD 2070 (Bandelin electronics, Berlin, Germany), the cells were incubated on ice for 30 min. Then the cells were disrupted by sonification on ice (7 x 10 s bursts). After centrifugation (20 000 rpm, 30 min) at 4 °C, the supernatant was loaded on a self-packed Ni-NTA column (II.5) for enzyme purification.

III.1.3.2 Immobilized-Metal-Affinity-Chromatography (IMAC)

The purification of heterologously expressed STR1 and its mutants was performed by affinity chromatography on Nickel-Nitrilotriacetic acid (Ni-NTA) Superflow column material. Ni-NTA is a tetradentate chelating adsorbent, charged with metal ions Ni^{2+} and coupled to Superflow resin.

Proteins containing one (or more) His_6-tags located at the N- or C-terminus bind with high affinity to the Ni-NTA groups on the matrix via histidine tail (His_6). Subsequent to the preparation of crude enzyme extract (III.1.3.1), binding was carried out in column mode at 4 ° C. Two practical procedures were applied (II.10; III.1.3.3; III.1.3.4). For both, self packed HR 10 chromatography columns from GE Healthcare Europe (Munich, Germany) were used.

Untagged proteins that have histidine residues in close proximity on their surface also bind to the Ni-NTA matrix. This was in part prevented by adding 10 mM imidazole to the lysis buffer. Proteins that interact with the Ni-NTA groups were washed out of the matrix with stringent conditions achieved by adding imidazole at 10 – 50 mM concentration. For elution of the His_6-tagged protein, the imidazole concentration was increased to 250 mM. In special cases, when elution seemed to be incomplete, 500 mM imidazole elution buffer was applied. The His_6-tagged protein dissociate because it can no longer compete for binding sites on the Ni-NTA resin.

III.1.3.3 Column chromatography under low pressure (cold-room)

The usual method for purification was the utilization of a peristaltic pump (ISMATEC, Basel, Switzerland) for loading the self-packed Ni-NTA Superflow column (II.5), which was connected to an UV-detector and a chart recorder (II.10). After loading the crude enzyme extract, the column was washed with different washing buffers (imidazole concentrations from 10 to 50 mM) to remove impurities and unspecifically bound proteins. Then, His_6-tagged enzymes were eluted with 250 mM imidazole (elution buffer, see II.4.1).

III.1.3.4 Fast protein liquid chromatography (FPLC)

FPLC method was carried out with ÄKTA-Explorer system (II.10) consisting of two pumps connected to a UV detector and a computer, using self-packed Ni-NTA Superflow columns (II.5). The system was operated in a MaxiColdLab-refrigerator (LKB, Sweden) at 4 °C. The results were evaluated using UNICORN software. After loading, the column was washed with 100 % of washing buffer containing 10 mM imidazole. Different amounts of elution buffer containing imidazole (250 mM) were mixed with washing buffer (containing 10 mM imidazole) so that the final concentration of the washing solution was 20 and later 50 mM imidazole. For elution of the His$_6$-tagged protein, 100 % elution buffer was applied. The eluent was automatically collected in fractions of 2 ml.

III.1.4 Exoproteolytic cleavage of N-terminal His$_6$-tag

The Qiagen TAGZyme system was applied for the removal of His$_6$-tag. This was necessary for crystallization of STR1. The TAGZyme system makes use of dipeptidyl aminopeptidase I (DAPase enzyme), which cleaves dipeptides from the N-terminus, until it hits an indigestible residue (intrinsic DAPase stop point). The N-terminal His$_6$-tag encoded by pQE-2 vector possesses a sequence optimized for TAGZyme enzyme digestion. This facilitates the removal of the His$_6$-tag and herewith the production of His$_6$-tag free protein, which was required for crystallization.

The recombinant DAPase enzyme contains a C-terminal His$_6$-tag and can be bound to Ni-NTA matrices too, which allows its removal from the reaction solution by Immobilized-Metal-Affinity-Chromatography (IMAC).

After purification of the crude extract (III.1.3), His$_6$-tagged protein was de-salted and exchanged into 1xTAGZyme buffer (II.4.2; III.1.5) by dialysis overnight. Prior to dialysis, 10 mM EDTA was added to the eluted protein fractions to remove nickel from the His$_6$-tag.

Prior to the His$_6$-tag cleavage, the concentration of the enzyme was determined. For an efficient cleavage a minimum concentration of 0.3 mg/ml was required. If necessary the solution was concentrated (III.1.7). The amount of DAPase enzyme used for digestion was 50 mU per mg of de-salted, His$_6$-tagged protein. After activation of DAPase enzyme by cysteamine-HCl according to the TAGzyme handbook recommendations, the enzyme mixture was added to the protein solution and incubated for 4 – 6 h at 30 °C. Incubation temperatures higher than 30 °C were detrimental to highly concentrated protein solutions because of the precipitation of protein.

Shortly after incubation, the digestion reaction mixture was purified: undigested STR1-His$_6$ and DAPase were removed by IMAC using Ni-NTA Superflow. The matrix was filled into a

disposable column provided in the TAGZyme kit (bed volume ca. 1 ml) and equilibrated with 10 column volumes of 1xTAGZyme buffer. The reaction mixture was passed through the column and flow through fractions were collected. Then the column was washed with 1xTAGZyme buffer until the flow through no longer contained protein (ca. 2 – 4 ml). Protein containing fractions were combined and were ready for further application (dialysis).

III.1.5 Dialysis of protein samples

Dialysis of proteins was used for de-salting proteins and exchanging buffers between different steps of the purification procedure or before crystallization and enzyme assay. It was performed at 4 °C against an excess of dialysi s buffer. Depending on the volume of the protein solution, dialysis tubes with diameters of 9, 16 or 29 mm (Servapor; II.9) were used. Dialysis tubes containing the protein solution were stirred in 5 – 10 l of dialysis buffer overnight.

III.1.6 Determination of protein concentration

Protein concentration was determined by the spectroscopic analytical procedure described by BRADFORD (1976) known as Bradford assay using BSA standard. The Bradford assay is a colorimetric protein assay. It is based on an absorbance shift in the dye Coomassie Brilliant Blue G-250 by the binding of proteins.

Coomassie reagent: 50 mg of Coomassie Brilliant Blue G-250 was dissolved in 50 ml ethanol and 100 ml of H_3PO_4 (85 %) were added. The solution was diluted to 1 l with water and filtered (circle filter papers Ø 15 cm).

50 µl of protein solution is mixed with 950 µl of Coomassie reagent. After 5 min the Coomassie-protein complex was built, which is stable for approximately 30 min. The absorbance at 595 nm was recorded on a Lambda 2-spectrometer (Perkin-Elmer, Überlingen, Germany) and the concentration was calculated via BSA-calibration curve. Later the absorbance at 595 nm was measured via Eppendorf Biophotometer.

The Bradford assay is linear over a short range, typically from 2 – 120 µg/ml; therefore dilutions of samples were often necessary for analysis fitting into this range.

III.1.7 Concentrating protein solutions

To achieve protein concentrations suitable for DAPase digestion and for crystallization, different types of concentrators were applied (0II.9).

Volumes larger than 2 ml were concentrated by centrifugation in Amicon Centriprep YM-10MW centrifugal filter units (Witten, Germany) or with Vivaspin 20 centrifugal concentrators

(Sartorius, Göttingen) at 4000 x g until the designated concentration was reached. For smaller volumes of protein solutions Vivaspin 500 Centrifugal concentrators were applied (10000 x g).

III.1.8 Electrophoretic analysis of proteins

III.1.8.1 Electrophoretic separation of proteins

SDS PAGE (sodium dodecyl sulfate polyacrylamide gel electrophoresis) is a firmly established procedure for the separation of proteins. The Laemmli modification of the discontinuous buffer system (LAEMMLI 1970) was used throughout this work with buffers described above (II.4.3). It provides high resolution patterns of proteins and allows estimation of their molecular weights.

First, the small-pored running gel (pH 8.8, 10 – 15 % acrylamide) was prepared (15 ml), filled between two glass plates (16 x 18 cm, distance 1.5 mm) and covered with water. After 1 h polymerization was finished. Then the water was removed and a comb with 15 wells (ca. 120 µl each), was inserted into the space between the plates. It was filled with the wide-pore stacking gel buffer solution (pH 6.8, 5 % acrylamide, ca. 6 ml). For polymerization another 45 – 60 min was necessary.

The protein solutions to be analyzed were mixed with sample buffer (containing Bromophenol-Blue 0.02 % (m/V)) 1:5 and heated at 95 °C for 10 min (sample volume 40 – 70 µl). After cooling they were applied into the wells. The electrophoresis was carried out at 4 °C in a vertical apparatus manufactured by Amers ham Pharmacia Biotech (Freiburg, Germany, II.10) using running buffer at a constant current of 20 mA until the Bromophenol-Blue dye reached to the bottom of the running gel (12 – 14 h for two gels). To shorten the running time, amperage was increased up to 50 mA. A quick analysis of a few samples was possible with COMPHOR Midi electrophoresis system (Biozym, Hess. Oldendorf, Germany). Buffers and procedures used for this purpose were the same as described above, but on small scale.

III.1.8.2 Coomassie staining

For visualization of protein bands Coomassie Brilliant Blue R-250 staining was used (II.4.3). The gels were soaked in dye (0.25 % Coomassie Brilliant Blue R-250, 45 % methanol, 9 % acidic acid) for 30 min continuously shaking and subsequently de-stained by shaking in the de-staining solution (30 % methanol, 10 % acidic acid) for 5 – 6 h. The solution was exchanged 3 – 4 times at intervals of 1 – 2 h.

III.2 Molecular Biology Methods

III.2.1 Site-directed mutagenesis procedure

Site-directed mutagenesis is the technique of creating a mutation at a defined site of a DNA molecule. It is a main tool for studying protein structure-function relationships, gene expression and vector modification.

In the current work, PCR was applied to introduce mutations into the *str1*-pQE2 plasmid. Wild-type *str1*-pQE2 plasmid served as template and the desired mutation was included into the oligonucleotide primers. After thermal cycling, parental (wild-type) DNA was digested with the restriction enzyme *DpnI*. Then PCR products were purified by agarose gel electrophoresis and extracted from the gel matrix (III.2.4; 0). Plasmids were subsequently transformed to *E. coli* Top10 cells for *in vivo* reproduction (III.2.7).

Since primer duplication or multiplication occurred in 50 – 80 % of the transformed colonies, a pre-selection by restriction digestion analysis was necessary. For this purpose, several colonies of freshly transformed cells were grown overnight and the plasmids were isolated (III.2.8). A small portion of each plasmid solution (usually 3 µl) was double digested with *HindIII* and *NdeI* or respectively *HindIII* and *SphI* (II.6.2; III.2.3); the fragments were electrophoretically separated and compared to a control digestion of wild-type plasmid (*str1*-pQE2). An agarose concentration of 1.5 % (m/V) allowed the detection of primer duplications and the selection of useable plasmids. The specific plasmids were sequenced by GENterprise Genomics (Mainz, Germany). After correct sequencing, the verified plasmid was finally transformed to the *E. coli* expression strain M15 (or Arctic™ Express for *str1_W149A*-pQE2 plasmid).

III.2.2 Polymerase chain reaction

Polymerase chain reaction (PCR) was developed in 1988 by Kary B. Mullis and it became a common technique for *in vitro* DNA amplification (SAIKI et. al., 1988). Throughout this work, PCR was used to generate point mutations in the *str1*-pQE2 plasmid. With this method, mutations (base substitution as well as insertions and deletions) can be easily generated from double-stranded plasmids. The procedure involves a PCR using a plasmid vector (*str1*-pQE2 plasmid) as the template and oligonucleotide primers containing the desired mutation (refer to Table 7). The oligonucleotide primers were constructed based on the cDNA of STR1 from *R. serpentina* (KUTCHAN et al., 1988; KUTCHAN 1993) and primers were purchased from MWG Biotech (Ebersberg, Germany).

Table 7. The basic components of PCR. The basic requirements for PCR are referred to the specific application in the current work.

Component and purpose of usage	PCR components applied in the current work
DNA template → target to be amplified	*str1*-pQE2 plasmid (wild-type plasmid)
Primers → oligonucleotides which are complementary to the DNA target's 5' and 3' ends	Two complementary oligonucleotide primers containing the desired mutation, supplied by MWG Biotech (Ebersberg, Germany)
DNA polymerase with a temperature optimum of 72 – 74 °C → amplification	- Phusion™ High Fidelity DNA polymerase (2 U/µl; New England Biolabs, Ipswich, USA) - Pfu Turbo polymerase (2.5 U/µl; Stratagene, La Jolla, CA, USA) - PfuPlus! DNA-Polymerase (5 U/µl; Roboklon, Berlin, Germany)
Deoxynucleotide triphosphates (dNTPs) → the building blocks for the new DNA strand	Promega (Madison, USA)
Buffer solution → providing a suitable chemical environment for the DNA polymerase	Buffer solutions respectively provided by the manufacturer of the DNA polymerases were used
Thermal cycler → raises and lowers temperature according to the program	- Genius Techne thermocycler - Mastercycler personal

PCR was carried out in a reaction volume of 50 µl in autoclaved reaction tubes (Biozym, Hess. Oldendorf, Germany) using a Genius Techne thermocycler (Jepson Bolton, Watford, UK) or a Mastercycler personal (Eppendorf, Hamburg, Germany). A layer of oil on top of the reaction mixture was not necessary since both thermocyclers had heated lids to prevent condensation on the top of the reaction tube. To reduce non-specific amplification during the initial set-up stages of the PCR, the Hot-start PCR technique was applied when necessary. For this purpose, the polymerase was manually added, after the reaction mixture was heated to the melting temperature of 95 °C for 2 min.

Subsequently to amplification, the template (*str1*-pQE2 plasmid) was removed by *DpnI* digestion. For digestion, 1 µl of *DpnI* recombinant enzyme (20,000 U/ml; NEB, Ipswich, USA) was added to the reaction tube after the PCR run and incubated for 2 h at 37 °C with constant shaking.

Products were routinely analyzed by agarose gel electrophoresis and visualized by ethidium bromide staining (III.2.4). Size and amount of PCR products were determined by comparison with a DNA ladder (III.2.6).

III.2.3 Restriction enzyme digestion of DNA

In addition to the removal of parental template described above, DNA fragmentation by restriction enzyme digestion was used to genotype the PCR product without completely sequencing it.

PCR products were electrophoretically separated (III.2.4), extracted from the gel (0) and transformed to *E. coli* Top10 cells for *in vivo* reproduction. The plasmids were isolated (III.2.8) and the enzymatic digestion accomplished by using two appropriate, commercially available restriction enzymes (double digest) and the buffer systems supplied with the enzymes (NEB, Ipswich, USA).

The following compounds were combined in a sterile reaction tube (volume 1.5 ml) in order:

- 3 µl 10x digestion buffer (supplied with the restriction enzymes)
- 21 - 24 µl sterile water (Ampuwa, Fresenius, Bad Homburg, Germany)
- 1 – 4 µl DNA (ca. 1 µg)
- 1 µl *HindIII*
- 1 µl *NdeI* or *SphI* (depending on availability)

This mixture, with a total volume of 30 µl, was incubated for 2 h at 37 ° C, shaking continuously (Eppendorf Thermomixer). Following, an agarose gel was run immediately to check the result and choose plasmids for sequencing. Results were predicted with NEBcutter, a freeware provided by New England Biolabs (Ipswich, USA).

Table 8. Restriction enzymes used in the current work. All enzymes were purchased from NEB (Ipswich, USA). Information taken from NEB web page (www.neb.com).

Enzyme	Concentration	Source	Cut
HindIII	20,000 units/ml	*Haemophilus influenzae*	5' --- A ▼ AGCTT --- 3' 3' --- TTCGA ▲ A --- 5'
NdeI	20,000 units/ml	*Neisseria denitrificans*	5' --- CA ▼ TATG --- 3' 3' --- GTAT ▲ AC --- 5'
SphI	10,000 units/ml	*Streptomyces phaeochromogenes*	5' --- G ▼ CATGC --- 3' 3' --- CGTAC ▲ G --- 5'
DpnI	20,000 units/ml	*Diplococcus pneumoniae*	5' --- G A(-CH$_3$) ▼ TG --- 3' 3' --- CT ▲ A(-CH$_3$)G --- 5'

III.2.4 Electrophoretic analysis of DNA

Agarose gel electrophoresis was applied to separate DNA molecules in order to analyze PCR products and DNA fragments after restriction digestion. Separation was achieved by moving negatively charged nucleic acid molecules through an agarose matrix (0.7 – 1.5 % agarose in TAE buffer), containing ethidium bromide within an electric field. Shorter molecules migrate further than longer ones, because they can move faster in the agarose matrix. Concentration of agarose depended on the separation range. A 1 % solution was appropriate for DNA molecules with 400 to 8000 bp.

First the agarose was melted in TAE buffer by heating until boiling in a microwave (Panasonic). After cooling down to 50 – 60 °C, eth idium bromide solution (10 mg/ml) was added (see Table 9), mixed gently and filled into the gel casting tray (avoiding bubbles) with the comb(s) positioned in the slots provided. After settling of the gel, the tray was placed in the apparatus and covered with 1xTAE buffer. Comb and casting gates were removed and the samples (mixed with loading buffer containing Bromophenol-Blue) were filled into the wells. The chamber was closed, the leads were connected to the power supply (Consort E844 or E835, Turnhout, Belgium) and voltage and current were set according to gel and apparatus (Table 9). When the Bromophenol-Blue front line reached the remaining 1/3 of the total running distance, electrophoresis was stopped. The gel was detected using UV-trans-illuminator at a wavelength of 302 nm (Bachofer, Reutlingen) and Canon Powershot G5 digital camera. Ethidium bromide was used for visualization of DNA strands. It fluoresces under UV light when intercalated into DNA (or RNA).

Table 9. Electrophoresis instruments. Specifications refer to a gel thickness of ca. 10 mm.

Instrument type	Blue marine 100	Blue marine 200	Blue marine 200
Size	7 x 10 cm	15 x 15 cm	15 x 20 cm
Gel volume	80 ml	150 ml	200 ml
Ethidium bromide solution 10 mg/ml	3 µl	5 – 6 µl	8 µl
Voltage	65 V	100 V	120 V

III.2.5 Extraction of DNA from agarose gel

After separation of PCR products via agarose electrophoresis, the designated DNA strand was excised from the gel by means of a scalpel. The extraction of the DNA from the gel matrix was achieved using NucleoSpin© Extract Kit (Macherey-Nagel, Düren, Germany) according to the manufacturer's recommendations with one exception: the elution buffer provided from the company was substituted with water.

III.2.6 Quantitative analysis of DNA

DNA was quantified via comparison of the DNA strand with a DNA ladder (λ DNA after *HindIII* digestion from NEB or Smart Ladder from Eurogentec, Cologne, Germany) by agarose gel electrophoresis.

DNA concentration was measured in aqueous solution by UV-spectrometry at 260 nm (WILLFINGER et al., 1997). Hereby a value of $OD_{260} = 1$ corresponds to 50 µg/ml DNA. Results were checked as following: due to possible protein impurities the absorption at 280 nm was additionally measured and the quotient OD_{260}/OD_{280} calculated (a quotient of 1.8 indicated a pure sample).

III.2.7 Transformation

Two transformation procedures were employed in the current work and they are described in the following paragraph.

III.2.7.1 Heat shock

Heat shock transformation procedure was applied for heat-competent *E. coli* Top10 and M15 cells. The cells were thawed on ice and 4 µl of the plasmid solution (10 – 100 ng) was mixed with 40 µl cell suspension. After 30 min on ice, the cells were briefly heat shocked by incubating the mixture for 1 min at 40 °C (water b ath). The cells were stored on ice for 2 min and subsequently the cell suspension was gently mixed with 500 µl pre-warmed (37 °C) LB-medium without antibiotics. For regeneration, incubation was carried out at 37 °C for 1 h. Finally, the cell suspension was streaked on LB agar plates, containing selective growth factors depending on the transformed *E. coli* strain. The plasmid pQE2 contained a gene coding for ampicillin resistance. Successfully transformed cells were able to grow on media containing this antibiotic. M15 competent cells additionally feature resistance to kanamycin.

Furthermore, a control transformation was performed with every transformation experiment. Instead of plasmid, 4 µl Ampuwa-water were used.

III.2.7.2 Electroporation

Electroporation was applied for transformation of plasmids into electro-competent M15 cells using an Easyject Optima electroporator (EQUIBIO, Ashford, UK) and 2 mm electroporation cuvettes.

Having thawed the cells on ice, 4 μl of the vector solution (10 – 100 ng) was mixed with 40 μl cell suspension and incubated on ice for 2 min. Then the mixture was transferred to a cooled, sterile electroporation cuvette, which was inserted into the electroporator and pulsed, using settings recommended by the manufacturer for *E. coli* cells (2500 V, 15 μF, 335 R). Immediately after pulsing, cells were diluted to 500 μl pre-warmed LB medium (without antibiotics) and transferred to a sterile 2 ml tube. The cell transformation mixture was incubated at 37 °C for 60 min before plating 200 – 500 μl onto LB agar plates containing selective growth factors (ampicillin 50 μg/ml and kanamycin 25 μg/ml). The plates were incubated overnight. Control transformation with Ampuwa-water was performed under identical conditions.

III.2.7.3 Preparation of competent *E. coli* cells

III.2.7.3.1 Heat competent cells

A single colony of M15 or Top10 cells was grown in 10 ml of LB-medium overnight with shaking at 37 °C; a 1 ml aliquot was used to inocu late 100 ml of LB-medium. The cells were grown at 37 °C until OD_{600} = 0.5 (90 – 120 min). Following the culture was cooled down on ice for 5 min and all further procedures were carried out at a temperature of ca. 4 °C. The culture was centrifuged at 4000 x g for 5 min. Subsequent to the removal of the supernatant the pellet was resuspended in TFB1 buffer (II.4.6) and the cells were incubated on ice for 90 min. To remove TFB1 buffer, the cells were centrifuged for 5 min at 4 °C and 4000 x g. After the supernatant was discarded, the pellet was resuspended in 4 ml TFB2 buffer (containing glycerol; II.4.6) and frozen in aliquots of 200 μl in liquid nitrogen. The cells were stored at - 80 °C.

III.2.7.3.2 Electro-competent cells

To obtain competent M15 cells for electroporation, 200 ml fresh LB-medium was inoculated with 4 ml of a fresh, overnight grown cell culture and grew at 37 °C continuously shaking until an OD_{600} of 0.6 was reached. Subsequently the culture was quickly cooled down on ice and all further steps of the procedure were carried out at 4 °C. The cells were harvested by centrifugation at 3000 x g for 10 min at 4 °C. The pellet was washed three times with 25 ml sterile water (4 °C). The pellet was resuspended i n 5 ml water (Ampuwa) and glycerol was

added to a final concentration of 10 % (V/V). The cell suspension was portioned in aliquots of 50 µl, frozen in liquid nitrogen and stored at -80 °C.

III.2.8 Plasmid DNA isolation from Top10 *E. coli* cells

For *in vivo* reproduction of plasmid DNA, *E. coli* Top10 cells were utilized. Single colonies were selected from bacterial plates and used to inoculate 10 ml of LB medium (containing 50 µg/ml ampicillin). The cultures were incubated overnight with shaking at 37 °C and then processed according to the descriptions given below.

Depending on the required purity of the plasmid, two methods were applied for the isolation of plasmid DNA from the bacterial cells. To obtain highly pure plasmid for sequencing and PCR, the commercially available NucleoSpin® Plasmid Kit (Macherey-Nagel) was used (III.2.8.1).

For restriction analysis (e.g. of PCR-mutagenesis-products from transformed Top10 cells), a plasmid gained from alkaline lyses (III.2.8.2) was sufficient. With this simple and cost-efficient procedure, a rapid preparation of up to 20 different small-scale bacteria cultures was possible in less than 45 min.

III.2.8.1 Plasmid DNA preparation with NucleoSpin® Plasmid Kit

NucleoSpin® Plasmid Kit yields highly pure plasmid solution by combination of alkaline lysis with special polypropylene spin column, which contains activated silica membrane filter. This filter traps nucleic acids and separates them from contaminating proteins and other cellular debris.

The pellet of 8 ml cell suspension was harvested by centrifugation in sterile microcentrifuge tubes (11000 x g, 2 min). The supernatant was discarded. Plasmid DNA preparation was carried out according to the manufacturer's recommendations with minor modifications using the provided buffers.

After the cell pellet was resuspended in buffer A1 and mixed gently with lysis buffer (A2) and binding buffer (A3), it was incubated at 4 °C for 10 min before centrifuged for 12 min at 11000 x g at 4 °C. Subsequently the supernatant was loaded onto the column, the silica membrane was washed once with optional wash buffer AW and then twice with concentrated wash buffer A4. Residual ethanol was removed and the silica membrane was dried via centrifugation (1 min, 11000 x g). Elution was carried out with water.

III.2.8.2 Alkaline lysis mini-preparation

For rapid batch-preparation of DNA, 2 ml of the overnight grown culture was pelleted via centrifugation (11000 x g, 2 min). The supernatant was discarded.

The pellet was resuspended in 150 µl Tris-HCl – EDTA buffer containing RNAse, and incubated at RT for 30 s. To lyse the cells, 150 µl of a highly alkaline solution containing 0.2 M NaOH and 1 % (m/V) SDS were added and mixed gently. Following 10 min incubation at RT, 150 µl of KAc buffer (3 M, pH 5.2) was added and mixed by vortexing. The addition of two drops of chloroform improved pelleting. The mixture was ensuing centrifuged (11000 x g, 5 min). The supernatant contained the soluble plasmid DNA and was separated from the pellet. Plasmid DNA was precipitated by adding 1 ml of ethanol and centrifugation (11000 x g, 4 °C, 10 min). The supernatant was discarded an d the pellet air-dried for 10 min at RT to allow the ethanol to evaporate. Then the pellet was dissolved in 50 µl TE buffer. This solution was used for restriction digestion and agarose electrophoresis analysis.

III.3 Crystallization and X-ray analysis

III.3.1 Hanging drop vapor diffusion method

A crystallization protocol for STR1 was previously published by MA et al. (2004). It represented the basis for all crystallization experiments performed in this work. MA et al. employed one of the most common methods for protein crystallization, which falls under the category of vapor diffusion and is known as the hanging drop method. It was maintained throughout this work. The hanging drop vapor diffusion method requires a droplet, composed of a mixture of protein solution (STR1 in Tris-HCl 10 mM, pH 8) and precipitation buffer 1:1, which was allowed to equilibrate with a larger reservoir containing similar buffers and precipitants in higher concentrations.

Highly purified protein was required. Since His$_6$-tagged STR1 (STR1-His6) was not suitable for crystallization (MA et al., 2004), the His$_6$-tag was removed by DAPase cleavage. The enzyme was then dialyzed twice against an excess of 10 mM Tris-HCl, pH 8 and then concentrated to 4 – 5 mg/ml before crystallization. Altogether enzyme concentrations of 3.5 - 10 mg/ml were tested. As precipitant different variants of the original precipitant buffer published by MA et al. (2004) were used (Table 10).

Crystallization experiments of STR1 were carried out in 24-well plates with sample volumes of 1 – 4 µl. Plates and cover slides were obtained from Hampton Research (Aliso Viejo, USA). Closed systems were achieved by sealing with grease (medium viscosity silicone oil,

Bayer, Leverkusen, Germany) between cover slides and reservoir edges at the crystallization plate surface.

Plates were prepared as follows: first silicon grease was applied and then 750 µl of precipitant buffer were filled into the reservoirs. 1 – 5 droplets were placed on a clean cover slide with 0.5 - 2 µl protein solution per drop. The same volume of precipitant buffer from the reservoir was pipetted into each drop and mixed gently. Next, the cover slide was inverted carefully so that the drops were hanging from the cover slide, and it was placed onto the bed of silicone grease on the reservoir. With gentle pressure, the slide was fixed to ensure a complete seal. Figure 8 depicts the hanging drop system (RHODES, 1993; MCREE, 1993).

Initially, the droplet of protein solution contains an insufficient concentration of precipitant for crystallization, but as water vaporizes from the drop and transfers to the reservoir, the precipitant concentration increases to a level optimal for crystallization – allowing the protein to precipitate out as a crystal.

Table 10. Composition of precipitant buffers. Buffers were prepared with 1M potassium sodium tartrate x 4 H_2O and 1 M HEPES stock solutions, diluted with water and sterile filtered.

Precipitant buffer No.	Potassium sodium tartrate x 4 H_2O (mol/l)	100 mM HEPES pH
1	0.70	7.5
2	0.75	7.5
3	0.80	7.5
4	0.85	7.5
5	0.90	7.5
6	0.80	7.0
7	0.80	7.3
8	0.80	7.7
9	0.70	7.3
10	0.75	7.3
11	0.85	7.3
12	0.90	7.3

Cover slide with protein solution droplet (light blue)

Silicon grease

H₂O

Reservoir with precipitant buffer
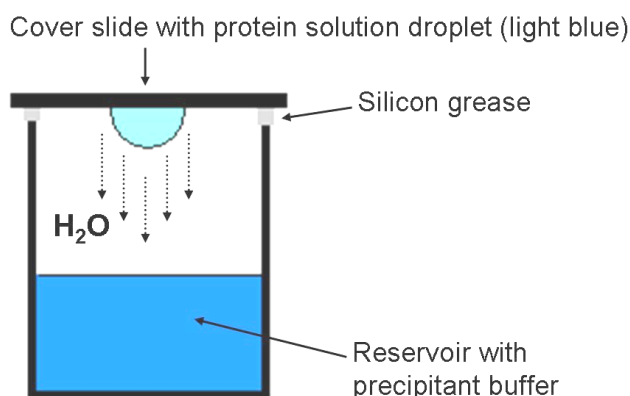
Figure 8. **Hanging drop vapor diffusion method.** The figure shows a single well containing precipitant buffer and the protein droplet hanging from the cover slide. Due to dilution 1:1 with protein solution, the drop contains lower precipitant concentration than the reservoir. To achieve equilibrium, water vapor leaves the drop (for the reservoir) and both, protein and precipitant increase in concentration.

III.3.2 Complex of enzyme with ligand

To obtain the structure of STR1 in complex with either strictosidine or inhibitor MIT as ligand, co-crystallization of enzyme and the individual compound, as well as soaking experiments were performed.

III.3.2.1 Co-Crystallization

For co-crystallization, the specific compound was present in the protein droplet for potential integration into the crystal structure. Co-crystallization of STR1 in complex with strictosidine was performed by mixing strictosidine with the enzyme solution to final concentrations of 1 to 10 mM strictosidine in the droplet. Enzyme concentrations were 5 – 10 mg/ml STR1. Crystals of strictosidine synthase in complex with inhibitor MIT were obtained by co-crystallization of STR1 in the presence of 0.1 and 0.5 mM inhibitor in the enzyme solution.

III.3.2.2 Soaking experiments

For soaking experiments, native crystals were removed from the droplet and transferred to a soaking buffer, the composition of which was similar to the droplet solution of the crystal. In addition to the components of the precipitant buffer, the soaking buffer contained the ligand and 21 – 25 % glycerol for cryo-protection purposes. After incubation the crystals were immediately frozen in liquid nitrogen. Incubation periods were ranged from 10 s up to 24 h.

The basic principle for soaking experiments is "trial and error". The range of soaking conditions tested is listed in Table 11.

Table 11. Soaking experiments. The range of different soaking conditions tested is shown.

Ligand	Concentration	Incubation time	Glycerol concentration (%) (V/V)
Strictosidine	2.5 – 10 mM	10 s – 8 h	25 %
Inhibitor MIT	0.1 – 10 mM	10 s – 7 min	23 – 25 %
Secologanin	5 mM	1 – 24 h	24 %

III.3.3 Distinction between protein and salt crystals

Control drops were routinely carried out in parallel. Additionally, the small molecule dye Izit Crystal Dye™ from Hampton Research was applied. Biological macromolecule crystals, like protein crystals, contain large solvent channels, allowing Izit to penetrate and color the crystal blue. The blue color intensifies in the crystal over time, becoming a darker blue than the solvent. 1 µl of dye solution or of a 1:10 dilution was placed in the sample drop and was allowed to incubate for 1 – 4 h. Crystal color was used to differentiate between protein crystals (blue crystals in light blue to clear drops) and salt contaminations (blue drops, clear crystals).

III.3.4 Freezing of crystals

Freezing *in situ* was the method of choice to inhibit radiation damage to STR1 crystals during data collection (cryo-crystallography). For this purpose, the crystals were carefully removed from the mother liquor by scooping up with a cryo loop (size 0.2, Hampton Research, II.7). The loop containing a crystal was immersed in a drop of cryo-protectant solution for a few seconds and frozen as it was placed on the goniometer head of the X-ray machine. Its magnetic base attached the loop to the goniometer and placed it into the nitrogen stream, provided by the cryo system. The crystals were flash cooled and maintained at -173 ° C under a stream of nitrogen gas during data collection.

The soaking of crystals in cryo-protectant solution, prior to flash freezing, was necessary to prevent the forming of ice during the process of freezing. The cryo-protectant solution was composed of the precipitant buffer additionally containing 21 – 25 % (V/V) glycerol as cryo-protectant. The appropriate concentration of glycerol and incubation time was determined by trial and error, via exposure of a frozen loop containing either cryo-protectant solution or test crystals to X-ray radiation.

III.3.5 X-ray measurement

X-ray data was collected by using the synchrotron radiation from the DORIS-III ring of the European Molecular Biology Laboratory (EMBL) Hamburg. The beamlines X11 and X13 were used. They are macromolecular crystallography beamlines on the DORIS Fan K, located in the HASYLAB Hall 5. Both are monochromatic fixed wavelength beamlines operated at a wavelength of 0.81 Å (15.3 keV) and equipped with a MARCCD detector (165 mm).

After mounting the crystal and flash cooling at -173 ° C in the liquid nitrogen stream, the crystal was centered in the X-ray beam, and the diffraction pattern was checked by initial shots (exposing a frame for an arbitrary length of time and oscillation range). This was necessary in order to determine the diffraction limit, and consequently the optimal distance between crystal and detector. Special problems, such as twinning or ice could be identified. X-ray dosage and oscillation angle were adapted according to distance in between the single reflections and the intensity of the spots. The crystal was rotated to take another exposure. In case the quality of the diffraction was satisfactory, settings were determined and data collection initiated. To collect all the necessary data, the crystal was rotated step-wise through 180 °, with an image recorded at every step .

III.3.6 Analysis of data set, structure elucidation and refinement

Data from X-ray measurements were processed by Dr. Santosh Panjikar (EMBL Hamburg) using the programs DENZO and SCALEPACK (OTWINOWSKI and MINOR, 1997).

The structures were solved by Dr. Santosh Panjikar (EMBL Hamburg) using molecular replacement method and the Auto-Rickshaw software pipeline (PANJIKAR et al. 2005). The high resolution structure of strictosidine synthase (PDB code 1fp8, MA et al., 2006) was used as a search model. Within the pipeline, the program MOLREP (VAGIN and TEPLYAKOV, 1997) was used for molecular replacement and the rigid body, positional as well as B-factor refinement was performed using the program CNS (BRÜNGER et al., 1998). The residual electron density for strictosidine and inhibitor was clearly visible and constructed using the graphics program COOT (EMSLEY and COWTAN, 2004). Subsequent refinement procedures were carried out using the program REFMAC5 (MURSHUDOV et al., 1997).

III.4 Synthesis and analysis methods

III.4.1 Activity assay for STR1 and its mutants

III.4.1.1 Basic activity assay with purified STR1-His$_6$ and its mutants

Enzyme activities of wild-type or mutants were determined using the HPLC method described below (III.4.3.1). His$_6$-tagged enzymes were used (~ 90 % purity as estimated by SDS PAGE). Protein concentration was measured by the Bradford method (III.1.6).

All activity tests were carried out in 50 mM KPi buffer, pH 7.0. In a standard volume of 50 µl an appropriate amount of enzyme was incubated in the presence of 1 mM tryptamine or one of its analogues and 1 mM secologanin at 28, 30 or 35 °C. Secologanin, tryptamine and its analogues were dissolved in Ampuwa water (sterile water, II.90) with the exception of certain substrates (such as 7-methyl- and 6-methoxy-tryptamine), which required the addition of small portions methanol or ethanol for solubility.

Incubation was accomplished using an Eppendorf thermomixer with constant shaking at 450 rpm. The enzyme reaction was terminated by the addition of 100 µl methanol followed by centrifugation at 12000 rpm (Biofuge A, Heraeus Christ GmbH, Osterode, Germany) for 5 min, to remove precipitated proteins. The supernatant was subjected to HPLC analysis and monitored at 250 or 280 nm. According to the tasks and requirements of the respective analysis, this standard assay was modified in substrate and enzyme concentrations, total incubation volume and temperatures. Modifications of the enzyme assay are described below in detail.

III.4.1.2 Substrate specificity study

For activity tests with different substrates, the His$_6$-tagged enzymes were incubated in a total volume of 500 µl KPi buffer (50 mM, pH 7.0; enzyme concentration of 2 – 20 µM) in the presence of 1 mM tryptamine or analogue and 1 mM secologanin. 50 µl aliquots were taken after selected time periods (0.5 – 24 h). The samples were analyzed via HPLC as described in paragraph III.4.3.1. Experiments in the absence of enzyme were performed to take into consideration background noise.

III.4.1.3 Kinetic analysis

Kinetic analysis was performed for wild-type STR1-His$_6$ and the mutants V208A-His$_6$, V208G-His$_6$ and E309D-His$_6$ by altering the concentration of tryptamine or its derivatives, while the secologanin concentration was held constant at 2 mM. Substrate decrease was monitored by HPLC at 280 nm.

Standard assay conditions were modified to obtain saturation conditions and a linear rate of conversion. Enzyme concentrations were 1 – 200 nmol/l. The standard assay was scaled-up (5-fold, total volume 250 µl) and assayed at three to four time points. Negative controls with denaturized enzyme (10 min, 95 ° C) were performed. After an initial experiment with 5 different substrate concentrations, kinetic parameters were estimated. For all following kinetic experiments, the minimum tryptamine or tryptamine derivative concentrations were 3-fold above and below the estimated K_M value. Each experiment included 10 – 12 different substrate concentrations, which were analyzed at least twice (n = 2 or 3).

For each tryptamine derivative, a calibration curve was generated by integration of peak area, which was used to calculate the change in concentration. HPLC detection limit was 0.001 mM, but substrate concentrations lower than 0.005 mM could not be detected reliably and had to be excluded in most cases (relative standard deviation >> 5 % as knock-out criterion). Reaction rates were calculated using Microsoft Excel software. Kinetic parameters were calculated by nonlinear regression analysis using GraphPad Prism 3 software and Microsoft Excel software.

All kinetic assays were repeated at least once (STR1 and mutant V208A twice) to ensure reproducibility. The results represented the average of 2 – 3 independent experiments (± standard deviation (SD)).

III.4.1.4 Relative activity

The calculation of relative activity was used to compare the activity of STR1-His$_6$ with different compounds and respectively with the different His$_6$-tagged mutants directly. For this purpose the standard assay described above (4.1.1 and 4.1.2) was used with identical conditions for all tested enzyme variants and substrates. Incubation time and temperature were 15 min and 35 °C.

Monitoring of tryptamine and strictosidine peaks were done by HPLC at 250 nm and peak areas were compared to the wild-type. Its activity was set to 100 %. Due to low expression of soluble enzymes, mutants V167A and V208G were tested in concentrations of 0.08 µM and 2.4 µM respectively. Relative activity was calculated with regard to the concentration difference.

For relative activity of STR1-His$_6$ with different substrates, lower enzyme concentrations (0.3 – 0.4 µM) were applied. Substrate loss and product formation were monitored at 250 nm and the peak area was integrated. Each experiment was done with active and denaturized enzymes to detect false conversion due to substrate instability.

III.4.1.5 Turn-over studies

In order to compare the conversion of STR1 wild-type and mutants, and to find optimal conditions for preparative enzymatic synthesis, turnover studies were performed for wild-type and mutant V208A using identical conditions. Enzyme assay containing 3.7 µM enzyme, 1 mM tryptamine derivative and 1 mM secologanin in a total volume of 700 µl was incubated at 35 °C or 28 °C. 50 µl aliquots were taken at spec ific time intervals (up to 48 h). They were analyzed via HPLC (III.4.3.1).

III.4.1.6 Inhibition studies

III.4.1.6.1 Substrate inhibition

To investigate whether a substrate inhibition of STR1 by tryptamine occurred, the standard assay was used with a maximum of 12 different tryptamine concentrations between 0.05 and 5 mM. Secologanin concentration was held constant at 1 mM. Several STR1 concentrations were tested and the enzyme was employed in a final concentration of 0.13 µM, which proved to achieve linear conversion of tryptamine. Substrate and product peaks were monitored at a wavelength of 250 nm. All conditions were carried out in either duplicate or triplicate and experiments were repeated for reproducibility.

III.4.1.6.2 Inhibition study with inhibitor MIT

To assess whether the compound obtained from Prof. Sarah O'Connor (MIT, Cambridge, MA, USA) for co-crystallization experiments, acts as an inhibitor for STR1 from *R. serpentina*, kinetic studies of STR1 with tryptamine were repeated with two different enzyme concentrations (0.02 and 0.9 µM) in the presence of 0.01 mM inhibitor MIT. K_i value was respectively calculated according to the equation (1).

(1) $K_M' = K_M \times (1 + I/K_i)$

In the current work the K_M value in the presence of inhibitor is referred to as K_M', and I as inhibitor concentration.

III.4.2 Enzymatic synthesis of strictosidine derivatives

III.4.2.1 Strictosidine and its 10-substituted derivatives

The following description of the enzymatic synthesis of 10-methyl-strictosidine is representative of all enzymatic synthesizes performed. According to the qualities of the different enzymes (wild-type and mutants) and the intended use of the product, the conditions varied in volume and amount of enzyme.

In a total volume of 5 ml KPi buffer (50 mM, pH 7.0) 5-methyl-tryptamine and secologanin (1 mM each) were incubated in presence of 260 µg STR1 mutant V208A (1.4 µM) for 90 min at 35 °C. The mixture was separated by TLC (III.4. 3.4). The 10-methyl-strictosidine formed, was eluted (CHCl$_3$/MeOH, 9:1), the solvent evaporated and the residue dried.

III.4.2.2 Enzymatic synthesis with immobilized mutant V208A – initial trial

His$_6$-tagged STR1 mutant V208A was purified and dialyzed for 12 h against an excess of 50 mM KPi buffer as described (III.1.5). Two Pasteur-pipettes (A and B) which were closed with cotton, served as the columns. Fresh Ni-NTA material was washed with water and suspended in the enzyme solution (1 g Ni-NTA suspension, 2 ml water and 1 ml of V208A preparation with a total concentration of 300 µg). The mixture was stirred for 60 min at 4 °C. The suspension was then filled into the columns. The protein concentration of the column flow was measured by Bradford method, to make sure the enzyme was completely loaded. By washing the column with water at RT, the flow rate was set to 2 – 3 ml/h. Aqueous, un-buffered, 10 mM solutions of the substrates (secologanin, 5-methyl- and 5-methoxy-tryptamine) were prepared. Both mixtures of substrates ((A) 5-methyl-tryptamine and secologanin; (B) 5-methoxy-tryptamine and secologanin) were separately transferred in alternating 300 µl steps onto the columns and mixed in the "column head", before slowly passing the Ni-NTA matrix with immobilized enzyme. The column eluate was collected in fractions. Samples were analyzed by HPLC.

III.4.3 Chromatographic and spectroscopic methods

III.4.3.1 High performance liquid chromatography

The enzyme activities of wild-type and mutant STR1 were determined using the High Performance Liquid Chromatography (HPLC) system from Merck-Hitachi (Darmstadt, Germany, II.10).

Table 12. HPLC gradient program for STR1 assay.

Time (min)	Acetonitrile (%)	Acidic water (%)
0.0	10	90
8.0	50	50
11.0	80	20
11.5	10	90
15.0	10	90

All analyses were carried out at RT on a LiChrospher 60 RP select B column (125 x 4 mm; 5 µm, Merck, Darmstadt, Germany). A pre-column (LiChrospher 60RP select B, 4 x 4 mm, 5 µm) was used in combination with the analytical column. The solvent system was acetonitrile/H_2O (pH 2.3 adjusted with H_3PO_4), using a gradient (described in Table 12) with a flow rate of 1.5 ml/min. The injection volume was varied in a range which was proven to be linear (20 – 80 µl). The absorbance was monitored at 250 and 280 nm. Acetonitrile was purchased from Fisher Scientific in HPLC grade and could be used without further treatment. Acidic water was prepared with de-ionized water and H_3PO_4, filtered through cellulose-acetate membrane filters (Ø 50 mm, pore size 0.45 µm) and finally degassed via ultrasonification (2.10).

III.4.3.2 Liquid chromatography-mass spectrometry analysis (LC-MS)

Strictosidine derivatives of wild-type STR1 and mutant V208A were identified by LC-MS analysis carried out by Dr. Matthias Unger and Dr. Andreas Frank (Institute of Pharmacy, Julius-Maximilians-University Würzburg) with a LC/MSD Trap system (Agilent, Waldbronn, Germany, II.10). The mass spectrometer was operated in the positive ion mode, using electrospray ionization. Nitrogen gas was used for the nebuliser (50 psi) and the drying gas (300 °C, 12 l/min).

The capillary voltage was – 3500 V and the skimmer, octopole 1, octopole 2 and capillary exit voltage were set to 40, 12, 1.7 and 104 V respectively.

For formation of strictosidine derivatives, a total volume of 500 µl containing 150 µg native wild-type or mutant enzyme, 1 mM tryptamine or derivative and 1 mM secologanin was incubated for 60 min at 35 °C. After addition of 1 ml MeOH and centrifugation, the reaction mixture was freeze-dried and 500 µl MeOH were added. After centrifugation, 25 µl of the clear supernatant was injected onto a 150 x 4.6 mm, 4 µm analytical HPLC column (Synergi Max-RP; Phenomenex, Aschaffenburg, Germany). The mobile phase consisted of 10 mM ammonium acetate (0.05 % acetic acid) (A) and acetonitrile (B). The flow rate was set to 0.8 ml/min and the following gradient (% B) was applied: 0 min: 20, 15 min: 60. After 15 min the column was flushed with 100 % (B) for 5 min and re-equilibrated with 20 % (A) for 5 min. The temperature for the analytical column was set to 25 °C.

III.4.3.3 ^{13}C- and ^{1}H-NMR analysis

For identification of 10-methyl-strictosidine and 10-methoxy-strictosidine, which were prepared according to the above described formation of 10-methyl-strictosidine (III.4.2.1), ^{13}C- and ^{1}H-NMR data were collected. Assignments were supported by HSQC experiments.

For the determination of C3-stereochemistry, ^{1}H-NMR data were collected for 10-methyl-strictosidine-lactam-tetraacetate and strictosidine-lactam-tetraacetate. The formations of both compounds are described below (III.4.4).

The compounds were respectively dissolved in CD_3OD. NMR spectra were recorded at the following institutions with technical support of staff members listed below, using the instruments written in brackets:

- Dr. Bernd Mathiasch, Johannes Gutenberg-University, Institute of Inorganic and Analytical Chemistry (Bruker DRX Avance 400 MHz instrument): 10-methyl-strictosidine and 10-methoxy-strictosidine

- Dr. Manfred Wagner, Max-Planck Institute for Polymer Research in Mainz (Bruker Avance 700 MHz instrument): 10-methyl-strictosidine and 10-methoxy-strictosidine

- Dr. Ulrich Braumann and Dr. Li-Hong Tseng, Bruker Company, Karlsruhe, Germany (Bruker 600 MHz, cryo probe, 5mm CPTCI): 10-methyl-strictosidine- lactam-tetraacetate

- Niklas Jänich, Johannes Gutenberg-University, Institute of Pharmacy (Bruker AC 300 MHz instrument): strictosidine-lactam-tetraacetate

Data were managed and analyzed by the author using MestRe-C software.

III.4.3.4 Thin layer chromatography (TLC)

TLC was applied for preparative purification of enzymatically synthesized strictosidine and analogous. TLC plates (20 x 20 cm, 1.0 mm, silica gel 60 F_{254}) were purchased from Merck (Darmstadt, Germany). Solvent system was benzene/ethyl acetate (1:2).

III.4.4 Determination of C3-stereochemistry

Wild-type STR1 is a highly stereo-selective enzyme, leading exclusively to 3α-(*S*)-strictosidine. To determine the stereo-selectivity of engineered mutants, ^{1}H-NMR data of the mutants' products were collected after lactamization and acetylation. This established NMR method was used among others by STÖCKIGT and ZENK (1977a, 1977b) to revise the originally incorrect 3-(*R*)-configuration to the 3-(*S*)-configuration of the biosynthetically correct precursor (strictosidine) for the monoterpenoid indole alkaloid family. According to them the ^{1}H-NMR data of the respective strictosidine-lactam-tetraacetate derived from the enzymatically formed strictosidine (analogue) provide clear evidence for the 3-(*S*)-stereochemistry. It was in every respect identical to the analysis of an authentic sample.

III.4.4.1 Determination of C3-stereochemistry of the STR1 mutant V208A

Incubation of 0.59 mg (2.8 µmol) 5-methyl-tryptamine hydrochloride and 1.087 mg (2.8 µmol) secologanin in the presence of 560 µg of pure His_6-tagged mutant V208A in 1.4 ml KPi buffer (50 mM, pH 7.0) was performed at 35 °C for 60 min. The mixture was diluted with 3 ml of MeOH, centrifuged and the supernatant was freeze-dried. Water (3 ml) and Na_2CO_3 (1.5 ml; 4.2 M) were added to the residue, saturated with N_2 gas, and heated for 4 h at 75 °C. NaCl was added for saturation and the mixture was extracted three times with 1 ml ethyl acetate, the solvents combined, evaporated and the residue dried. A mixture of acetic anhydride/pyridine (1:1; total volume of 0.2 ml) was added and incubated for 14 h. The solvents were evaporated. The residue was dissolved in 0.1 ml of $CHCl_3$/MeOH (3:1) and separated on TLC plates in solvent benzene/ethyl acetate (1:2). The 10-methyl-strictosidine-lactam-tetraacetate formed was eluted ($CHCl_3$/MeOH, 8:2), the solvent evaporated and the residue dried. The sample was dissolved in 160 µl CD_3OD and measured in 3 mm NMR tubes at 600 MHz (cryo probe, 5 mm CPTCI). The instrument and measurement facilities were provided by Bruker, Karlsruhe, Germany.

III.4.4.2 Determination of C3-stereochemistry STR1 mutant E309D

The stereo-selectivity of mutant E309D was determined via ^{1}H-NMR analysis of strictosidine-lactam-tetraacetate, which was obtained by incubation of 5.3 mg tryptamine (30 µmol) and 10.1 mg secologanin (30 µmol) in the presence of 2.6 mg of pure His_6-tagged mutant E309D in 5 ml KPi buffer (50 mM, pH 7.0) at 35 °C for 8 h. The mixture was diluted with 10 ml MeOH, centrifuged and the supernatant freeze-dried. The lactamization and acetylation were carried out according to the description above. After purification by TLC, the strictosidine-lactam-tetraacetate was dissolved in 500 µl CD_3OD and measured on a Bruker AC 300 MHz instrument (Johannes Gutenberg University, Institute of Pharmacy).

III.4.5 Online-tools and programs

Table 13. List of online-tools and software programs applied in the current work.

Program	Source	Purpose
Blast 2 Sequences	TATUSOVA and MADDEN (1999) http://www.ncbi.nlm.nih.gov/blast/bl2seq/wblast2.cgi	Sequence alignment of DNA and proteins
ClustalW	LARKIN et al. (2007) http://www.ebi.ac.uk/Tools/clustalw2/	Multiple sequence alignment of DNA and proteins
ChemDraw Ultra 0.8	ChemOffice 2004	2D structure
DaliLite workbench	HOLM and PARK (2000) http://www.ebi.ac.uk/DaliLite/index.html?	Pairwise comparison of proteins structures
ExPASy Translate Tool	GASTEIGER et al. (2003) Expert Protein Analysis System, Institute of Bioinformatics, Geneva, Switzerland http://expasy.org/tools/dna.html	Translation of nucleotide sequence to the respective protein sequence
GraphPad Prism	GraphPad Software Inc. (San Diego, USA)	Scientific graphic, statistics and curve fitting (kinetics, non-linear regression)
MestRe-C	Mestrelab Research NMR solutions Santiago de Compostela, Spain	Analysis of NMR data
MolProbity	LOVELL et al. (2003) ; DAVIS et al. (2007); http://molprobity.biochem.duke.edu/	Web service for structure validation
MS Office	Microsoft Corporation (Redmond/Seattle, USA)	Office software suite
NEB Cutter V2.0	VINCZE et al. (2003); http://tools.neb.com/NEBcutter2/index.php	Program to cleave DNA with restriction enzymes
PyMol	DELANO (2002) http://www.pymol.org	3D structure viewer
wwPDB	worldwide Protein Data Bank http://www.pdb.org/pdb/home	Archive of macromolecular structural data that is freely and publicly available to the global community
TINKER (Force Field Explorer)	PONDER and RICHARDS (1987)	Computational modeling of STR1 mutants
Xtalview	MCREE (1999)	Software package for solving a macromolecular crystal structure

IV. Results

IV.1 Expression and purification of STR1

In order to obtain homogeneous STR1 suitable for crystallization experiments, activity tests and kinetics, the *str1*-pQE2 plasmid, constructed by Dr. Xueyan Ma (MA et al. 2004) was transformed into the *E. coli* strain M15[pREP4]. The *str1*-pQE2 expression vector introduced a hexa-histidine tag (His$_6$-tag) at the N-terminus of the enzyme (STR1-His$_6$), enabling the purification by affinity chromatography on Nickel-Nitrilotriacetic acid (Ni-NTA) Superflow matrix. Expression was carried out according to the standard protocol described in III.1.1, and the purification procedure given in III.1.3 was used. Figure 9 displays the individual steps of expression and purification depending on the respective application.

Growing host cells → Induction → Expression →

Cell harvest

Crude extract preparation

Affinity chromatography on Ni-NTA matrix

Dialysis against 50 mM KPi buffer pH 7.0

➤ Enzyme assay

➤ Substrate specificity

➤ Enzymatic synthesis

➤ Enzyme kinetics

➤ etc.

Dialysis against 1xTAGZyme buffer

Removal of His$_6$-tag by DAPase digestion

Affinity chromatography on Ni-NTA matrix

Dialysis against 10 mM Tris HCl, pH 8.0

➤ Crystallization

Figure 9. Schematic diagram of the purification procedure. Individual steps for the recovery of STR1 are displayed. After growing and inducing the host cells (*E. coli* M15 cells) in 1l-Erlenmeyer flasks containing 500 ml LB-medium, *str1* gene was expressed. Cell harvest and crude extract preparation were followed by purification using affinity chromatography on Ni-NTA matrix. Depending on the enzyme's applications, it was either directly used for activity tests (left) or the His$_6$-tag was removed by DAPase digestion for crystallization purposes, which is shown in the right path.

Figure 10 shows a representative absorption profile of the purification of STR1-His$_6$, carried out with the ÄKTA Explorer system. UV absorption at 280 nm is plotted against the elution

volume. After equilibration of the self-packed Ni-NTA column with wash buffer containing 10 mM imidazole, the crude protein extract (see III.1.3.1 for preparation details), was loaded to the column. For washing steps increasing imidazole concentrations were used to remove unspecifically bound proteins. The washing buffers contained 10, 20 and 50 mM imidazole (ca. 30 ml each). Best elution was achieved with an imidazole concentration of 250 mM in the elution buffer. The purity of the eluted fractions (volume of 1.5 ml) was evaluated by SDS PAGE (Figure 11). Even though the elution of STR1-His$_6$ was already observed several times with the 50 mM imidazole wash fractions, the amounts were negligible.
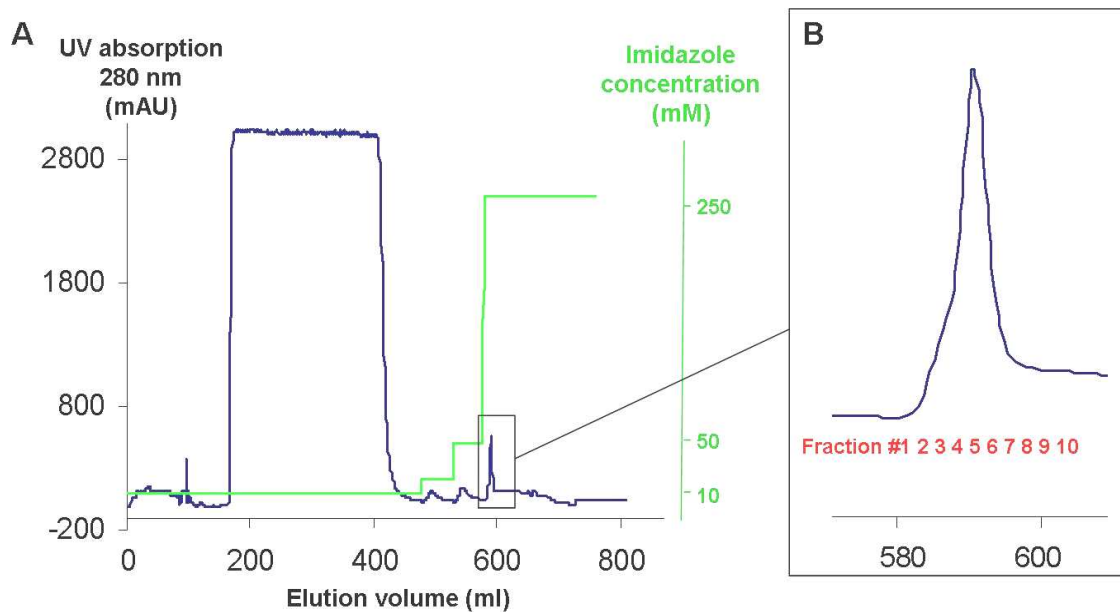
Figure 10. Representative absorption profile of STR1-His$_6$ purification. Purification of heterologously expressed STR1-His$_6$ by affinity chromatography on Ni-NTA matrix is shown. (A) The absorption profile at 280 nm (mAU, blue) is plotted against the elution volume (ml). The imidazole concentration of wash and elution buffers is shown in green (10 – 250 mM). The protein is eluted with 250 mM imidazole elution buffer and the eluted peak is zoomed in (B). Fractions collected are numbered in red.

M$_A$ et al. (2004) reported that most of the expressed STR1 enzyme accumulated as so called inclusion bodies. These are aggregates of unfolded, insoluble proteins. SDS PAGE confirmed that a major part of the expressed enzyme remained in the pellet. Figure 11 shows a representative Coomassie-stained SDS PAGE after purification of STR1-His$_6$. Pellet is applied next to crude extract (P and CE) and can be directly compared. The elution fractions generally exhibit > 90 % purity as shown in Figure 11.

The formation of inclusion bodies can pose serious problems for the recovery of functionally active and soluble protein. Nevertheless, 5 – 10 mg enzymatically active, soluble STR1-His$_6$ could be purified from a 20 l-bacterial culture (0.35 (± 0.19) mg/l). This amount was sufficient

for activity tests, DAPase digestion, as well as enzymatic synthesis, and even for crystallization experiments.
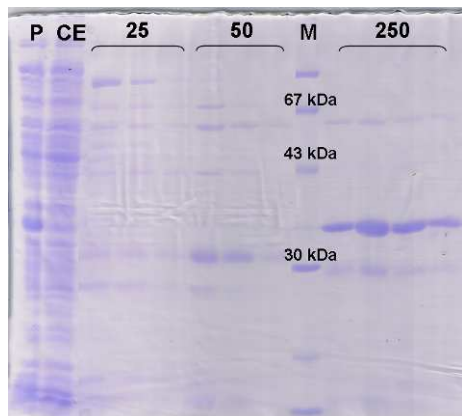
Figure 11. Coomassie-stained SDS PAGE of STR1. SDS PAGE shows different fractions for the purification of STR1-His$_6$ from *E. coli* by affinity chromatography on Ni-NTA matrix. P = pellet, CE = crude extract, 25 = fractions eluted with 25 mM imidazole wash solution, 50 = fractions of 50 mM imidazole wash solution, M = marker proteins, 250 = fractions eluted with elution buffer (250 mM imidazole) containing STR1-His$_6$ (ca. 37 kDa).

IV.2 Substrate specificity of STR1 wild-type

A detailed, systematic analysis of STR1 substrate specificity was performed, using the His$_6$-tagged enzyme expressed and purified according to the standard protocol described (III.1).

The study was focused on commercially available tryptamine analogues. Enzyme activity was measured by HPLC, in which the amine starting material disappearance and product formation were monitored by UV at 250 nm (III.4.3.1).

Figure 12 shows tryptamine and all 17 analogues analyzed in this study. Some of the compounds are very similar to the native substrate tryptamine. Others like dopamine, histamine or phenylalanine have only basic structural similarity. Out of the 17 tested tryptamine analogues, 7 were accepted by STR1-His$_6$. Derivatization caused a significant loss of relative enzyme activity as shown in Figure 12. Accepted derivatives were fluorinated, hydroxylated, methoxylated and methylated at the aromatic moiety of the indole ring system, which seemed to be required for recognition and turnover by the enzyme. At positions 5 and 6, STR1 accepted a range of different derivatives, but the enzyme activity compared to the native substrate decreased tenfold. Remarkably those tryptamine derivatives with bulky groups at positions 5 and 6 acted as poor substrates or were not converted at all.

The electron-withdrawing group fluorine was a competent functional group. Both tested fluorine-derivatives of tryptamine were accepted. The carbon-5-hydroxylated tryptamine-derivative serotonin was converted by the enzyme with 10 % relative activity compared to the native substrate tryptamine. The compounds 5-methoxy- and 5-methyl-tryptamine were not accepted by STR1. With a methyl- or methoxy-group at carbon 6, poor conversions were observed (2 % relative activity, respectively). Carbon-7-methylated tryptamine was accepted as well. A hydroxyl-group at carbon 7 prevented the reaction: no conversion with 5,7-

dihydroxy-tryptamine, while the 5,6-dihydroxy-tryptamine derivative was accepted. A difficulty with di-hydroxyl-compounds was their instability. After incubation for 15 min at 35 °C, the solutions were colored (grey and pink) and a large variety of novel peaks was monitored by HPLC. This also happened with the control incubations using denaturized enzyme.
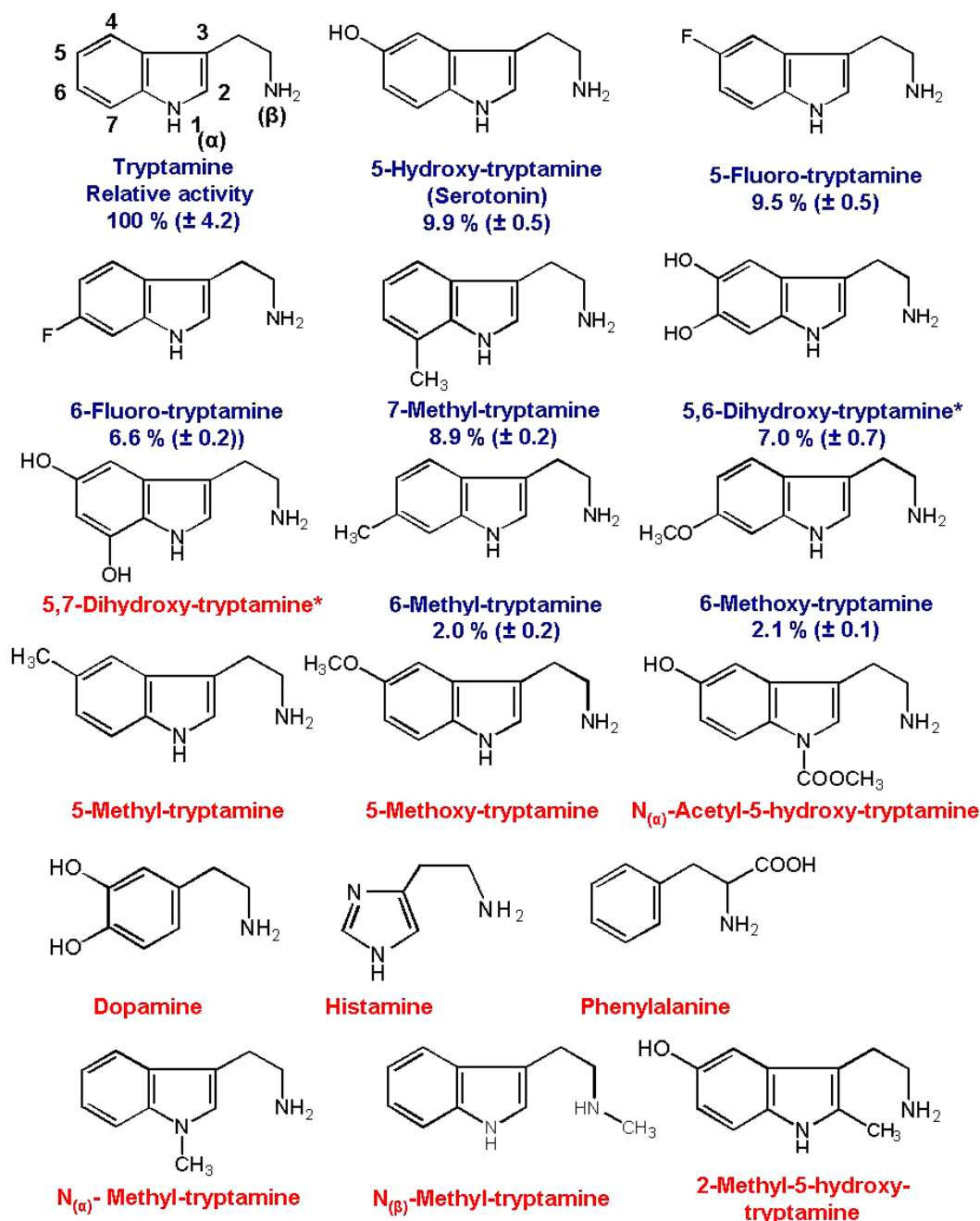
Figure 12. Substrate specificity of STR1-His$_6$. Presentation of all compounds tested in the current work. Relative activity is referred to the activity of STR1-His$_6$ with tryptamine, whose specific activity is 2.99 (± 0.8) μmol/min/mg (= 100% relative activity). Accepted substrates are labeled in blue. For substrates labeled in red, no conversion was detected. * = instable compounds.

Comparison of the peak pattern of incubation with either natural or denaturized enzyme led to the identification of one peak as a potential product of 5,6-dihydroxy-tryptamine. Relative activity was estimated by the comparison of peak area with strictosidine, which was produced under identical assay conditions. Calculation of substrate loss could not be applied, since it faked high turnover due to instability. In the peak pattern of 5,7-dihydroxy-tryptamine, a product peak could not be clearly identified. Therefore it was concluded that no conversion had taken place.

Derivatization at other positions of tryptamine, thus different from the aromatic moiety of the indole ring system of tryptamine (for example $N_{(\alpha)}$-acetyl-5-hydroxy-tryptamine or 2-Methyl-5-hydroxy-tryptamine) did not show any turnover. Substrates without the indole framework were not accepted by STR1 as judged by the lack of detectable turnover (< 0.1 % relative activity).

IV.2.1 Spectroscopic product identification

The condensation product of 6-methyl-tryptamine and secologanin converted by STR1-His$_6$ was analyzed by LC-MS using a LC/MSD Trap system (Agilent, Waldbronn, Germany). Measurement was carried out by Dr. Matthias Unger and Dr. Andreas Frank (Institute of Pharmacy, Julius-Maximilians-University Würzburg, Germany) as described in III.4.3.2.

Compound 6-methyl-tryptamine was of particular interest, since it was not accepted by the strictosidine synthase from *C. roseus* (McCoy et al., 2006). Therefore a reliable proof of identity was necessary. Figure 13 shows the HPLC and the LC-MS trace of the conversion of 6-methyl-tryptamine and secologanin by STR1-His$_6$ from *R. serpentina*. Identity was clearly demonstrated. $[M + H]^+$ was 545.6 m/z for 11-methyl-strictosidine.

Furthermore, this analysis was successful in the identification of a formerly unknown peak as the lactamization product of 11-methyl-strictosidine. $[M + H]^+$ of the unknown peak was 513 m/z for 11-methyl-strictosidine-lactam (M_r 512.6). Lactam peaks appeared in incubations longer than 15 – 30 min (wild-type as well as mutants) and it was observed ca. 1 – 2 min after the respective strictosidine product peak.
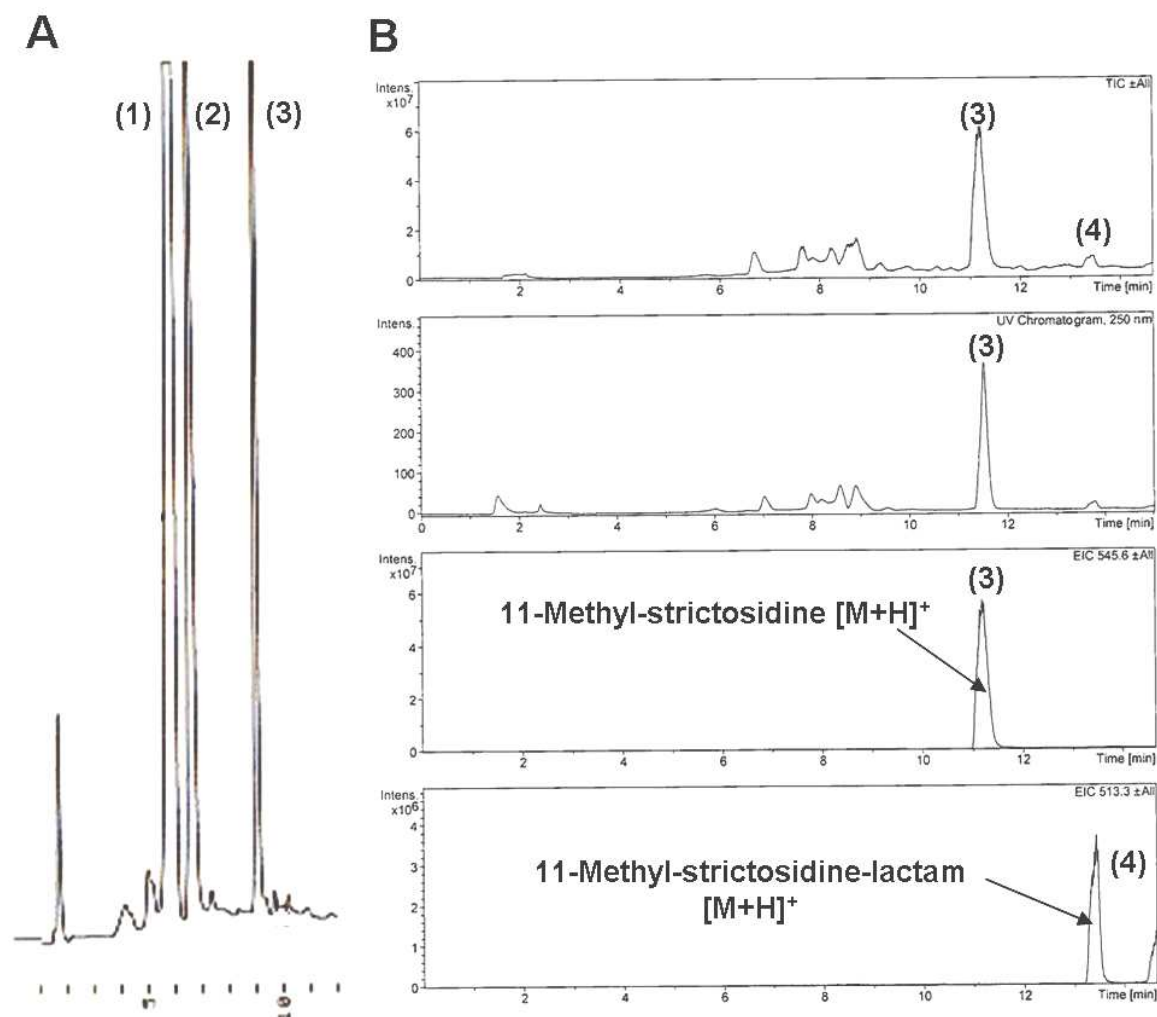
Figure 13. Formation and identity of 11-methyl-strictosidine. (A) HPLC trace displays the enzymatic formation of 11-methyl-strictosidine (3) coming from secologanin (1) and 6-methyl-tryptamine (2) with STR1-His$_6$ after 15 min. Retention times: (1) 5.8 min, (2) 6.4 min, (3) 8.9 min. (B) LC-MS analysis shows total ion current (TIC), UV-chromatogram and extracted ion current (EIC); from top to bottom). [M + H]$^+$ of reaction product was 545 m/z for 11-methyl-strictosidine (3) and 513 m/z for 11-methyl-strictosidine-lactam (4). The last EIC represents the first identity evidence for the lactam (4). (A) and (B) derive from different incubations of 6-methyl-tryptamine and secologanin with STR1-His$_6$.

IV.3   Inhibition experiments

IV.3.1 Substrate inhibition

The question whether high tryptamine concentrations were inhibitory or not to the *R. serpentina* STR1 reaction should be definitely answered by an inhibition study performed with STR1-His$_6$. Though several studies investigated the substrate inhibition of STR from different species (TREIMER and ZENK, 1979b; HAMPP and ZENK, 1988; STEVENS et al., 1993; KUTCHAN et al., 1994; DE WAAL et al., 1995; YAMAZAKI et al., 2003b), not a single one was performed with recombinant, His$_6$-tagged STR1 from *R. serpentina*. The utilized enzymes were derived from cell suspension cultures of the respective plants. Furthermore the results were contradicting and will be discussed in conjunction with the results from the current work in V.3.2.

The substrate inhibition study of STR1-His$_6$ was performed with an enzyme concentration of 0.13 µM, which proved to be within a linear activity range during 15 min of incubation. The standard enzyme assay was used (in 50 mM KPi, pH 7.0). Tryptamine concentrations were increased up to 5 mM. Strictosidine formation and substrate loss were monitored by HPLC analysis at 250 nm and peaks were automatically integrated. The conversion of tryptamine was calculated by means of a calibration curve.
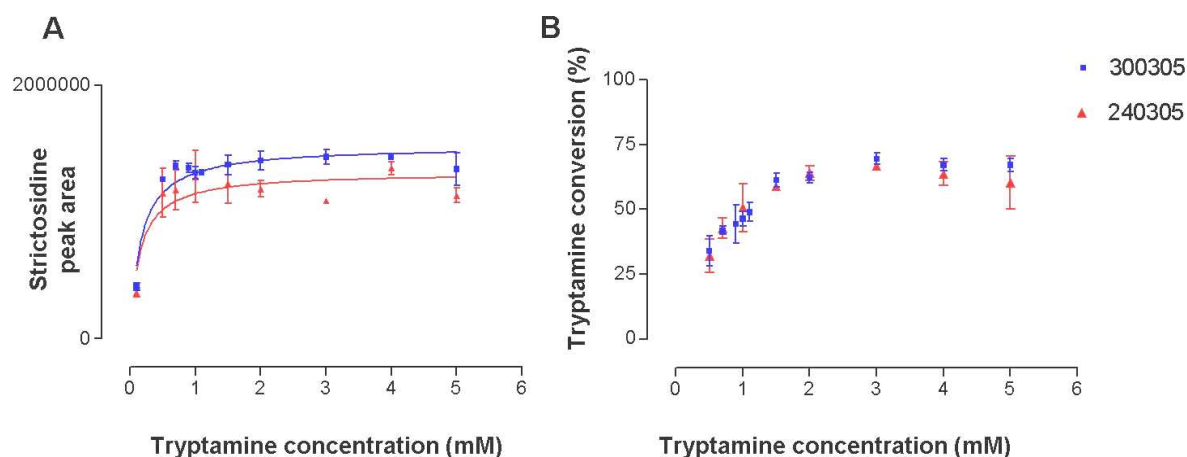
Figure 14. STR1-His$_6$ inhibition study. (A) Formation of strictosidine and (B) conversion of tryptamine are plotted against the tryptamine concentration (mM). Two independent experiments (▲ 240305 and ■ 300305, n = 3 respectively) were performed using respectively up to 5 mM tryptamine.

No substrate inhibition was observed. Two independent experiments with 10 different tryptamine concentrations between 0.05 and 5 mM showed constant strictosidine formation with increasing tryptamine concentrations (Figure 14 A). Moreover, tryptamine conversion

was steadily rising. At a concentration of 5 mM, 60 – 67 % of tryptamine was converted in 15 min by the enzyme, yielding strictosidine (Figure 14 B).

IV.3.2 Inhibition study with compound MIT

The compound MIT (Figure 15 B) was demonstrated to be a potent inhibitor of STR from *Catharanthus roseus* with an IC_{50} value of 3 (± 0.5) nM (MARESH et al., 2008). An inhibition study was performed to assess whether the compound acted also as an inhibitor for STR1 from *R. serpentina*. Pilot experiments confirmed an inhibitory effect, and kinetic values in the presence of compound MIT (0.01 mM) were determined by two independent experiments (III.4.1.3). K_M value in presence of inhibitor (referred to as K_M' in the current work), was calculated using non-linear regression (GraphPad Prism 3 software) and confirmed by the generation of Michaelis-Menten plot and Lineweaver-Burk linear regression using MS Excel (Figure 15 A). K_M' was determined to be 0.189 (± 0.08) mM.
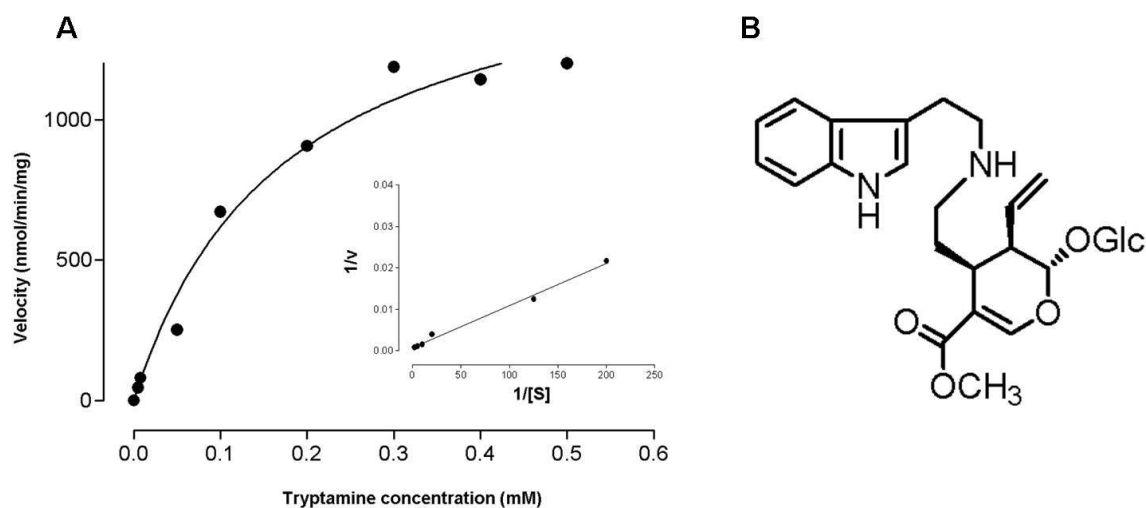
Figure 15. Compound MIT. (A) Michaelis-Menten plot of STR1-His$_6$ in presence of 0.01 mM compound MIT with Lineweaver-Burk plot included. (B) The structure of compound MIT is displayed. Glc = glucose.

Then the inhibitor constant K_i at this specific inhibitor concentration $K_{i\,(0.01)}$ was calculated according to equation (1).

(1) $K_M' = K_M \times (1 + I/K_i)$

K_M' = K_M value in presence of inhibitor, K_M = K_M of STR1-His$_6$ with tryptamine without inhibitor, and I = inhibitor concentration. The results are displayed in Table 14.

Table 14. Catalytic constants of STR1 with tryptamine in the presence of 0.01 mM inhibitor MIT.

	K_M (mM)	K_M' (mM)	$K_{i\ (0.01)}$
STR1-His$_6$	0.072 (± 0.02)	0.189 (± 0.08)	0.006

IV.4 Crystal structures of STR1 complexes

IV.4.1 Crystallization

Crystallization of STR1 succeeded for the first time in 2004. MA et al. (2004) and KOEPKE et al. (2005) described the expression, purification and crystallization procedure in detail. It was known that His$_6$-tagged STR1 did not crystallize and the purification procedure described by MA et al. (2004) included a second step of chromatography on Ni-NTA column, which was adopted in the present work.

As displayed in Figure 9, the affinity chromatography purification of His$_6$-tagged STR1 from crude extract of *E. coli* was followed by DAPase digestion (III.1.4) in order to remove the N-terminal His$_6$-tag. For this purpose, the eluted fractions of the first purification step were combined and the buffer was exchanged by overnight dialysis against an excess of 1xTAGZyme buffer (pH 7.0).

When working with proteins, purified by affinity chromatography using Ni-NTA matrixes, metal ions may be leached from the matrix. These metal ions may have an inhibitory effect on the DAPase digestion. Addition of EDTA (final concentration ca. 10 mM) to the protein preparation prior to dialysis had a positive effect on the digestion efficiency. Although the manufacturer denied this leaking of nickel ions from the matrix, digestion after dialysis without EDTA resulted in up to 80 % loss of enzyme due to insufficient cleavage.

Subsequent to DAPase digestion, the reaction mixture was purified by a second affinity chromatography step on Ni-NTA matrix. Due to the C-terminal His$_6$-tag of recombinant DAPase enzyme, it was bound to Ni-NTA matrixes, allowing its removal from the reaction solution by affinity chromatography. Efficiency of the digestion and purity of the obtained STR1 solution was checked by SDS PAGE (Figure 16). The latter, namely the purity of STR1 preparation after the removal of the His$_6$-tag was ca. 90 % as estimated by SDS PAGE (Figure 16) and this was rated suitable for crystallization. Further purification on Mono Q column resulted in a much purer enzyme preparation; however the enzyme was reluctant to crystallize or formed mostly twins (KOEPKE et. al., 2005). It was supposed, that some components of the STR1 preparation facilitate the nucleation procedure during STR1

crystallization. Therefore the author desisted from further purification. Crystals grew with the hanging drop vapor diffusion method at 32 °C (usin g Hampton Research equipment, see III.3) within 3 to 14 days.
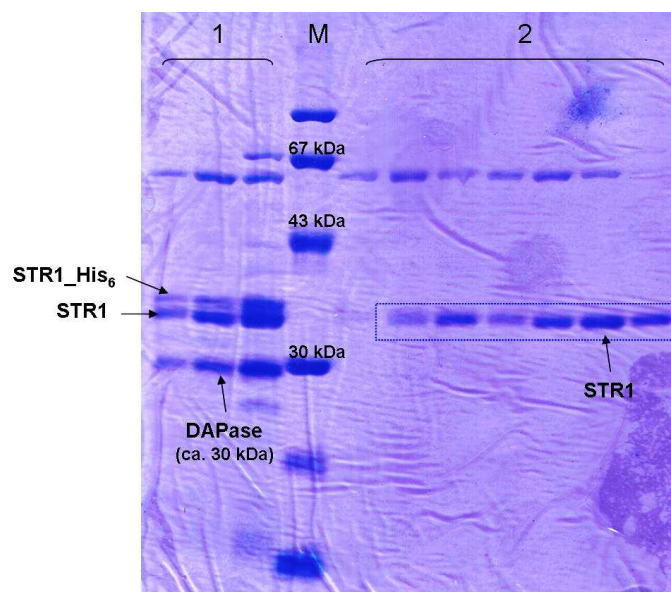
Figure 16. SDS PAGE presenting the results of DAPase digestion. M = marker proteins. Lanes left of the marker (1) are samples from the DAPase reaction mixture in different concentrations. Separation of STR1 with and without His_6-tag is highlighted by arrows. Lanes on the right (2) show fractions from second affinity chromatography on Ni-NTA column. STR1 is highlighted in the blue frame.

IV.4.2 STR1-Strictosidine-complex

IV.4.2.1 Crystallization

Co-crystallization experiments with STR1 and strictosidine were performed using precipitant buffer 3 (0.8 M potassium sodium tartrate x 4 H_2O and 100 mM HEPES, pH 7.5; II.7.1 and III.3). Crystals grew within four days. Successful experiments contained either 2 or 10 mM strictosidine in the enzyme solution (5 and 10 mg/ml). However, being extremely small and clustered, the co-crystals were not suitable for X-ray analysis. The crystal structure of strictosidine bound to STR1 was finally elucidated by X-ray analysis of native STR1 crystals after soaking with cryo-protection solution (0.8 M potassium sodium tartrate x 4 H_2O, 100 mM HEPES, pH 7.5 and 25 % glycerol) containing strictosidine (3 mM). The basic principle for soaking experiments was "trial and error". High ligand concentrations and unsuitable buffer compositions damaged the crystal and resulted in low diffraction. Too much glycerol caused damage as well, however, too low concentrations led to ice rings.

The native STR1 crystals were grown at 32 °C with the hanging drop vapor diffusion method described above (III.3.1) using STR1 (without His_6-tag) in concentrations of 3 – 5 mg/ml. After DAPase digestion, the de-tagged protein was dialyzed twice against the crystallization

buffer (10 mM Tris-HCl, pH 8) and concentrated (III.1.5; III.1.7). Best results were achieved in experiments with 4 – 5 mg/ml STR1. High quality crystals were obtained with precipitation buffers 3 and 5 (containing either 0.8 or 0.9 M potassium sodium tartrate x 4 H_2O and 100 mM HEPES, pH 7.5, Figure 17). Buffers 11 and 12 generated beautiful, big crystals, which did not diffract at all, proving that appearance can not be the only criterion for the selection of good quality crystals.

Figure 17. Crystals of native STR1. The rhombohedral crystals of STR1 belong to the space group of *R*3 with unit cell parameters of a = b = 150.18, c = 121.71. The length of the crystals was approximately 0.08 - 0.2 mm. The complete data of STR1 in complex with strictosidine were collected to 3.0 Å resolution at the X13 beamline of EMBL Hamburg, Germany.

Other conditions led to extremely small, frequently clustered crystals or to the occurrence of brown amorphous precipitate, which is a characteristic for denaturized protein. A skin on the drop was observed several times. It was probably a layer of denaturized protein. The question whether there was a negative effect of the skin on the crystallization process, such as through attenuation of vapor diffusion rate, could not be addressed, since both non-crystal-reservoirs and successful crystallization experiments showed this phenomenon. Improved sealing of the reservoir with more silicone grease did not affect the formation of skin. Apparently STR1 tended towards skin formation, but this did not disturb crystallization. Wrapped around a crystal, the skin could affect the limit of diffraction. Therefore it was carefully removed prior to the mounting of crystals.

Since STR1 crystals were relatively stable in regards to vibration and temperature variations, they could be transported (by car) in the multi-well plates (containing crystals in the drops) to the synchrotron facilities in Hamburg, Germany. Pre-freezing in liquid nitrogen and storage in a Dewar were not necessary. Freezing *in situ* was used to inhibit radiation damage to STR1 crystals during data collection (cryo-crystallography). A crystal was carefully removed from the mother liquor by scooping up with a cryo loop (size 0.2, Hampton Research, II.7.2), in which it was held by surface tension.

IV.4.2.2 Measurement, structure elucidation and refinement

The STR1 crystals were soaked for 10 min in the cryo-protection solution (composed of 0.8 M potassium sodium tartrate x 4 H_2O, 100 mM HEPES, pH 7.5) containing 25 % glycerol and 3 mM strictosidine prior to flash cooling at 100K in a liquid nitrogen stream. X-ray data were collected using synchrotron radiation at the X13 beamline of EMBL-Hamburg. The complete

data were collected to a resolution of 3.0 Å. The data were processed and the structure solved and refined by Dr. Santosh Panjikar as previously described (III.3.6).

A commonly used indicator of the data quality is the so called merging factor (R-merge). It depends on the redundancy of the data, which may be problematic. R-merge at the highest resolution bin was 75.8 %, and one of the reasons for the high value was the occurrence of 11.8-fold redundancies. However, the signal-to-noise-ratio ($I/\sigma(I)$) at this bin was 3.7, and with this improved value, data to 3.0 Å were utilized. As the data was non-isomorphous with the native data, the structure of STR1-strictosidine complex was solved using the molecular replacement protocol of Auto-Rickshaw which is an automated crystal structure determination pipeline (PANJIKAR et al., 2005). The high resolution structure of STR1 (PDB code 1fp8, MA et al., 2006) was used as a search model. The strictosidine was built in the residual electron density using the graphics program COOT (EMSLEY and COWTAN, 2004). Subsequent refinement procedures were carried out using the program REFMAC5 (MURSHUDOV et al. 1997). Out of all non-glycine residues, 83.1 % fall in the most favored regions of a Ramachandran plot (RAMAKRISHNAN and RAMACHANDRAN 1965) generated by PROCHECK (LASKOWSKI et al. 1993, see Table 15) and MolProbity (LOVELL et al., 2003, see Figure 18). The data collection and the refinement statistics are summarized in Table 15. PDB ID code for the structure of STR1-strictosidine complex is 2v91. The number of STR1 molecules in the asymmetric unit was two.

The crystal structure of *R. serpentina* STR1 has been previously published for the native protein, and in complex with both substrates (tryptamine and secologanin) at resolutions ranging from 2.3 to 3.0 Å (MA et al., 2004 and 2006; KOEPKE et al. 2005). Structural alignment of STR1-strictosidine complex with the native protein structure was performed using PyMol software (DELANO, 2002) and DaliLite (HOLM and PARK, 2000). Root mean square deviation (RMS deviation) between aligned α-carbons of the protein structures was of 0.3 – 0.4 Å. RMS deviation is a measure of the average deviation in distance between the backbones of the superimposed proteins. The structure of STR1-strictosidine complex will be discussed in detail in section V.1.

Table 15. Data collection and refinement statistics of STR1-strictosidine complex.

Crystal	STR1-strictosidine
Wavelength (Å)	0.8076
Space group	*R*3
Cell parameters (Å)	a=b=150.18, c=121.71
Crystal size, mm^3	0.05x0.05x0.08
Matthews coefficient	3.6
Solvent content, %	60
Beamline/Detector	X13/Mar165
Resolution range (Å)	20 - 3.00
Total reflections	239481
Unique reflections	20295
Redundancy	11.8
Completeness $^\Gamma$ (%)	100 (100)
R-merge $^\Gamma$ (%) [a]	12.7 (75.8)
I/σ(I) $^\Gamma$	21.2 (3.7)
R-factor/R-free (%) [b]	19.2/23.4
RMS deviation bonds (Å)/angle (°)	0.018/1.84
Average B-factor of protein	26.0
Average B-factor of strictosidine	51.6
Average B-factor for water	47.8
Ramachandran plot (PROCHECK)	
Residues in most favorable regions (%)	83.1
Residues in additional allowed regions (%)	16.1
Residues in generously allowed regions (%)	0.8

$^\Gamma$ Value in the parentheses are for the highest resolution bin (3.05 – 3.00 Å)

[a] $R_{merge} = \Sigma_{hkl}\Sigma_i|I_i (hkl) - < I(hkl) >|/\Sigma_{hkl}\Sigma_i< I_i(hkl) >$, where $< I(hkl) >$ is the average intensity over symmetry equivalent reflections.

[b] $R_{cryst} (R_{free}) = \Sigma_{hkl}||F_o(hkl)| -|F_c(hkl)|| /\Sigma_{hkl}|F_o(hkl)|$, where F_o and F_c are observed and calculated structure factors, respectively.

Figure 18. Ramachandran analysis of STR1-strictosidine complex. The refined pdb-file of STR1-strictosidine complex was analyzed using MolProbity (LOVELL et al., 2003). 99.2 % of all residues were in allowed regions. There were 4 outliers (phi, psi); chain A: 71 Asn, 173 Asp, 301 Pro (see proline plot, appendix IX.6.1); chain B: 173 Asp. Outliers signify unusual conformations of the protein backbone and are highlighted in purple. These residues are still located within generously allowed regions.

IV.4.3 STR1-Inhibitor-complex

IV.4.3.1 Crystallization and X-ray measurement

To resolve the structure of STR1 in complex with the inhibitor MIT, both co-crystallization and soaking experiments were performed.

The native STR1 crystals used for soaking with inhibitor were grown as described (III.3; IV.4.1) by using precipitation buffer 3 and 5. Soaking conditions were investigated by trial and error with low quality crystals using EMBL beamline BW7B. Soaking and cryo-protect solutions were combined. A glycerol concentration of 24 % in the soaking solution was determined to be suitable. Inhibitor concentrations of > 0.5 mM immediately damaged the crystals. With 0.4 mM inhibitor added to the soaking solution, the crystals survived up to 10 min without visible damage, but the diffraction quality suffered during long incubation times (resolution after soaking for 8 min in 0.1 mM ca. 3.5 Å). An incubation time of 20 s in 0.4 mM inhibitor solution was not sufficient to detect inhibitor density in the active site. The best

dataset obtained from soaking experiments was measured at a resolution of 3.0 Å with a STR1 crystal soaked for 3 min in 0.15 mM inhibitor-cryo-solution. After the processing of the data, clear density for inhibitor was found in only one of the two STR1 molecules in the asymmetric unit (data not shown). Since this dataset obtained by soaking did not deliver optimal results for the solution of this complex structure, no further refinement but co-crystallization was performed.

Co-crystallization of STR1 and inhibitor MIT was performed in presence of 0.1 and 0.5 mM inhibitor respectively in the enzyme solution according to the STR1 crystallization protocol described (III.3.2.1). Precipitant buffers 3 (0.8 M potassium sodium tartrate x 4 H_2O, HEPES 0.1 M, pH 7.5) and 7 (0.8 M potassium sodium tartrate x 4 H_2O, HEPES 0.1 M, pH 7.3) were applied. STR1 concentration amounted to 4.6 – 5.3 mg/ml. The formation of single crystals was achieved with all conditions within 14 days. They differed in size as well as in the quality of diffraction. The data sets of STR1-inhibitor MIT co-crystals were collected at the X11 beamline of EMBL Hamburg, Germany. Again appearance misled. Especially big (ca. 0.1 x 0.1 x 0.3 mm; Figure 19), perfectly shaped crystals did not diffract as powerfully as their appearance promised. Better results were achieved with small crystals. A dataset was recorded from a crystal grown with buffer 7 and inhibitor concentration of 0.1 mM up to a resolution of 3.0 Å. Glycerol concentration in the cryo-protectant solution amounted to 22 %. After processing the data, clear density in both molecules of the asymmetric unit was apparent and it was decided to continue with this dataset.
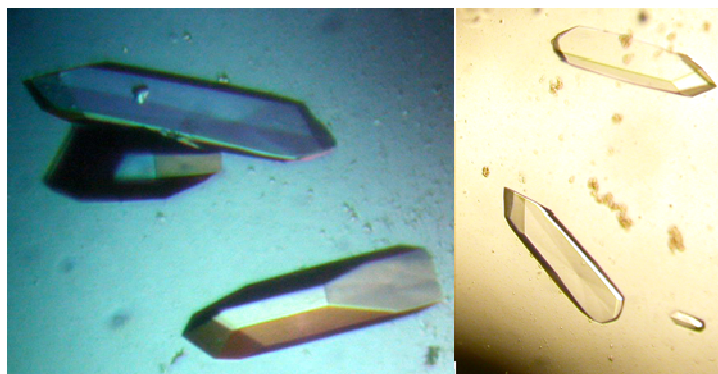
Figure 19. STR1-inhibitor MIT co-crystals. Like native STR1-crystals, the co-crystals were rhombohedral and belonged to the space group *R*3 with unit cell parameters of a=b=150.0, c=121.7. Crystal length varied between 0.05 and 0.3 mm. Very big exemplars (≥ 0.2 mm) did not diffract.

IV.4.3.2 Structure elucidation and refinement

The structure was solved and refined by Dr. Santosh Panjikar as described above (III.3.6). The final R-factor was 18.7 % for all data in the resolution range 20 -3.0 Å (R-free = 24.7 %). Of the non-glycine residues, 85.0 % fell in the most favored regions of a Ramachandran plot (RAMAKRISHNAN and RAMACHANDRAN 1965) generated by PROCHECK (LASKOWSKI et al. 1993). The refinement statistics are summarized in Table 16. In Figure 20 the Ramachandran plot generated by MolProbity (LOVELL et al., 2003) is displayed. The number

of STR1 molecules in the asymmetric unit was two. PDB ID code for the structure of STR1-inhibitor complex is 2vaq.

Structural alignment of STR1-inhibitor complex with the three previously solved enzyme structures (namely native STR1, PDB code 2fp8; STR1-tryptamine complex, PDB code 2fpb and STR1-secologanin complex, PDB code 2fpc; MA et al., 2006) and the structure of the STR1-strictosidine complex (PDB code 2v91; LORIS et al., 2007) resulted in RMS deviation of 0.2 – 0.8 Å. The crystal structure of STR1-inhibitor complex as well as STR1-strictosidine complex will be discussed in section V.1.
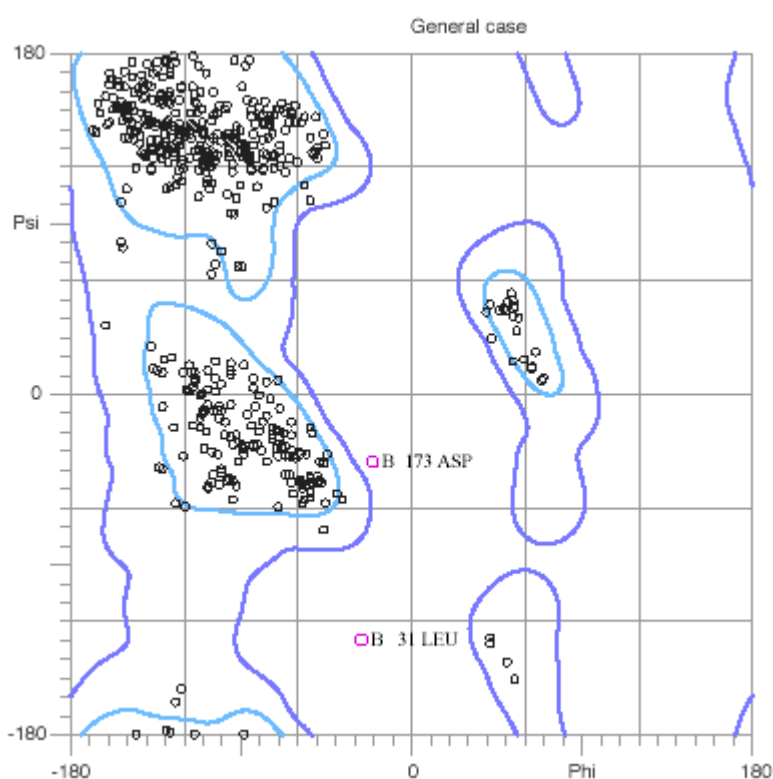
Figure 20. Ramachandran analysis of STR1-inhibitor complex. The PDB file of STR1-inhibitor complex was analyzed using MolProbity (LOVELL et al., 2003). 99.3 % of all residues were in allowed regions. There were 4 outliers (phi, psi); chain A: 301 Pro (see proline plot, appendix IX.6.2); chain B: 31 Leu, 173 Asp, 301 Pro. Outliers are highlighted in purple.

Table 16. Data collection and refinement statistics of STR1-inhibitor complex.

Crystal	STR1-inhibitor
Wavelength (Å)	0.8148
Space group	*R*3
Cell parameters (Å)	a=b=150.0, c=121.7
Crystal size, mm^3	0.05x0.05x0.08
Matthews coefficient	3.6
Solvent content, %	60
Beamline/Detector	X11/Mar165
Resolution range (Å)	20 - 3.00
Total reflections	119018
Unique reflections	20319
Redundancy	5.86
Completeness $^\Gamma$ (%)	100 (100)
R-merge $^\Gamma$ (%) [a]	10.1 (52.9)
I/σ(I) $^\Gamma$	18.1 (3.6)
Mosaicity	1.0
R-factor/R-free (%) [b]	18.7/24.7
RMS deviation bonds (Å)/angle (°)	0.019/1.921
Average B-factor of protein	48.6
Average B-factor of inhibitor MIT	52.4
Average B-factor for water	30.5

Ramachandran plot (PROCHECK)

Residues in most favorable regions (%)	85.0
Residues in additional allowed regions (%)	14.2
Residues in generously allowed regions (%)	0.4

$^\Gamma$ Value in the parentheses are for the highest resolution bin (3.05 – 3.00 Å)

[a] $R_{merge} = \Sigma_{hkl}\Sigma_i|I_i (hkl) - < I(hkl) >|/\Sigma_{hkl}\Sigma_i< I_i(hkl) >$, where $< I(hkl) >$ is the average intensity over symmetry equivalent reflections.

[b] $R_{cryst} (R_{free}) = \Sigma_{hkl}||F_o(hkl)| - |F_c(hkl)|| /\Sigma_{hkl}|F_o(hkl)|$, where F_o and F_c are observed and calculated structure factors, respectively.

IV.5 Structure-based re-engineering of Strictosidine Synthase

IV.5.1 Engineering strategy

The rational re-design of the *R. serpentina* STR1 active site was performed based on the structural analysis of STR1-strictosidine complex, which will be presented in V.2V.2.2.

Initially, a detailed analysis of the active site was performed with the STR1-strictosidine structure, considering the results of the substrate specificity study. This will be presented and discussed below (V.2.2). The aim was the finding of crucial residues for substrate acceptance and the determination of the respective mutations. Table 17 summarizes the mutagenesis strategy by listing the proposed mutations according to the target substrates.

Mutant E205V/V208A was generated due to an error in the ordered primer's sequence (Primer V208A-rev1). Residue E205V was located in a distance of > 13 Å afar from the active site. Its influence on the catalytic pocket and the occurring interactions could not be foreseen. Therefore the mutant was included in this study though its generation was indirectly based on the structural analysis.

Table 17. Proposed mutations for the conversion of so far not accepted STR1 substrates. The respective residues and mutations were selected due to their position related to strictosidine in the catalytic pocket of STR1-strictosidine complex.

Target substrate	Proposed mutations
5-Methoxy-tryptamine	V208A, V208G, V167A, V167G
5-Methyl-tryptamine	V208A, V208G, V167A, V167G
5,7-Dihydroxy-tryptamine	W149A
$N_{(\alpha)}$-Acetyl-5-hydroxy-tryptamine	W149A
$N_{(\alpha)}$-Methyl-tryptamine	W149A
$N_{(\beta)}$-Methyl-tryptamine	W149A
2-Methyl-5-hydroxy-tryptamine	W149A, E309D

IV.5.2 Generation, expression and purification of STR1 mutants

The structure-based, rational re-design of the active site of *R. serpentina* STR1 was performed by site-directed point mutagenesis. STR1 mutants were generated by PCR amplification using *str1*-pQE2 plasmid as template and two complementary oligonucleotide primers, which contained the desired point mutation (III.2.2). Primers were designed based on the cDNA sequence of STR1 from *R. serpentina* (KUTCHAN et al., 1988) and the desired mutation was introduced by the exchange of one or two nucleotides. The respective nucleotide and protein sequence regions of the mutants as well as the primer sequences and melting temperatures (T_m) are listed in

Table 18. The complete nucleotide and protein sequence of STR1 wild-type is shown in appendix IX.2.

STR1 plasmid *str1*-pQE2 served as the template with two exceptions: double mutant V167G/V208A was created with *str1_V208A*-pQE2 plasmid as the template and V208A with *str1_E205V/V208A*-pQE2 plasmid. Numerous PCR experiments were carried out for the generation of the mutants. The following conditions were varied with the aim to produce a sharp product band, detectable by agarose gel electrophoresis (Figure 21 C): annealing temperature, type of polymerase, number of cycles, concentration of primer as well as template and dNTPs. PCR conditions and procedures are exemplified using mutant E309D as a case study in Figure 21, which is representative for the generation of all mutants described. Exact settings and compositions of PCR experiments leading to the other mutants are listed in appendix IX.4.

After completion of PCR, the template was removed by restriction enzyme digestion (III.2.3). The restriction enzyme *DpnI* is specific for methylated DNA. Due to the enzymatic equipment of *E. coli* (dam⁺), the *E. coli*-derived template was dam-methylated. Dam methylase adds a methyl group on the nitrogen at position 6 of adenosine. *DpnI* cuts dam-methylated DNA specifically. The mutated plasmid remained intact, since the deployed dNTPs were not methylated. The enzyme was added directly to the reaction mixture (0.5 µl, 10 U) and incubated for 2 h at 37 °C shaking constantly. PCR reaction mixture was separated by agarose gel electrophoresis and visualized by ethidium bromide staining (III.2.4). The size of PCR products was determined by comparison with a DNA ladder (II.6). Figure 21 C shows a typical agarose gel. PCR product size was expected to be 5.78 kb (pQE2 vector 4.76 kb and

str1-insert 1.02 kb). Sharp bands in this area of the DNA ladder were cut out and extracted from the gel matrix, using NucleoSpin© Extract Kit.

Table 18. Peptide, nucleotide and primer sequence of STR1 variants. For each generated mutant, the mutated regions of the nucleotide and amino acid sequence are shown (5' – 3'). Primer used for site-directed mutagenesis are listed together with their sequences and melting temperatures (T_m).

Trp149Ala (W149A):

144	G	V	P	F	K	A	L	Y	A	V	T	V
430	GGA	GTG	CCA	TTC	AAG	GCG	CTC	TAT	GCA	GTA	ACA	GTT

Primer name	Nucleotide sequence	T_m (°C)
W149A-for:	5'-GGA GTG CCA TTC AAG gcG CTC TAT GCA GTA ACA G –3'	71.9
W149A-rev:	5'-C TGT TAC TGC ATA GAG Cgc CTT GAA TGG CAC TCC –3'	71.9

Val167Ala (V167A):

162	V	Y	F	T	D	A	S	T	L	Y	D
484	GTT	TAC	TTC	ACC	GAT	GCT	AGC	ACC	TTA	TAT	GAT

Primer name	Nucleotide sequence	T_m (°C)
V167A-for	5'– GTT TAC TTC ACC GAT GcT AGC ACC TTA TAT GAT –3'	65.8
V167A-rev	5'– ATC ATA TAA GGT GCT AgC ATC GGT GAA GTA AAC –3'	65.8

Val167Gly (V167G):

162	V	Y	F	T	D	G	S	T	L	Y	D
484	GTT	TAC	TTC	ACC	GAT	GGT	AGC	ACC	TTA	TAT	GAT

Primer name	Nucleotide sequence	T_m (°C)
V167G-for	5'– GTT TAC TTC ACC GAT GgT AGC ACC TTA TAT GAT –3'	65.8
V167G-rev	5'– ATC ATA TAA GGT GCT AcC ATC GGT GAA GTA AAC –3'	65.8

Val208Ala (V208A):

203	L	K	E	L	H	A	P	G	G	A	E	V
607	TTG	AAA	GAG	CTA	CAC	GCG	CCA	GGT	GGC	GCA	GAA	GTC

Primer name	Nucleotide sequence	T_m (°C)
V208A-for	5'-G TTG AAA GAG CTA CAC Gcg CCA GGT GGC GCA GAA G –3'	>75
V208A-rev2	5'-C TTC TGC GCC ACC TGG cgC GTG TAG CTC TTT CAA C –3'	>75

Val208Gly (V208G):

203	L	K	E	L	H	G	P	G	G	A	E	V
607	TTG	AAA	GAG	CTA	CAC	GGT	CCA	GGT	GGC	GCA	GAA	GTC

Primer name	Nucleotide sequence	T_m (°C)
V208G-for	5'– GTT GAA AGA GCT ACA C GgT CC AGG TGG GGC AGA AG –3'	>75
V208G-rev	5'– CT TCT GCC CCA CCT GG AcC G TGT AGC TCT TTC AAC –3'	>75

▼
Table 19. Continued.

Double mutant Glu205Val+Val208Ala (E205V/V208A):

203	L	K	E	L	H	G	P	G	G	A	E	V
607	TTG	AAA	GAG	CTA	CAC	GGT	CCA	GGT	GGC	GCA	GAA	GTC

Primer name	Nucleotide sequence	T_m (°C)
V208A-for	5'– G TTG AAA GAG CTA CAC Gcg CCA GGT GGC GCA GAA G –3'	>75
V208A-rev1	5'– C TTC TGC GCC ACC TGG cgC GTG TAG CaC TTT CAA C –3'	>75

Glu309Asp (E309D):

304	A	G	E	H	F	D	Q	I	Q	E	H
910	GCA	GGT	GAA	CAC	TTC	GAC	CAA	ATT	CAA	GAG	CAT

Primer name	Nucleotide sequence	T_m (°C)
E309D-for	5'– GCA GGT GAA CAC TTC GAc CAA ATT CAA GAG CAT G –3'	69.5
E309D-rev	5'– C ATG CTC TTG AAT TTG gTC GAA GTG TTC ACC TGC –3'	69.5

Double mutant Val167Gly+Val208Ala (V167G+V208A):

162	V	Y	F	T	D	G	S	T	L	Y	D	...
484	GTT	TAC	TTC	ACC	GAT	GGT	AGC	ACC	TTA	TAT	GAT	...
20	L	L	K	E	L	H	A	P	G	G	A	E	V
604	CTG	TTG	AAA	GAG	CTA	CAC	GCG	CCA	GGT	GGC	GCA	GAA	GTC

Primer name	Nucleotide sequence	T_m (°C)
V208A-for	5'– G TTG AAA GAG CTA CAC Gcg CCA GGT GGC GCA GAA G –3'	>75
V208A-rev2	5'– C TTC TGC GCC ACC TGG cgC GTG TAG CTC TTT CAA C –3'	>75
V167G-for	5'– GTT TAC TTC ACC GAT GgT AGC ACC TTA TAT GAT –3'	65.8
V167G-rev	5'– ATC ATA TAA GGT GCT AcC ATC GGT GAA GTA AAC –3'	65.8

Next step was the transformation of the extracted DNA sample into Top10 *E. coli* cells for *in vivo* reproduction (see III.2.7). The successfully transformed cells were grown overnight in a volume of ca. 10 ml LB medium (containing 50 µg/ml ampicillin) and plasmids were isolated using NucleoSpin© Plasmid Kit. Intention was to increase the amount of DNA in order to have enough material for restriction digest, sequencing and further transformations. The alkaline lyses mini preparation was a cost-efficient alternative for the rapid preparation of a large

amount of samples. Up to 20 different small-scale bacteria cultures were processed in less than 45 min.

(A) Composition of PCR reaction mixture	
str1-pQE2 (ca. 10 ng/ml)	2.0 µl
Primer E309D-for (10 pmol/µl)	1.0 µl
Primer E309D-rev (10 pmol/µl)	1.0 µl
5xPhusion Control buffer	10.0 µl
dNTP's (20 mM)	2.5 µl
Phusion™ Polymerase (2U/µl)	1.0 µl
Ampuwa water	ad 50.0 µl

(B) PCR cycler program

Temperature (°C)	Time (min)	Cycles
95	2	1
95	0.5	
54	1	26
72	4	
72	10	1

(C) Agarose electrophoresis

Figure 21. Representative procedure for the generation of mutants. (A) Composition of the PCR reaction mixture for the generation of mutant E309D. (B) PCR process: time and temperature program run by thermocycler. After completion of PCR, the template was removed by restriction enzyme digestion, and the reaction mixture was separated by agarose gel electrophoresis. (C) Electrophoretic separation of PCR products. M = DNA ladder; Band 1 shows the result of unsuitable PCR conditions and the bands summarized as 2 are the product of a successful PCR amplification (both E309D).

Prior to sequencing, the isolated plasmids were pre-analyzed by restriction enzyme digestion with the enzymes *HindIII* and, depending on availability, *SphI* or *NdeI* (2 h, 37 °C). The digestion mixture was analyzed by agarose gel electrophoresis and the restriction pattern was compared to likewise digested STR1 native plasmid, which served as a positive control. Solely plasmids which match the fragments of the positive control were selected for sequencing. The sequencing of selected plasmids was performed by GENterprise Genomics (Mainz, Germany). The results were compared to the sequence of native STR1. Alignment was performed by means of the following online tools: ClustalW (EMBL-EBI), Blast2Sequences (NCBI) and ExPASy translation tool. Exclusively verified, homogenous plasmids containing the desired mutation were accepted and transformed into *E. coli* M15 cells, which were used for expression of the engineered plasmid. The sequencing results of the generated mutants are shown in appendix IX.5.

Expression and purification procedure were similar to the expression and purification of native STR1 (III.1) and the results are described below (IV.6.1). Exceptions were made due to optimization efforts and are described in section IV.8.

The purity of His$_6$-tagged STR1 mutants was checked by SDS PAGE and the protein concentration was determined by the Bradford method as it had been performed for STR1

wild-type (III.1.8; III.1.6). Activity tests were carried out with His_6-tagged enzymes using the enzyme assay for STR1 wild-type (III.4.1).

IV.6 Enzyme properties of STR1 - mutants

The mutants of STR1 highly differed in expression, in protein yield after purification and in activity. There were significant differences in comparison to the wild-type enzyme STR1 as well as between the individual mutants. The following chapter presents the results achieved with the mutants.

IV.6.1 Expression and purification

For expression, the re-engineered plasmids, which were verified by sequencing, were transformed into M15 cells. Except for initial small scale experiments and optimization efforts, the methodologies of expression and purification as well as employed amounts were similar to expression and purification of native STR1 (Figure 22 and Figure 23 show representative SDS PAGE).

Since the mutants of STR1 highly differed in expression and protein yield (Table 30), it was found advantageously to screen the transformed M15 cells for high expression colonies. For this purpose, several single colonies of freshly transformed cells were grown in 20 ml LB-medium containing 50 µg/ml ampicillin and 25 µg/ml kanamycin with shaking (160 rpm) at 37 °C for 8 h. Subsequently the cultures were divided into two parts: one part was induced by adding IPTG to a final concentration of 1 mM while the other stood non-induced. Both were grown overnight shaking at RT. Then aliquots of the cells were analyzed by SDS PAGE. Figure 22 shows the result of a colony screening.
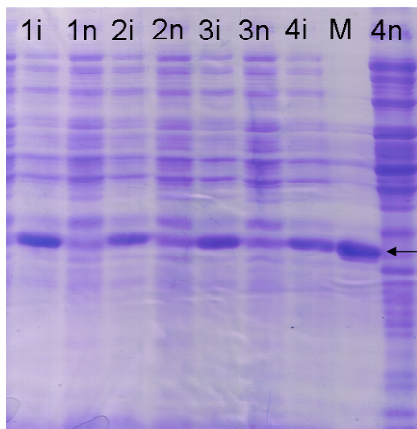
Figure 22. SDS PAGE of several colonies of mutant V208G. Analysis of 4 different colonies of M15 cells containing the engineered plasmid *str1_V208G*-pQE2. 1n, 2n, 3n, 4n = non-induced cells; 1i, 2i, 3i, 4i = induced with IPTG. M = authentic STR1-His$_6$ was used as marker protein. The arrow highlights the area of 37 kDA, where the STR1 band is localized. Remarkably in presence of IPTG the expression of other genes seemed to be suppressed. Colony 1i was selected for expression in production-scale.

Reportedly a majority of the STR1-His$_6$ protein expressed formed insoluble aggregates of unfolded or misfolded proteins, so called inclusion bodies (MA et al., 2004). Over-expression of the engineered plasmids led to the same phenomenon and several mutants showed extreme lack of solubility compared to the wild-type enzyme. In some cases (such as mutant W149A and E309D) 80 – 90 % of the expressed enzyme accumulated as inclusion bodies

and stayed in the pellet (Figure 23). This posed serious problems in the recovery of functionally active and soluble protein and led to low protein yields (Table 30).

In addition to this, weak binding of His_6-tagged mutants was observed and made the production of pure protein in usable amounts more difficult: His_6-tagged enzyme was already washed out of the column with 50 mM imidazole wash buffer and only a small part of the expressed soluble enzyme was eluted with the 250 mM imidazole elution buffer. Though this phenomenon occurred with wild-type STR1-His_6 as well, the amount lost was negligible. Less stringent conditions were used for the purification of mutant enzymes (such as washing with maximum 40 mM imidazole, lower flow rates) and the protein yields could be optimized.
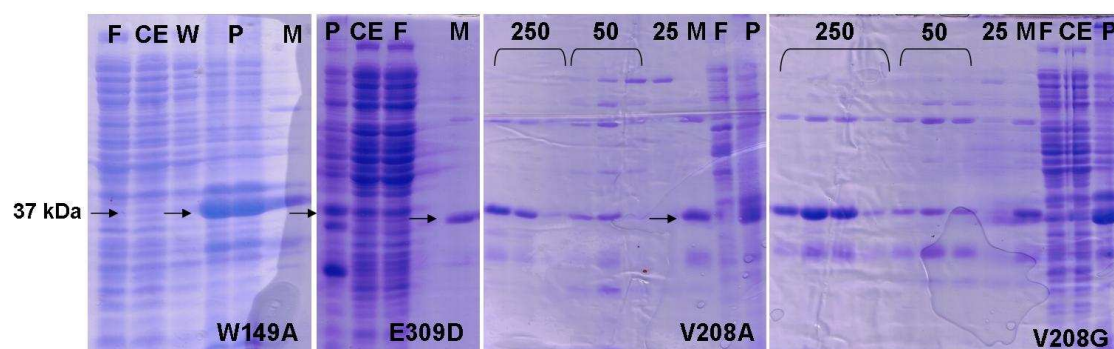
Figure 23. SDS PAGE of the purification procedure of STR1 mutants W149A, E309D, V208A and V208G. F= flow through, CE = crude extract, W = pellet washing solution, P = pellet, M = authentic STR1 as marker. 25 = wash fraction(s) eluted with 25 mM imidazole, 50 = wash fraction(s) eluted with 50 mM imidazole, 250 = 250 mM imidazole elution fractions containing His_6-tagged proteins. Arrows highlight the position of the mutant's protein bands at 37 kDa.

The average yield of soluble, His_6-tagged V208A enzyme from standard purification was 0.21 ($\pm$ 0.16) mg from one liter bacterial culture in LB-medium. Mutants E309D, V208G, E205V/V208A and W149A were available in similar or slightly lower amounts. Mutant's V167A protein yield was < 0.01 mg/l LB while V167G could not be obtained at all. No activity was detected in the elution fractions from affinity chromatography. The protein yields are shown in Table 30 at the end of this chapter (IV.8), when optimization efforts are presented. The mutation of residue V167 seemed to be particularly critical and only limited analysis could be performed with these two mutants. SDS PAGE showed a phenomenon which is described in detail below (IV.6.6).

IV.6.2 Relative activity of His$_6$-tagged mutants with the native substrates tryptamine and secologanin

Relative activity of STR1 mutants compared to conversion of tryptamine by STR1 wild-type enzyme was used as initial activity measure. It was determined for every generated mutant using the standard enzyme assay (III.4.1.4) with His$_6$-tagged enzymes and HPLC (III.4.3.1). Strictosidine formation and substrate loss were monitored at 250 nm and were both used for calculation. Enzyme concentration for relative activity of mutants compared to wild-type enzyme was 13.5 μM. The relative activity of the engineered mutants with the native substrates compared to the conversion by STR1 wild-type enzyme is shown in Figure 24.
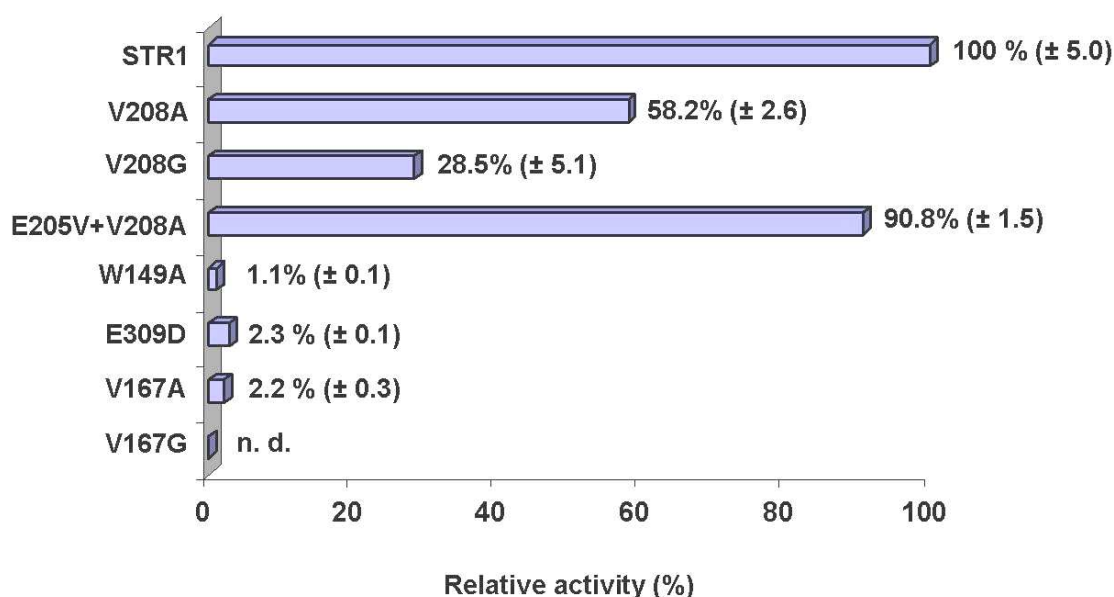
Figure 24. Relative activity of mutants compared to wild-type enzyme. Calculation was based on activity with the native substrates. Activities of STR1 mutants compared to conversion of tryptamine by STR1 wild-type enzyme are shown.

Unsurprisingly no mutant provided benefit for turnover of the native substrate tryptamine; however, the double mutant E205V/V208A converted the native substrate nearly in the same extent as the wild-type enzyme. Mutants V208A and V208G exhibited good conversion of tryptamine, indicating that these enzymes were suitable for further (kinetic) analysis. In contrast to the other mutants, W149A, E309D and V167A showed extreme decrease in activity. Mutant's V167G relative activity was not determined due to the reasons mentioned above.

IV.6.3 Substrate specificity

IV.6.3.1 Qualitative analysis

The mutants' substrate specificity was initially investigated by substrate screenings using the standard enzyme assay and HPLC as described above. Negative control was carried out with denaturized enzyme, using identical conditions. Figure 25 represents a typical HPLC trace, showing the enzymatic formation of 10-methoxy-strictosidine by mutant V208A (A) and negligible peak with wild-type STR1-His$_6$ (B). The retention times of substrates and products are listed in appendix IX.1.
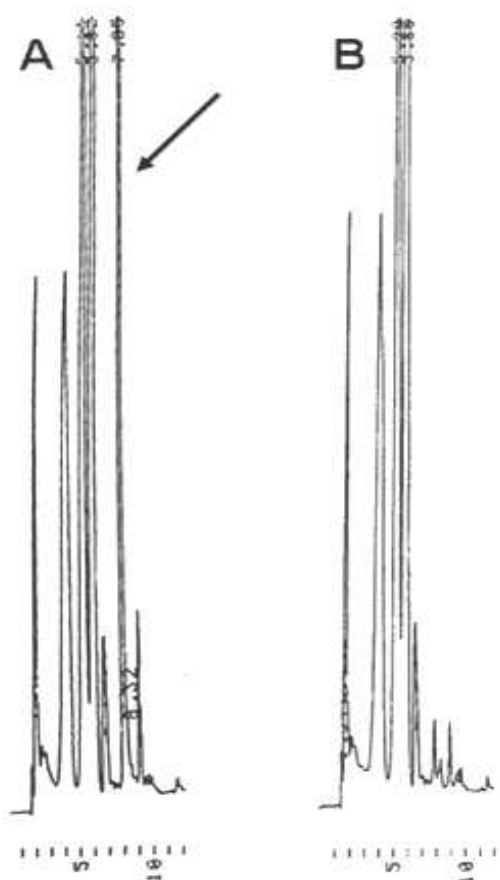
Figure 25. Representative HPLC trace. The enzymatic formation of 10-methoxy-strictosidine (retention time ca. 8 min, see the arrow) from 5-methoxy-tryptamine and secologanin by the His$_6$-tagged mutant V208A and negligible peak with wild-type STR1-His$_6$ (B).

In the case turnover was not detectable with standard conditions, the enzyme concentration was increased up to 40 µM (ca. 20-fold) and the incubation time extended up to 48 h. The number of tested substrates and the enzyme concentration used depended on the available amount of His$_6$-tagged protein. Mutant V167A gave little scope for activity tests because of extremely poor expression. Section IV.6.6 is dealing with this special case.

The initial substrate screening gave first information on substrate specificity and activity of the generated mutants. The results were decisive for further analysis and are summarized in Table 19. Definitely accepted substrates (++ in Table 19) showed significant substrate loss

as well as product formation with standard activity assay. Both substrate loss and product formation increased with respectively prolonged time of incubation and increasing enzyme concentration. Poorly converted substrates, which could exclusively be detected using high enzyme concentrations and long incubation times (conversion estimated < 1 nmol/min/mg by HPLC plot and calibration curve) were marked with +. Results from probably accepted substrates (+/-) indicated conversion, but definite conclusions could not be drawn. The above mentioned detection rules (such as appearance of potential product peak or significant product peak pattern and significant substrate loss) were not completely fulfilled. A reason for this was an extremely poor conversion or the instability of substrates and product(s), which complicated the detection.

The substitution of residue V208 completely met the expectations (see Table 19; IV.5.1, Table 17). The resulting mutants V208A and V208G as well as double-mutant E205V/V208A exhibited conversion of 5-methyl- and 5-methoxy-tryptamine to the corresponding substituted strictosidine in the presence of secologanin, which was confirmed using HPLC, NMR and LC-MS (see IV.6.3.2). Except for these two novel compounds, the mutants' substrate scope was similar to the wild-type. The fact that double mutant E205V/V208A also converted the carbon-5-methylated and -methoxylated tryptamine derivatives, supported the reliability and reproducibility of the engineering strategy.

Shielding the carbon 7 of tryptamine, residue W149 was replaced by Ala and the resulting mutant exhibited conversion of 7-methyl-tryptamine. This compound was also converted by the wild-type, broadening of substrate range was not necessary, but because of low activity of wild-type with 7-methyl-tryptamine, mutant W149A was expected to be more efficient. This was to be investigated in the following quantitative analysis of conversion. Furthermore, mutant W149A converted $N_{(\alpha)}$-acteyl-5-hydroxy-tryptamine at least to a very low extent (conversion estimated < 1 nmol/min/mg by HPLC plot and calibration curve). This compound was not accepted by STR1 wild-type and represented a new substrate due to the novel mutation.

As mentioned above, the substitution of residue V167 was critical: the extraction of V167G failed several times. V167A yield was poor. Nevertheless, it was tested with several substrates and exhibited high substrate specificity, accepting only a few compounds besides tryptamine. Remarkably, among the converted substrates were the carbon-5-substituted tryptamine analogues 5-methyl- and 5-methoxy-tryptamine, which were not accepted by STR1. Apparently the substitution of residue Val167 by a smaller amino acid residue also resulted in an enlarged substrate spectrum.

Table 19. Substrate specificity of STR1 and mutants. (++ = definitely accepted substrate, + = accepted substrate with conversion < 1 nmol/min/mg, +/- = probably accepted substrate, no distinct conclusion, 0 = no turnover measurable, / = not tested).

Enzyme / mutant	STR1	V208A	V208G	E205V/V208A	W149A	E309D	V167A
Tryptamine	++	++	++	++	++	++	++
5-Fluoro-tryptamine	++	++	++	/	++	/	++
6-Fluoro-tryptamine	++	++	++	/	++	/	0
5-Hydroxy-tryptamine (Serotonin)	++	++	++	/	+	/	+/-
5,6-Dihydroxy-tryptamine	++	+/-	/	/	/	/	/
5,7-Dihydroxy-tryptamine	0	0	/	/	0	/	/
5-Methyl-tryptamine	0	++	++	++	+	/	++
6-Methyl-tryptamine	++	++	++	/	++	/	/
7-Methyl-tryptamine	++	++	++	/	++	/	++
5-Methoxy-tryptamine	0	++	++	++	++	/	++
6-Methoxy-tryptamine	++	++	++	/	++	/	0
2-Methyl-5-hydroxy-tryptamine	0	0	+	0	0	0	0
$N_{(\alpha)}$-Methyl-tryptamine	0	0	0	/	0	/	0
$N_{(\alpha)}$-Acetyl-5-hydroxy-tryptamine	0	0	0	/	+	/	0
$N_{(\beta)}$-Methyl-tryptamine	0	0	0	0	0	0	0
Phenylalanine	0	0	/	/	/	/	/
Histamine	0	0	/	/	/	/	/
Dopamine	0	0	/	/	/	/	/

IV.6.3.2 Spectroscopic product identification

Novel strictosidine analogues 10-methyl- and 10-methoxy-strictosidine, which were so far not available by wild-type enzyme, were identified by NMR and LC-MS analysis.

Strictosidine and the derivatives 10-methyl- and 10-methoxy-strictosidine, generated by mutant V208A, were analyzed by LC-MS using a LC/MSD Trap system (Agilent, Waldbronn, Germany). Measurement was carried out by Dr. Matthias Unger and Dr. Andreas Frank (Würzburg, Germany) as described in III.4.3.2. [M + H]$^+$ of reaction products were 531, 545, 561 m/z for strictosidine and its 10-methyl- and 10-methoxy-derivative (Figure 27).

^{13}C- and ^{1}H-NMR data were collected for 10-methyl-strictosidine and 10-methoxy-strictosidine (Figure 26), which were generated by mutant V208A according to the description given in chapter III.4.2. The NMR spectra were recorded in CD$_3$OD on a Bruker DRX Avance 400 MHz instrument by Dr. Bernd Mathiasch (Johannes Gutenberg-University, Institute of Inorganic and Analytical Chemistry) and on a Bruker Avance 700 MHz instrument by Dr. Manfred Wagner (Max-Planck Institute for Polymer Research in Mainz). Assignments were supported by HSQC experiments and by comparison with the stereo-chemical analysis of strictosidine by PATTHY-LUKÁTS et al. (1997, 1999). Data were managed and analyzed using MestRe-C software. ^{13}C- and ^{1}H-NMR chemical shifts of 10-methyl- and 10-methoxy-strictosidine in CD$_3$OD are listed in Table 20 and Table 21 respectively.
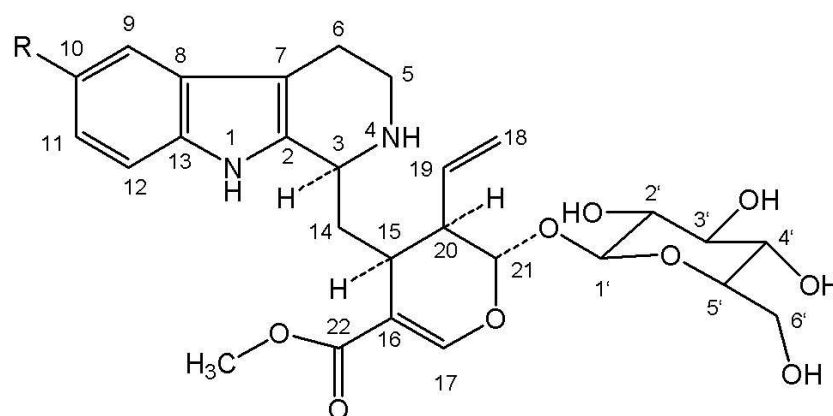
Figure 26. Structure and numbering of 10-methyl-strictosidine (R = CH$_3$) and 10-methoxy-strictosidine (R = OCH$_3$).
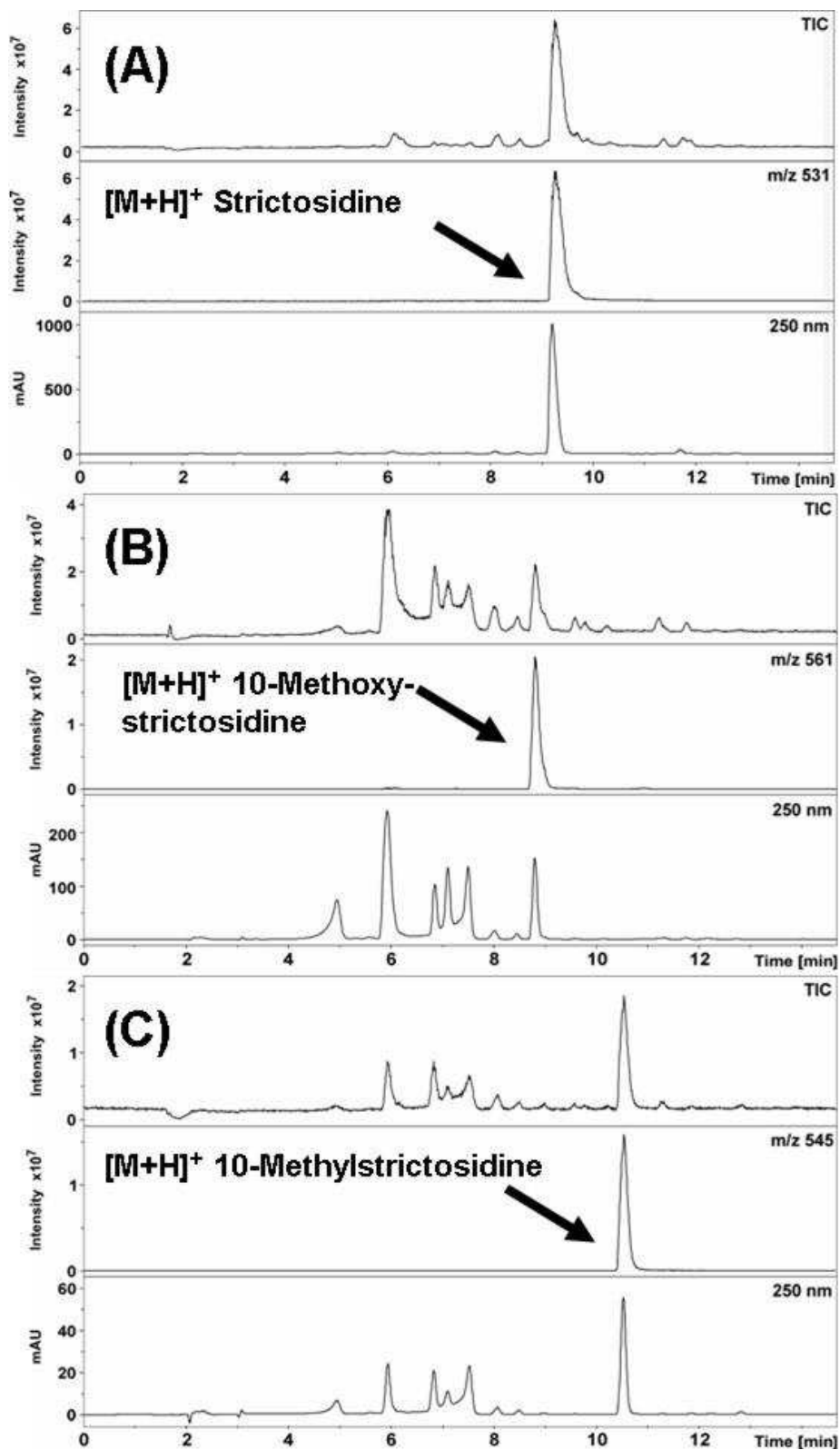
Figure 27. LC-MS traces for the identification of enzymatically formed strictosidine and derivatives. (A) strictosidine, (B) 10-methoxy-strictosidine and (C) 10-methyl-strictosidine; total ion current (TIC), the MS and UV traces (from top to bottom for each picture).

Table 20. ^{13}C- and ^{1}H-NMR Chemical shifts of 10-methyl-strictosidine in CD$_3$OD. Internal standard; $\delta_{TMS} = 0.0$ (br = broad, s = singlet, d = doublet, dd = double doublet, dt = double triplet, m = multiplet).

10-methyl-strictosidine	δ_C	δ_H
C-2	131.6	-
C-3	50.1	3.91 (brd, J $_{3,14R}$ 10.9, 1H)
C-5	41.7	α: 2.71-2.80 (m, 1H); β: 3.20-3.25 (m, 1H)
C-6	20.9	α: 2.63-2.70 (m, 1H); β: 2.72-2.81 (m, 2H; overlap with H-20)
C-7	106.4	-
C-8	127.2	-
C-9	116.7	7.14 (brs, 1H)
C-10	134.4	-
CH$_3$ at C-10	20.0	2.36 (s, 3H)
C-11	121.8	6.84 (dd, J $_{11,12}$ 8.2, J $_{9,11}$ 1.5, 1H)
C-12	109.8	7.11 (d, J $_{11,12}$ 8.2, 1H)
C-13	135.0	-
C-14	35.6	*R, S* 1.93-2.10 (m, 2H)
C-15	31.1	3.02 (m, 1H)
C-16	109.3	-
C-17	153.6	7.67 (s, 1H)
C-18	117.4	*E*: 5.22 (dt, J 10.6, 2.3, 2.3, 1H); *Z*: 5.30 (dt, J 17.0, 2.6, 2.6, 1H)
C-19	134.5	5.85 (m, 2H; overlap with H-21)
C-20	44.3	2.66 (m, 1H)
C-21	96.0	5.81(d, 1H, J $_{20,21}$ 9.1)
C-22	168.5	-
OCH$_3$ ester	50.5	3.74 (s, 3H)
C-1'	98.7	4.77 (d, J $_{1',2'}$ 7.9, 1H)
C-2'	77.1	3.18-3.45
C-3'	76.4	3.18-3.45
C-4'	73.1	3.18-3.45
C-5'	70.1	3.18-3.45
C-6'	61.3	3.93 (dd, J $_{6'a, 6'b}$ 11.7, J $_{5',6'a}$ 2.1, 1H); 3.64 (dd, J $_{6'a, 6'b}$ 12.0, J $_{5', 6'b}$ 6.7, 1H)

Table 21. ^{13}C- and ^{1}H-NMR Chemical shifts of 10-methoxy-strictosidine in CD$_3$OD. Internal standard; $\delta_{TMS} = 0.0$ (br = broad, s = singlet, d = doublet, dd = double doublet, dt = double triplet, m = multiplet).

10-methoxy-strictosidine	δ_C	δ_H
C-2	131.3	-
C-3	50.2	3.91 (brd, J $_{3,14R}$ 9.4, 1H)
C-5	41.7	α: 2.72-2.81 (m, 1H); β: 3.20-3.24 (m, 1H)
C-6	20.9	α: 2.62-2.70 (m, 1H); β: 2.72-2.81 (m, 2H; overlap with H-20)
C-7	106.8	-
C-8	127.3	-
C-9	117.0	6.87 (d, J 2.3, 1H)
C-10	158.7	-
OCH$_3$ at C-10	54.7	3.78 (s, 3H)
C-11	120.2	6.67 (dd, J $_{11,12}$ 8.8, J $_{9,11}$ 2.3, 1H)
C-12	110.1	7.12 (d, J $_{11,12}$ 8.5, 1H)
C-13	135.8	-
C-14	35.5	*R, S*: 1.92-2.04 (m, 2H)
C-15	31.1	3.02 (m, 1H)
C-16	109.3	-
C-17	153.6	7.66 (s, 1H)
C-18	117.5	*E*: 5.21 (dt, J 10.5, 2.3, 2.3, 1H); *Z*: 5.30 (dt, J 17.6, 2.6, 2.6, 1H)
C-19	134.5	5.85 (m, 2H: overlap with H-21)
C-20	44.3	2.65 (m, 1H)
C-21	96.0	5.81 (d, J $_{20,21}$ 9.1, 1H)
C-22	169.6	-
OCH$_3$ ester	50.5	3.74 (s, 3H)
C-1'	98.7	4.77 (d, J $_{1', 2'}$ 7.9, 1H)
C-2'	77.1	3.18-3.45
C-3'	76.4	3.18-3.45
C-4'	73.1	3.18-3.45
C-5'	70.1	3.18-3.45
C-6'	61.3	3.94 (dd, J $_{6'a, 6'b}$ 11.7, J $_{5',6'a}$ 2.2, 1H); 3.64 (dd, J $_{6'a, 6'b}$ 11.7, J $_{5', 6'b}$ 6.8, 1H)

IV.6.3.3 Quantitative analysis

The quantitative analysis of enzyme activity was performed with the His$_6$-tagged wild-type enzyme and its individual His$_6$-tagged mutants after purification by affinity chromatography on Ni-NTA column. The standard HPLC assay was used for detection of substrate loss and product formation at 250 nm and 280 nm. The reaction rate was calculated by substrate loss. Calibration curves at 250 and 280 nm were generated for each tryptamine analogue by integration of peak area.

Initial experiments, with up to five different substrate concentrations, provided information on the enzymes' activity, and kinetic parameters could be estimated. They showed that a quantification of the mutants' activity could not be carried out consistently, since the differences in activity were too large. Therefore, kinetic analysis was focused on mutants that were available in high amounts and which exhibited sufficient activity (V208A, V208G, and E309D). For mutants exhibiting (partly extremely) low conversion of several tryptamine analogues (W149A, V167A), a basic quantitative analysis was performed by the determination of specific activity under selected, benefiting conditions such as incubation periods > 1 h and high enzyme concentrations. All quantitative assays were repeated at least once (STR1 and V208A twice) to ensure reproducibility. The results are shown in Table 22 and Table 23. They represent the average of 2 – 3 independent experiments, respectively with n = 2 or 3.

Independent experiments were carried out with different charges of enzyme, coming from independent purifications. The respective purifications yielded protein solutions differing in protein concentration (measured with Bradford method) and purity (STR1 wild-type ca. 90 %, an increased amount of impurities was observed for mutants, 75 – 90 %). This may have major influence on the behavior and the properties of the respective enzyme preparations. The author decided to include all experiments with standard error ≤ 10 % and value of non-linear regression coefficient R^2 > 0.9, despite partly differing kinetic constants of the individual experiments. It should reflect the features of different enzyme preparations, which can influence the activity results.

Differing kinetic values were no result of aged enzyme preparations. The substrate inhibition study (IV.3.1) was performed twice with the same protein charge within 6 days. No activity loss was monitored. Furthermore the activity of a 10-day old enzyme preparation was determined and compared to the activity achieved with the same solution at day 2. The 10 day old solution lost 90 % activity compared to day 2. The author decided to use each enzyme preparation for a period of 6 days and excluded elder enzymes from quantitative studies. All protein solutions were stored at 2 – 8°C.

(A) Michaelis-Menten plot

(B) Lineweaver-Burk plot
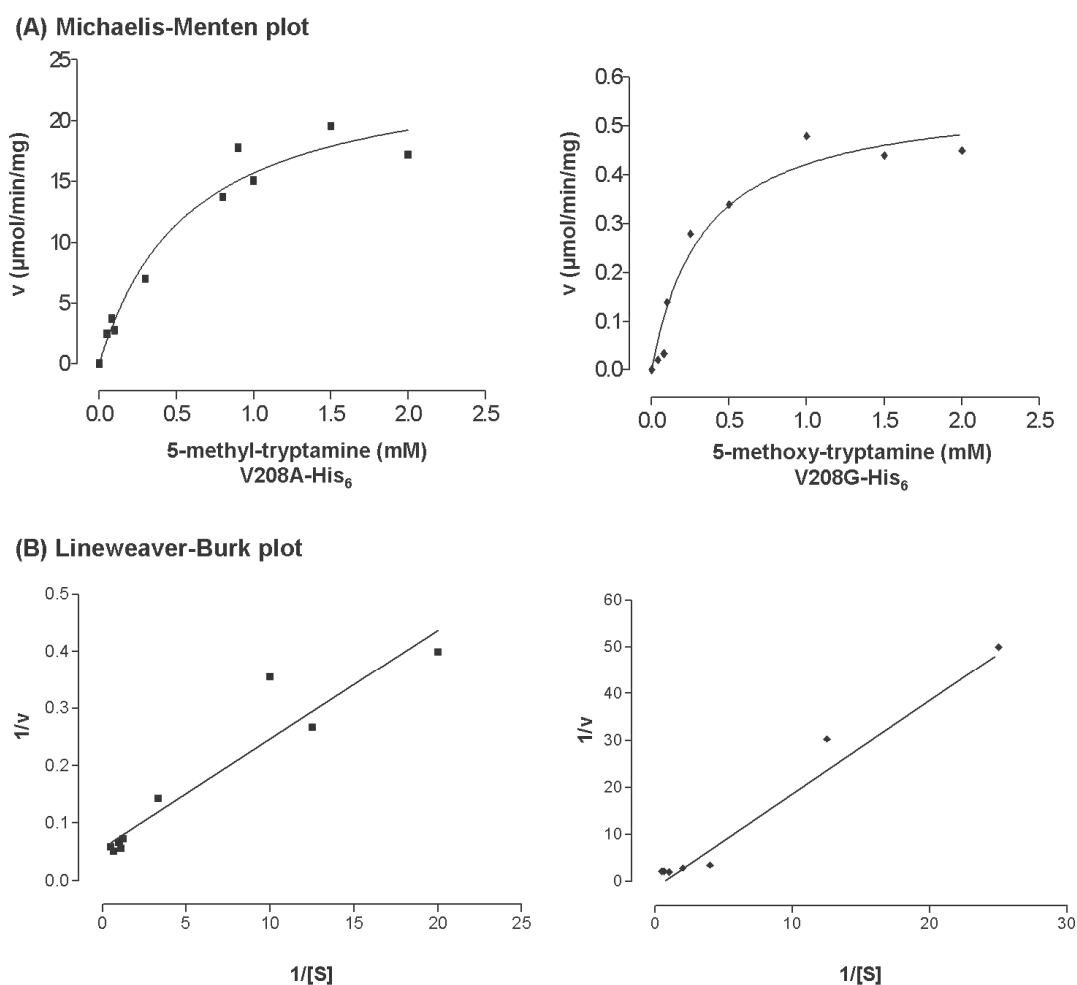
Figure 28. The kinetic diagrams of 5-methyl-tryptamine with V208A and 5-methoxy-tryptamine with V208G.
(A) Michaelis-Menten plots and (B) Lineweaver-Burk plots. The kinetic constants were calculated by non-linear regression. Lineweaver-Burk linear regression served as a control.

Detailed kinetic analysis was performed with STR1 wild-type and the mutants V208A and V208G (III.4.1.3) with varying substrate concentrations ranging from 0.001 – 2 mM while the concentration of secologanin was constantly 2 mM. Saturation conditions were achieved with substrate concentrations much higher than the respective enzyme concentration (up to 1000-fold) and at least 3-fold higher than the expected K_M value. Wild-type and engineered enzymes displayed Michaelis-Menten kinetics (MICHAELIS and MENTEN, 1913). Representative Michaelis-Menten plots of STR1 wild-type and several mutants, showing the relation between substrate concentration and reaction rate are given in Figure 28 and Figure 29. The kinetic results obtained in the current work are listed inTable 22. The Michaelis constant K_M is defined as the substrate concentration at which the velocity of the enzyme reaction is half the maximum reaction rate (v_{max}). It represents an affinity measure. The calculation of turnover number k_{cat} is based on the kinetic values obtained by non-linear regression. It represents the maximum number of enzymatic reactions catalyzed per second and together with the K_M value it allows for the calculation of the specificity constant k_{cat}/K_M

which gives a measure of the enzyme's conversion efficiency. The double reciprocal Lineweaver-Burk plot was used to illustrate the kinetic data. Thus the K_M and v_{max} values obtained by non-linear regression (using GraphPad Prism 3 software) were evaluated. Figure 28 shows two examples.
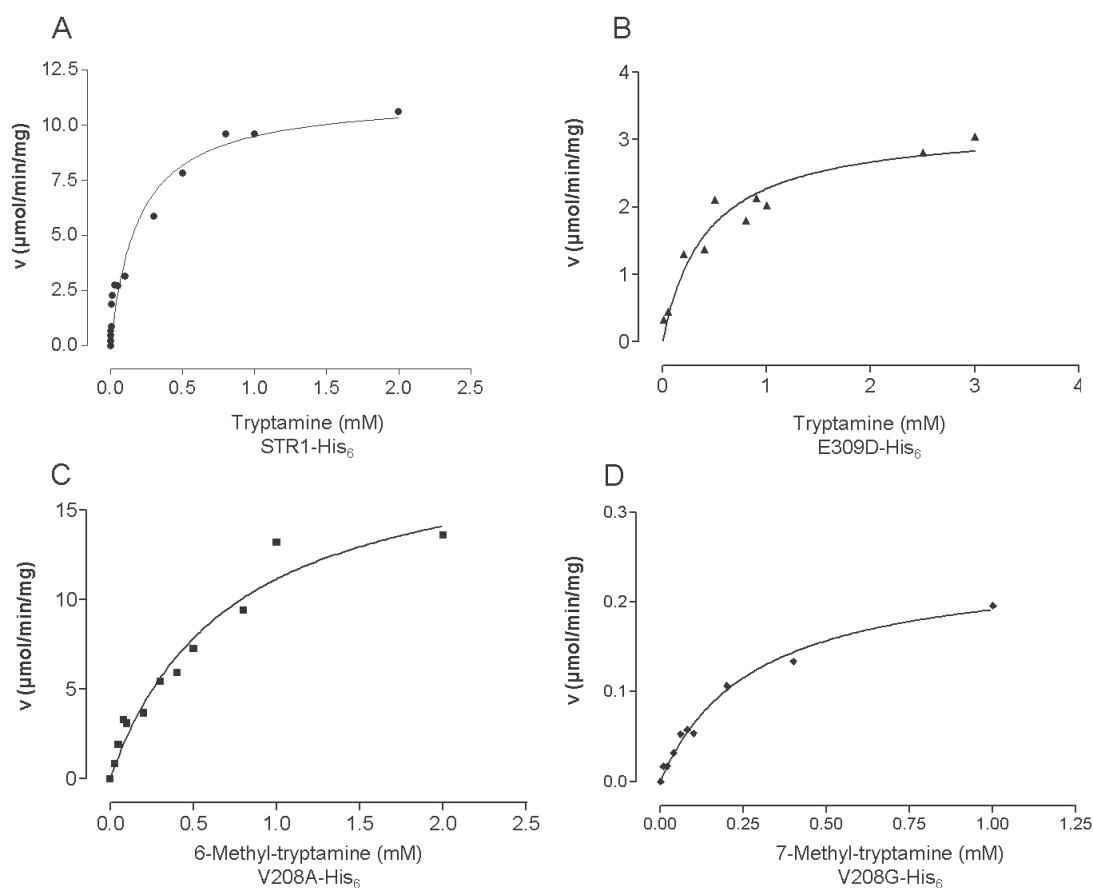
Figure 29. Selection of representative Michaelis-Menten plots. (A) STR1 wild-type with tryptamine, (B) E309D with tryptamine, (C) V208A with 6-methyl-tryptamine and (D) V208G with 7-methyl-tryptamine as substrate.

The kinetic results corresponded to the observations of relative activity and turnover studies and were consistent compared to each other. Highest affinity (e.g. lowest K_M value) was observed for the wild-type STR1 with its native substrate tryptamine (0.072 mM (± 0.02)). With 7-methyl-tryptamine the mutant V208A exhibited a similar K_M value (0.092 (± 0.03)) but the turnover number was very low. All other K_M values determined were higher than 0.1 mM. The mutants could not compete with the conversion efficiency of the wild-type enzyme. The native substrate tryptamine, together with both fluorine derivatives, was the best substrate for STR1, showing specificity constants of $k_{cat}/K_M > 100$ mM^{-1}/s^{-1}. Only the mutant V208A could approximate this level. For several substrates, such as 6-methyl-, 6-methoxy-tryptamine, and 5-hydroxy-tryptamine, the conversion by the mutant was more efficient than the wild-type conversion (ca. 2 – 10 times). Furthermore, the novel substrates 5-methyl- and 5-methoxy-

tryptamine were exclusively converted by the mutants with good efficiency (V208A k_{cat}/K_M > 20 mM^{-1}/s^{-1}).

For the determination of specific activity, substrate concentrations of 1 mM were used. Substrate decrease was monitored together with product formation, which served as a control. The reaction rate was calculated by substrate loss, using a calibration curve of the respective compound. The specific activity of mutant W149A was determined using high enzyme concentrations (10 – 40 µM) and long incubation times. This was necessary because W149A exhibited extremely low activity. Mutants V167A and E205V/V208A were more active and enzyme concentrations < 5 µM were employed. The results are given in Table 23.

Table 22. Kinetic data for wild-type His$_6$-tagged STR1 from *R. serpentina* and several mutants. (n.d. = reaction not detectable).

Substrate	Enzyme	K_M (mM)	k_{cat} (s^{-1})	k_{cat}/K_M (mM^{-1}/s^{-1})
Tryptamine	**STR1**	0.072 (± 0.02)	10.65	147.92
	V208A	0.219 (± 0.15)	11.31	51.64
	V208G	0.235 (± 0.05)	0.77	3.28
	E309D	0.418 (± 0.12)	1.98	4.73
5-Methyl-tryptamine	**STR1**	n. d.	n. d.	n. d.
	V208A	0.281 (± 0.13)	6.56	23.35
	V208G	0.356 (± 0.12)	0.35	0.99
6-Methyl-tryptamine	**STR1**	0.393 (± 0.17)	2.32	5.90
	V208A	0.762 (± 0.21)	10.95	14.37
	V208G	0.394 (± 0.01)	0.51	1.28
7-Methyl-tryptamine	**STR1**	0.367 (± 0.12)	1.02	2.78
	V208A	0.091 (± 0.03)	0.2	2.18
	V208G	0.279 (± 0.04)	0.14	0.49
5-Methoxy-tryptamine	**STR1**	n. d.	n. d.	n. d.
	V208A	3.592 (± 1.12)	79.66	22.18
	V208G	0.433 (± 0.14)	0.32	0.73

▼

91

Table 22. Continued.

6-Methoxy-tryptamine	**STR1**	0.962 (± 0.15)	5.32	5.53
	V208A	0.307 (± 0.01)	16.66	54.27
	V208G	0.286 (± 0.02)	0.13	0.44
5-Fluoro-tryptamine	**STR1**	0.259 (± 0.10)	37.46	144.63
	V208A	1.302 (± 0.13)	21.24	16.31
	V208G	0.860 (± 0.24)	0.68	0.79
6-Fluoro-tryptamine	**STR1**	0.136 (± 0.05)	23.37	171.84
	V208A	0.356 (± 0.09)	13.63	38.29
	V208G	0.404 (± 0.08)	0.84	2.07
5-Hydroxy-tryptamine	**STR1**	1.036 (± 0.25)	11.13	10.74
	V208A	0.844 (± 0.34)	18.12	21.47
	V208G	0.980 (± 0.18)	1.12	1.14

Table 23. Specific activity of mutants W149A and V167A, and double mutant E205V/V208A. His_6-tagged enzymes were employed. (n.d. = not detectable; / = not determined)

Mutant / Substrate	W149A (µmol/min/mg)	V167A (µmol/min/mg)	E205V/V208A (µmol/min/mg)
5-Methyl-tryptamine	< 0.001	0.29	0.15
5-Methoxy-tryptamine	0.001	0.23	0.13
N$_{(\alpha)}$-Acetyl-5-hydroxy-tryptamine	< 0.001	n.d.	n.d.
5-Fluoro-tryptamine	0.001	0.13	/
6-Fluoro-tryptamine	0.001	n.d.	/
5,7-dihydroxy-tryptamine	n.d.	/	/
6-Methyl-tryptamine	0.002	/	/
7-Methyl-tryptamine	0.002	0.48	/
6-Methoxy-tryptamine	0.001	n.d.	/

IV.6.4 Stereo-selectivity

A distinct feature of wild-type STR1 was its complete stereo-selectivity. The enzymatic Pictet-Spengler reaction, catalyzed by STR1, was leading exclusively to 3α-(*S*)-strictosidine. Therefore, the question whether the reaction catalyzed by the engineered mutants of STR1 exhibited full stereo-selectivity as well was investigated for at least one representative mutant, which was chosen to be V208A. The specific point mutation was carried out in the line of hydrophobic residues, which shielded the aromatic moiety of the indole framework (Val208, Val167, Trp149, Gly210). These residues supported the tryptamine position in the active site by means of van der Waals interactions. Since the indole sandwich, which contributed extensively to the orientation of tryptamine remained untouched, it was assumed that the exchange of any hydrophobic residue in this area did not disturb the stereo-selectivity of the enzymatic reaction.

The mutation E309D was an exception, since it was localized in close proximity to the primary amine group of tryptamine. Therefore, mutant V208A could not be representative in this case. Furthermore, the mutation E309D putatively influenced the stereo-specificity of the reaction. Though indole sandwich and hydrophobic line were still present, E309D offered certain flexibility near the reaction centre due to size reduction (about the size of one methylene group).

To investigate the stereochemistry at carbon 3, a method was applied which was used amongst others in 1977 by STÖCKIGT and ZENK to revise the originally incorrect assumption that the precursor of the monoterpenoid indole alkaloid family, arising from the enzymatic condensation of tryptamine and secologanin, would be 3-β-(*R*)- vincoside, the epimere of 3α-(*S*)-strictosidine. Until then, this compound had been assumed to be the common precursor of the monoterpenoid indole alkaloids. STÖCKIGT and ZENK proved 3α-(*S*)-strictosidine to be the key intermediate by ^{1}H-NMR analysis of acetylated strictosidine-lactam, which was obtained by lactamization and acetylation of strictosidine. The ^{1}H-NMR spectrum was in every respect identical to that of an authentic sample. The characteristic feature was an anomalous acetate signal shifted to higher field. The ^{1}H-NMR signals of 4 acetyl groups of strictosidine-lactam-tetraacetate were δ ($CDCl_3$, Me_4Si, 90 MHz) 2.06 ppm, 1.98 ppm and 1.87 ppm (9 H), and the anomalous acetate signal at 1.23 ppm (3H; STÖCKIGT and ZENK, 1977a).

A large-scale enzymatic preparation was carried out: 10-methyl-strictosidine and strictosidine were generated using the mutants V208A-His$_6$ and E309D-His$_6$ respectively as described in III.4.2. The compounds were isolated as lactam (strictosidine-lactam and 10-methyl-strictosidine-lactam) after heating the incubation mixture (4 h, 75 ° C; III.4.4). The

lactamization product was extracted into ethyl acetate and freeze dried. It was then acetylated and purified by thin layer chromatography (TLC; III.4.3.4). The obtained lactam-tetraacetate (Figure 30 B and Figure 31 B) was identified by ^{1}H-NMR spectroscopy. The ^{1}H-NMR data provided clear evidence for the 3-(S)-stereochemistry generated by the STR1 mutants.

Signals of four acetyl groups: 2.05 s (3H), 1.98 s (3H), 1.86 s (3H) and 1.18 s (3H) ppm for 10-methyl-stricosidine-lactam-tetraactetate (V208A); 2.03 s (3H), 1.96 s (3H), 1.83 s (3H) and 1.13 s (3H) ppm for strictosidine-lactam-tetraacetate (E309D). The high field shift of the acetyl group at 1.18 ppm in the 10-methyl-stricosidine-lactam-tetraacetate and at 1.13 ppm the strictosidine-lactam-tetraacetate spectrum indicates the 3α-(S)-configuration of the compounds (highlighted with #) in both Figure 30 and Figure 31).

10-Methyl-strictosidine-lactam-tetraacetate, R=CH₃
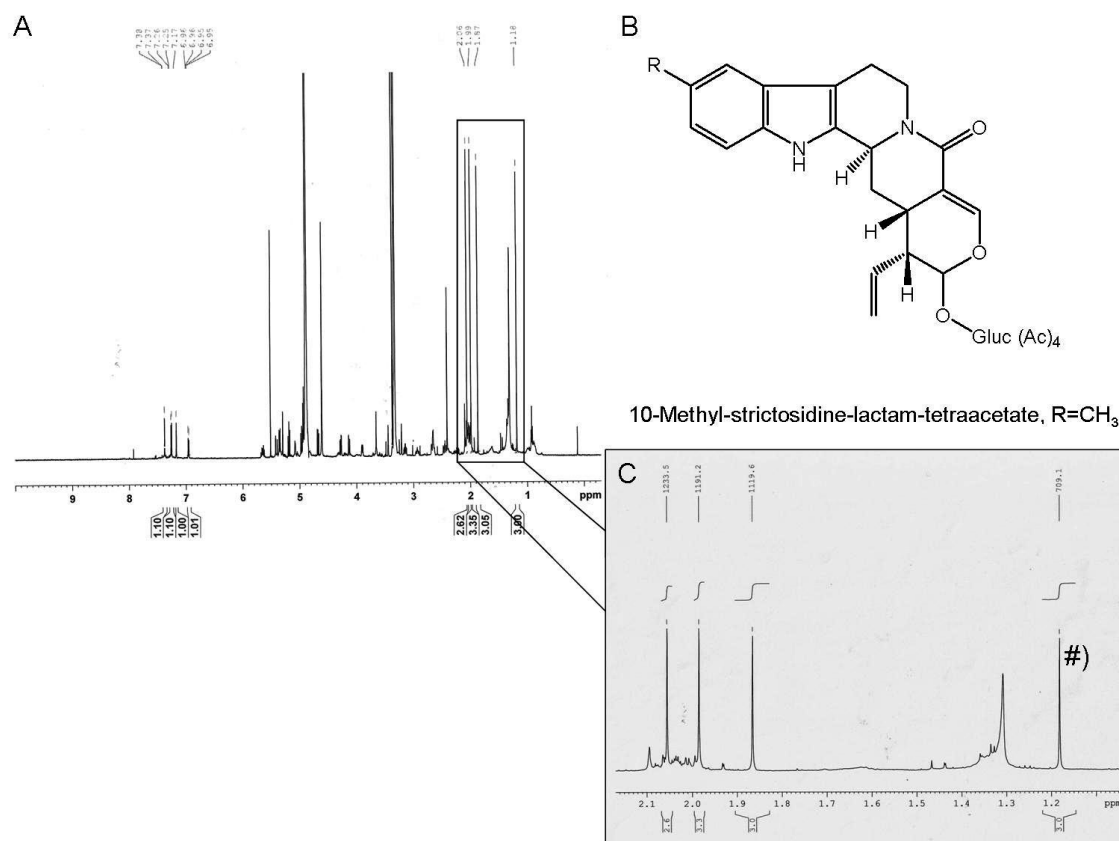
Figure 30. Identification of 10-methyl-strictosidine-lactam-tetraacetate. ^{1}H-NMR data of 10-methyl-strictosidine-lactam-tetraacetate, generated through the lactamization and acetylation of V208A product 10-methyl-strictosidine. (A) represents the overall ^{1}H-NMR spectrum, (B) its structure and (C) illustrates the zoomed region between 1.1 and 2.1 ppm. The high field shift of the acetyl group at 1.18 ppm #) indicates the 3α-(S)-configuration of the enzymatically formed 10-methyl-strictosidine.
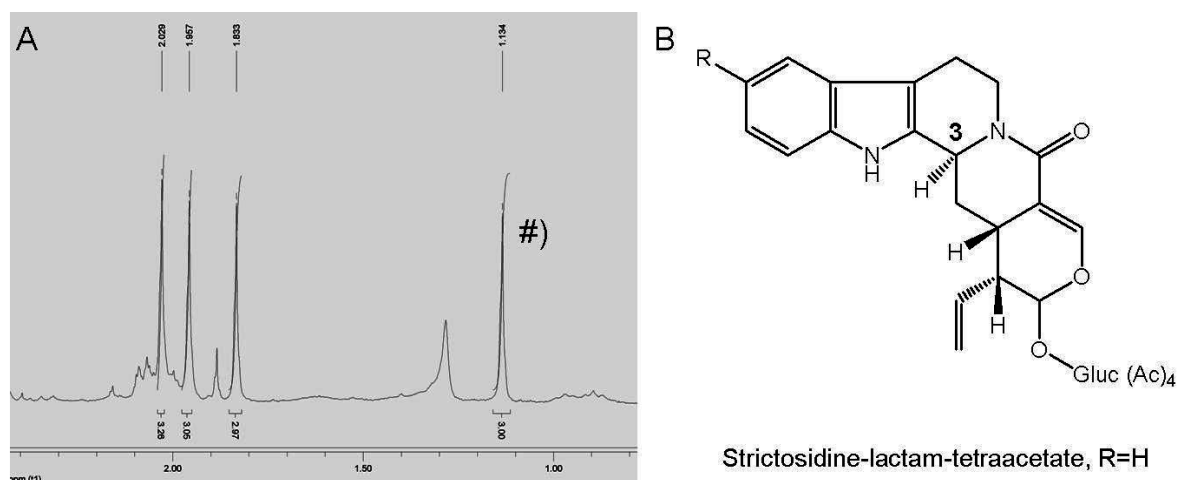
Figure 31. Identification of strictosidine-lactam-tetraacetate. ^{1}H-NMR data of strictosidine-lactam-tetraacetate (B) coming from strictosidine which was generated by STR1 mutant E309D. (A) represents a sequence from the overall ^{1}H-NMR spectrum and illustrates the region between 1.1 and 2.1 ppm. #) highlights the anomalous acetyl signal at 1.13 ppm, clearly indicating 3α-(*S*)-configuration.

IV.6.5 Basic research on the application of mutants for enzymatic synthesis of strictosidine analogues

This chapter summarizes all investigations performed in view of the preparative enzymatic synthesis of strictosidine analogues with engineered mutants. Namely, the time-conversion relationship and the effect of temperature and pH on the enzymatic reaction were investigated. Furthermore, initial experiments with immobilized enzyme were performed to explore whether this facile approach could be considered in future.

IV.6.5.1 Turnover-studies

The rational, efficient production of novel strictosidine derivatives with engineered mutants of STR1 is a major prospect of this work. Therefore it was necessary to investigate the time-conversion relationship in order to find the requirements for an optimal conversion of the respective tryptamine derivatives and efficient enzymatic synthesis of strictosidine analogues. The results are presented in two major groups: the first represents the substrates which are not accepted by the wild-type enzyme and can exclusively be converted by engineered mutants (namely 5-methyl- and 5-methoxy- tryptamine, IV.6.5.1.1). The second includes compounds which are available with STR1 wild-type. The enzymatic synthesis of the respective strictosidine derivatives should be optimized by use of engineered mutants. In order to check the benefit of mutants for this purpose and to obtain direct comparison, turnover studies were performed for selected mutants and tryptamine analogues and are presented in paragraph IV.6.5.1.2.

Considering the results from substrate screening and enzyme kinetics, a preliminary selection was made. Due to low reaction rates, mutants V208G, E205V/V208A and W149A were not included, although the latter apparently accepted $N_{(\alpha)}$-acetyl-5-hydroxy-tryptamine, a compound which was not converted by STR1 or by another mutant. Conversion was too low, even to prove identity of the product peak. Mutants V167A and V167G were not available in suitable amounts due to low expression rates. Therefore the studies focused on mutant V208A.

IV.6.5.1.1 Enzymatic synthesis of novel strictosidine analogues, 10-methyl- and 10-methoxy-strictosidine, by mutant V208A-His$_6$

For the two tryptamine analogues, which could be converted for the first time with the mutant V208A, a conversion on preparative level was confirmed. The novel strictosidine analogues 10-methyl- and 10-methoxy-strictosidine were available in mg amounts. The other re-engineered enzyme with mutation of 208 (V208G) can not compete with V208A in terms of activity as shown by the obtained kinetic results (IV.6.3.3, Table 22). Double mutant E205V/V208A (His$_6$-tagged) also exhibits significantly lower activity with the novel compounds. Relative activity of E205V/V208A compared to V208A is shown in Table 24. Using V208A, it was possible to convert > 90 % 5-methyl-tryptamine within 90 min and > 50 % of 5-methoxy-tryptamine (each 1mM in the incubation mixture) within 240 min (Figure 32).

Table 24. Relative activity of E205V/V208A-His$_6$ compared to V208A-His$_6$. Relative activity was determined using identical incubation conditions for both enzymes (n = 2). Activity of V208A was referred to as 100 %. Substrate concentration was 1 mM. Two different enzyme concentrations were employed.

Enzyme concentration	10-Methyl-strictosidine	10-Methoxy-strictosidine
5.4 µM	41.4 %	10.8 %
21.6 µM	77.4 %	7.9 %

The comparison of two tested incubation temperatures (28 °C and 35 °C) showed no major differences in the time-conversion plot of 5-methyl-tryptamine (Figure 32 A). With the investigated conditions (each substrate 1 mM, V208A 3.7 µM), it was possible to produce 1 mg of 10-methyl-strictosidine within less than 2 h using the enzyme yield from ca. 1.5 l bacterial culture (Table 25).

For the enzymatic synthesis of 1 mg 10-methoxy-strictosidine the enzyme yield from at least 2.5 l bacterial culture was necessary. The conversion of 5-methoxy-tryptamine at 35 °C demonstrated higher efficiency (Figure 3 B) compared to 28 °C. Increasing the enzyme's

concentration, together with a reduction of substrate concentration accelerated the conversion significantly. By changing the enzyme-substrate ratio from 1:270 to 1:67 as shown in Table 25, a 3.2-fold reduced incubation time is sufficient for the recovery of 1 mg 10-methoxy-strictosidine.
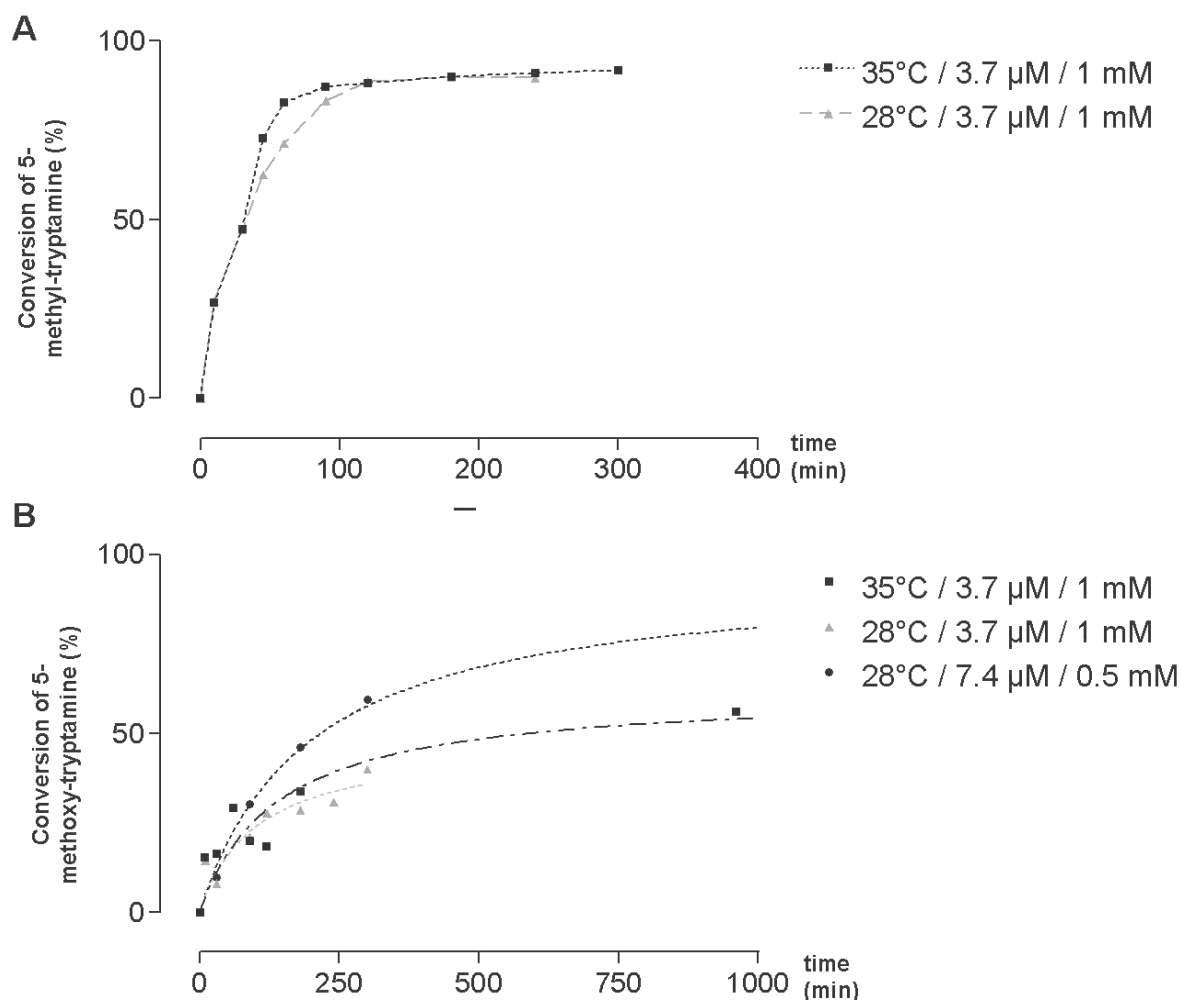
Figure 32. Conversion of 5-methyl-and 5-methoxy-tryptamine by mutant V208A. (A) shows the conversion (%) of 5-methyl-tryptamine by V208A at two different temperatures. (B) compares the conversion of 5-methoxy-tryptamine at two different temperatures (28 ° C versus 35 ° C) and two different enzyme-subst rate ratios. The conversion is plotted against the time (min).

Lactam formation was observed in all incubations longer than 30 min. The retention time of 10-methyl-strictosidine-lactam was ca. 10 min and 10-methoxy-strictosidine-lactam ca. 9 min using the HPLC assay described in III.4.3.1. As shown in Figure 33 lactam formation depended on incubation temperature. Low temperatures benefit the stability of 10-methyl-strictosidine and reduced lactamization. High temperatures and long incubation times accelerated the lactamization. The lactam formation increased in the beginning, and settled

down on a more or less constant level after different periods of time (30 – 300 min). Apparently it did not influence the strictosidine formation very much, presumably due to a compensating reaction. Although lactamization was clearly reduced at 28 °C (Figure 33 A, B), the product formation was initially equal. Later the reaction at 35 °C was benefited from the higher temperature.
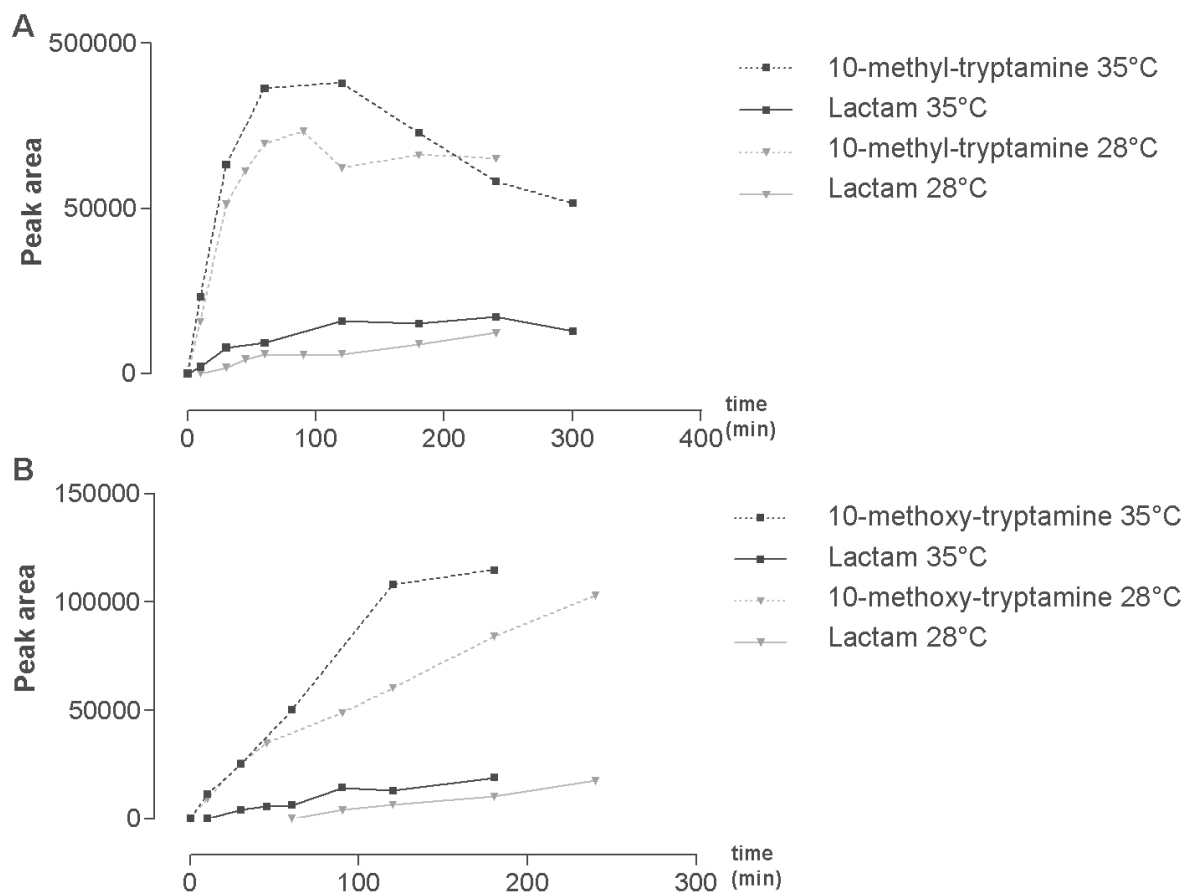
Figure 33. Formation of 10-methyl- and 10-methoxy-strictosidine by mutant V208A- His$_6$. The peak area is plotted against the time (min). Reaction was performed using two different incubation temperatures (28 °C versus 35 °C) while all other parameters were identical. Furthermore the respective lactam formation is included. (A) The formation of 10-methyl-strictosidine and its lactamization product is presented. (B) shows the formation of 10-methoxy-strictosidine and its lactam.

Table 25. How to get 1 mg of 10-methyl- and 10-methoxy-strictosidine. Conclusions are drawn from turnover studies under the listed conditions. The amount of enzyme for the synthesis of 1 mg of the novel strictosidine analogues and respectively required volume of bacterial culture were calculated on the basis of the time-conversion plot and the yield of expression and purification. 5-Me = 5-methyl-tryptamine, 5-MOX = 5-methoxy-tryptamine.* referred to standard expression protocol.

Incubation conditions (compound and respective concentration / temperature / enzyme concentration)	Amount of V208A necessary to yield 1 mg product		Incubation time (h)	Substrate conversion (%)
	V208A (mg)	Bacterial culture volume*		
5-Me 1 mM / 35°C / 3.7 µM	0.3	ca. 1.5 l	< 2	90
5-Me 1 mM / 28°C / 3.7 µM	0.3	ca. 1.5 l	< 2	90
5-MOX 1 mM / 35°C / 3.7 µM	0.6	ca. 3 l	16	60
5-MOX 1 mM / 28°C / 3.7 µM	0.4	ca. 2 l	16	60
5-MOX 0.5 mM / 35°C / 7.4 µM	1.6	ca. 8 l	5	60
5-MOX 0.5 mM / 35°C / 7.4 µM	1.3	ca. 7.5 l	22	80

IV.6.5.1.2 Comparison: wild-type versus mutant activity with tryptamine analogues

Turnover studies were performed under identical conditions for wild-type and mutant to provide comparability. Time-conversion plots were generated based on middle-scale incubations of the respective compounds and enzymes (STR1-His$_6$ and V208A-His$_6$; 35 °C). Enzyme assay contained, respectively 3.7 µM enzyme, 1 mM tryptamine analogue and 1 mM secologanin in a total volume of 700 µl. Aliquots of 50 µl were taken after different time periods and analyzed via HPLC (t = 0 – 1200 min). Strictosidine analogue formation as well as substrate loss was monitored by HPLC.

The graphs A, B1 and C of Figure 34 display the representative raw data (integrated peak area) obtained by HPLC for the conversion of 6-methyl-tryptamine by mutant V208A, and illustrate the investigation procedure. As shown in Figure 34 A, product formation and substrate loss corresponded to each other. After 30 min, 6-methyl-tryptamine ("6-Me" in Figure 34 A) and secologanin were converted almost 90 %. The HPLC trace B1 in Figure 34 represents the mutant preparation at t = 30 min. The comparison of the wild-type HPLC trace with these substrates after the same period of time under identical conditions (B2) illustrates and emphasizes the difference in activity with this substrate. The formation of 11-methyl-strictosidine ("11-Me") by mutant and wild-type is compared in Figure 34 C, as well as 6-methyl-tryptamine conversion in Figure 34 D.
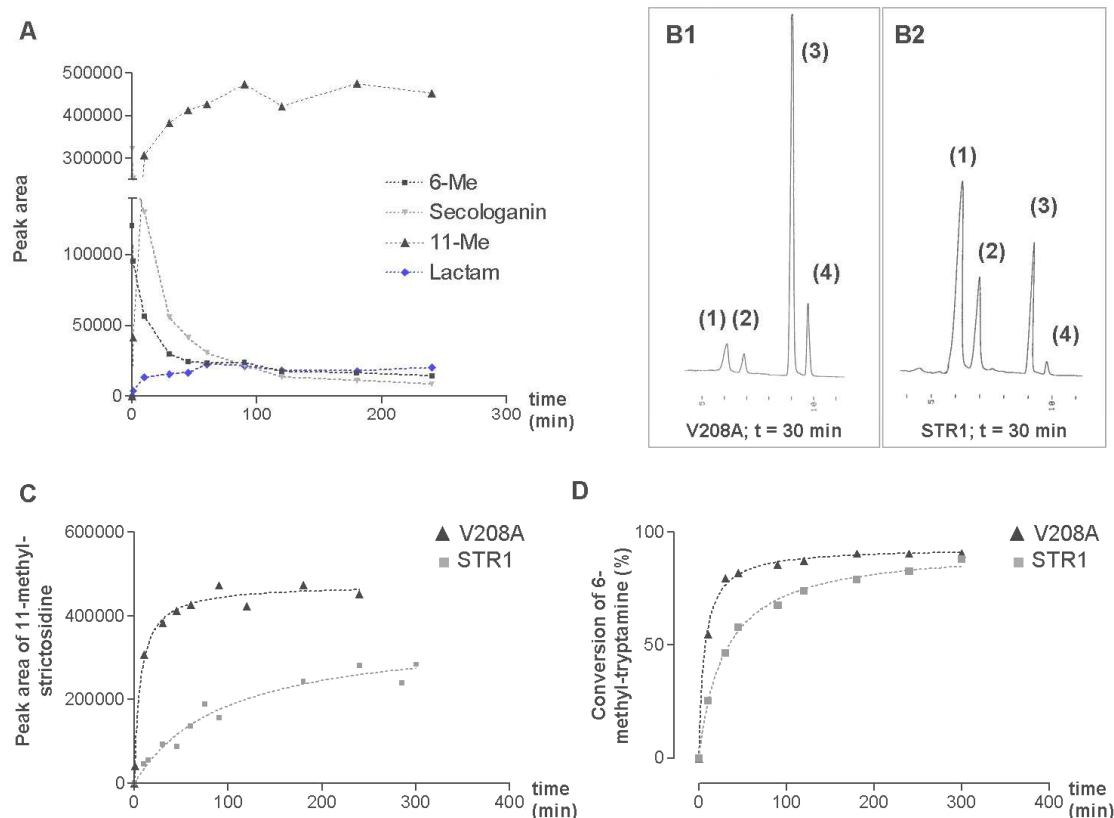
Figure 34. Activity of mutant V208A-His$_6$ with 6-methyl-tryptamine compared to wild-type. (A) Raw data of HPLC detection are shown; namely product formation by mutant V208A-His$_6$ (11-methyl-strictosidine ▲ "11-Me"), substrate loss (6-methyl-tryptamine ■ "6-Me" and secologanin ▽) and lactam formation (in blue). (B1) and (B2) HPLC traces provide direct comparison of 11-methyl-strictosidine formation by mutant V208A-His$_6$ (B1) and STR1 wild-type (B2) after 30 min reaction time. Retention times were: (1) secologanin 5.9 min; (2) 6-methyl-tryptamine 6.8 min; (3) 11-methyl-strictosidine 8.9 min; (4) 11-methyl-strictosidine lactam 9.8 min. (C) 11-methyl-strictosidine formation by mutant V208A (▲) and wild-type STR1 (■); the peak area is plotted against the time. (D) Time-conversion plot of 6-methyl-tryptamine by STR1 wild-type (■) and mutant V208A (▲).

Five tryptamine derivatives (listed in Table 26) were investigated as exemplified above by compound 6-methyl-tryptamine. The turnover studies exhibited two substrates, whose conversion clearly benefit from the engineered mutant: 6-methyl- and 6-methoxy-tryptamine. As shown in Figure 34, the enzymatic synthesis of 11-methyl-strictosidine, employing the mutant V208A-His$_6$, was more efficient than wild-type synthesis. The same was found for the conversion of 6-methoxy-tryptamine, which is illustrated in Figure 35.
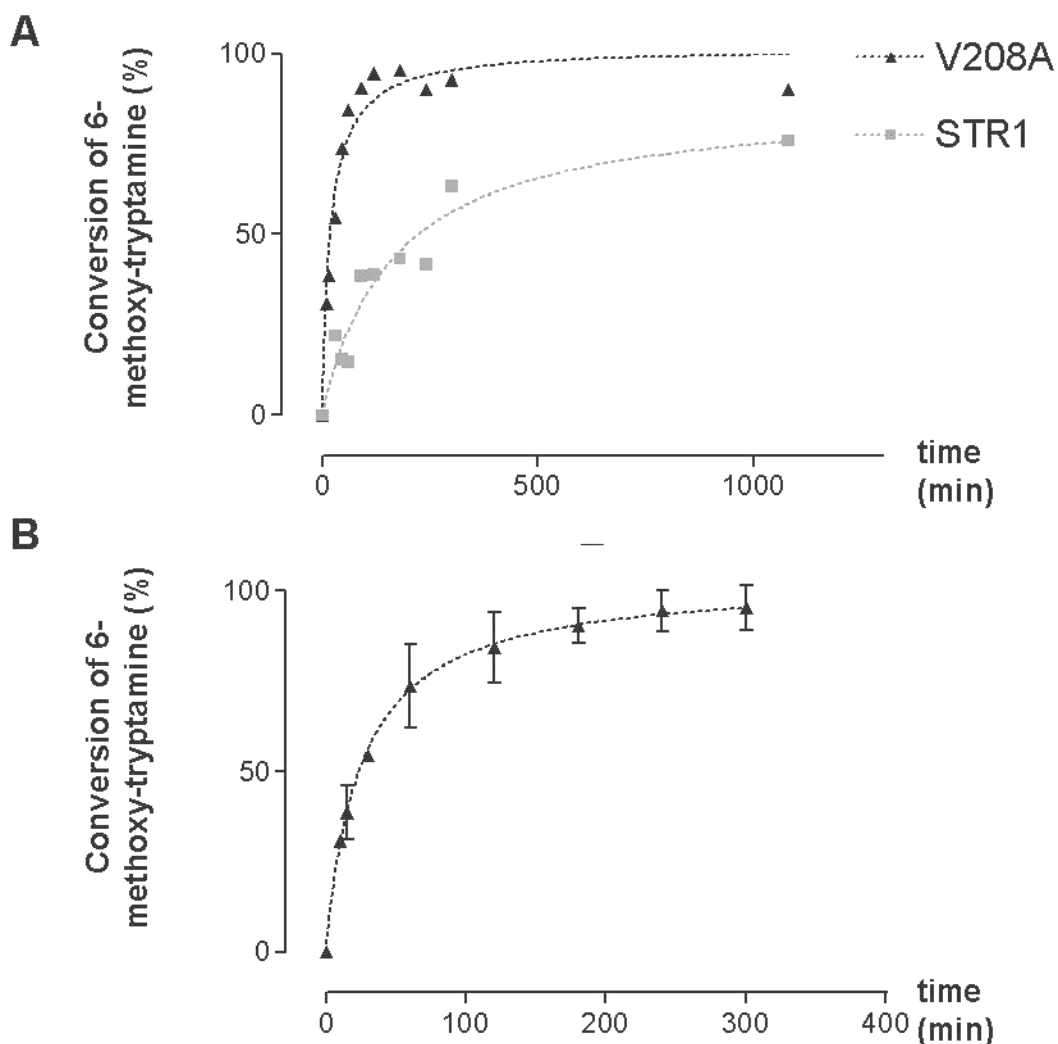
Figure 35. Conversion of 6-methoxy-tryptamine by wild-type and mutant V208A. (A) Direct comparison of the conversion of 6-methoxy-tryptamine by STR1 wild-type (■) and mutant V208A-His$_6$ (▲) is displayed. Further experiments with mutant V208A-His$_6$ confirmed reproducibility. The representative time – conversion plot (B) shows the average conversion of 6-methoxy-tryptamine by mutant V208A-His$_6$ obtained from 3 independent experiments.

To estimate the practical use of the re-engineered enzymes for preparative enzymatic synthesis of strictosidine derivatives, the requirements for the recovery of 1 mg strictosidine analogue were investigated. A reaction mixture containing 1 mM 6-methoxy-tryptamine, 1 mM secologanin and 3.7 µM STR1-His$_6$ needs 18 h to yield 1 mg product (conversion 75 %) while the mutant V208A-His$_6$ achieved this result within 3 h under identical conditions. With the 6-methyl-derivative the mutant achieved a 5.4-fold reduced incubation time. Results are listed in Table 26.

For the conversion of compound 5-hydroxy-tryptamine by mutant V208A, a benefit could be detected compared to wild-type STR1. The kinetic results provided a 2-fold higher specificity constant (k_{cat}/K_M) indicating an increased conversion efficiency of the mutant (k_{cat}/K_M of

V208A was 21.47 mM^{-1}/s^{-1} versus 10.74 mM^{-1}/s^{-1} for STR1). However, the current turnover study exhibited similar activity levels for the employed conditions.

Table 26. Preparative enzymatic synthesis of selected strictosidine analogues. Listed incubation conditions were investigated. The results represent theoretical calculations based on the observed reaction rates and purification yields. 6-Me = 6-methyl-tryptamine, 6-MOX = 6-methoxy-tryptamine, 5-F = 5-fluoro-tryptamine, 6-F = 6-fluoro-tryptamine, 5-OH = 5-hydroxy-tryptamine. * referred to standard expression protocol.

Strictosidine (analogue)	Incubation conditions (substrate and its concentration / temperature / enzyme concentration)	Requirements to yield 1 mg product			Yield of converted substrate (%)
		Enzyme (mg)	Bacterial culture volume*	Time (h)	
Strictosidine	TRM 1 mM / 35 °C / 3.7 µM	0.30 STR1	ca. 1 l	0.05	> 95 %
11-Methyl-strictosidine	6-Me 1 mM / 35 °C / 3.7 µM	0.28 STR1	< 1 l	2.7	88 %
	6-Me 1 mM / 35 °C / 3.7 µM	0.32 V208A	2 l	0.5	80 %
	6-Me 1 mM / 28 °C / 3.7 µM	0.28 V208A	1.5 l	1.5	93 %
11-Methoxy-strictosidine	6-MOX 1 mM / 35 °C / 3.7 µM	0.32 STR1	1 l	18	75 %
	6-MOX 1 mM / 35 °C / 3.7 µM	0.33 V208A	2 l	3	75 %
	6.MOX 1 mM / 28 °C / 3.7 µM	0.30 V208A	1.5 l	3	85 %
10-Fluoro-strictosidine	5-F 1 mM / 35 °C / 3.7 µM	0.27 STR1	< 1 l	0.5	90%
	5-F 1 mM / 35 °C / 3.7 µM	0.28 V208A	ca. 1.5 l	5	90 %
11-Fluoro-strictosidine	6-F 1 mM / 35 °C / 3.7 µM	0.26 STR1	< 1 l	0.5	95%
	6-F 1 mM / 35 °C / 3.7 µM	0.28 V208A	ca. 1.5 l	5	9 2 %
10- Hydroxy-strictosidine	5-OH 1 mM / 35 °C / 7.4 µM	0.27 STR1	< 1 l	4	90%
	5-OH 1 mM / 35 °C / 7.4 µM	0.28 V208A	ca. 1.5 l	4	90%

IV.6.5.1.3 Effect of temperature and pH on activity of STR1 mutants V208G-His$_6$ and W149A-His$_6$

The mutants W149A and V208G were not suitable for turnover studies due to poor activity with tryptamine derivatives. Nevertheless, they should be characterized. Temperature- and pH-optima were determined using the standard activity assay. The conversion of tryptamine was tested at different incubation temperatures, ranging from 5 – 70 °C. The enzymes were applied in concentrations of respectively 1.2 µM (V208G) and 10 µM (W149A). For investigation of the pH-effect, the enzymes were incubated with tryptamine and secologanin (each 1 mM) in KPi buffer of different pH values, ranging from 4.8 – 8.8. Mixtures of 1M

KH_2PO_4 and 1M K_2HPO_4 were used to adjust pH, and were diluted to a final concentration of 50 mM. Enzyme concentrations were 2.5 µM (V208G) and 10 µM (W149A).

The highest enzyme activity was detected at a temperature of 50 °C for both mutants (Figure 36). The pH-optimum for mutant V208G activity was detected to be 7.0. For mutant W149A the pH-optimum was shifted to pH 6.2 (Figure 37). At pH 4.8, W149A still exhibit 75.6 % relative activity, while mutant V208G showed only 41.6 %.
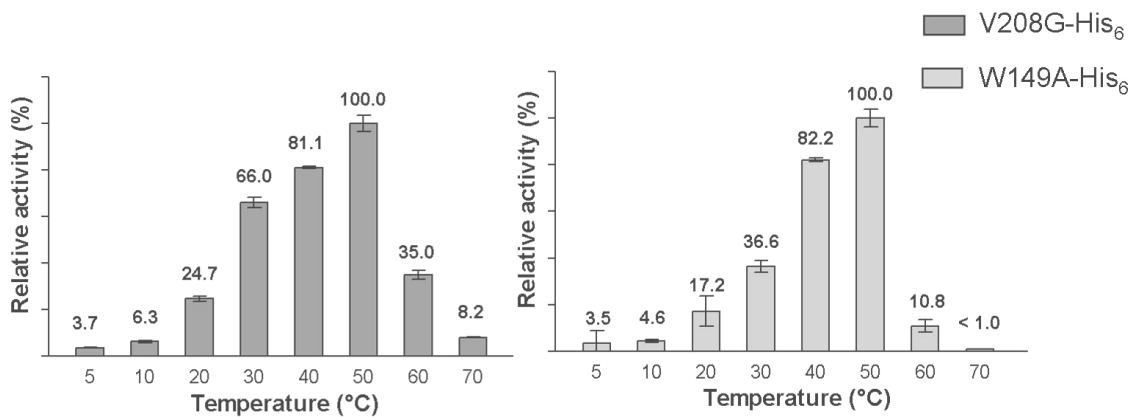
Figure 36. The effect of temperature on the relative activity of STR1 mutants V208G (■) and W149A (■). The optimum temperature for the enzymes' activity was 50 °C. Specific activity was 0.52 µmol/min/mg fo r V208G and 0.03 µmol/min/mg for W149A (respectively relative activity of 100 %).
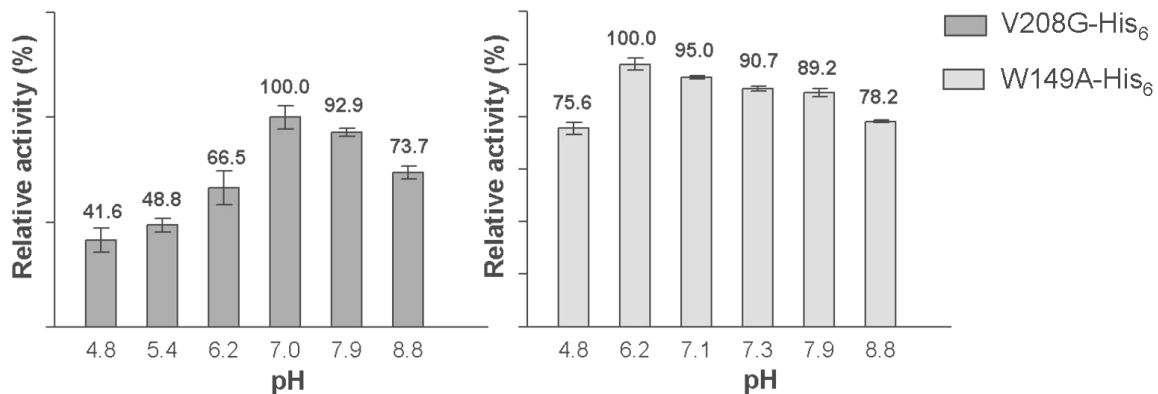
Figure 37. The effect of pH on the relative activity of His₆-tagged V208G and W149A. The pH-optimum is determined to be 7.0 for mutant V208G (with specific activity of 0.37 µmol/min/mg as relative activity of 100 %) and 6.2 for mutant W149A (specific activity of 0.007 µmol/min/mg referred to as relative activity of 100 %).

IV.6.5.2 Experiments with immobilized STR1-mutant V208A

The opportunities of a flow through assay, by use of His$_6$-tagged enzymes and Ni-NTA matrix, were investigated. The question, whether His$_6$-tagged STR1 (and its mutants) bound to Ni-NTA matrix was active, should be answered. The experiment was inspired by a successful and efficient approach to preparative synthesis of strictosidine with immobilized STR from *C. roseus* described by PFITZNER and ZENK (1982).
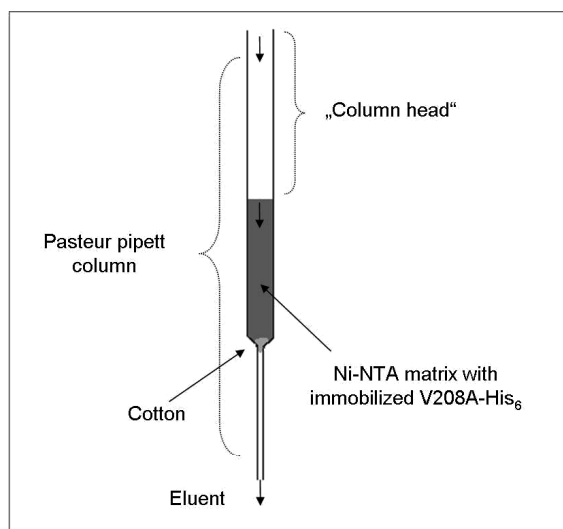
Figure 38. Experiment with immobilized V208A-His$_6$. The illustration of the applied column is displayed above. Below: parameters of the experimental procedure with immobilized V208A-His$_6$ are listed.

Column	A	B
Bed volume	0.6 ml	0.8 ml
Amount of V208A_His$_6$	129 µg	171 µg
Substrates	5-methyl-tryptamine + secologanin	5-methoxy-tryptamine + secologanin
Product	10-methyl-strictosidine	10-methoxy-strictosidine

For an initial investigation His$_6$-tagged STR1 mutant V208A was purified and dialyzed against an excess of 50 mM KPi buffer pH 7.0 as described (III.4.2.2). The final concentration of the enzyme preparation was 300 µg/ml. Fresh Ni-NTA material (1 g) was suspended in 2 ml distilled water and 1 ml V208A preparation, for loading the enzyme to the Ni-NTA matrix (stirring for 60 min at 4 °C). Two Pasteur-pipette s (A and B), which were closed with cotton, served as columns (Figure 38). The suspension was filled into the columns (Ni-NTA bed volume (A) 0.6 and (B) 0.8 ml), and the protein concentration of the flow through measured by Bradford to make sure, the enzyme was completely loaded. No enzyme was detected in the flow through fractions of the loading procedure, and the amount of immobilized enzyme on the columns was calculated to be (A) 129 µg and (B) 171 µg per column. This corresponds to a concentration of 5.8 µM, considering the Ni-NTA bed volume. By washing

the column with water at RT, the flow rate was set to 2 – 3 ml/h. Aqueous, un-buffered, 10 mM solutions of the substrates (secologanin, 5-methyl- and 5-methoxy-tryptamine) were separately transferred onto the columns in alternating steps. They were mixed in the "column head" by up and down pipetting, before slowly passing the Ni-NTA matrix with the immobilized enzyme. The column eluent was collected in fractions. Samples were analyzed by HPLC. Features of the columns are summarized in Figure 38.
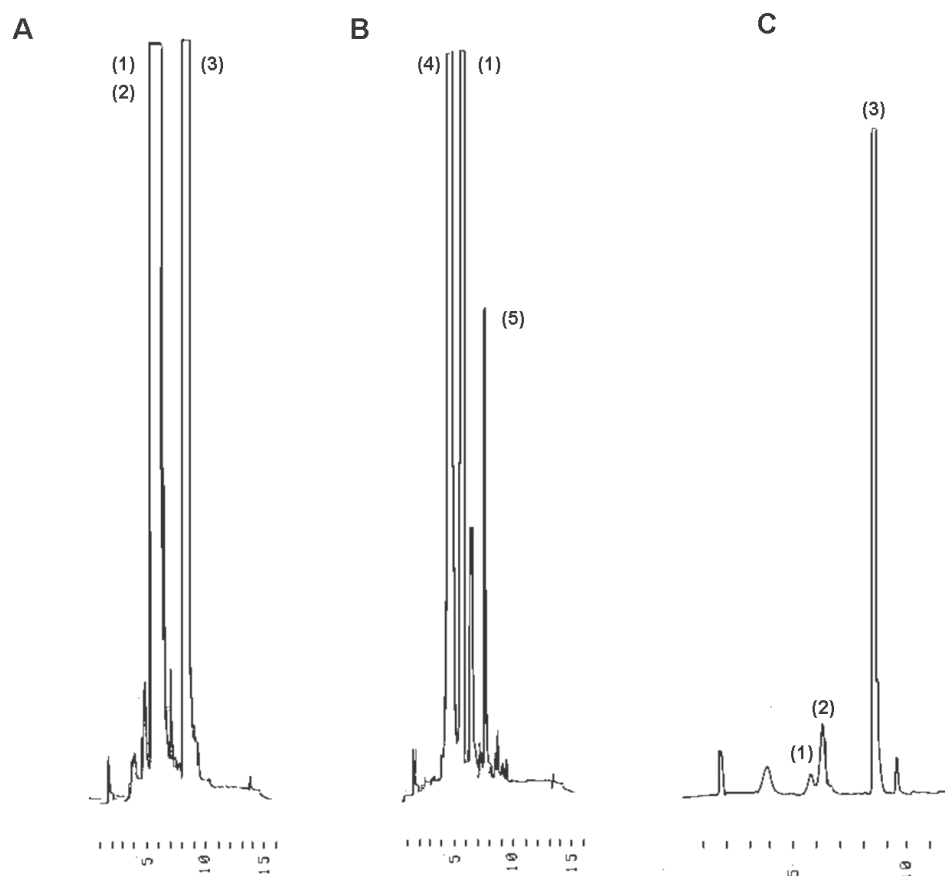
Figure 39. HPLC analysis of enzymatic synthesis with immobilized V208A-His$_6$. (A) and (B) show HPLC traces of reaction fractions passing the columns A and B respectively, with a flow rate of ca. 2 – 3 ml/h. (C) displays the HPLC trace of a diluted fraction of column A which stayed 14 h (overnight) in the column exhibiting almost 90 % conversion of the substrates. Retention times: (1) secologanin 5.7 min; (2) 5-methyl-tryptamine 5.9 min; (3) 10-methyl-strictosidine 8.6 min; (4) 5-methoxy-tryptamine 4.8 min; (5) 10-methoxy-strictosidine 7.6 min.

His$_6$-tagged mutant V208A, immobilized on Ni-NTA matrix, was active, as shown in Figure 39. It can be applied for preparative synthesis of strictosidine (analogues), in a flow through assay. It was concluded, that this was true for His$_6$-tagged STR1 wild-type and the other mutants as well. Buffered solutions were not mandatory, but conversion in aqueous solution was not optimal. By use of a flow rate of 2 – 3 ml/h, a complete conversion of the substrates was not achieved. The product amount was ca. 25 % 10-methyl-strictosidine and 3 % 10-

methoxy-strictosidine as estimated from the HPLC trace. Figure 39 C displays the HPLC trace of a reaction fraction that stayed in the column for 14 h. Here the product amount was higher (ca. 70 %). A column system, allowing for a better regulation of the flow volume and velocity, is recommended for preparative synthesis. A better conversion and reaction yield can be expected from longer residence of substrates in the column: the solutions should pass the immobilized enzyme more slowly. The stability of the immobilized enzyme was given up to 24 h at RT.

IV.6.6 Special case: The low expression of V167A-His$_6$ und V167G-His$_6$

The mutagenesis of the residue V167 resulted in critical enzyme variants. Both generated mutants (V167A-His$_6$ and V167G-His$_6$) could not be purified in higher yields by Ni-NTA affinity chromatography using natural conditions (without denaturizing agents). Mutant V167A-His$_6$ was only available in extremely low yields (< 0.01 mg/l LB culture), while V167G-His$_6$ was not obtained in soluble form at all. No activity was detected in the elution fractions (using maximum amount of enzyme solution and incubation times up to 24 h). A protein band at 37 kDa (where V167G-His$_6$ was expected) was not detected by SDS PAGE analysis. Instead, a band of ca. 15 kDa was observed in crude extracts of both, V167G-His$_6$ and V167A-His$_6$. In contrast to V167G-His$_6$, in the eluent fractions of V167A-His$_6$, a protein band at 37 kDa was clearly detectable and the enzyme was active with tryptamine and several other compounds.

Similar protein bands were never detected in any other mutant preparation or in native M15 cells (see Figure 40 A, line 1 and 2). Therefore it was concluded that this unknown protein was no genuine protein of M15 cells. It clearly correlated with the plasmids *str1_V167A*-pQE2 and *str1_V167G*-pQE2. Figure 40 A shows that these bands exclusively occurred in M15 cells containing the specific plasmids. Neither W149A nor "native" M15 cells (line 1 and 2) expressed such proteins. Their occurrence appeared to depend on the concentration of IPTG during gene expression (Figure 40 B): with increasing IPTG levels, the size of the protein bands increased too. Without IPTG, the specific bands were not observed[9].

---

[9] The sequencing of the unknown protein bands should be considered in future.
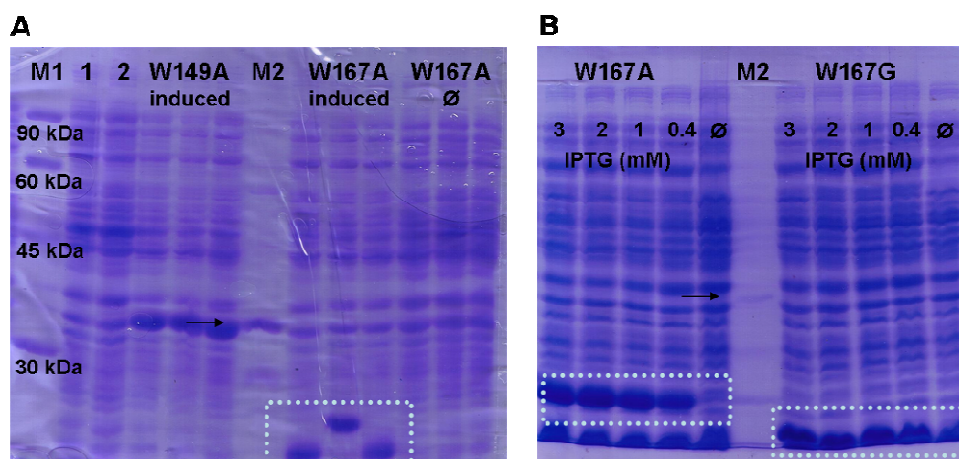
Figure 40. Protein artifacts of *str1_V167A*-pQE2- and *str1_V167G*-pQE2-competent M15 cells. (A) three different colonies of M15 cells expressing *str1_V167A*-pQE2 or *str1_W149A*-pQE2 plasmid ("induced"). The three lines on the right show the three *str1_V167A*-pQE2 containing colonies without IPTG induction. M1 = marker proteins, M2 = authentic STR1-His$_6$ as marker. The lines 1 and 2 represent M15 cells without expression vector (native M15 cells) induced (1) and not induced (2) by IPTG addition. (B) SDS PAGE of V167A and V167G colonies, which were induced by addition of different concentrations of IPTG (0 – 3 mM). An arrow highlights STR1-His$_6$ at 37 kDa. The light blue frames include the unknown protein bands which occurred after induction.

IV.7 The structure of the engineered STR1 variants

IV.7.1 Crystallization experiments

The observed substrate specificity of the His$_6$-tagged mutants V208A, V208G and the double mutant E205V/V208A confirmed the author's structural analysis and engineering strategy. It was a main concern to illustrate this with the crystal structures of the mutant(s). To obtain insight into the mutants' structures, crystallization experiments were carried out several times with the de-tagged mutants V208A and V208G. The enzymes were produced and purified as described for the wild-type enzyme's crystallization (III.3), including the removal of His$_6$-tag by DAPase digestion. After dialysis against the crystallization buffer (10 mM Tris-HCl, pH 8.0), the purity of the enzyme preparations was evaluated by SDS PAGE, and the protein solutions concentrated to final concentrations of > 5 mg/ml. As successfully applied previously, the hanging drop vapor diffusion method was used (III.3.1).

Unfortunately, none of the crystallization experiments resulted in crystals. In most cases brown amorphous precipitate was observed which was a characteristic of denaturized protein. Skin on the drops occurred several times. This too was believed to be a layer of denaturized protein. The denaturation of proteins can be reduced by slowing down the rate of vapor diffusion, e.g. by lowering the temperature.
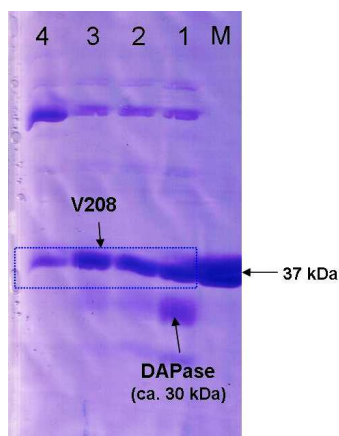
Figure 41. SDS PAGE showing the DAPase digest result of mutant V208A. M = authentic STR1-His$_6$ as marker (partly overlaid from a neighboring band, which is not displayed); 1 = DAPase reaction mixture after an incubation period of 6h, displaying complete digestion; 2 = eluted fraction of the purification of digestion mixture by affinity chromatography on Ni-NTA; 3 and 4 = two different charges of V208A solutions ready for crystallization (both desalted and concentrated up to > 5 mg/ml); 3 comes from a standard elution with 250 mM imidazole buffer, 4 includes the 50 mM imidazole wash buffer fractions which contain high concentrations of V208A-His$_6$. Both did not successfully crystallize.

Another reason for the failing of crystallization experiments was probably an insufficient purity of the enzyme preparation for crystallization experiments (Figure 41). Unlike the wild-type, the mutants were partly accompanied by higher amounts of persisting impurities, which might have disturbed crystallization. The wild-type crystallization preparation exhibited ca. 10 % impurities, which were supposed to facilitate the nucleation procedure during STR1 crystallization and therefore benefit the crystal growth (KOEPKE et al., 2005). This was not confirmed for the mutants. Further purification of the enzyme preparation with Mono Q represents an option that should be considered in the future[10].

IV.7.2 Computer modeling of STR1 mutants

A visualization of the mutant's structure was important to demonstrate the engineering strategy and to understand the observed substrate specificity. Since crystallization of STR1 mutants V208A and V208G failed, it was necessary to perform theoretical calculations in order to obtain insight into their molecular structure. Each mutant was simulated using the program PyMol (DELANO, 2002) and the energy minimized conformation was calculated by the Force Field Explorer tool of the TINKER software (PONDER and RICHARDS, 1987). In the subsequent section the modeling procedure and its results are described and will be discussed in V.2.4. The modeling was performed after the site-directed mutagenesis experiments. The modeling results had no influence on the engineering strategy and were exclusively used as illustration tools.

---

[10] MonoQ is a high resolution, anion exchange column. It has been used for further purification of wild-type STR1 and provided highly pure enzyme preparations (MA et al., 2004; KOEPKE et al., 2005).

IV.7.2.1 Computer-modeling validation

Validation of the modeling with TINKER, in matters of significance and reliability has been performed because the results should represent the structural and geometrical features of the mutants as accurately as possible. To check the accuracy of the modeling results, native STR1 enzyme was modeled by TINKER. The computer-modeling results (STR1-model) were compared to the crystal structures of native STR1 (PDB code 2fp8) and STR1-strictosidine complex (PDB code 2v91). Structural alignment was performed with the EMBL-EBI online tool DaliLite (Holm and Park, 2000) and superposition of the structures was done with PyMol (DeLano, 2002). The latter focused on the conformation of the active site. Furthermore, a Ramachandran plot of the STR1-model was generated using the structural validation web service MolProbity (Lovell et al., 2003). 99.3 % of all residues were in allowed regions (see Figure 42).

> 93.3 % of all residues were in favored regions.
> 99.3 % of all residues were in allowed regions.
> There were two outliers (phi, psi):
>> 9 Ser and 57 Phe
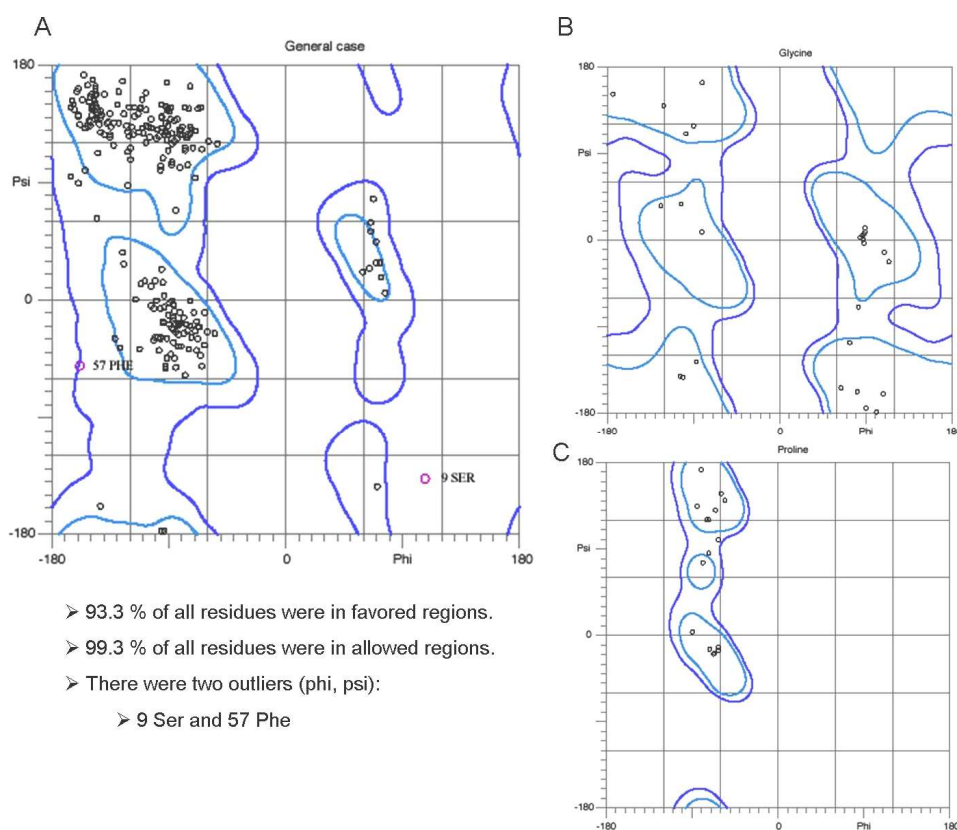
Figure 42. The Ramachandran analysis of STR1-model generated by Molprobity. Outliers signify unusual conformations of the protein backbone and are highlighted in purple in the general plot (A). (B) represents the analysis of glycine residues and (C) the proline plot .

In general the calculated model of the STR1 corresponded to the crystal structures and turned out satisfactory. Comparison of the α-carbon backbones by structural alignment with DaliLite gave a root mean square deviation (RMS deviation) of α-carbon atoms of 0.9 – 1 Å. With an average distance of ca. 1 Å the protein backbones calculated by TINKER did not

highly differ from the structures obtained by crystallization and X-ray analysis (see Figure 43 A). Superimposition of the individual crystal structures resulted in RMS deviation values of 0.3 – 0.8 Å. Though the average deviations between aligned α-carbons of the crystal structures were lower, all values ranged ≤ 1 Å.
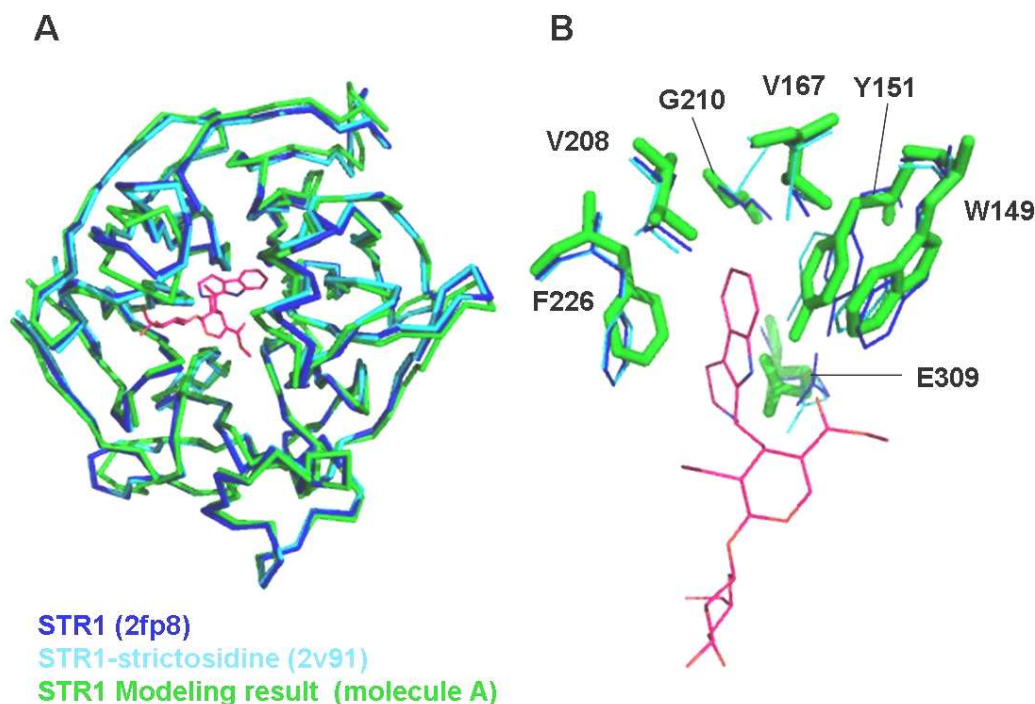
Figure 43. Structural alignment of STR1-model and the crystal structures of STR1. (A) Ribbon representation of the α-carbon backbone. Alignment of STR1 high resolution crystal structure (2fp8; blue), STR1-strictosidine complex (2v91, cyan) and the modeling result STR1 (molecule A; green) are presented. Strictosidine is shown as stick representation in pink in the catalytic pocket. (B) Active site of the STR1-model (green, stick representation) aligned to the crystal structures (2fp8 in blue, 2v91 in cyan, both as line representation).

Backbone differences were particularly located at the enzyme surface. Helix α3 and the loop connecting blades 5 and 6, as well as the N-terminus, showed slightly different conformation compared to the crystal structures (Figure 43). With increasing distance from the α-backbone, larger differences between the side chains of STR1-model and crystal structures occurred. The pdb-files were aligned and the average distances between corresponding atoms of the single were measured with PyMol Wizard measurement tool. The values reflected the average deviation and were listed in Table 27. Figure 43 B represents an alignment of key residues in the active site. The average distance was ca. 1 Å. Residues like Phe226 and Gly210 exhibited larger deviations (see Table 27). Remarkably the values of the two STR1 molecules (A and B) occurring in the asymmetric unit partly highly differed from each other. The deviation between the STR1-model and the STR1 high resolution structure (PDB code 2fp8) was lower than between the STR1-model and the strictosidine complex

structure (PDB code 2v91). Both deviations did not highly differ from the corresponding values of the alignment of the two crystal structures.

Table 27. Distances between the key residues of the active site of the STR1-model and the crystal structures. Comparison of model and PDB structures 2fp8 and 2v91 by superimposition using PyMol. The average distances between selected residues of model and crystal structure were determined: measurements were carried out between corresponding atoms using the Wizard measurement tool. [1] PDB code 2fp8; [2] PDB code 2v91. The distances are given in Å.

| Residue | Average distance between corresponding side chain atoms | | | | | |
| | STR1-model aligned with STR1 crystal structure[1] | | STR1-model aligned with STR1-strictosidine complex[2] | | STR1 crystal structure[1] aligned with STR1-strictosidine complex[2] | |
Molecule	A	B	A	B	A	B
W149	0.6 (± 0.2)	0.6 (± 0.5)	1.1 (± 0.4)	1.3 (± 0.4)	0.7 (± 0.2)	1.3 (± 0.6)
Y151	0.7 (± 0.3)	0.9 (± 0.2)	1.2 (± 0.7)	1.8 (± 0.6)	1.3 (± 0.6)	2.3 (± 0.9)
V167	0.6 (± 0.4)	0.4 (± 0.2)	1.8 (± 0.4)	1.2 (± 0.4)	1.3 (± 0.1)	1.0 (± 0.3)
V208	0.6 (± 0.1)	0.7 (± 0.1)	2.1 (± 0.1)	1.2 (± 0.3)	1.6 (± 0.1)	1.7 (± 0.2)
G210	0.5 (± 0.1)	0.6 (± 0.1)	0.8 (± 0.2)	1.8 (± 0.1)	0.6 (± 0.2)	2.0 (± 0.1)
F226	1.1 (± 0.4)	1.0 (± 0.5)	2.3 (± 0.1)	2.0 (± 0.5)	1.83 (± 0.1)	2.0 (± 0.2)
E309	1.0 (± 0.6)	1.9 (± 1.0)	2.4 (± 0.6)	1.0 (± 0.2)	1.72 (± 0.3)	1.8 (± 0.2)

IV.7.2.2 Computer-modeling results

The theoretical structures of the mutants were calculated as described above (IV.7.2). Relevant models have been compared pairwise to the STR1-strictosidine complex structure (PDB code 2v91) using DaliLite (HOLM and PARK, 2000) and a Ramachandran plot has been generated via MolProbity. The quality parameters determined (RMS deviation and Ramachandran plot) are listed in Table 28.

Structural alignment with focus on the conformation of the active site was performed using PyMol (DELANO, 2002). Distances between selected key residues in the active site and the ligand were measured with the Wizard measurement tool. The results are listed and compared to correspondent distances in the STR1-strictosidine complex structure in Table 29.

Table 28. Structural analysis of the TINKER models. RMS deviation has been determined by pairwise comparison of the respective model with STR1-strictosidine complex using DaliLite. The Ramachandran plots have been generated by MolProbity.

Model	RMS deviation (Å)	Ramachandran plot		
		Residues in most favorable regions	Residues in allowed regions	Outliers
W149A-model	1.0	94.7 %	99.7 %	0.3 %
V167A-model	1.0	94.3 %	99.7 %	0.3 %
V167G-model	1.1	94.7 %	99.7 %	0.3 %
V208A-model	1.1	95.0 %	99.7 %	0.3 %
V208G-model	1.0	93.7 %	100 %	0 %
E309D-model	1.1	93 %	99.7 %	0.3 %

Table 29. Average distances between strictosidine and mutated residues. The average distances between selected residues and strictosidine were determined by structural alignment of the respective model with the crystal structure of STR1-strictosidine complex using the Wizard measurement tool of PyMol. * = STR1-strictosidine complex PDB code 2v91.

	Tinker model of enzyme (variant):						
Residue	V208A	V208G	W149A	E309D	V167A	V167G	STR1*
149	5.1 (± 0.01)	4.9 (± 0.04)	8.5 (± 0.40)	5.2 (± 0.51)	5.0 (± 0.51)	5.5 (± 1.0)	4.7 (± 1.1)
167	--------------------- similar 4.9 (± 0.7) -------------------				5.5 (± 0.47)	6.5 (± 0.46)	4.6 (± 0.48)
208	4,8 (± 0.35)	5.6 (± 0.53)	3.3 (± 0.38)	3.6 (± 0.39)	3.7 (± 0.38)	3.7 (± 0.40)	3.9 (± 0.28)
309	3.2 (± 0.66)	2,2 (± 0.67)	3.2 (± 0.62)	2,7 (± 0.90)	2.5 (± 0.81)	2.5 (± 0.85)	3.2 (± 0.42)

IV.8 Optimization of expression and purification of STR1 and mutants

MA et al. (2004) reported on the phenomenon that most of the STR1 enzyme expressed in M15 cells formed inclusion bodies due to protein misfolding. Inclusion bodies are defined as insoluble aggregates of unfolded or misfolded proteins. Over-expression of recombinant proteins frequently comes along with the production of inclusion bodies. Over-expression of STR1 mutants resulted in partly extremely increased lack of solubility. In some cases (such as mutant W149A and E309D) 80 – 90 % of the expressed enzyme accumulated as inclusion bodies and stayed in the pellet (Figure 23, page 78). The recovery of functionally active and soluble protein was difficult and resulted in lower protein amounts (Table 30).

Table 30. Results achieved with standard expression and purification of the respective enzymes. Values represent the average of all experiments carried out with the respective enzyme. High standard deviations reflect the wide range of possible results, due to the complex procedure and a large number of influencing factors.

Enzyme	Bacterial mass (g/l) 24 h	Protein yield average (mg/l)
STR1-His$_6$	2.5	0.35 (± 0.19)
V208A-His$_6$	2.2	0.21 (± 0.16)
V208G-His$_6$	3.6	0.16 (± 0.12)
W149A-His$_6$	2.3	0.12 (± 0.09)
E309D-His$_6$	2.3	0.19 (± 0.02)
E205V/V208A-His$_6$	1.8	0.17 (± 0.10)
V167A-His$_6$	/	< 0.01
V167G-His$_6$	/	< 0.01

Since purification under denaturizing conditions and particularly the refolding of the respective protein was difficult and posed serious problems with the recovery of functionally active protein, the author tried to prevent inclusion bodies from being formed in order to increase solubility. This was achieved by lowering the level of expression (decreased IPTG concentration, time of induction), lowering temperature, increasing osmotic stress and co-expression of chaperones.

Unsurprisingly, the increase of IPTG concentration resulted in increased protein expression level and *vice versa* lower IPTG addition led to minor expression. The amount of soluble

enzyme that was extracted decreased with increased expression level. Thus, IPTG concentration was lowered from 0.5 mM to 0.2 mM.

Reduced inoculums together with elongation of growing interval from 24 h to 48 h after inoculation resulted in an increased bacterial mass, but provided only minor advantages for the recovery of protein probably due to denaturalization processes in dead cells. The large quantity of bacterial mass complicated the purification procedure. Protein yield from small or middle scale bacterial cultures (≤ 20 l) was the best. Due to the applied procedure the results varied in a relatively wide range. Lowest protein yield was achieved from big scale cultures with up to 40 l volume (> 20 l; results are shown in Table 31). The purification of middle and small scale cultures was easier to handle and provided best results for the recovery of soluble enzyme.

The time of induction did not significantly influence the expression of soluble protein. No differences were observed between induction subsequently to inoculation and induction 2 – 12 h later (data not shown).

Table 31. Results of optimization efforts with STR1-His$_6$. Bacterial mass and protein yield from standard (24 h) and longtime (48 h) cultures are shown. The average protein yield from middle scale purifications (up to 20 l culture volume) is compared to large scale (> 20 l). AE = Arctic Express competent *E. coli* cells.

	Bacterial mass (g/l) 24 h	Bacterial mass (g/l) 48 h	Protein yield average 24 h (mg/l) ≤ 20 l culture	Protein yield average 24 h (mg/l) > 20 l culture	Protein yield average (mg/l) 48 h	Protein yield average 24 h (mg/l) in AE
STR1-His$_6$	2.5	3.1	0.35 (± 0.2)	0.14 (± 0.01)	0.14 (± 0.01)	0.45
V208A-His$_6$	2.2	2.7	0.24 (± 0.2)	< 0.1	0.38 (± 0.1)	/

A lower growing temperature for overnight cultures (24 – 30 °C, standard protocol planed 36 °C) provided no advantage for protein expressio n and yield, whereas the expression of STR1-His$_6$ in Arctic Express (AE) competent *E. coli* cells (STR1-His$_6$-AE), which allowed for expression at 12 °C, resulted in ca. 30 % higher p rotein yield (Table 31). This proved that the standard host, *E. coli* strain M15, did not represent the optimal method for the expression of STR1-His$_6$. Unfortunately the facilities did not allow for more than small scale expression at 12 °C (max. 2.5 l). Therefore this procedure wa s not suitable for routine recovery of

STR1-His$_6$ in order to obtain sufficient protein amounts for crystallization experiments and kinetics.

The expression of mutant W149A-His$_6$ in AE at 12 °C led to a more than 80 % decreased total protein yield compared to M15 host (< 0.01 mg/l) and proved to be no alternative, although SDS PAGE analysis showed that W149A-His$_6$ was obviously well expressed in AE (Figure 44, CE). Ca. 50 % of the enzyme expressed, was detected in the pellet fraction (Figure 44, P), which was quite good compared to expression of W149A-His$_6$ in M15, where ca. 80 % stayed as insoluble protein in the pellet (Figure 23, page 78). By SDS PAGE analysis of mutant W149A-His$_6$ in AE, a protein band at 37 kDa representing W149A-His$_6$ was not detected in the elution fraction (Figure 44, line E). Instead, a strong protein band at ca. 58 kDA appeared (Figure 44). This was assumed to be a chaperone, expressed by AE to allow proper protein folding which probably competed against the His$_6$-tagged enzyme and displaced it from Ni-NTA binding sites. A putative W149A-His$_6$ band was detected in the flow through fraction (Figure 44, line F). Incubation of the elution fraction in presence of tryptamine and secologanin (1 mM, 30 min, and 30 ° C, with maximal elution fraction volume) showed activity and confirmed the presence of W149A-His$_6$. In the crude extract conversion of tryptamine and secologanin was detected as well. Total W149A-His$_6$ yield was estimated by SDS PAGE and enzyme assay to be < 0.01 mg/ml in the elution fraction.
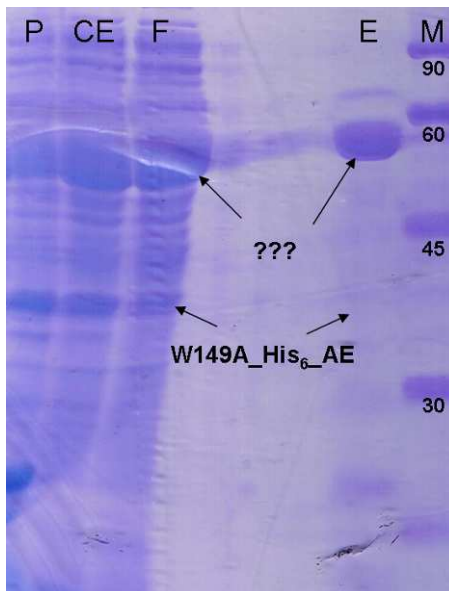
Figure 44. SDS PAGE of W149A-His$_6$ from Arctic Express (AE) expression. P = pellet, CE = crude extract, F = flow through, E= elution fraction, M = marker proteins.

The cell disruption represented another crucial step of the purification procedure and to increase its efficiency, was one of the opportunities, how to optimize the amount of soluble STR1-His$_6$. In the current work sonification together with lysozyme was applied for cell disruption. The sonification of small volumes benefit the productivity (< 10 ml), but it was difficult to handle large volumes of crude extract (e.g. 300 ml). The employment of a "French Press" for cell disruption proved to be of advantage (Dr. Hongbin Zou, personal communication).

V. Discussion

V.1 Crystal structure of STR1-strictosidine and STR1-inhibitor complex

V.1.1 Overall architecture

Both novel X-ray structures presented in the current work, namely STR1-strictosidine and STR1-inhibitor MIT complex, were determined at a resolution of 3.0 Å. In accordance with previous results (MA et al., 2006), the novel complex structures displayed the typical overall architecture of STR1 which was the six-bladed β-propeller-fold: six blades (labeled 1 to 6 in Figure 45), radially arranged around a central six-fold pseudo-symmetry axis and each containing four β-strands (labeled a – d). The β –strands of the propeller blades were twisted so that they were approximately perpendicular to the first inner strand, resulting in a propeller-like appearance. Three strands (6a – c) from the C-terminus and one strand (6d) from the N-terminus formed the so called velcro-closure in blade six of both structures, which was a characteristic structural motif of this fold (JAWAD and PAOLI, 2002; HAREL et al., 2004). There were no significant deviations in the α-carbon backbone compared to the previously determined (complex-) structures of STR1 (MA et al., 2006). They superimposed with a RMS deviation of < 0.5 Å.
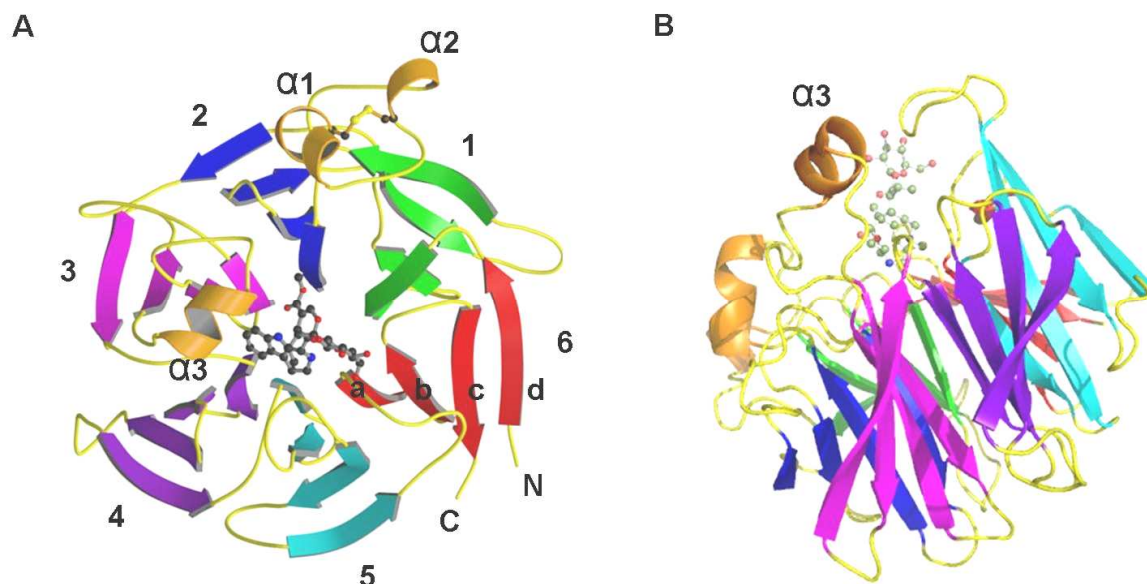
Figure 45. Ribbon diagram of STR1 complexes with strictosidine (A) and inhibitor MIT (B). The overall architecture of *R. serpentina* STR1 resembles a six-bladed β-propeller-fold. The active site is located near the pseudo-six-fold-symmetry axis. (A) Front view of the six-bladed β-propeller in complex with strictosidine. (B) A side view of the propeller in complex with inhibitor MIT.

Two of the three helices, existing in STR1, were located in the loop, connecting the outermost strand d of blade 1 and the innermost strand a of blade 2. They were connected by a disulfide bridge between residues Cys89 and Cys101 which pulled the two helices closer together. The two cysteine residues were conserved throughout the STR family (see appendix IX.3). MA et al. (2006) assumed that this was a distinct feature of the STR family and proved that the disulfide bridge was essential for the integrity of the catalytic pocket and for the overall architecture, because the mutation of residue Cys89 (serine substitution) resulted in poor expression and a complete loss of enzyme activity.

The third helix (α3), which was located between strands b and c in blade 3, formed a cap over the active site. Together with a loop that connected strands b and c in blade 5, the helix α3 shaped the substrate binding pocket and contributed to form an entrance for the substrates.

V.1.2 Architecture of the active site

The data sets presented here were of sufficient quality to clearly define the binding mode of the product strictosidine and the inhibitor MIT. Both ligands were bound to the enzyme, with the tryptamine moiety located deep within the catalytic pocket and the glucose moiety exposed to the solvent. The active site was situated on top of the propeller, near the pseudo-symmetry axis. The structural elucidation of STR1 in complex with strictosidine and inhibitor MIT corresponded to the formerly published substrate complexes and supported the conclusions drawn by MA et al. (2006). The novel crystal structures extended the three-dimensional image of STR1 from *R. serpentina* and provided valuable insight into advanced phases of the reaction mechanism. Together they allowed the determination of residues involved in substrate binding and catalysis.

The main amino acid residues involved in forming the active centre were Tyr105, Trp149, Tyr151, Val167, Met180, Val208, Phe226, Ser269, Met276, His277, His307, Phe308, Glu309, Leu323, and Phe324 (Figure 46). The closed structure of the catalytic pocket, which was created by helix α3 and the loop in blade 5, provided a hydrophobic environment in the catalytic center. Polar residues were located at the entrance in proximity to helix α3 (His307 and His277) and in the environment of the tryptamine binding site (Glu309; MA et al., 2006). Most of the residues in the active site of STR1 were conserved in the sequences of STR from *C. roseus* and *O. pumila* (STÖCKIGT et al., 2008; see appendix IX.3) with the exception of Val208, Met276 and His277.

The tryptamine deriving part of both, the strictosidine molecule as well as the inhibitor molecule, was embedded deep in the substrate binding pocket surrounded by the residues

Trp149, Tyr151, Val167, Val208, Gly210 and Phe226 (contacts < 4Å; Figure 46). These residues built a hydrophobic cleft for the tryptamine moiety, which was extended by residues Tyr105, Val176, Met276 and Leu323. They encased the monoterpenoid part of strictosidine. The glucose moiety was connected with His227 and His307 via hydrogen bonds whereas Phe324 lay in close proximity to the hydrophobic face. The majority of these residues (with the exceptions of Val208, Met276 and His277) were conserved in the sequences of STR from *C. roseus* and *O. pumila* (see sequence alignment in appendix IX.3).
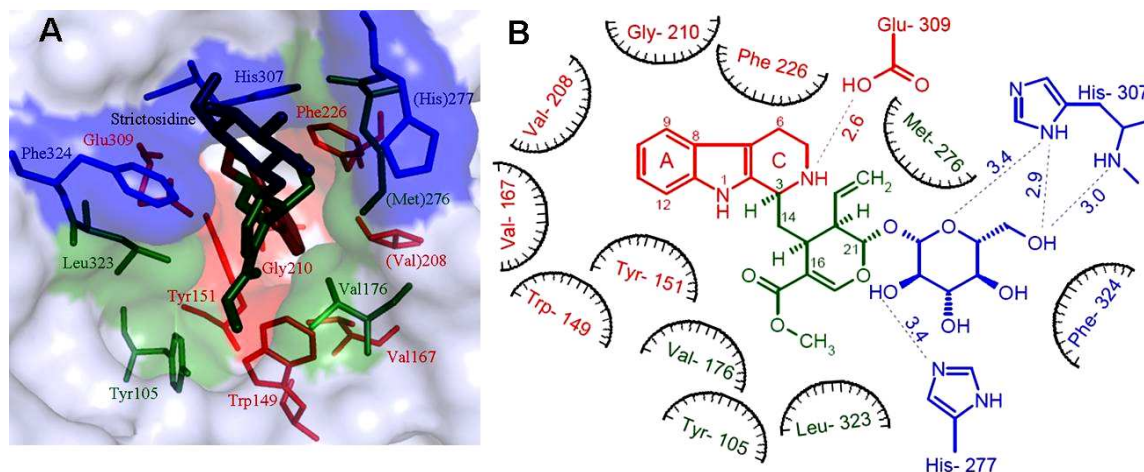
Figure 46. Crystal structure of the active centre of STR1 from *R. serpentina* in complex with strictosidine. (A) Red residues interact with the indole moiety of strictosidine, green and blue residues with the secologanin and glucose moieties of secologanin respectively. The grey surface corresponds to amino acids located more than 4.0 Å away from strictosidine. Amino acid names in brackets are not conserved in *C. roseus* and *O. pumila*. (B) 2D-representation of STR1 in complex with strictosidine (colors as in figure A). Picture taken from STÖCKIGT et al. (2008).

V.1.2.1 The position of strictosidine in STR1-strictosidine complex

The STR1-strictosidine complex provided molecular insight into the late phase of the reaction mechanism. In the STR1-tryptamine complex structure (MA et al., 2006) the ligand occupies approximately the same position as the corresponding indole moiety of strictosidine in the STR1-strictosidine complex. It was slightly shifted compared to tryptamine (average deviation of corresponding ligand atoms: 1.02 Å (± 0.52) and 1.69 Å (± 0.75) in molecule A and B respectively; see Figure 47) indicating a certain amount of flexibility in the binding mode. In the STR1-tryptamine complex structure, the primary amine group was connected with the residue Glu309 by a hydrogen bond. This residue was identified as a catalytic residue which played an important role in the reaction mechanism (MA et al., 2006, MARESH et al., 2008). In the STR1-strictosidine complex, Glu309 was in close proximity to the secondary amine in ring C with an average distance of 3.2 Å (± 0.4). One of the Glu309 oxygen was located in a distance of 2.6 Å. These distances allowed a connection via hydrogen bonds. It was

hypothesized that a further involvement of Glu309 in the catalytic processes after the amine deprotonation was likely to occur.

Further key residues involved in the binding of the tryptamine part of strictosidine were Phe226 and Tyr151. As in the tryptamine complex, the aromatic ring of strictosidine was stacked between these two aromatic residues, which lay parallel to the aromatic indole ring system. Including the indole they appeared like a sandwich and therefore they were referred to as the "indole sandwich" in the current work. Phe226 and Tyr151 acted as a scaffold and fixed the conformation of the indole moiety by way of π-π interactions (average distances between Phe226 and strictosidine: 5.0 (± 1.0) Å and 5.2 (± 0.8) Å in molecule A and B respectively; between Tyr151 and strictosidine 4.1 (± 0.2) Å and 3.9 (± 0.3) Å in molecule A and B respectively).

Four hydrophobic residues (Trp149, Val167, Val208, and Gly210) participated via van der Waals interactions in keeping the indole ring in place (Figure 46). In the hydrophobic cleft the residues Val208, Val167 and Gly210 shielded the steric positions 10 and 11 of strictosidine (positions 5 and 6 according to the tryptamine numbering) at an average distance of 4.2 Å (± 0.53), 4.6 Å (± 0.42) and 4.0 (± 0.36) respectively. The large residue Trp149 was approximating the carbons 11 and 12 of strictosidine with an average distance of 4.2 (± 0.3) Å and 5.1 (± 0.5) Å (in the molecules A and B of the asymmetric unit respectively).

In agreement with previously published data regarding the STR1-secologanin complex (MA et al., 2006), the monoterpenoid part of strictosidine was positioned at the top of the binding pocket, with the ester group facing towards the bottom. The hydrophilic glucose unit was located at the entrance and was accessible to the solvent. Two of the glucose oxygen atoms were coordinated with the nitrogen atoms of His307 (Figure 46). In the STR1-secologanin complex, the aldehyde group of the secologanin molecule pointed towards Glu309 and when superimposed with the STR1-tryptamine complex, it was located in close proximity to the amine group of tryptamine. In STR1-strictosidine complex, the corresponding carbons occupied the identical position, connected to tryptamine. The binding mode of the monoterpenoid compound in STR1 was obviously less flexible compared to tryptamine. The structural alignment of the active site of the STR1-strictosidine complex with the crystal structures of STR1-substrate complexes is displayed in Figure 47.
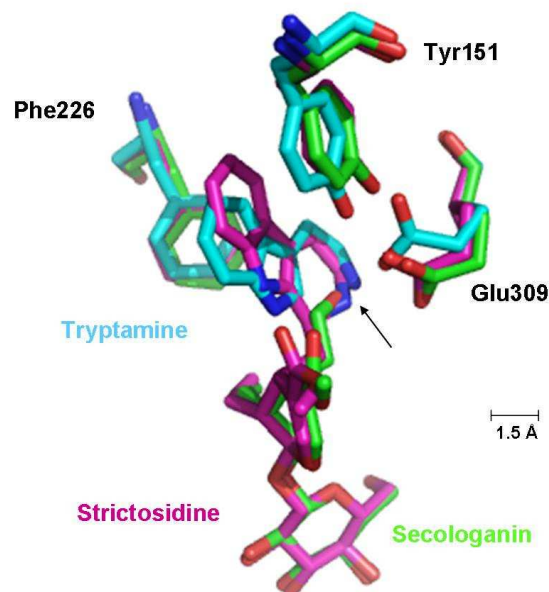
Figure 47. Structural alignment of STR1-strictosidine complex active site with STR1 substrate complexes.
STR1-strictosidine = magenta (2v91), STR1-tryptamine = blue (2fpb), STR1-secologanin = green (2fpc). The arrow highlights the catalytic site.

V.1.2.2 The position of inhibitor MIT bound to STR1

The structural alignment of the STR1-inhibitor complex with the other crystal structures of STR1 showed no major differences in the α-carbon backbone and the overall architecture. Superimposing the crystal structures of the ligands bound to the active site of the STR1-inhibitor and STR1-strictosidine complex allowed one to visualize the overlapping of the monoterpenoid moiety in both structures. The same was true for the alignment with the STR1-secologanin complex (Figure 48). As observed for the STR1-strictosidine complex, it appeared that due to the rigid conformation, only a single orientation of secologanin was acceptable.

To the contrary, the orientation of the indole system of the inhibitor was significantly different, as compared to the positions of strictosidine and tryptamine in the respective STR1 complexes. There was a shift and incline so that it did not fit perpendicularly into the sandwich scaffold provided by the two aromatic residues Tyr151 and Phe226 (Figure 48 C, D). The sp^3 hybridization of the inhibitor with its flexible amine linkage between the indole and the secologanin moieties allowed for this orientation. In the strictosidine molecule this part was fixed by ring closure at carbon 3 as shown in Figure 48 B.
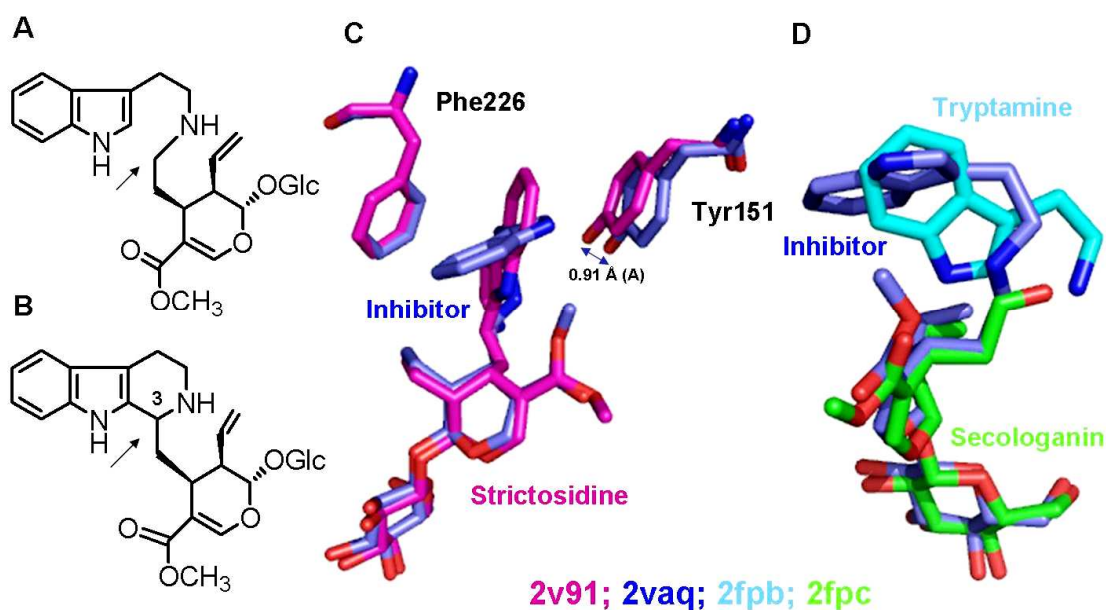
Figure 48. Structural alignment of inhibitor MIT bound to STR1 with the other STR1 complex structures. (A) the structure of inhibitor MIT; (B) the structure of strictosidine; (C) alignment of inhibitor position with strictosidine in the active site, including sandwich residues Tyr151 and Phe226; (D) alignment of inhibitor with tryptamine and secologanin. The arrows highlight the flexible amine linkage of inhibitor MIT in A and the inflexible formation of strictosidine in B. The deviation of the Tyr151-hydroxyl function: 0.91 Å and 1.56 Å in molecule A and B respectively.

Apparently STR1 allowed different orientations of tryptamine in the active site, including positions in which tryptamine was inclined to the sandwich and the "hydrophobic line" of residues. On the other hand, the distance between Glu309 and the primary amine group of tryptamine in the STR1-tryptamine complex (3 Å) was similar to the corresponding positions in the inhibitor complex. It was concluded that though the binding mode of tryptamine was flexible, the ligand could not bind in any order and only certain conformations were possible due to the interactions with the indole sandwich and the "hydrophobic line". However, this did not suffice to maintain the inhibitor molecule in a productive conformation; there may have been other contributing factors such as the sp^2 hybridization of the iminium intermediate occurring during the reaction mechanism. It possibly contributed to the correct orientation as discussed in the following paragraph (V.1.2.3).

V.1.2.3 Conclusions for the reaction mechanism

STR1 catalyzes the condensation of tryptamine and secologanin by way of a completely stereo-selective Pictet-Spengler type reaction (Figure 49). The product of this condensation, the glucoalkaloid 3α-(S)-strictosidine (syn. isovincoside), is likely to be the common biosynthetic precursor of all monoterpenoid indole alkaloids in higher plants (see introduction, I.2). The Pictet-Spengler reaction is known from synthetic chemistry where it is applied in alkaloid synthesis. It basically involves an aromatic amine and a carbonyl component under acidic conditions in a two-part reaction (type Mannich reaction, respectively α-amino-methylation). Initially an iminium ion (Schiff base, Figure 49) is formed between an aldehyde group and a primary or secondary amine compound, followed by the intra-molecular addition of a CH-acidic substrate (nucleophilic substitution). In contrast to the biological Pictet-Spengler reaction catalyzed by STR1 (which leads exclusively to 3α-(S)-strictosidine), the chemical variant is not stereo-selective and yields the 3β-(R) epimer (vincoside) as well.
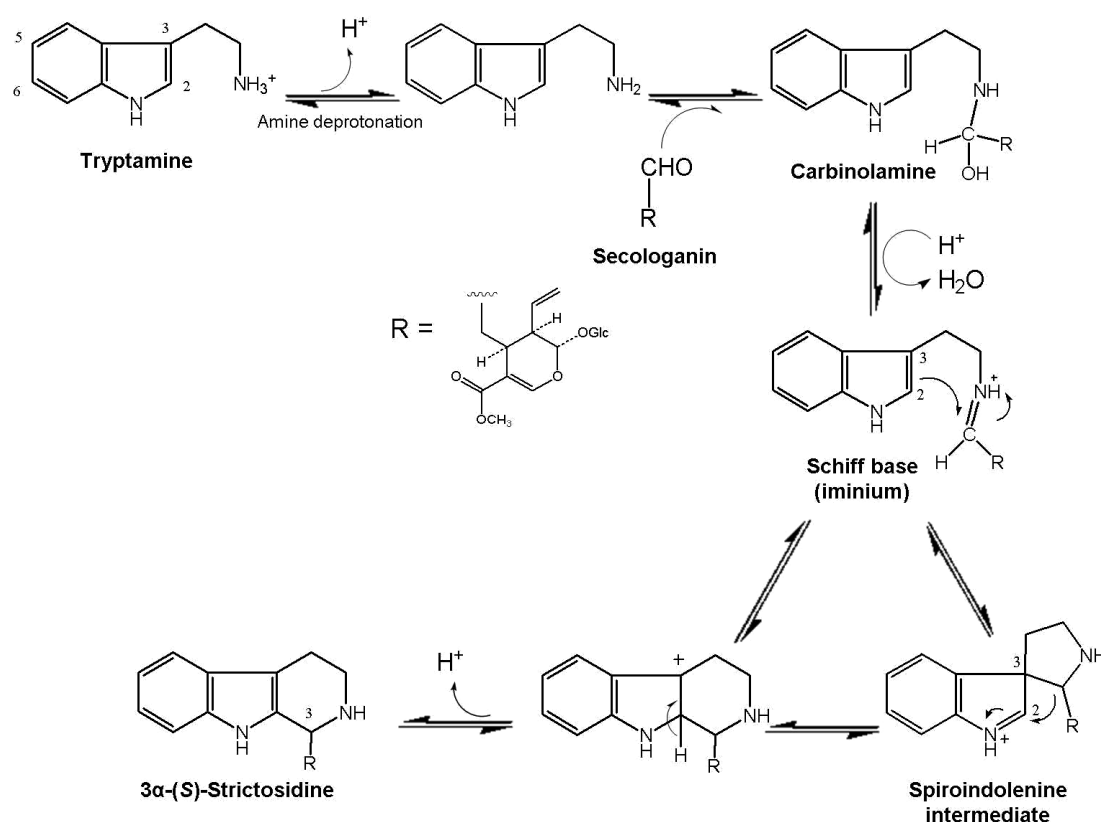
Figure 49. Mechanism of the Pictet-Spengler reaction. Detailed Pictet-Spengler reaction mechanism as proposed by MARESH et al., 2008.

Figure 49 displays the reaction mechanism as it was proposed for an *in vitro* (not enzyme catalyzed) Pictet-Spengler condensation of tryptamine and secologanin (MARESH et al., 2008). The Schiff base is formed between the secologanin-aldehyde and the primary amine group of tryptamine after its deprotonation (pK$_b$ value of tryptamine is close to 10). According to MARESH et al. (2008) this is a two-step process consisting of the carbinolamine formation and the subsequent dehydration to the Schiff base. The CH-acidic center, which reacts under ring-closure with the Schiff base, is the nucleophilic carbon 2 of tryptamine (Figure 49). Notably, though it is a common rule, that 6-endo-ring closures are favored over 5-endo cyclizations, carbon 3 of tryptamine is nucleophilic too and can theoretically attack the Schiff base yielding a spiroindolenine intermediate (MARESH et al., 2008). That requires a subsequent 1,2-alkyl-shift to form the product. For the chemical reaction in solution evidence was found for both mechanisms (BAILEY 1987; IBACETA-LIZANA et al., 1987; KOWALSKI and MOKROSZ 1997; UNGEMACH and COOK 1978; MARESH et al., 2008), whereas little is known about the mechanism of the enzymatic reaction.

After the determination of the three-dimensional structure of STR1, the hydrophobic nature of the substrate binding pocket was revealed. It was elucidated that there were only three polar residues (Glu309, Tyr151, and His307) around the active site, which could contribute to the conditions required for a Pictet-Spengler condensation to occur. With Glu309, a catalytic residue was identified and confirmed by site-directed mutagenesis studies (MA et al., 2006). MA et al. suggested an important role of Glu309 in catalysis, namely in the initial amine deprotonation. The mutation of Glu309 to Ala resulted in approximately a 900-fold decrease in turnover rate, whereas the influence on the K$_M$ for tryptamine was negligible (MA et al., 2006). As the only possible proton acceptor, the removal of Glu309 resulted in a limited conversion of tryptamine, though the tryptamine molecule still fit into the active site of the mutated enzyme (as reflected by the K$_M$ value).

The crystal structures presented in this work completed the molecular image of STR1 catalysis and allowed for the first time a detailed analysis of the active site in all phases of the enzymatic reaction. Investigation of the reaction mechanism was extended to the final part of the strictosidine formation. Furthermore, the STR1-inhibitor complex represented an intermediate conformation.
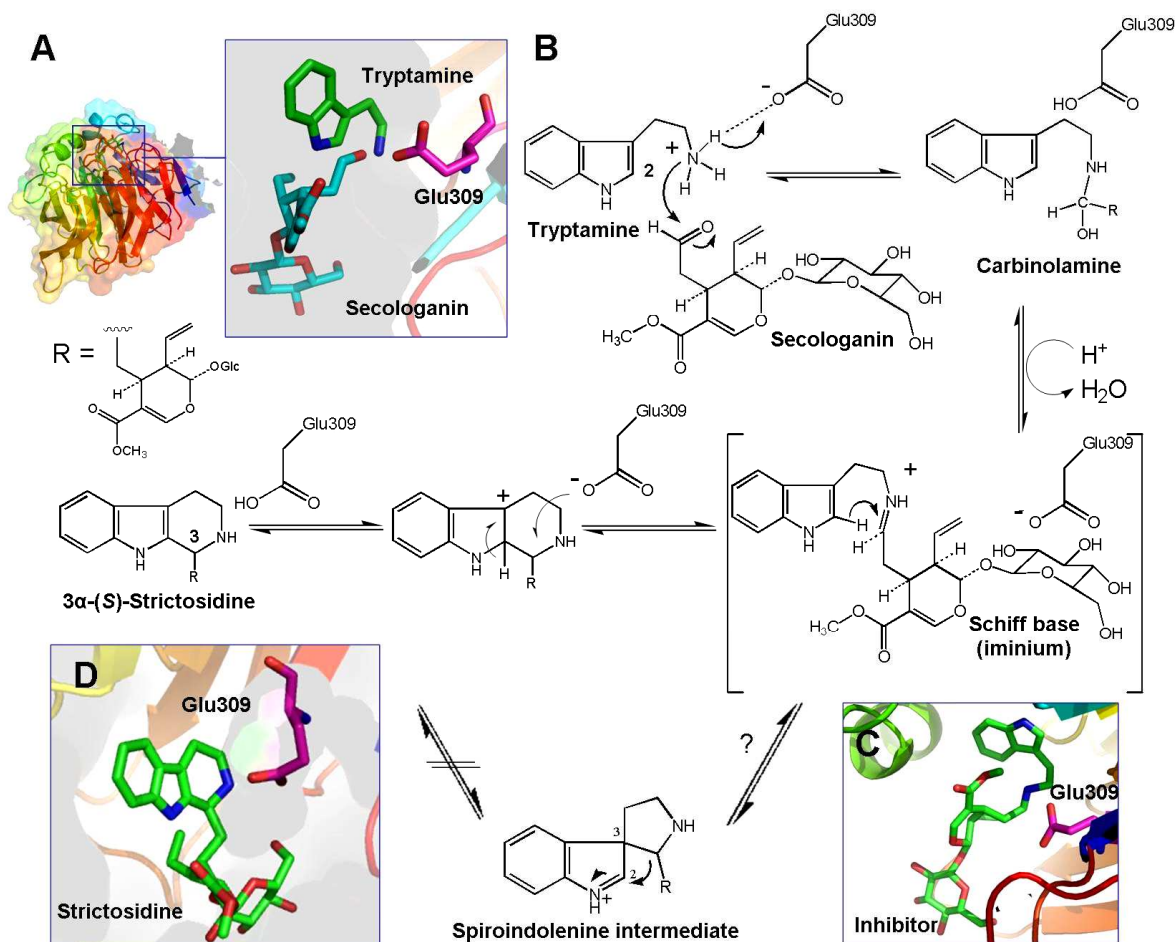
Figure 50. Reaction mechanism of STR1-catalyzed Pictet-Spengler condensation as it may occur in the enzyme. (A) Left: Side view of STR1 in complex with tryptamine, superimposed with STR1-secologanin structure; right: close-up view of the active site. Glu309 is highlighted in pink. (B) The reaction mechanism as it may occur in the substrate binding pocket of STR1, leading to 3α-(*S*)-strictosidine. Prior to the Schiff base formation tryptamine is deprotonated. Addition of the amine to the secologanin aldehyde yields a carbinolamine intermediate and is followed by dehydration to the Schiff base. Subsequently the electrophilic substitution occurs at carbon 2 of tryptamine, which represents the CH-acidic centre, and the product is formed under ring closure. (C) and (D) Crystal structures of STR1-inhibitor and STR1-strictosidine complex respectively, close-up view of the catalytic residue Glu309 and the ligand.

The structural analysis of the substrate binding pocket of STR1-strictosidine complex revealed that the amine group of the newly formed ring C was in close proximity to Glu309. This corresponded to the STR1-tryptamine structure where the primary amine group was hydrogen bonded to the same residue. Similar distances were measured in the STR1-inhibitor complex and indicated an important role of the catalytic residue Glu309, not only in the beginning but throughout the reaction process. Obviously this residue was also involved in the catalytic events after the amine deprotonation as shown in Figure 50. Previous studies of LORENTZEN et al. (2005) and ST-JEAN et al. (2005) on the enzymatic iminium formation in different enzymes (e. g. fructose-1,6-bisphosphate aldolase) demonstrated that it was often a catalytic glutamic acid residue, which was responsible for the carbinolamine protonation

(which finally catalyzed its dehydration). It was evident, since there were no alternatives, that in STR1, Glu309 was the catalytic residue involved in the acid catalyzed dehydration of the carbinolamine. FULLERTON et al. (2006) reported the possibility of catalysis by an ordered water molecule, but in the active site of STR1, none existed.

The Schiff base is subsequently attacked by the nucleophilic carbon 2 and ring closure occurs. This is the crucial step for the stereo-selectivity of the reaction because the stereo center carbon 3 is formed. The enzyme provides the scaffold to adopt the molecule in the right orientation, but a rigid conformation of the iminium molecule itself is most probably required to fix the correct binding mode because in addition the active site allows for unproductive orientations (as demonstrated in the STR1-inhibitor complex). Cyclization yields a positively charged intermediate, which is finally deprotonated to 3α-(S)-strictosidine. The proximity of nitrogen and Glu309 in the two novel STR1 complexes and the lack of alternatives indicated that the residue might be involved in the final deprotonation step as well. Kinetic analysis by MARESH et al. (2008) found a carboxylate ion adequate to catalyze the deprotonation. Thus Glu309 is likely involved in a total of three steps of the reaction mechanism (Figure 50). Like most of the active site residues, Glu309 was conserved in the STR sequences from *C. roseus* and *O. pumila* (sequence alignment in appendix IX.3).

The compound MIT is the reductive amination product of tryptamine and secologanin. It has a flexible amine linkage between the indole and secologanin moieties and approximates the structure of the iminium intermediate which occurs during catalysis (Figure 50, Schiff base). Until now the intermediate itself could not be isolated and its instability issues do not allow crystallization experiments. It is proposed that the compound MIT imitates its conformation (MARESH et al., 2008). Figure 51 illustrates the inhibitor MIT in association with the conformations of strictosidine, tryptamine and secologanin bound to the enzyme. Furthermore the proposed structure of the iminium intermediate is shown. The crystal structure of STR1 in complex with inhibitor MIT was expected to allow for further conclusions on the enzymes mechanism. The electron density suggested binding of the inhibitor's indole moiety in a significantly different conformation compared to strictosidine and tryptamine bound to STR1 (Figure 48, Figure 51). Due to structural reasons, it was not plausible that strictosidine could adopt the inhibitor's conformation in the active site and the same was true for the sp^2 hybridized iminium intermediate. The nucleophilic carbon 2 (according to tryptamine numbering; see the red arrow in Figure 51), which was assumed to attack the Schiff base, was located at a distance of 3.5 Å from the iminium nitrogen and it was 4.8 Å afar from the carbon which corresponded to the electrophilic iminium carbon (next to the iminium nitrogen). The distance was too substantial to allow for a reaction. In comparison: the distance in the STR1-tryptamine complex structure between carbon 2 and the primary

amine was 2.5 Å (see the arrows in Figure 51 C) and superimposed with the STR1-secologanin complex, the distance measurement between carbon 2 of tryptamine and the aldehyde moiety of secologanin yielded < 1 Å in both molecules A and B; in STR1-strictosidine complex the distance between carbon 2 and the nitrogen was 2.3 Å (Figure 51 D). The inhibitor conformation with a distance of 3.5 Å did not represent a productive cyclization state.
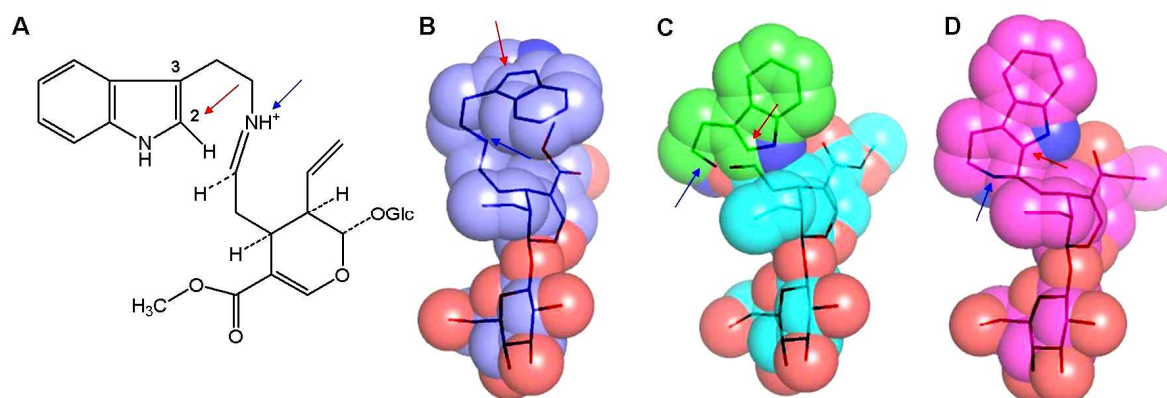
Figure 51. Conformation comparison. (A) The putative structure of the iminium intermediate. The red arrow highlights the nucleophilic carbon 2 that reacts under ring-closure with the Schiff base (blue arrow) and corresponding positions in figure B, C and D. (B) The conformation of inhibitor MIT bound to STR1. (C) Superimposition of STR1-tryptamine (green) and –secologanin complex (cyan). (D) The conformation of strictosidine in the active site of STR1. Line representations including the atom spheres. Red = oxygen; dark blue = nitrogen.

As mentioned above, the nucleophilic carbon 3 can theoretically attack the Schiff base to perform a ring-closure. However, distance measurements did not support this theory: carbon 3 was 3.8 Å afar from the putative reaction site (iminium carbon), whereas carbon 2 was 4.8 Å (see above). Therefore, in the inhibitor structure, this alternative nucleophilic center (carbon 3) was not in suitable proximity to the Schiff base either. Though carbon 3 was 1 Å closer (as carbon 2) to the position representing the electrophilic reaction center, it appeared unlikely that compound MIT demonstrated a productive cyclation state for the spiro-indolenine variant of the reaction. MARESH et al. (2008) also reported *ab initio* calculations which pointed to the unlikelihood of such a reaction taking place. According to MARESH et al., this intermediate was not an important part of the enzymatic Pictet-Spengler condensation and the 1,2-alkyl-shift required for product formation apparently did not occur. Transition state searches rather resulted in a rearrangement into the iminium intermediate. It was assumed that (in the case this variant does exist) it may not contribute significantly to the reaction mechanism.

In the current work, the part of the catalytic residue Glu309 was further investigated by site-

directed mutagenesis. Glu309 was replaced by Asp, an amino acid featuring similar properties (acidic amino acid, pK_a values 4.1 and 4.8), but differing in size so that the distance between the catalytic residue and the ligands and herewith the scope for the ligand's orientation was putatively enhanced (Figure 52). Kinetic analysis of the resulting mutant E309D showed a 5.8-fold higher K_M value (0.418 mM) and more than 31.3-fold lower specificity constant (k_{cat}/K_M 4.73 mM^{-1}/s^{-1}; see IV.6.3.3) in comparison to the wild-type enzyme (K_M 0.072 mM; k_{cat}/K_M 147.92 mM^{-1}/s^{-1}). As reflected by the kinetic constants the substitute Asp309 did not benefit the catalytic process. It was assumed that it was in an unfavorable position to the amine function probably due to a large spatial separation. To more accurately interpret the results, the structure of E309D was simulated (PyMol) and an energy minimized conformation was calculated via TINKER Force Field Explorer software. The resulting model (E309D-model) exhibited a RMS deviation of 1.1 Å when superimposed with the STR1-strictosidine complex (DaliLite). A similar value was calculated for the structural alignment of STR1-model with the STR1 crystal structures during the computer-modeling validation, while the RMS deviations between the individual crystal structures of STR1 were ≤ 0.8 Å (see sectionV.2.4).

The E309D-model showed that the introduction of the smaller Asp residue at position 309 had unexpected consequences on the conformation of the active site. Structural alignment of the E309D-model with STR1-strictosidine complex (Figure 52 A) demonstrated that Asp309 (model) was turned in a way that it was ca. 1 Å closer to the strictosidine molecule than Glu309 (crystal structure). This mutation was expected to offer greater flexibility for the orientation of the tryptamine molecule, however, the contrary was observed. According to the structural alignment, it was not a larger distance, which constricted the catalytic process, but rather a sterical interference by the approximation of residue and ligand. One must be precautious when drawing conclusions from the theoretical model (V.2.4). It was determined that the replacement of Glu by Asp resulted in an enhanced K_M value and reduced conversion efficiency, however, it remained unclear whether these changes were due to enhanced distances in the active site or due to sterical interferences.

The modeling result was supported by the outcome of the ^{1}H-NMR analysis of strictosidine-lactam-tetraacetate derived from the mutant (IV.6.4). It was assumed that this alteration would allow for a reduced stereo-selectivity of the reaction, since it probably offered a more flexible binding mode. This theory was not confirmed. The ^{1}H-NMR analysis of the lactamized and quadruple acetylated E309D product strictosidine clearly demonstrated the carbon-3-stereochemistry to be 3α-(*S*).

Glu309 was not likely to be the sole crucial residue for the stereo-selectivity of the reaction, instead the contribution of the overall architecture of the active site (indole sandwich,

hydrophobic cleft) and the rigid molecule structure must be taken into consideration. No evidence was given concerning the orientation of the mutated residue Asp309 and a future determination of the crystal structure is required to draw a definite conclusion.
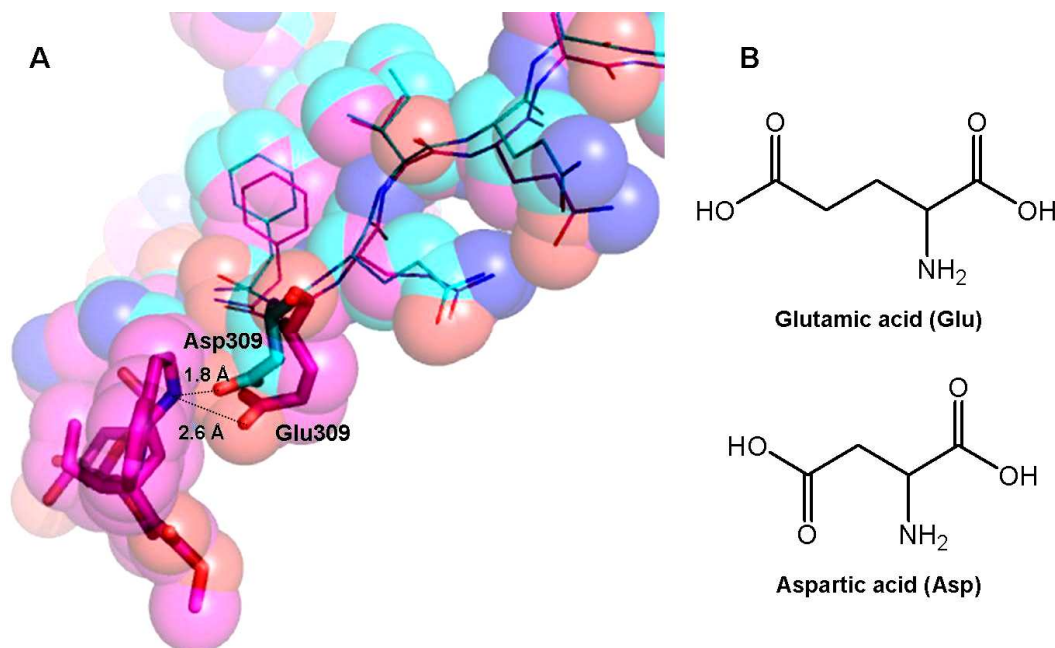
Figure 52. Structural alignment of Mutant E309D-model and STR1-strictosidine complex. (A) Sequence from the crystal structure of STR1-strictosidine complex (pink) superimposed with the calculated TINKER-model of mutant E309D (cyan); spheres and lines are displayed, residue 309 and strictosidine are highlighted in stick representation. (B) Structures of the acidic amino acids Glu and Asp.

V.2 Modulation of substrate specificity by rational site-directed mutagenesis

V.2.1 Substrate specificity of wild-type STR1

To broaden the substrate scope of STR1 (in order to produce novel strictosidine derivatives), the knowledge of the wild-type's substrate acceptance was required. Besides the crystal structures, it represented a cornerstone of the engineering strategy. A detailed, systematic analysis of STR1 substrate specificity was carried out, using the His$_6$-tagged enzyme from *R. serpentina* (III.1, III.4.1.2). It focused on commercially available tryptamine analogues (Figure 1, page 58).

Though substrate specificity studies of STR from various sources were previously carried out (*R. serpentina*: HAMPP and ZENK, 1988; *C. roseus*: TREIMER and ZENK 1979b; MCCOY et al., 2006; *Cinchona robusta*: STEVENS et al., 1993) the investigation of the His$_6$-tagged enzyme was an important achievement. In accordance with the previous studies, a coherent image of
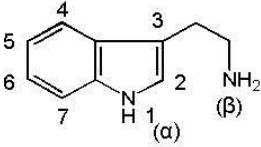
the enzymes substrate acceptance was drawn. Table 32 and Table 33 summarize the analysis. His$_6$-tagged STR1 from *R. serpentina* exhibited distinct substrate specificity, accepting only a few substrates (7 out of 17 in the current work). TREIMER and ZENK (1979b) demonstrated the enzyme to be highly substrate specific in particular for the monoterpenoid substrate. The aldehyde substrates secologanic acid, iridotrial and tarennoside were not converted by STR from *C. roseus*, whereas methylated secologanin and dihydrosecologanin proved to be accepted. Furthermore *C. roseus* STR accepted several ester derivatives of secologanin, but derivatization of secologanin at the vinyl position completely prevented turnover (CHEN et al., 2006; MCCOY et al., 2006).

For amine substrates, the enzyme appeared to be more tolerant; however, it retained a high degree of substrate selectivity. STR1-His$_6$ tolerated a range of different substituents, e.g. hydroxyl-, fluorine-, methyl- and methoxy-groups, but the activity of the enzyme with the tryptamine analogues compared to the native substrate decreased dramatically (approximately 10-fold). The following tendencies were observed in the current study, which were supported by the outcomes of other substrate specificity studies (TREIMER and ZENK, 1979b; HAMPP and ZENK, 1988; STEVENS et al., 1993; MCCOY et al., 2006):

1. Similarity to the native substrate tryptamine favored turnover by STR1. Hence, the indole ring system was highly required for recognition and turnover by the enzyme. Non-indole-substrates with only basic structural similarity (such as dopamine, histamine or phenylalanine) were not accepted by the wild-type enzyme (Table 33). This observation was true for *R. serpentina* and *C. roseus* enzyme and showed that the indole-framework was crucial for conversion. Alone the substitution of the indole-nitrogen resulting in a benzothiophene or benzofuran system was tolerated by the enzyme from *C. roseus* (MCCOY et al., 2006; Table 33).

2. All accepted amine compounds were substituted at the aromatic moiety of the indole framework (carbons 4 – 7, Table 32). Derivatization at other tryptamine positions (such as N$_{(\alpha)}$-acetyl-serotonin or 2-methyl-serotonin, Table 32) resulted in complete abolition of turnover.

3. With increasing size of the functions introduced into the aromatic moiety of tryptamine, the conversion of the compound became more critical. Those tryptamine derivatives with relatively small substituents (fluoro, hydroxyl) were in principle accepted. Larger substituents, such as methyl- or methoxy-groups, resulted in poor conversion or appeared to prevent it completely.
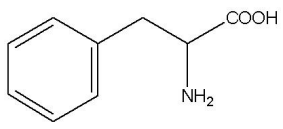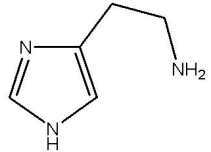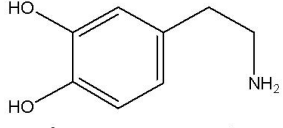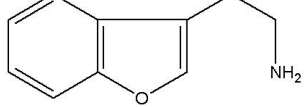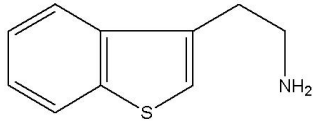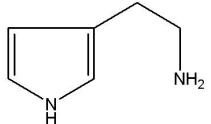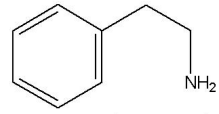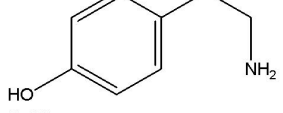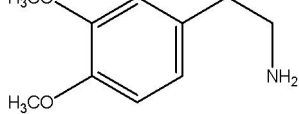
The electron-withdrawing group fluorine yielded competent substrates for STR in all studies; fluorine-functions were accepted at all positions of the aromatic indole moiety (carbon 4 – 7). While carbon 5-fluorinated and -hydroxylated tryptamine-derivatives were converted (both exhibited almost 10 % relative activity), those substrates possessing a bulky methyl- or methoxy-function at this position showed no turnover: 5-methoxy- or 5-methyl-tryptamine were **not** accepted by STR1. In contrast, at carbon 6, methyl- or methoxy-groups did not in general prevent the conversion. *R. serpentina* STR1-His$_6$ accepted 6-methyl- and 6-methoxy-tryptamine, although relative activity was only about 2 % compared to tryptamine. For the *C. roseus* enzyme, this result was not reproducible: conversion of 6-methoxy-tryptamine was detected, but no 6-methyl-tryptamine conversion was observed (MCCOY et al., 2006). Carbon-7-methylated tryptamine was accepted by both, STR1 from *R. serpentina* and STR from *C. roseus* (TREIMER and ZENK, 1979b; MA et al., 2006; MCCOY et al., 2006). A hydroxyl-group at carbon 7 appeared to prevent the reaction as shown by compound 5,7-dihydroxy-tryptamine. Whereas the 5,6-dihydroxy-tryptamine derivative was accepted. Due to their instability, conversion of dihydroxy-compounds was difficult to detect. The large number of novel peaks monitored by HPLC complicated, however, the identification of a putative product peak. The comparison of the peak pattern with the control incubations using denaturized enzyme was employed in order to detect a product peak. In contrast to 5,6-dihydroxy-tryptamine, a product peak was not clearly identified for 5,7-dihydroxy-tryptamine. This was rather an unexpected result, since the 5,6-dihydroxy compounds should be more unstable due to easier oxidation compared to the 5,7-hydroxylated tryptamine derivative.

Table 32. Tryptamine derivatives tested as substrates for STR from different plant origin. Results from the present study on the substrate specificity of His$_6$-tagged STR1 from *R. serpentina* (published in MA et al., 2006) are presented together with data taken from TREIMER and ZENK (1979b; *C. roseus*); HAMPP and ZENK (1988; *R. serpentina*); STEVENS et al. (1993; *C. robusta*) and McCOY et al. (2006; *C. roseus*). + = reaction; 0 = no reaction detectable; - = not tested; +/0 = different results.

	Rauvolfia serpentina	*Catharanthus roseus*	*Cinchona robusta*
Tryptamine	+	+	+
Serotonin (5-Hydroxy-tryptamine)	+/0	+	0
4-Fluoro-tryptamine	-	+	-
4-Methyl-tryptamine	-	+	-
4,5-Dimethyl-tryptamine	0	-	-
4-Methyl-5-methoxy-tryptamine	0	-	-
5-Fluoro-tryptamine	+	+	-
5-Methyl-tryptamine	0	0	0
5-Methoxy-tryptamine	0	0	+
5,6-Dihydroxy-tryptamine	+	0	-
5,7-Dihydroxy-tryptamine	0	0	-
6-Hydroxy-tryptamine	-	+	-
6-Fluoro-tryptamine	+	+	-
6-Methyl-tryptamine	+	0	-
6-Methoxy-tryptamine	+	-	-
7-Fluoro-tryptamine	-	+	-
7-Methyl-tryptamine	+	+	-
N$_{(\alpha)}$-Acetyl-5-hydroxytryptamine	0	-	-
N$_{(\alpha)}$-Methyl-tryptamine	0	0	-
N$_{(\beta)}$-Methyl-tryptamine	0	-	-
2-Methyl-5-hydroxy-tryptamine	0	-	-
α-Methyl-tryptamine	-	+/0	-
α-Dimethyl-tryptamine	-	0	-
α-Ethyl-tryptamine	-	0	-
D-, L-Tryptophan	0	0	0
5-Hydroxy-tryptophan	-	-	0
5-Methoxy-D,L-tryptophan	-	-	0
3-Methylamine-indole	-	0	-
3-Propylamine-indole	-	0	-

Table 33. Non-indole compounds tested as putative substrates of STR of different plant origin. Beside the results of the current work, data taken from McCoy et al. (2006), and Treimer and Zenk (1979b) are presented. + = reaction; 0 = no reaction detectable; - = not tested).

		Rauvolfia serpentina	*Catharanthus roseus*
Phenylalanine		0	-
Histamine		0	0
Dopamine		0	0
3-(2- Aminoethyl) – benzofuran		-	+
3-(2-Aminoethyl)– benzothiophene		-	+
2-Pyrrole-3-ethylamine		-	0
Phenylethylamine		-	0
Tyramine		-	0
Homoveratrylamine		-	0

The substrate specificity of STR1 mostly corresponded to the substrate spectra reported for STR from *C. roseus* (STR_CR) and *C. robusta*. There were three exceptions: the above mentioned 6-methyl-tryptamine (STR1 +, STR_CR 0), serotonin STR1 +, STR_CR +, STR from *C. robusta* 0) and 5-methoxy-tryptamine (STR from *C. robusta* +, STR1 0, STR_CR 0). Sequence alignment of STR from different species (see appendix IX.3) showed that most residues in the active site were conserved in the STR enzymes. In particular the aromatic

residues forming the indole sandwich (Tyr151, Phe226) and the hydrophobic residues Trp149, Val167, Va208 and Gly210 shielding the positions 4 – 5 (tryptamine numbering) existed in both STR1 and STR_CR. Since there were no differences in the immediate vicinity of the ligand binding site, it was concluded that far-reaching structural interactions within the enzymes may contribute to the observed substrate preference. Though the three-dimensional image of STR1 contributed to the understanding of the enzyme's function, interactions of this type were difficult to predict without molecular insight into the architecture of STR_CR. The determination of further crystal structures (such as STR_CR), and more detailed investigations on the substrate specificity of STR are required to arrive to a conclusion.

The question why STR from *C. robusta* featured the conversion of 5-methoxy-tryptamine (relative activity 10 %; STEVENS et al., 1993), which was reportedly no substrate for STR1 and STR_CR remained open, since the sequence of *C. robusta* was not available. As aforementioned, more information about the enzyme is required in order to interpret the observed differences in the substrate spectrum.

V.2.2 Structural analysis and engineering strategy

The crystal structure of STR1-strictosidine complex provided structural understanding of the observed substrate preference and represented the basis for its rational modulation. As shown in Figure 46 (page 118), the indole ring of the tryptamine unit was located deep in a hydrophobic cleft, containing six hydrophobic residues in immediate proximity. The two aromatic "sandwich" residues Phe226 and Tyr151 kept the indole ring in place via π-π interactions. Shielding the plane face of the indole, no benefit was expected from their mutagenesis for the substrate acceptance and therefore these residues were not considered. In between the sandwich, Trp149, Val167, Val208 and Gly210 shielded the steric positions 10, 11 and 12 of strictosidine (5, 6 and 7 respectively according to the tryptamine numbering) in a distance of ≤ 4 Å (Figure 53). They contributed to the orientation of the indole via van der Waals interactions in the active site. The space between the aromatic indole moiety and the adjoining residues was limited. Considering the results of the substrate specificity study (IV.6.3), which showed that those tryptamine derivatives with bulky groups at positions 5 and 6 acted as poor substrates, it was proposed that space limitations were the major constraint against the conversion of these compounds. It was assumed that creating more space in this part of the active site, would reduce the discrimination against substitutions at the indole ring. Focus was on the residues in close proximity: Trp149, Val167 and Val208.
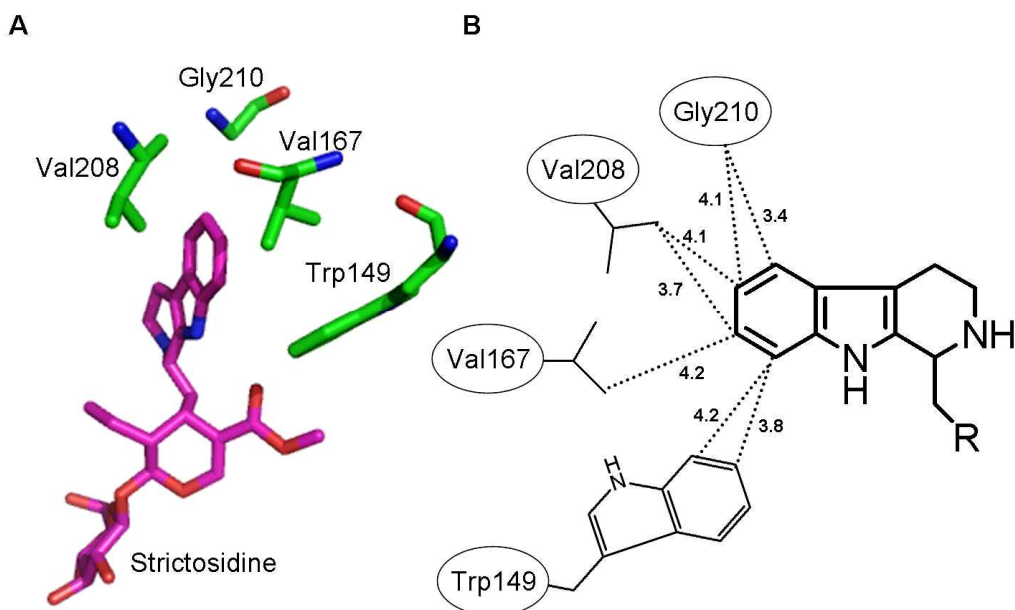
Figure 53. Active site of STR1 with strictosidine. (A) Crystal structure of STR1 active site harboring strictosidine. Hydrophobic residues shielding the aromatic part of the indole moiety are highlighted in green. (B) 2D drawing of strictosidine and the residues lining the carbons 9 – 12. Distances are drawn as dotted lines and charted in Å.

The residues shielding the aromatic moiety of the substrate were replaced by smaller residues featuring similar qualities. Mutants V208A, V208G, V167A, V167G and W149A were generated with the aim to create space for substituents at carbon 5 and 6 of tryptamine while the local hydrophobic environment persisted. These tryptamine positions appeared to be crucial for pharmacological activity: several commonly used drugs such as vinblastine, vincristine, reserpine or quinine, harbor a methoxy-group at these positions. In order to design mutants which can (in contrast to the wild-type) accept 5-methyl- and 5-methoxy-tryptamine as a substrate, Val208 was replaced by the smaller residues Ala and Gly. Furthermore, the conversion of 6-methyl- and 6-methoxy-tryptamine (so far the poorest substrate for the wild-type, relative activity of 2 %) was expected to be enhanced by customizing the binding site in this way.

Though the overall nature of the binding pocket was hydrophobic, hydroxyl-derivatives were among the accepted substrates, whereas the bulky methyl- and methoxy-derivatives were not converted or were accepted to a limited extent only. The hydrophobic nature of the active site was not a constraint and an introduction of polar residues was not required for the conversion of substrates with polar functions. Therefore, it did not represent a crucial condition for substrate acceptance.

According to the rules established in 1994 by DE FILIPPIS et al. which were based on the comparison of crystal structures of point mutants and wild-types (n = 83), the mutagenesis

experiments performed were categorized under the so called X → Ala and X → Gly mutations, where X represented a more voluminous residue. In these cases the residue was replaced by a similar, but smaller residue and no strain was introduced into the structure by the mutation. The mutated residue was expected to adapt an orientation according to the cavity available and no large changes were expected in the local structure. The structural effect of a point mutation was often limited: adoptions were made mainly by the mutated residue and the overall (secondary) structure was not dramatically effected (DE FILIPPIS et al, 1994).

The replacement of residue Trp149 by Ala represented the largest structural change in the active site. Tryptophan represents the largest amino acid, extending ca. 10 Å, while alanine is one of the smallest. It was likely that this significant difference in size influenced the stability and function of the resulting mutant. Shielding the carbon 7 of tryptamine, there were only a few interesting substrates available for mutant W149A (such as 7-methyl-tryptamine, $N_{(\alpha)}$-methyl-tryptamine, $N_{(\alpha)}$-acetyl-5-hydroxy-tryptamine). Since 7-methyl-tryptamine was accepted to a modest extent by the wild-type enzyme, a more efficient conversion was expected with the mutant W149A.

Interactions over greater distances within a protein can hardly be predicted, thus the double mutant E205V/V208A was included in the current study. Residue Glu205 is located at the enzymes surface (blade 3 strand d) at a distance of > 13 Å from the active site.

The mutant E309D was not constructed for broadening the substrate specificity. Rather, mutant E309D represented a small digression concerning the investigation of the reaction mechanism and stereo-selectivity. The effect of a shorter aliphatic chain on the stereo-selective orientation during the enzymatic reaction was investigated (It has been discussed in section V.1.2.3).

Double mutants combining the replacement of Val167 and Val208 were planned, but could not be achieved. Sequencing results showed multiple primer doubling and all selected colonies had to be rejected. However, the mutagenesis of residue Val167 was in general critical. Mutant V167A exhibited poor yield and activity (IV.6). V167G was not obtained in soluble form and no activity was detected. Both mutants revealed an unknown band of ca. 15 kDa in SDS PAGE analysis, which obviously came from the plasmid (*str1_V167A*-pQE2 and *str1_V167G*-pQE2) and depended on IPTG induction (IV.6.6).

V.2.3 Broadening the substrate specificity of STR1

The structure–based, rational re-design of *R. serpentina* STR1 active site in order to modulate activity and substrate specificity was successfully used to broaden the substrate scope of this enzyme. The generated mutants V208A, V208G and E205V/V208A exhibited the ability to convert 5-methyl- and 5-methoxy-tryptamine in the presence of secologanin to the corresponding strictosidine derivatives which broadened the substrate specificity for tryptamine derivatives and consequently the variety of strictosidine derivatives. The novel isolation of 10-methyl- and 10-methoxy-strictosidine with a mg yield was possible via enzymatic synthesis. This was confirmed using HPLC, LC-MS, ^{1}H- and ^{13}C-NMR analysis (IV.6.3.2). Furthermore, kinetic studies showed a 2 – 8-fold increase in conversion efficiency of 5-hydroxy-, 6-methyl- and 6-methoxy-tryptamine. The modeling results by TINKER Force Field Explorer were consistent with the engineering strategy and supported it. The calculated models showed that the space provided for the tryptamine molecule was enhanced and allowed for substituents at the carbons 5 and 6 (Figure 54). Based on the validation of the computer modeling procedure (IV.7.2), it was concluded that the calculated models represented the three-dimensional structure of the mutants accurately enough for the current purpose. It is discussed in the subsequent section (V.2.4).

The mutants W149A and V167A represented two further re-engineered enzymes which broadened the substrate specificity for 5- and 6-substituted tryptamine analogues: both accepted 5-methyl- and 5-methoxy-tryptamine as substrates. Although the activity was in part extremely low (specific activity of V167A 0.13 – 0.48 µmol/min/mg; W149A ≤ 0.002 µmol/min/mg; see IV.6.3.3), the mutants confirmed the results achieved with the mutagenesis of residue Val208. Furthermore, mutant W149A featured the conversion of another novel substrate: N$_{(\alpha)}$-acetyl-5-hydroxy-tryptamine was accepted by this re-engineered enzyme. Though the activity of W149A was poor and the identity of the putative product peak could not yet be confirmed by NMR or LC-MS, HPLC analysis indicated the formation of a product peak. This putative product peak did not occur in the control incubation with denaturized enzyme. It gained area with increasing enzyme concentration and incubation time and the substrate loss was significant.
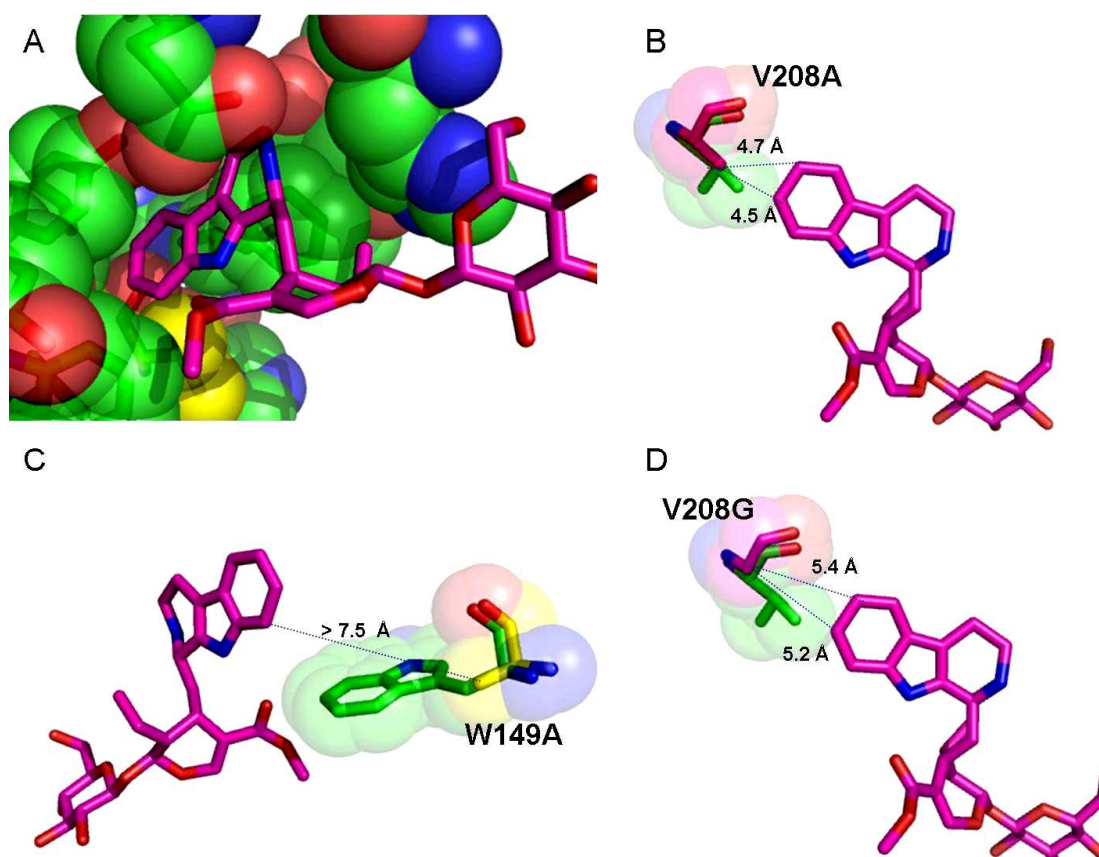
Figure 54. Structural analysis of generated mutants. (A) The crystal structure of STR1-strictosidine complex active site. The spheres of the residue are displayed. Strictosidine is surrounded by residues in close proximity (ca. 4 Å). Residue Val208 is highlighted in yellow, the strictosidine molecule in magenta. (B) The structural alignment of Val208 of STR1-strictosidine complex (green) with the model of mutant V208A calculated by TINKER (in pink). Spheres are displayed and emphasize the enhanced space available in the active site of mutant V208A. Distances between the mutated Ala208 and the carbons 5 and 6 of the strictosidine molecule (magenta) are shown. (C) Mutant V208G: residue Gly208 (magenta) is superimposed with STR1-strictosidine complex. Residue Val208 is shown in green. (D) Mutant W149A: residue Trp149 is superimposed with STR1-strictosidine complex: Trp149 green, Ala149 yellow.

The results demonstrated the potential of rational site-directed mutagenesis and re-engineering of STR1. The calculation and modulation of substrate's acceptance has become practicable and will constitute an attractive strategy for the efficient generation of novel strictosidine derivatives and new alkaloids derived from them. To the author's knowledge it represents the first rational approach to predict and modulate the substrate spectrum of STR1 from *R. serpentina*. It is expected that via further structure-based re-engineering, an additional rational modulation of activity and substrate selectivity of STR1 will be possible. In conclusion, it is assumed that a structure-based re-design strategy may be applicable to other enzymes. Hereby, the structural knowledge of enzyme-ligand complex structures represents the major requirement.

The modulation of substrate specificity by saturation mutagenesis of STR from *C. roseus* (STR_CR) represented a different approach. It required facilities for the expression and purification of a large number of randomly generated enzyme variants and a rapid method for identification of competent mutants. With this random approach, two mutants were obtained with enhanced substrate spectrum (BERNHARDT et al., 2007). The mutation site Val214 in STR_CR found by the screening of randomly generated enzyme variants corresponded to the point mutations at residue Val208 in STR1. A mutant where the Val residue 214 was replaced by a less voluminous amino acid (Met in STR_CR) also converted 5-methyl-tryptamine. It confirmed that this residue (Val208) was a crucial constraint for the turnover of carbon-5-substituted tryptamine analogues and supported the successful engineering strategy developed in the current work.

CHEN et al. (2006) demonstrated that the generation of several strictosidine derivatives containing alterations within the monoterpenoid unit by engineered enzyme variants of STR from *C. roseus* was superior to the wild-type conversion. A broadening of the substrate specificity for the monoterpenoid unit, which could not be achieved until now, could be the next aim for a rational re-design of STR1.

V.2.4 Computer modeling results

Performance and validation of the computer modeling by TINKER Force Field Explorer is described in section IV.7.2. A model of native STR1 was generated and aligned to the crystal structure of STR1 (native, PDB code 2fp8) and STR1-strictosidine complex (PDB code 2v91). Structural alignment of crystal structure and model showed that the calculated STR1-model in generally corresponded to the crystal structures. The root mean square deviation (RMS deviation) of 0.9 – 1 Å between the aligned α-carbon atoms indicated that the protein backbones calculated by TINKER did not highly differ from the structures obtained by crystallization and X-ray analysis (see Figure 43, page 109). Though the superimposition of the individual crystal structures resulted in significant lower RMS deviation values (0.3 – 0.4 Å), considering the resolution range of 20 – 3.0 Å, the computer modeling was satisfactory. Backbone differences were particularly located at the enzyme surface, far from the active site and were considered as negligible. An explanation for these variances may be the fact that the influence of the aqueous medium remained unconsidered during the simulations. Solvation energies, e.g. interactions of residues at the enzyme surface with the solvent could not be accurately simulated in the modeling procedure.

In the binding pocket, the side chain deviations between the STR1-model and the crystal structures were investigated in detail and showed an average difference of ca. 1 Å. Residues including F226 and G210 exhibited an average distance of > 1.5 Å, but still match the

conformation tolerably. By comparison of the individual crystal structures, similar differences were detected between the corresponding residues. Moreover, the comparison of the two STR1 molecules (A and B) located in the asymmetric unit exhibited similar values. Therefore it was concluded that the conformation of the active site was accurately represented in the STR1-model. The models calculated by TINKER approximated the 3D-structure of the mutants and in particular the conformation of the active site satisfactorily and were therefore chosen as adequate models for illustration purposes. Nevertheless one should keep in mind that these models and hereby all further conclusions based on theoretical calculations and do not necessarily reflect the molecule's structure and properties in the physiological environment.

V.3 Application-oriented conclusions

V.3.1 Enzyme activity and application of re-engineered enzymes

The results from enzyme kinetics, activity tests and turnover studies presented in this work are important for one basic reason: they are measures for the efficiency of the engineered enzymes and indicate how they may be applied in preparative enzymatic syntheses.

Figure 55 displays representative raw data (peak area) of the conversion of tryptamine and secologanin by wild-type STR1 obtained by HPLC. It hereby illustrates the efficiency of the wild-type enzyme with the native substrates. Within 5 min, a total conversion of both substrates was achieved as shown in the HPLC trace (1 mM each in the incubation mixture). The turnover number (k_{cat} = 10.65 s^{-1}) and specificity constant (k_{cat}/K_M = 147.92 mM^{-1}/s^{-1}) determined, reflected the catalytic power of the enzyme. The K_M value of the conversion of tryptamine by the wild-type enzyme (0.072 (± 0.02) mM) represented the lowest K_M observed in the current study.

Kinetic analysis of STR from different sources was performed several times during the last decades and the K_M values reported ranged between 0.0062 mM and 5.8 mM for the conversion of tryptamine by STR from *Rauvolfia* species (TREIMER and ZENK, 1979a; HAMPP and ZENK, 1988; KUTCHAN et al., 1994; MA et al., 2006). Differences in source and methodology may have caused these extremely variable results. The only investigation comparable to the current analysis was performed by MA et al. (2006) using His$_6$-tagged enzyme from *R. serpentina*. They report a K_M value of 6.2 µM for tryptamine and a turnover number (k_{cat}) of 1.3 s^{-1}. The present kinetic results for STR1 wild-type with tryptamine as substrate, namely the K_M value as well as the turnover number k_{cat} were ca. 10-fold higher than the values determined by MA et al. (2006). However, these values were in accordance with the current observations from relative activity and turnover studies and additionally lie

within the range given in the literature. Moreover, the above mentioned K_M and k_{cat} values are consistent with the other kinetic values determined in the present context.
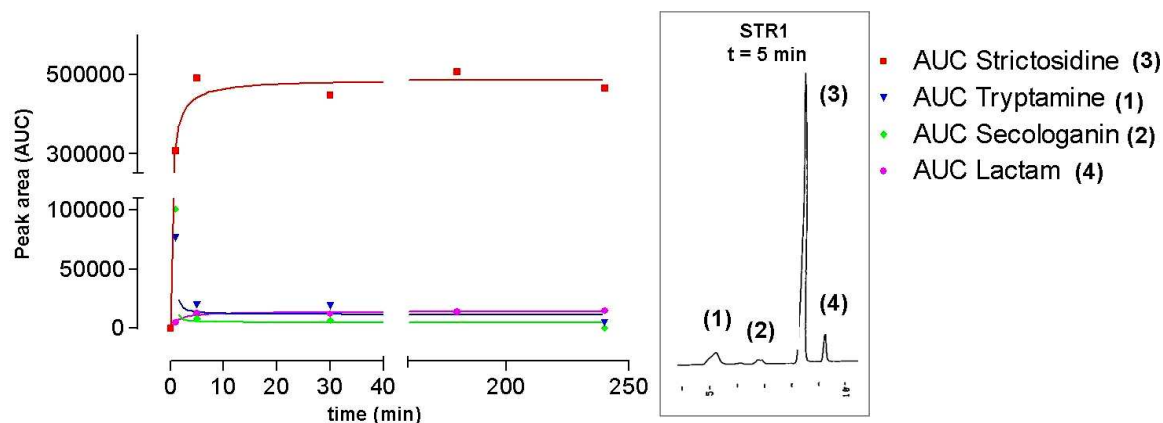
Figure 55. The high conversion of tryptamine and secologanin by wild-type STR1-His$_6$. Diagram on the left: product formation (red) and substrate loss (tryptamine in blue, secologanin in green) are plotted against the incubation time. The purple line represents the lactam formation. HPLC trace on the right: within 5 minutes, the wild-type enzyme converts > 95 % of the native substrates. Data obtained by a turnover study according to III.4.1.5.

The investigation of the relative activity of the wild-type enzyme with different tryptamine analogues showed that wild-type STR1-His$_6$ was highly substrate specific and a high-power conversion comparable to the turnover of tryptamine (relative activity 100 %) was not achieved with other compounds (relative activity < 10 %; see IV.2). The employment of re-engineered enzyme variants changed this situation: several mutants exhibited an enhanced substrate spectrum (W149A, V167A, V208A, V208G, and E205V/V208A) and for a minimum of two substrates a more efficient turnover was achievable with the re-engineered enzyme variant V208A (6-methyl- and 6-methoxy-tryptamine).

For compounds, clearly exhibiting the best results with the wild-type enzyme (such as the formation of native strictosidine as well as 10- and 11-fluoro-strictosidine), no assay modifications were further tested. The rational re-design of STR1 was focused on rejected and less active tryptamine analogues, e.g. 5-methyl- and 5-methoxy-tryptamine, 6-methyl- and 6-methoxy-tryptamine. Here significant progress was achieved by the utilization of re-engineered mutants.

The substrate scope of STR1 was extended by two compounds, namely 5-methyl- and 5-methoxy-tryptamine. Conversion was achieved by mutants V208A, V208G, W149A, V167A and E205V/V208A. Mutant V208A enabled the recovery of the resulting strictosidine derivatives in mg yield and herewith fulfilled the prerequisite for the further application of

these compounds in the biomimetic approach mentioned above (I.5) and presented in section V.4.

In general, the generation of 11-methyl- and 11-methoxy-strictosidine by wild-type STR1 was feasible, but the efforts were considerable compared to mutant V208A. For example the difficulty of the formation of 11-methoxy-strictosidine can be observed as following: 18 h were necessary to yield 1 mg product (conversion 75 %) while an equivalent amount was achieved in 3 h under identical conditions by use of mutant V208A. By the employment of the re-engineered enzyme, a 5.4-fold and 6-fold reduced incubation time was suitable for the recovery of 11-methyl- and 11-methoxy-strictosidine. The turnover study clearly demonstrated that the conversion of 6-methyl- and 6-methoxy-tryptamine by V208A was more efficient than the wild-type conversion and approved its future utilization.

The kinetic results obtained for the conversion of 5-hydroxy-tryptamine strongly suggested a higher efficiency of V208A (2-fold higher specificity constant k_{cat}/K_M compared to the wild-type conversion; see section IV.6.3.3), however, the current turnover study did not confirm this result: no significant benefit was detected under the applied conditions (IV.6.5.1.2). It is expected that further optimization efforts, e.g. a change in enzyme-substrate ratio as successfully applied for the conversion of other compounds (5-methyl- and 5-methoxy-tryptamine; see IV.6.5.1.1) can change this situation and will certainly exhibit the differences in activity.

The analysis of the substrate specificity of mutant W149A indicated that this enzyme provided the turnover of $N_{(\alpha)}$-acetyl-5-hydroxy-tryptamine. This compound represented a novel compound, which was not accepted by any other enzyme variant (including the wild-type). However, the experimental evidence was up to now rudimentary and spectroscopic product identification is still required to confirm this assumption. Due to the low expression and activity, the mutant did not allow for further investigation and at this point it is suggested for future studies to begin with the optimization of the W149A expression.

Concerning the relative enzyme activity with the native substrates, double mutant E205V/V208A was the most active STR1 mutant (ca. 90 % relative activity). It converted tryptamine almost to the same extent as the wild-type enzyme. The mutation E205V was located at the enzyme's surface and it represented the replacement of an acidic, relatively large residue (Glu205) with a smaller, uncharged Val residue. Due to the spatial separation between the mutation site and binding pocket the effect could not be predicted. Interactions over distances of this nature, were technically not conceivable, nevertheless, it appeared to benefit the turnover of tryptamine. The double-mutant E205V/V208A converted 17 % (± 1.6)

of 5-methyl-tryptamine and < 1 % of 5-methoxy-tryptamine to the corresponding novel strictosidine derivatives in the presence of secologanin within 15 min (substrate concentration 1 mM, standard incubation at 35 °C). Under identical conditions, the mutant V208A converted 54 % (± 5.8) of 5-methyl-tryptamine and 21 % (± 6.2) 5-methoxy-tryptamine. Though the double-mutant exhibited only weak turnover of 5-methyl- and 5-methoxy-tryptamine, it demonstrated the importance of the residue Val208 for the conversion of substrates with bulky groups at these positions and supported the engineering strategy.

The highest affinity for the substrate 5-methoxy-tryptamine was exhibited by the mutant V208G (as reflected by the K_M value of 0.433 (± 0.14) mM) but its turnover activity was extremely low, resulting in a specificity constant k_{cat}/K_M of 0.73 mM^{-1}/s^{-1}. Low turnover numbers were a general feature of this mutant (k_{cat} < 2 s^{-1}). Though the K_M value of V208A was 8.3-fold higher (3.592 (± 1.12) mM), the most efficient enzymatic synthesis of 10-methoxy-strictosidine was achieved with this mutant (k_{cat}/K_M 22.18 mM^{-1}/s^{-1}). This also applied to 10-methyl-strictosidine.

For a highly efficient enzymatic synthesis, the knowledge of the impact of temperature and pH on the enzyme's activity is essential. In the literature, several studies on temperature and pH dependence of STR from different plant species have been published. For *R. serpentina* STR1 two sources reported a pH optimum of pH 6.5 (HAMPP and ZENK, 1988; KUTCHAN et al. 1994). As optimal temperature 45 °C (HAMPP and ZENK, 1988) and 55 °C (KUTCHAN et al. 1994) were stated. This difference might be caused by different sources and methodology: HAMPP and ZENK (1988) investigated cell culture derived STR1 while KUTCHAN et al. (1994) used the Baculovirus system for expression of recombinant STR1 in Sf9 cells. Until today, His$_6$-tagged STR1's temperature and pH optimum was not investigated.

Due to instability reasons temperature optima of > 40 °C were not applicable, because they frequently damaged the product and benefit lactamization. In the current work, the main aspect of the investigation of temperature and pH effect was their influence on a preparative synthesis of strictosidine derivatives. For enzymes featuring sufficient activity at 28 – 35 °C (such as STR1 and mutant V208A), turnover studies were executed using two different temperatures below the reported optima (28 °C versus 35 °C, see section IV.6.5.1) in order to find the most efficient conditions and enzyme variants. The results permitted conclusions in regards to the amount of enzyme necessary for the enzymatic synthesis of 1 mg of the novel strictosidine analogues. The volume of bacterial culture was calculated on the basis of the time-conversion plot and the yield of expression and purification.

The results showed that high temperatures (35 ° C) in generally benefit the product formation; however, they also increased the lactamization, which putatively led to lower product yield. The poorly converted substrates (such as 5-methoxy-tryptamine) benefit slightly from higher temperatures, however, compounds which were already converted with good activity showed no significant differences (5-methyl-tryptamine). The lactam formation was detectable at ca. 20 and 60 min at 35 and 28 ° C respectively. Unexpectedly there was no influence on the strictosidine formation, which may have been the result of a high reaction rate, which compensated the loss due to lactamization.

The temperature alone was not the crucial determinant. For enzymatic synthesis of 10-methoxy-strictosidine in particular the change in enzyme-substrate ratio (from 1:270 to 1:67), favored a fast conversion: by reducing the substrate excess from 1:270 to 1:67, the reaction rate was boosted significantly. To yield 1 mg 10-methoxy-strictosidine a 4.4-fold reduced incubation time (from 22 h to 5 h) was sufficient. Until today 5-methoxy-tryptamine remained the least efficient in the current array of substrates. Nevertheless, even this critical compound was converted by an engineered enzyme in satisfactory quantities so that the respective strictosidine analogue was accessible in mg yield.

The investigation of temperature- and pH-optima of the mutants W149A and V208G contributed to the understanding of their poor activity with tryptamine derivatives (IV.6.5.1.3). Both showed optimal conversion of tryptamine at 50 ° C – a temperature which was not suitable for preparative enzymatic synthesis. At the standard temperature (30 ° C) V208G still converted with 66 % of the optimal activity while W149A had only 37 %. It was concluded that elevating the incubation temperature can significantly improve the activity of W149A and represents an option for optimization procedures. The effect of pH on the relative activity of the two mutants was not distinct. The employed KPi buffer pH 7.0 represented the pH optimum for V208G while W149A featured 95 % activity (pH-optimum was pH 6.2).

V.3.2 Substrate inhibition

A putative inhibitory effect of high tryptamine concentrations on the activity of His$_6$-tagged STR1 and its engineered variants would have significant influence on the analysis of the enzymes and eventually it could limit their further application. Therefore a careful analysis was performed to answer the question whether high tryptamine concentrations were inhibitory or not, to the activity of His$_6$-tagged STR1 from *R. serpentina*. In the current work, experiments using tryptamine concentrations of up to 5 mM have been applied and no substrate inhibition was detected (IV.3.1).

In the literature, several studies have dealt with the substrate inhibition of STR from different sources (TREIMER AND ZENK, 1979b; HAMPP and ZENK, 1988; STEVENS et al., 1993; KUTCHAN et al., 1994; DE WAAL et al., 1995; YAMAZAKI et al., 2003b). However, it was difficult to draw any conclusions for the present work, since recombinant His$_6$-tagged STR1 from *R. serpentina* has never been tested before, for a putative substrate inhibition. The enzymes employed in previous studies were mostly derived from cell suspension cultures of *R. serpentina, C. roseus, C. robusta,* and *O. pumila*. Furthermore the authors arrived to various conclusions.

Inhibition of enzyme activity at elevated tryptamine levels was described by HAMPP and ZENK in 1988 for STR1 from *R. serpentina*. The enzyme was derived from cell suspension cultures and tryptamine concentrations higher than 0.9 mM caused a strong substrate inhibition. KUTCHAN et al. (1994) also reported an inhibitory effect of tryptamine concentrations higher than 0.7 mM. In that work, the enzyme was cloned and heterologously expressed in Sf9 cells using Baculovirus system. For STR from *C. roseus*, different results were published: while TREIMER and ZENK (1979b) reported that tryptamine concentrations higher than 1.2 mM were inhibitory to the enzyme reaction, DE WAAL et al. (1995) did not observe this phenomenon. Though they investigated tryptamine concentrations of up to 5 mM, no substrate inhibition was detected. No inhibitory effects of tryptamine were detected for the reaction catalyzed by STR from *O. pumila* (YAMAZAKI et al, 2003b) and *C. robusta* (STEVENS et al., 1993).

V.3.3 Strictosidine synthesis by immobilized His$_6$-tagged enzymes

For over 15 years, PFITZNER AND ZENK (1982) described a successful approach for the preparative synthesis of strictosidine using immobilized STR from *C. roseus*. The enzyme was extracted from cell suspension cultures of *C. roseus* and was immobilized on CNBr-activated sepharose. Beside an enhanced thermostability, the preparation of gram quantities of 3α-(*S*)-strictosidine was reported.

The prospects of a flow-through assay by use of His$_6$-tagged enzymes bound to Ni-NTA matrix were investigated in the current work. The conversion of 5-methyl- and 5-methoxy-tryptamine by mutant V208A immobilized on Ni-NTA matrix served as a case study. It clearly demonstrated that His$_6$-tagged enzyme bound to Ni-NTA was active and could be employed for the preparative synthesis of strictosidine (analogues) in a flow-through assay. It was concluded that this was true for His$_6$-tagged STR1 wild-type and the other mutants as well.

Considering the poor quality of expression and purification of soluble, His$_6$-tagged STR1 and mutants, the main advantage of a flow-through assay utilizing immobilized enzyme, is the re-use of the enzyme. Furthermore, the separation of the product from the enzyme and a highly

pure product (in the case of complete conversion) are advantageous. Even a salt-free product is achievable, if the activity in un-buffered aqueous solution is sufficient. Buffered solutions are not mandatory. Therefore a flow-through assay is an attractive strategy for the mass production of strictosidine derivatives.

The subsequent optimization efforts are required in order to achieve sufficient conversion. For an analytical scale, the utilization of Pasteur pipettes as columns represented a makeshift solution. A column system allowing for a better regulation of flow volume and velocity appeared more suitable for a large-scale preparative synthesis. A higher conversion and reaction yield was expected from a longer residence of the substrates in the column: the solutions should pass the immobilized enzyme as slowly as possible. However, increasing the amount of enzyme bound to the Ni-NTA matrix and its optimal activity will additionally benefit the conversion. The advantage of a salt-free product by use of an aqueous solution can be neglected with regard to a more efficient reaction.

The stability of the immobilized enzyme was proved over a period of 24 h at RT. PFITZNER and ZENK (1982) reported a remarkable increase in thermostability of immobilized enzyme compared to soluble enzyme: after 68 days at 37 °C about 50 % activity was observed, while soluble enzyme had a half-life of 5 h under identical conditions. It is likely that the stability of STR1 mutant V208A is given beyond the investigated period of 24 h.

V.3.4 The heterologous expression of STR1-His$_6$ and its re-engineered variants

The current production of biologically active, recombinant STR1-His$_6$ by use of M15 cells and pQE2 vector was complicated by the formation of insoluble inclusion bodies (MA et al., 2006). In particular the engineered mutants W149A and V208G accumulated to a large extent as insoluble complexes, detectable in the pellet fraction via SDS PAGE. In these aggregates, the proteins were present in a misfolded, denaturized state, precipitated with other cell constituents (such as ribosomes, nucleic acids and other cytoplasmic proteins; HARTLEY and KANE, 1988; BLACKWELL and HORGAN, 1991).

It was however the denaturation and the heterogeneous character of the precipitates, which made the recovery of soluble, active enzyme from inclusion bodies a difficult task. *In vitro* re-folding and re-naturation were complex procedures and no general techniques had been developed until today. Since the formation of inclusion bodies depended on the protein synthesis rate and growth conditions, the optimization efforts described in section IV.8 focused on the manipulation of the current protocol in order to increase the yield of soluble protein. Modest success was achieved by lowering the level of expression (reduction of IPTG concentration and temperature).

Best results were achieved with the utilization of the *E. coli* strain Arctic Express (AE), instead of M15. AE provided the co-expression of cold-adapted chaperones (cpn60 and cpn10) and enabled the expression of the *str1*-pQE2 and *str1_W149A*-pQE2 plasmids at temperatures of 12 – 15 °C. The expression of *str1*-pQE2 in AE resulted in an almost 30 % higher yield of soluble, active STR1-His$_6$. Unfortunately, this result was not reproducible to the mutant W149A. Furthermore, the technical requirements were a limiting factor for expression at low temperatures.

A more effective cell disruption technique would benefit the recovery of soluble STR1 as well. In general the purification of low quantities of bacterial masses (deriving from cultures ≤ 20 l) achieved the best results due to the convenient handling.

However, in view of a future mass-production of strictosidine and its analogous via enzymatic synthesis, the protein yield required will most probably exceed the capacities of the current expression system and further investigations will be necessary. For a large scale production of recombinant STR1, a new production strategy is recommended in order to reduce the formation of inclusion bodies significantly, since a real breakthrough is not yet achieved. To overcome this future challenge, three promising strategies are presented below. They are suggested for the recovery of STR1 and the engineered variants.

1. BLACKWELL and HORGAN (1991) reported a novel strategy for the high-yield production of recombinant protein: they produced large amounts of active, soluble protein (reportedly an increase of > 400-fold) under an elevated osmotic pressure by growing and inducing the cells in the presence of sorbitol and glycyl betaine. Osmotic stress facilitated the uptake of glycyl betaine, which acted as a "compatible solute" (BROWN, 1976; BLACKWELL and HORGAN, 1991) and favored the production of active, soluble protein. This resulted in the disappearance of the protein from the pellet fraction. The authors suggested that this treatment may be widely applicable to the production of other recombinant proteins and it is proposed that it could benefit the expression of STR1 as well.

2. *E. coli* cells represent a well characterized and cost-efficient prokaryotic expression system. However, the direct expression of His$_6$-tagged STR1 and the engineered mutants, did not deliver an optimal performance. A fusion expression of STR1 (e.g. pMAL Protein Fusion and Purification system provided by New England Biolabs, Ipswich, USA) represents another opportunity, which is in particular recommended to overcome the insolubility of STR1. *E. coli* maltose-binding protein (MPB) has been demonstrated to enhance the solubility of its fusion partners (KAPUST and WAUGH, 1999). An attempt to use fusion protein expression systems in place of the current standard protocol is highly recommended. Sub-

cloned in frame with a MBP-encoding gene, STR1 can be expressed as a MBP-fusion protein, which can be purified via one-step affinity purification process. By use of specific proteases the enzyme can be cleaved from MPB.

3. The replacement of the current host (*E. coli*) represents a further option. *Saccharomyces cerevisiae* yeast expression (by use of pYES2/CT vector encoding for C-terminal His-tag; McCoy et al., 2006) proved to be highly efficient for the production of recombinant STR from *C. roseus* (S. E. O'Connor, personal communication).

Though the potential of the present expression system is not yet totally exploited, a novel efficient method for the recovery of STR1 is required to overcome the problem of inclusion body formation and to meet the future challenge of a large scale production of recombinant STR1.

V.4   Future prospect

Future outlooks include the further processing of the newly accessible strictosidine analogues by subsequent catalytic steps of the monoterpenoid indole alkaloid biosynthetic pathway – if necessary by means of further (rationally) re-engineered enzymes. Several of the "unnatural" strictosidine compounds demonstrated successful implementation in downstream pathways in *C. roseus* cell cultures (CHEN et al., 2006; McCoy et al., 2006; McCoy and O'Connor 2006). It is likely that this also applies to STR1 from *R. serpentina* and future interest will be directed toward strictosidine glucosidase (SG; BARLEBEN et al., 2005 and 2007), the enzyme which follows STR in the biosynthesis of the indole alkaloid family. It catalyzes the de-glycosylation of strictosidine and yields the highly reactive strictosidine-aglycon (GERASIMENKO et al., 2002). The recently determined crystal structure of SG from *R. serpentina* (BARLEBEN et al., 2007; PDB code 2jf6 and 2jf7) and the investigation of the substrate specificity of SG from *C. roseus* (YERKES et al., 2008) turned out to be promising.

The structure of SG in complex with strictosidine showed the glucose moiety located deep in the binding pocket, with the indole portion in close proximity to the surface (Figure 56). Putative structural interferences of active site residues with substituents at the indole ring (as observed in the STR1 structure, see Figure 56) are not likely to occur. It is hypothesized that the active site of SG does not generally constrict the conversion of these strictosidine derivatives. Furthermore, the substrate specificity study by YERKES et al. (2008) demonstrated SG from *C. roseus* to be highly tolerant to substitutions at these specific positions of strictosidine. Methyl- and methoxy-functions, including 10-methyl- and 10-methoxy-strictosidine, were tolerated in general. YERKES et. al (2008) concluded that SG does not discriminate against substitutions at the indole ring and that the specificity of the initial stages of the biosynthetic pathway is in large part controlled by STR.

It is concluded that a rational re-engineering of SG from *R. serpentina* in order to act in concert with the re-engineered STR1 variants will probably not be necessary. Nevertheless, this option must be taken into consideration for future metabolic progressing, since experimental evidence on the substrate specificity of SG from *R. serpentina* is not yet available. However, the current structure-based engineering strategy proved to be successful. Overall, the results suggested that it is plausible to apply a rational re-design to other enzymes subsequent to STR1 in the biosynthetic pathway. However, the elucidation of the three-dimensional structures remains essential.
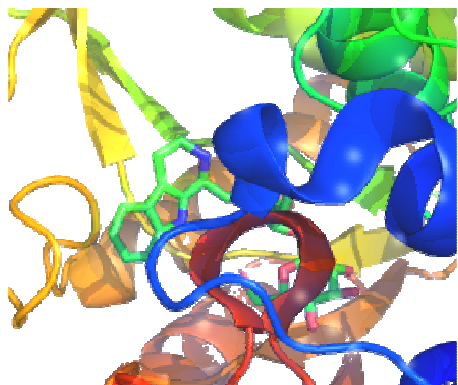
Figure 56. Crystal structure of an inactive mutant of SG with strictosidine bound to the active site. Barleben et al. (2007), PDB code 2jf6. The surface representation demonstrates the position of the indole moiety of strictosidine at the entrance of the binding site with the glucose portion deep in the catalytic pocket.

The currently accessible novel strictosidine derivatives will be used as source material for further chemo-enzymatic modifications. The potential lying in strictosidine and its derivatives is exemplified by a so called biomimetic approach developed by H. Schübel and J. Stöckigt (LORIS et al., 2007). It combines the enzymatic reactions catalyzed by STR1 and SG with further synthetic modulations to a chemo-enzymatic (e.g. biomimetic) approach as shown in Figure 57.

The observation that in presence of NH_4^+-ions, N-heteroyohimbine alkaloids are formed in enzyme assays (HEINSTEIN et al., 1979) inspired to attempt the application of the biomimetic approach, which incorporates the enzymatic and chemical reactions in "one pot". The main requirement is initially a sufficient amount of strictosidine, which is provided due to STR1 and its variants. The incubation of the strictosidine (-derivative) is performed using 0.1 M KPi buffer (pH 7.0) in the presence of an excess of a primary amine compound (such as tryptamine, Figure 57) and a crude enzyme preparation containing SG at 30 °C for several hours. Since SG is the sole required compound of the crude enzyme extract, it is possible to use any indole alkaloid-producing cell system, including *Rauvolfia* (originally the crude enzyme was derived from *C. roseus* cell suspension cultures). Furthermore, it is feasible to employ recombinant SG and engineered SG variants with modified substrate spectra to produce the aglycon (in case the substrate specificity of SG does not allow for the conversion of individual strictosidine derivatives).
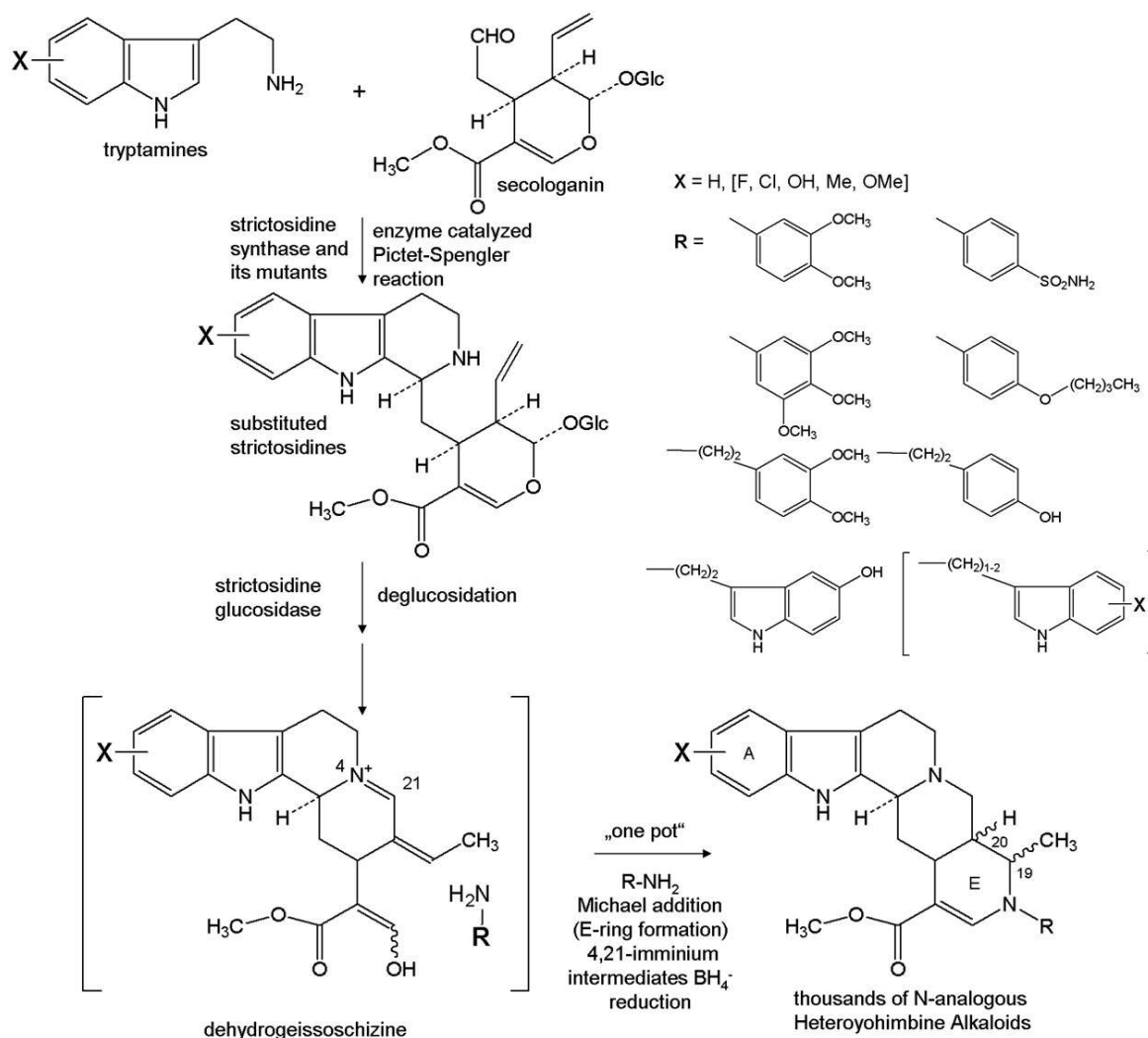
Figure 57. Chemo-enzymatic synthesis of novel N-analogous heteroyohimbine alkaloids. The illustrated combination of X with mono- and di-substitution and with R substitution (including R-X-substitution) delivers thousands of new alkaloids of the heteroyohimbine type. Each "one pot" experiment leads to four diastereomeric alkaloids (at positions 19 and 20). R residues in brackets represent novel determinants which have not yet been tested with the biomimetic approach. The figure was published in LORIS et al., 2007.

In the current approach, the aglycon serves as a potent building block for biomimetic generation of novel alkaloids (STÖCKIGT and RUPPERT, 1999; BARLEBEN et al., 2005; LORIS et al., 2007). It rearranges into 4,21-dehydrogeissoschizine, which subsequently incorporates the amine compound under ring-closure. The variability of this combinatorial approach and the biochemical potential of reactive alkaloid intermediates allows for the insertion of various substituents into the heteroyohimbine structure by way of this facile reaction which can be systematically applied for preparative structure modifications. The subsequent reduction via NaBH$_4$ yields four different diastereomeric products (carbon 19 and 20).
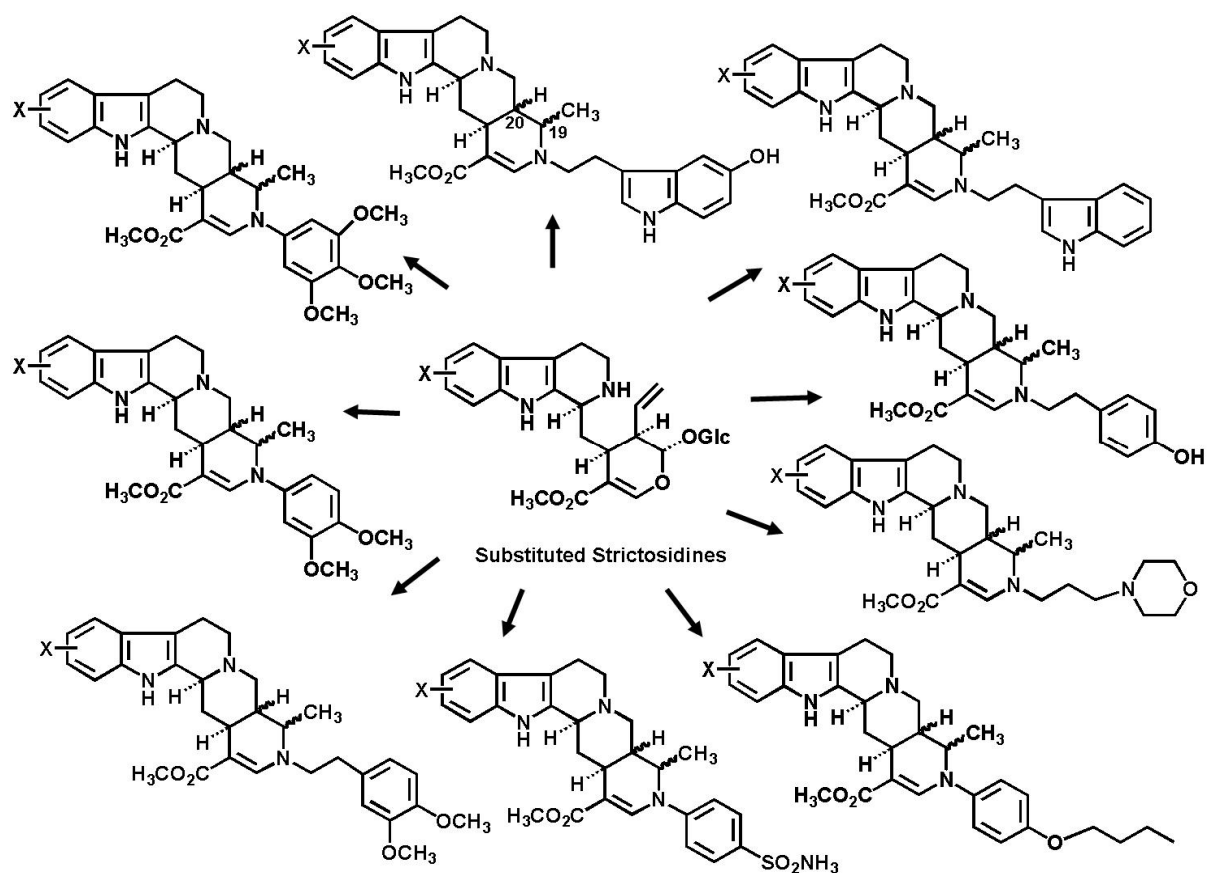
Figure 58. Variety of heteroyohimbine analogs obtained by the "one pot" approach. Starting from strictosidine, the compounds illustrated above were generated by the biomimetic approach described (X = H). It can now be extended by novel strictosidines analogous, generated by rationally re-engineered enzyme variants.

The "one pot" approach has proven to be successful with different substituted primary amines (Figure 57 and 58) using a crude enzyme extract from *C. roseus* cell suspensions starting with strictosidine. It can now be extended via the use of STR1 mutants from *R. serpentina,* using a combination of X-substituted tryptamine derivatives and various substituted primary amines as shown in Figure 57 and 58. The fact that the number of strictosidine derivatives can now be enhanced significantly and their yield allows for further chemical modifications enables the generation of a large number of novel alkaloid compounds via biomimetic synthesis. Each strictosidine derivative, that is processed in this way, delivers 36 novel N-analogous heteroyohimbine alkaloids (including stereo-isomers; using the currently employed amine compounds, Figure 57), e.g. with novel 10-methyl- and 10-methoxy-strictosidine, 72 additional alkaloids are available. The individual application of all proposed amine components, illustrated in Figure 57, would allow for an increased number of products. Large libraries of novel, biologically valuable indole alkaloid analogues are expected to be generated in the near future (STÖCKIGT and RUPPERT, 1999; LORIS et al., 2007). Enzymes from *R. serpentina,* native or re-engineered, will play an essential role in achieving this goal.

VI. Summary

The current work relates to the structure and the rational re-design of strictosidine synthase from the Indian medicinal plant *Rauvolfia serpentina* (STR1; EC 4.3.3.2), which is one of the most detailed investigated enzymes in alkaloid biosynthesis. As a so called Pictet-Spenglerase it catalyzes the Pictet-Spengler condensation between tryptamine and secologanin, yielding the central biosynthetic precursor of probably all monoterpenoid indole alkaloids (MIA) occurring in higher plants, namely, 3α-(*S*)-strictosidine. This alkaloid family consists of approximately 2000, structurally complex and diverse compounds, which furthermore feature a wide range of pharmacological activities. Though the yields of MIA are usually very poor, the extraction from botanical resources remains economically more efficient than total synthesis. The current work investigated the plausibilities of a chemo-enzymatic approach for the production of MIA. It focused on the initial step, namely the synthesis of strictosidine (-analogues) using STR1 and engineered variants of STR1. A chemo-enzymatic approach is an interesting new production strategy, particularly if it can be optimized by rational site-directed mutagenesis of wild-type STR1. This was the major aim of the current work.

The expression and purification procedure was based on the protocol published by MA et al. (2004) and employed the *str1*-pQE2 expression vector which introduced a hexa-histidine-tag (His$_6$-tag; STR1-His$_6$) at the N-terminus of the enzyme, enabling the purification by affinity chromatography on Ni-NTA Superflow column material. With the exception of crystallization, all experiments of the present work (such as activity tests, kinetics, enzymatic synthesis, etc.) were carried out using His$_6$-tagged enzyme.

Initially the influence of elevated tryptamine concentrations (up to 5 mM) on the activity of STR1-His$_6$ was investigated. No inhibitory effect was detected, though several previous studies reported this phenomenon (TREIMER and ZENK, 1979b; HAMPP and ZENK, 1988; KUTCHAN et al., 1994). A putative interference with the preparative enzymatic synthesis of strictosidine (-analogues) was not expected.

A detailed, systematic analysis of STR1-His$_6$ substrate specificity was performed, using the His$_6$-tagged enzyme and 17 commercially available tryptamine derivatives. It was demonstrated that the enzyme had a narrow substrate spectrum.

Two novel crystal structures (STR1 in complex with its product strictosidine and in complex with a bisubstrate inhibitor) were presented and discussed in the current work. The results provided a more complete three-dimensional image of STR1 and valuable insight into advanced stages of the reaction mechanism.

The two structures represented the basis for the first rational re-design of STR1. Based on the structural analysis, an engineering strategy was developed with the aim to broaden the substrate specificity of STR1. A set of seven mutants was generated by site-directed mutagenesis experiments, namely W149A, V167A, V167G, E205V/V208A, V208A, V208G, and E309D. Out of the seven STR1 variants, five mutations (W149A, V167A, E205V/V208A, V208A, and V208G) resulted in a broadened substrate scope, accepting two compounds (5-methyl- and 5-methoxy-tryptamine) which were not converted by the wild-type enzyme. Moreover the mutant W149A was assumed to permit the conversion of another novel substrate, $N_{(\alpha)}$-acetyl-5-hydroxy-tryptamine. The structure-based re-engineering of STR1 enhanced the number of available strictosidine derivatives and it furthermore benefit an efficient enzymatic production of certain strictosidine derivatives derived from 6-methyl-tryptamine, 6-methoxy-tryptamine and 5-hydroxy-tryptamine. It was demonstrated that a calculation and rational modification of substrate specificity was practicable.

The opportunities of a flow through assay, by use of His_6-tagged enzymes and Ni-NTA matrix, were investigated. His_6-tagged mutant V208A, immobilized on Ni-NTA matrix, proved to be active and was applied for preparative synthesis of strictosidine analogues in a flow through assay.

In particular mutant V208A-His_6 featured adequate activity and allowed for the first time a preparative enzymatic synthesis of several strictosidine derivatives in mg amounts, which can be used as source material for further chemo-enzymatic modifications. In the current work, the novel generation of two of these derivatives, namely 10-methyl- and 10-methoxy-strictosidine was made possible for the first time.

154

VII. Zusammenfassung

Die vorliegende Arbeit befasst sich mit der Struktur und der rationalen Re-Strukturierung des Enzyms Strictosidine Synthase aus *Rauvolfia serpentina* (STR1; EC 4.3.3.2). STR1 katalysiert die Pictet-Spengler-Kondensation von Tryptamin und Secologanin, wobei stereoselektiv 3α-(*S*)-Strictosidin gebildet wird. Es handelt sich hierbei um eine zentrale Reaktion im Biosyntheseweg der monoterpenen Indol-Alkaloide. Die vorliegende Arbeit demonstriert die Möglichkeiten eines rationalen Enzym-Designs und legt die Weichen für eine präparative, enzymatische Synthese von Strictosidin und Derivaten des Strictosidins. Dabei wurde die in der Literatur beschriebene Expression und Reinigung mit dem *str1*-pQE2 Vektor via Affinitätschromatographie an Ni-NTA (Nickel-Nitrilo-triessigsäure) verwendet (MA et al., 2004). Der Vektor codiert für einen N-terminalen, sechsfachen Histidin-Anhang (His$_6$-tag, STR1-His$_6$). Mit Ausnahme der Kristallisation, welche eine Abspaltung des His$_6$-tags erforderte, wurden alle Versuche (Aktivitätstests, Kinetik, enzymatische Synthese etc.) der vorliegenden Arbeit mit STR1-His$_6$ (bzw. mit den His$_6$-Mutanten) durchgeführt.

Zunächst wurde der Einfluss hoher Tryptamin Konzentrationen (bis zu 5 mM) auf die Enzymaktivität untersucht. Diese hatten keine negativen Auswirkungen auf die Aktivität der STR1-His$_6$ und eine mögliche Substrat-Hemmung durch Tryptamin konnte ausgeschlossen werden.

In einer Analyse der Substrat-Akzeptanz mit verschiedenen Tryptamin-Derivaten, erwies sich die STR1-His$_6$ als höchst substrat-spezifisch: von 17 getesteten Substanzen wurden nur sieben umgesetzt und die relative Aktivität (im Vergleich zur Aktivität mit dem natürlichen Substrat Tryptamin) war nur maximal 10 %.

Die vorliegende Arbeit präsentiert zwei neue Kristallstrukturen des Enzyms: STR1 im Komplex mit dem Produkt Strictosidin sowie im Komplex mit einem synthetischen Inhibitor, der einen Übergangszustand der enzymatischen Reaktion nachahmt. Sie ermöglichten zum ersten Mal einen molekularen Einblick in späte Phasen der Reaktion und erlaubten Rückschlüsse auf den Reaktionsmechanismus.

Außerdem bildeten die dreidimensionalen Strukturen die Grundlage für das rationale Enzym-Design der STR1. Unter Berücksichtigung der Substrat-Spezifität, wurden diese analysiert und eine Mutagenesestrategie erarbeitet, mit dem Ziel, maßgeschneiderte Enzym-Mutanten für die Umsetzung neuer Substrate zu generieren. Mit folgenden Mutationen wurden Veränderungen im aktiven Zentrum der STR1 vorgenommen: W149A, V167A, V167G, E205V/V208A, V208A, V208G, and E309D. Fünf der sieben generierten Mutanten zeigten eine, im Vergleich zum Wildtyp, erweiterte Substrat-Spezifität (nämlich W149A-His$_6$, V167A-

His$_6$, E205V/V208A-His$_6$, V208A-His$_6$ und V208G-His$_6$). Sie akzeptierten 5-Methyl- und 5-Methoxy-tryptamin, zwei Substrate, die der Wildtyp nicht umsetzt. HPLC-Ergebnisse deuteten außerdem darauf hin, dass die Mutante W149A-His$_6$ ein weiteres neues Substrat, nämlich N$_{(\alpha)}$-acetyl-5-hydroxy-tryptamin, zum entsprechenden Strictosidin-Derivat umsetzte.

Die Mutante-His$_6$ V208A ermöglichte die Synthese der beiden neuen, „unnatürlichen" Strictosidin-Derivaten nämlich 10-Methyl- und 10-Methoxy-Strictosidin, im mg-Maßstab. HPLC, LC-MS und NMR-Analysen bestätigten deren Identität. Des Weiteren zeigten kinetische Untersuchungen und Umsatzstudien die Überlegenheit dieser STR1-Variante in der Umsetzung der Substanzen 6-Methyl-, 6-Methoxy- und 5-Hydroxy-tryptamin. Es wurde bewiesen, dass die Mutationen die Stereoselektivität der Kondensationsreaktion nicht beeinflussen.

Weiterhin konnte am Beispiel der STR1 Mutante V208A-His$_6$ gezeigt werden, dass das via His$_6$-tag an Ni-NTA immobilisierte Enzym aktiv ist und sich für die präparative, enzymatische Synthese von Strictosidin (-derivaten) eignet.

VIII. References

BAILEY, P. D. (1987). Direct proof of the involvement of a spiro intermediate in the Pictet-Spengler reaction. J. Chem. Res. (S), 202-203.

BAGAUTDINOV, B., KUNISHIMA, N. (2007). Crystal structures of shikimate dehydrogenase AroE from Thermus thermophilus HB8 and its cofactor and substrate complexes: insights into the enzymatic mechanism. J. Mol. Biol. 373, 424-438.

BAKER, E. D., DODSON, G. G. (2005). Proteins – discovery and detail. Curr. Opin. Struct. Biol. 15, 652-654.

BARLEBEN, L., MA, X., KOEPKE, J., PENG, G., MICHEL, H., STÖCKIGT, J. (2005). Expression, purification, crystallization and preliminary X-ray analysis of strictosidine glucosidase, an enzyme initiating biosynthetic pathways to a unique diversity of indole alkaloid skeletons. Biochim. Biophys. Acta. 1747, 89-92.

BARLEBEN, L., PANJIKAR, S., RUPPERT, M., KOEPKE, J., STÖCKIGT, J. (2007). Molecular architecture of strictosidine glucosidase: the gateway to the biosynthesis of the monoterpenoid indole alkaloid family. Plant Cell 19, 2886-2897.

BATTERSBY, A. R., LEWIS, N. G., TIPPETT, J. M. (1978). The basic glucosides related to the biosynthesis of indole and ipecac alkaloids. Tetrahedron Lett. 19, 4849-4852.

BERKNER, H., SCHWEIMER, K., MATECKO, I., RÖSCH, P. (2008). Conformation, catalytic site, and enzymatic mechanism of the PR10 allergen-related enzyme norcoclaurine synthase. Biochem. J. 413, 281-290.

BERNHARDT, P., MCCOY, E., O'CONNOR S. E. (2007). Rapid Identification of Enzyme Variants for Reengineered Alkaloid Biosynthesis in Periwinkle. Chem. Biol. 14 , 888-897.

BERTANI, G. (1951). Studies on lysogenesis. I. The mode of phage liberation by lysogenic *Escherichia coli*. J. Bacteriol. 62, 293-300.

BERTANI, G. (2004). Lysogeny at Mid-Twentieth Century: P1, P2, and Other Experimental Systems. J. Bacteriol. 186, 595-600.

BLACKWELL, J. R., HORGAN, R. (1991). A novel strategy for production of a highly expressed recombinant protein in an active form. FEBS Lett. 295, 10-2.

BRACHER, D., KUTCHAN, T. M. (1992). Strictosidine synthase from Rauvolfia serpentina: analysis of a gene involved in indole alkaloid biosynthesis. Arch. Biochem. Biophys. 294, 717-723.

BRADFORD, M. M. (1976). A rapid and sensitive method for the quantitation of microgram quantities of protein utilizing the principle of protein-dye binding. Anal. Biochem. 72, 248-254.

BROWN, D. (1976). Microbial water stress. Bacteriological Reviews 40, 803-846.

BROWN, R. T., LEONARD, J. (1977a). Reversible trapping of labile 21-dehydroheteroyohimbines as 21-cyano adducts. Tetrahedron Lett. 18, 4251-4254.

BROWN, R. T., LEONARD, J., SLEIGH S. K. (1977b). „One-pot" biomimetic synthesis of 19β-heteroyohimbine alkaloids. J. Chem. Soc. Chem. Commun. 18, 636-638.

BROWN, R. T., LEONARD, J., SLEIGH S. K. (1978) The role of Strictosidine in Monoterpenoid Indole Alkaloid Biosynthesis. Phytochemistry 17, 899-900.

BRÜNGER, A. T., ADAMS, P. D., CLORE, G. M., DELANO, W. L., GROS, P., GROSSE-KUNSTLEVE, R. W., JIANG, J. S., KUSZEWSKI, J., NILGES, M., PANNU, N. S., READ, R. J., RICE, L. M., SIMONSON, T., WARREN, G. L. (1998). Crystallography and NMR system: A new software suite for macromolecular structure determination. Acta. Crystallogr. D 54, 905 - 921.

CANEL, C., LOPES CARDOSO, M. I., WHITMER, S., VAN DER FITS, L., PASQUALI, G., VAN DER HEIJDEN, R., HOGE, J. H. C., VERPOORTE R. (1998) Effects of over-expression of strictosidine synthase and tryptophan decarboxylase on alkaloid production by cell cultures of Catharanthus roseus. Planta 205, 414-419.

CHAPMAN K. R., CHOMCHALOW, N. (1996). Production of Medicinal Plants in Asia. First Asian Symposium on Industrial Utilization of Medicinal and Aromatic Plants in FAO/RAP, Bangkok, November 1996.

CHEN, R. (2001). Enzyme engineering: rational redesign versus directed evolution. Trends in Biotechnology 19, 13-14.

CHEN, S., GALAN, M. C., COLTHARP, C., O'CONNOR, S. E. (2006). Redesign of a central enzyme in alkaloid biosynthesis. Chem. Biol. 13, 1137-1141.

COX, E. D., COOK, J. M. (1995). The Pictet-Spengler Condensation: A New Direction for an Old Reaction. Chem. Rev. 95, 179 -1842.

DAVIS, I. W., LEAVER-FAY, A., CHEN, V. B., BLOCK, J. N., KAPRAL, G. J., WANG, X., MURRAY L. W., ARENDALL, W. B. 3rd, SNOEYINK, J., RICHARDSON, J. S., RICHARDSON D. C. (2007). MolProbity: all-atom contacts and structure validation for proteins and nucleic acids. Nucleic Acids Res. 35 (Web Server issue), W375-W383.

DE-EKNAMKUL, W., OUNAROON, A., TANAHASHI, T., KUTCHAN, T. M., ZENK, M. H. (1997). Enzymatic condensation of dopamine and secologanin by cell-free extracts of *Alangium Lamarckii*. Phytochemistry 45, 477 - 484.

DE-EKNAMKUL, W., SUTTIPANTA, N., KUTCHAN, T. M. (2000). Purification and characterization of deacetylipecoside synthase from *Alangium Lamarckii* Thw.. Phytochemistry 55, 177-181.

DE FILIPPIS, V., SANDER, C., VRIEND, G. (1994). Predicting local structural changes that result from point mutations. Protein Eng. 7, 1203-1208.

DELANO, W. L. (2002). The PyMOL Molecular Graphics System. DeLano Scientific, Palo Alto, CA, USA.

DEUS-NEUMANN, B., ZENK, M. H. (1984). Instability of Indole Alkaloid Production in *Catharanthus roseus* Cell Suspension Cultures. Planta Med. 50, 427-431.

DE WAAL, A., MEIJER, A. H., VERPOORTE, R. (1995). Strictosidine synthase of *Catharanthus roseus*: purification and characterization of multiple forms. Biochem. J. 306, 571-580.

DOGRU, E., WARZECHA, H., SEIBEL, F., HAEBEL, S., LOTTSPEICH, F., STÖCKIGT, J. (2000). The gene encoding polyneuridine aldehyde esterase of monoterpenoid indole alkaloid biosynthesis in plants is an ortholog of the alpha/betahydrolase super family. Eur. J. Biochem., 267, 1397-1406.

DUTTA, P. K., CHOPRA, I. C., KAPOOR, L. D. (1963). Cultivation of *rauvolfia serpentina* in India. Econ. Bot. 17, 243-251.

EMSLEY, P., COWTAN, K. (2004). Coot: model-building tools for molecular graphics. Acta Crystallogr. D 60, 2126-2132.

FALKENHAGEN, H., POLZ, L., TAKAYAMA, H., KITAJIMA, M., SAKAI, S.-I., AIMI, N., STÖCKIGT. J. (1995). Substrate Specificity of Vinorine Hydroxylase, a novel Membrane-bound Key Enzyme of *Rauwolfia* Indole Alkaloid Biosynthesis. Heterocycles 41, 2683-2690.

FALKENHAGEN, H., STÖCKIGT, J. (1995). Enzymatic Biosynthesis of Vomilenine, a Key Intermediate of the Ajmaline Pathway, Catalyzed by a Novel Cytochrome P 450-Dependent Enzyme from Plant Cell Cultures of *Rauwolfia serpentina*. Z. Naturforsch. 50c, 45-53.

FINTELMANN, V., MENßEN, H. G., SIEGERS, C. P. (1989). Phytotherapie Manual. Hippokrates Stuttgart, 122-123.

FULLERTON, S. W. B., GRIFFITHS, J. S., MERKEL, A. B., CHERIYAN, M., WYMER, N. J., HUTCHINS, M. J., FIERKE, C. A., TOONE, E. J., NAISMITH, J. H. (2006). Mechanism of the Class I KDPG aldolase. Bioorg. Med. Chem. 14, 3002-3010.

FULZELE, D. P., HEBLE, M. R. (1994). Large-scale cultivation of *Catharanthus roseus* cells: production of ajmalicine in a 20-l airlift bioreactor. J. Biotechnol. 35, 1-7.

GAO, S., VON SCHUMANN, G., STÖCKIGT, J. (2002). A Newly-Detected Reductase from *Rauvolfia* Closes a Gap in the Biosynthesis of the Antiarrhythmic Alkaloid Ajmaline. Planta Medica 68, 906-911.

GASTEIGER, E., GATTIKER, A., HOOGLAND, C., IVANYI, I., APPEL, R. D., BAIROCH A. (2003). ExPASy: the proteomics server for in-depth protein knowledge and analysis. Nucleic Acids Res. 31, 3784-3788.

GEERLINGS, A., REDONDO, F. J., CONTIN, A., MEMELINK, J., VAN DER HEIJDEN, R., VERPOORTE, R. (2001). Biotransformation of tryptamine and secologanin into plant terpenoid indole alkaloids by transgenic yeast. Appl. Microbiol. Biotechnol. 56, 420-424.

GERASIMENKO, I., SHELUDKO, Y., MA, X., STÖCKIGT, J. (2002). Heterologous expression of a *Rauvolfia* cDNA encoding strictosidine glucosidase, a biosynthetic key to over 2000 monoterpenoid indole alkaloids. Eur. J. Biochem. 269, 2204-2213.

GETZOFF, E. D., CABELLI, D. E., FISHER, C. L., PARGE, H. E., VIEZZOLI, M. S., BANCI, L., HALLEWELL R. H. (1992). Faster superoxide dismutase mutants designed by enhancing electrostatic guidance. Nature 358, 347-351.

GRÄTHER, O., SCHNEIDER, B. (2001). The metabolic diversity of Plant Cell and Tissue Cultures. In: Progress in Botany Volume 62. ESSER, K., LÜTTGE, U., BEYSCHLAG, W. (et al.) (Eds.) Springer Verlag Berlin, Heidelberg, New York, 266-304.

HAMPP N., ZENK M.H. (1988). Homogeneous strictosidine synthase from cell suspension cultures of *Rauvolfia serpentina*, Phytochemistry 27, 3811-3815.

HÄNSEL R. (2004). Alkaloide. In: Pharmacognosie – Phytopharmazie. Hänsel, R. and Sticher, O. (Eds.) Springer Verlag, Berlin, Heidelberg, New York, 985-998.

HAREL M., AHARONI A., GAIDUKOV L., BRUMSHTEIN B., KHERSONSKY O., MEGED R., DVIR H., RAVELLI R. B. G., MCCARTHY A., TOKER L., SILMAN I., SUSSMAN J. L., TAWFIK D. S. (2004). Structure and evolution of the serum paraoxonase family of detoxifying and anti-atherosclerotic enzymes. Nat. Struct. Mol. Biol. 11, 412-419.

HARTLEY, D. L., KANE, J. F. (1988). Properties of inclusion bodies from recombinant Escherichia coli. Biochem. Soc. Trans. 16, 101-102.

HEINSTEIN, P., HÖFLE, G., STÖCKIGT, J. (1979). Involvement of Cathenamine in the Formation of N-analogues of Indole Alkaloids. Planta Medica 37, 349-357.

HOLM, L., PARK, J. (2000). DaliLite workbench for protein structure comparison. Bioinformatics 16, 566-567.

HUGHES, E. H., SHANKS, J. V. (2002). Metabolic Engineering of Plants for Alkaloid Production. Met. Eng. 4, 41-48.

IBACETA-LIZANA, J. S., JACKSON, A. H., PRASITPAN, N., SHANNON, P. V. R. (1987). Electrophilic substitution in indoles. Part 13. The synthesis and rearrangement of 2-deuteriospiro[cyclopentane-3'-indolenine]. J. Chem. Soc., Perkin Trans. II, 1221-1226.

JALEEL, C. A., GOPI, R., MANIVANNAN, P., SANKAR, B., KISHOREKUMAR, A., PANNEERSELVAM, R. (2007a). Antioxidant potentials and ajmalicine accumulation in *Catharanthus roseus* after treatment with giberellic acid. Colloids Surf B Biointerfaces 60, 195-200.

JALEEL, C. A., MANIVANNAN, P., SANKAR, B., KISHOREKUMAR, A., GOPI, R., SOMASUNDARAM, R., PANNEERSELVAM, R. (2007b). Water deficit stress mitigation by calcium chloride in *Catharanthus roseus*: effects on oxidative stress, proline metabolism and indole alkaloid accumulation. Colloids Surf B Biointerfaces 60, 110-116.

JALEEL, C. A., SANKAR, B., MURALI, P. V., GOMATHINAYAGAM, M., LAKSHMANAN, G. M., PANNEERSELVAM, R. (2008). Water deficit stress effects on reactive oxygen metabolism in *Catharanthus roseus*; impacts on ajmalicine accumulation. Colloids Surf B Biointerfaces 62, 105-111.

JAZIRI, M., ZHIRI, A., GUO, Y. W., DUPON, J. P., SHIMONURA, K., HAMADA, H., VAN HAELEN, M., HOMES, J. (1996). *Taxus* sp. cell, tissue and organ cultures as alternative sources for taxoids production: a literature survey. Plant Cell Tissue Organ Cult. 46, 59-75.

Jawad, Z., Paoli, M. (2002). Novel Sequences Propel Familiar Folds. Structure 10, 447-454.

KAPUST, R. B., WAUGH, D. S. (1999). *Escherichia coli* maltose-binding protein is uncommonly effective at promoting the solubility of polypeptides to which it is fused. Protein Sci. 8, 1668–1674.

KINAST, G., TIETZE, L. F. (1976) Biogenetic type synthesis of secologanin- and sweroside aglycon O-methyl ether. Chem. Ber. 109, 3626-3639.

KOEPKE, J., MA, X. Y., FRITZSCH, G., MICHEL, H., STÖCKIGT, J. (2005). Crystallization and preliminary X-ray analysis of strictosidine synthase and its complex with the substrate tryptamine, Acta Crystallogr. D Biol. Crystallogr. 61, 690-693.

KOWALSKI, P., MOKROSZ, J. L. (1997). Structure and spectral properties of β-carbolines. Part 9. New arguments against direct rearrangement of the spiroindolenine intermediate into β-carboline system in the Pictet-Spengler cyclization. Bull. Soc. Chim. Belg. 106, 147-149.

KUTCHAN, T. M., BOCK, A., DITTRICH, H., (1994). Heterologous expression of the plant proteins strictosidine synthase and berberine bridge enzyme in insect cell culture. Phytochemistry 35, 353-360.

KUTCHAN T. M. (1989). Expression of enzymatically active cloned strictosidine synthase from the higher plant *Rauvolfia serpentina* in Escherichia coli, FEBS Lett. 257, 127-130.

KUTCHAN T. M. (1993). Strictosidine: from alkaloid to enzyme to gene. Phytochemistry 32, 493-506.

KUTCHAN, T. M. (2000). The Biotechnological Exploitation of Medicinal Plants. Ernst-Schering Research Foundation workshop 32, 269-283.

KUTCHAN, T. M. (2005). Predictive metabolic engineering in plants: still full of surprises. TRENDS in Biotechnology 23, 381-383.

KUTCHAN, T. M., HAMPP, N., LOTTSPEICH, F., BEYREUTHER, K., ZENK, M. H. (1988). The cDNA clone for strictosidine synthase from *Rauvolfia serpentina*. DNA sequence determination and expression in *Escherichia coli*. FEBS Lett. 237, 40-44.

LAEMMLI, U. K. (1970). Cleavage of structural proteins during the assembly of the head of bacteriophage T4. Nature. 227, 680-685.

LARGHI, E. L., AMONGERO, M., BRACCA, A. B. J., KAUFMAN, T. S. (2005). The intermolecular Pictet-Spengler condensation with chiral carbonyl derivatives in the stereoselective syntheses of optically-active isoquinoline and indole alkaloids, ARKIVOC xii, 98-153.

LARKIN, M. A., BLACKSHIELDS, G., BROWN, N. P., CHENNA, R., MCGETTIGAN, P. A., MCWILLIAM, H., VALENTIN, F., WALLACE, I. M., WILM, A., LOPEZ, R., THOMPSON, J. D., GIBSON, T. J., HIGGINS, D. G. (2007). ClustalW2 and ClustalX version 2. Bioinformatics 2321, 2947-2948.

LASKOWSKI, R. A., MACARTHUR, M. W., MOSS, D. S., THORNTON, J. M. (1993). PROCHECK: A program to check the stereochemical quality of protein structures. J. Appl. Cryst. 26, 283-291.

LEETE, E. (1961). Biogenesis of Rauwolfia alkaloids. II. Incorporation of tryptophan into serpentine and reserpine. Tetrahedron 14, 35-41.

LEWIS, S. E. (2006). Recent advances in the chemistry of macroline, sarpagine and ajmaline-related indole alkaloids. Tetrahedron 62, 8655-8681.

LI, Q.Y., ZU, Y. G., SHI, R. Z., YAO, L. P. (2006). Review camptothecin: current perspectives. Curr Med. Chem. 13, 2021-2039.

LORENCE, A., NESSLER, C. L. (2004). Camptothecin, over four decades of surprising findings. Phytochemistry 65, 2735-2749.

LORENTZEN, E., SIEBERS, B., HENSEL, R., POHL, E. (2005). Mechanism of the Schiff Base Forming Fructose-1,6-bisphosphate Aldolase: Structural Analysis of Reaction Intermediates. Biochemistry 44, 4222-4229.

LORIS, E. A., PANJIKAR, S., RUPPERT, M., BARLEBEN, L., UNGER, M., SCHÜBEL, H., STÖCKIGT, J. (2007). Structure-Based Engineering of Strictosidine Synthase: Auxiliary for Alkaloid Libraries. Chem. Biol. 14, 979-985.

LOVELL, S. C., DAVIS, I. W., ARENDALL III, W. B., DE BAKKER, P. I. W., WORD, J. M., PRISANT, M. G., RICHARDSON, J. S., RICHARDSON D. C. (2003). Structure Validation by Cα Geometry: φ,ψ and Cβ Deviation. Proteins: Structure, Function and Genetics 50, 437-450.

LUK, L. Y. P., BUNN, S., LISCOMBE, D. K., FACCHINI, P. J., TANNER M. E. (2007). Mechanistic Studies on Norcoclaurine Synthase of Benzylisoquinoline Alkaloid Biosynthesis: An Enzymatic Pictet-Spengler Reaction. Biochemistry, 46, 10153 -10161.

MA, X., KOEPKE, J., BAYER, A., FRITZSCH, G., MICHEL, H., STÖCKIGT, J. (2005a) Crystallization and Preliminary X-ray Analysis of native and Selenomethionyl Vinorine Synthase from *Rauvolfia serpentina*. Acta Crystallogr. Sect. D. 61, 694-696.

MA X. Y., KOEPKE J., FRITZSCH G., DIEM R., KUTCHAN T. M., MICHEL H., STÖCKIGT J. (2004). Crystallization and preliminary X-ray crystallographic analysis of strictosidine synthase from *Rauvolfia* - the first member of a novel enzyme family, Biochim. Biophys. Acta 1702, 121-124.

MA, X., KOEPKE, J., PANJIKAR, S., FRITZSCH, G., STÖCKIGT, J. (2005b). Crystal structure of vinorine synthase, the first representative of the BAHD superfamily. J. Biol. Chem. 280, 13576-13583.

MA X.Y., PANJIKAR S., KOEPKE J., LORIS E., STÖCKIGT J. (2006). The structure of *Rauvolfia serpentina* strictosidine synthase is a novel six-bladed beta-propeller fold in plant proteins. Plant Cell 18, 907-920.

MARESH, J. J., GIDDINGS, L. A., FRIEDRICH, A., LORIS, E. A., PANJIKAR, S., TROUT, B. L., STÖCKIGT, J., PETERS, B., O'CONNOR, S. E. (2008). Strictosidine synthase: mechanism of a Pictet-Spengler catalyzing enzyme. J. Am. Chem. Soc. 130, 710-723.

MCCOY E., GALAN M.C., O'CONNOR S.E. (2006). Substrate specificity of strictosidine synthase. Bioorg. Med. Lett. 16, 2475-2478.

MCCOY, E., O'CONNOR S. E. (2006). Directed Biosynthesis of Alkaloid Analogs in the Medicinal Plant *Catharanthus roseus*. J. Am. Chem. Soc. 128, 14276-14277.

MCKNIGHT, T. D., ROESSNER, C. A., DEVAGUPTA, R., SCOTT, A. I., NESSLER, C. L. (1990). Nucleotide sequence of a cDNA encoding the vacuolar protein strictosidine synthase from *Catharanthus roseus.* Nucleic Acids Research 18, 4939.

MCREE, D. E. (1993). Practical Protein Crystallography. San Diego: Academic Press, 1-23.

MCREE, D. E. (1999). XtalView/Xfit - A Versatile Program for Manipulating Atomic Coordinates and Electron Density. J. Struct. Biol. 125, 156-165.

MICHAELIS, L., MENTEN, M. (1913). Die Kinetik der Invertinwirkung. Biochem. Z. 49, 333 – 369.

MINAMI, H., DUBOUZET, E., IWASA, K., SATO, F. (2007). Functional Analysis of Norcoclaurine Synthase in *Coptis japonica*. J. Biol. Chem. 282, 6274-6282.

MISHRA, M. (2000). Harvesting practices and management of two critically endangered medicinal plants in the natural forests of India. In: Seminar Proceedings Harvesting of non-wood forest products. The International Agro-Hydrology Research and Training Center in Menemen-Izmir (Turkey) October 2000.

MIZUKAMI, H., NORDLÖV, H., LEE, S. L., SCOTT, A. I. (1979). Purification and properties of strictosidine synthase (an enzyme condensing tryptamine and secologanin) from *Catharanthus roseus* cultured cells. Biochemistry 18, 3760-3763.

MORENO-VALENZUELA, O. A., MINERO-GARCÍA, Y., CHAN, W., MAYER-GERALDO, E., CARBAJAL, E., LOYOLA-VARGAS, V. M. (2003). Increase in the indole alkaloid production and its excretion into the culture medium by calcium antagonists in *Catharanthus roseus* hairy roots. Biotechnol Lett. 25, 1345-1349.

MURSHUDOV, G. N., VAGIN, A. A., DODSON, E. J. (1997). Refinement of macromolecular structures by the maximum-likelihood method. Acta Crystallogr. D 53, 240-255.

MUTSCHLER, E., GEISSLINGER, G., KROEMER, H. K., SCHÄFER-KORTING, M. (2008). Arzneimittelwirkungen. 9th edition, Wissenschaftliche Verlagsgesellschaft mbH (WVG), Stuttgart.

NAGAKURA, N., RÜFFER M., ZENK, M. H. (1979). The biosynthesis of monoterpenoid indole alkaloids from strictosidine. J. Chem. Soc. Perkin Trans. 1, 2308-2312.

NAMDEO, A., PATIL, S., FULZELE, D. P. (2002). Influence of fungal elicitors on production of ajmalicine by cell cultures of *Catharanthus roseus*. Biotechnol Prog. 18, 159-62.

O'CONNOR S. E., MARESH J. J. (2006). Chemistry and biology of monoterpene indole alkaloid biosynthesis. Nat. Prod. Rep. 23, 532-547.

OTWINOWSKI, Z., MINOR, W. (1997). Processing of X-ray diffraction data collected in oscillation mode. Methods Enzymol. 276, 307-326.

PANJIKAR, S., PARTHASARATHY, V., LAMZIN, V. S., WEISS, M. S., AND TUCKER, P. A. (2005) Auto-Rickshaw: An automated crystal structure determination platform as an efficient tool for the validation of an X-ray diffraction experiment. Acta Crystallogr. D 61, 449-457.

PATTHY-LUKÁTS, A., KÁROLYHÁZY, L., SZABÓ, L. F., PODÁNYI, B. (1997). First Direct and Detailed Stereochemical Analysis of Strictosidine. J. Nat. Prod. 60, 69-75.

PATTHY-LUKÁTS, A., KOCSIS, A. SZABÓ, L. F., PODÁNYI, B. (1999). Configurative Correlation and Conformational Analysis of Strictosidine and Vincoside Derivatives. J. Nat. Prod. 62, 1492-1499.

PARK, H. H., CHOI, S. K., KANG, J. K., LEE, H. Y. (1990). Enhancement of producing catharanthine by suspension growth of *Catharanthus roseus*. Biotechnology Letters 12, 603-608.

PASQUALI, G., PORTO, D. D., FETT-NETO, A. G. (2006). Metabolic engineering of cell cultures versus whole plant complexity in production of bioactive monoterpene indole alkaloids: recent progress related to old dilemma. J. Biosci. Bioeng. 101, 287-296.

PASQUO, A., BONAMORE, A., FRANCESCHINI, S., MACONE, A., BOFFI, A., ILARI, A. (2008). Cloning, expression, crystallization and preliminary X-ray data analysis of norcoclaurine synthase from *Thalictrum flavum*. Acta Crystallogr. Sect. F Struct. Biol. Cryst. Commun. 64, 281-283.

PENNINGS E. J .M., VAN DEN BOSCH R. A., VAN DER HEIJDEN R., STEVENS L. H., DUINE J. A., VERPOORTE R. (1989). Assay of Strictosidine Synthase of plant cell cultures by High-Performance Liquid Chromatography. Anal. Biochem. 176, 412-415.

PFITZNER, A., POLZ, L., STÖCKIGT, J. (1986). Properties of Vinorine Synthase – the *Rauwolfia* Enzyme Involved in the Formation of the Ajmaline Skeleton. Z. Naturforsch., 41c, 103-114.

PFITZNER, A., STÖCKIGT, J. (1982). Partial Purification and Characterization of Geissoschizine Dehydrogenase from Suspension Cultures of *Catharanthus roseus*. Phytochemistry, 21, 1585-1588.

PFITZNER, A., STÖCKIGT, J. (1983a). Characterization of Polyneuridine Aldehyde Esterase, a Key Enzyme in the Biosynthesis of Sarpagine/Ajmaline Type Alkaloids. Planta Medica, 48, 221-227.

PFITZNER, A., STÖCKIGT, J. (1983b). Polyneuridine Aldehyde Esterase: An Unusually Specific Enzyme involved in the Biosynthesis of Sarpagine Type Alkaloids. J. Chem. Soc. Chem. Comm., 459-560.

PFITZNER, U., ZENK, M. H. (1982). Immobilization of strictosidine synthase from *catharanthus* cell cultures and preparative synthesis of strictosidine. Planta Med. 46, 10-14.

PFITZNER, U., ZENK, M. H. (1989). Homogeneous Strictosidine Synthase Isoenzymes from Cell Suspension Cultures of *Catharanthus roseus*. Planta Med. 55, 525-530.

PICTET, A., SPENGLER, T. (1911). Über die Bildung von Isochinolin-Derivaten durch Einwirkung von Methylal auf Phenyl-Äthylamin, Phenyl-Alanin und Tyrosin. Ber. Dtsch. Chem. Ges. 44, 2030-2036.

PONDER, J. W., RICHARDS, F. M. (1987). An Efficient Newton-like Method for Molecular Mechanics Energy Minimization of Large Molecules. J. Comput. Chem. 8, 1016-1024.

RAMAKRISHNAN, C., RAMACHANDRAN, G. N. (1965). Stereochemical criteria for polypeptide and protein chain conformations. Biophys. J. 5, 909-933.

RHODES, G. (1993). Crystallography Made Crystal Clear. San Diego: Academic Press, 8-10, 29-38.

ROESSNER, C. A., DEVAGUPTA, R., HASAN, M., WILLIAMS, H. J., SCOTT, A. I. (1992). Purification of an indole alkaloid biosynthetic enzyme, strictosidine synthase, from recombinant strain of *Escherichia coli*. Prot. Expr. Purif. 3, 295-300.

ROSENTHAL, C., MUELLER, U., PANJIKAR, S., SUN, L., RUPPERT, M., ZHAO., Y., STÖCKIGT, J. (2006). Expression, purification, crystallization and preliminary X-ray analysis of perakine reductase, a new member of the aldo-keto reductase enzyme superfamily from higher plants. Acta Cryst. F. 62, 1286-1289.

ROST, B. (1998). Marrying structure and genomics, Structure 6 (1998) 259-263.

ROST, B. (2001). Review: protein secondary structure prediction continues to rise. J Struct. Biol. 134, 204-218.

ROST, B., O'DONOGHUE, S. (1997). Sisyphus and prediction of protein structure. Cabios 13, 345-356.

RUEFFER, M., EL-SHAGI, H., NAGAKURA, N., ZENK, M. H. (1981). (S)-Norlaudanosoline synthase: the first enzyme in the benzylisoquinoline biosynthetic pathway. FEBS 129, 5-9.

RUEFFER, M., NAGAKURA, N., ZENK, M. H. (1978). Strictosidine, the common precursor for monoterpenoid indole alkaloids with 3 α and 3 β configuration. Tetrahedron Lett. 19, 1593-1596.

RUPPERT, M., WOLL, J., GIRITCH, A., GENADY, E., MA, X., STÖCKIGT, J. (2005). Functional expression of an ajmaline pathway-specific esterase from *Rauvolfia* in a novel plant-virus expression system. Planta, 222, 888-898.

SAIKI, R. K., GELFAND, D. H., STOFFEL, S., SCHARF, S. J., HIGUCHI, R., HORN, G.T., MULLIS, K. B., ERLICH, H. A. (1988). Primer-directed enzymatic amplification of DNA with a thermostable DNA polymerase. Science 239, 487-491.

SAHU, B. N. (1979). Rauvolfia serpentina – Sarpagandha. Vol. I. Today's and Tomorrow's Printers and Publishers, New Delhi.

SAMANANI, N., LISCOMBE, D.K., FACCHINI, P.J. (2004). Molecular cloning and characterization of norcoclaurine synthase, an enzyme catalyzing the first committed step in benzylisoquinoline biosynthesis. Plant Journal 40, 302-313.

SATDIVE, R. K., FULZELE, D. P., EAPEN, S. (2003). Studies on production of ajmalicine in shake flasks by multiple shoot cultures of *Catharanthus roseus*. Biotechnol Prog. 19, 1071-1075.

SCHMIDT, D., STÖCKIGT, J. (1995). Enzymatic Formation of the Sarpagan-Bridge, a Key Step in the Biosynthesis of Sarpagine- and Ajmaline-Type Alkaloids. Planta Medica, 61, 254-258.

SCHÜBEL, H. STÖCKIGT, J. (1984). RLCC-isolation of Raucaffricine from its most efficient source – cell suspension cultures of *Rauwolfia serpentina* Benth.. Plant Cell Reports, 3, 72-74.

SEVESTRE-RIGOUZZO, M., NEF-CAMPA, C., GHESQUIÈRE, A., CHRESTIN, H. (1993). Genetic diversity and alkaloid production in *Catharanthus roseus*, *C. trichophyllus* and their hybrids. Euphytica 66, 151-159.

SIATKA, T., KASPAROVÁ, M. (2008). Effects of auxins on growth and scopoletin accumulation in cell suspension cultures of *Angelica archangelica* L.. Ceska Slov. Farm. 57, 17-20.

STEVENS, L. H., GIROUD, C., PENNINGS, E. J. M., VERPOORTE, R. (1993). Purification and characterization of strictosidine synthase from a suspension culture of *Cinchona robusta*. Phytochemistry 33, 99-106.

ST-JEAN, M., LAFRANCE-VANASSE, J., LIOTARD, B., SYGUSCH, J. (2005). High resolution reaction intermediates of rabbit muscle fructose-1,6-bisphosphate aldolase: Substrate cleavage and induced fit. J. Biol. Chem. 280, 27262-27270.

STÖCKIGT, J. (1995). Biosynthesis in Rauwolfia serpentina – Modern Aspects of an old Medicinal Plant. In: The Alkaloids (Cordell, G.A. Ed.), Academic Press, 47, 115-172.

STÖCKIGT, J., BARLEBEN, L., PANJIKAR, S., LORIS, E. A. (2008). 3D-Structure and Function of Strictosidine Synthase – the Key Enzyme of Monoterpenoid Indole Alkaloid Biosynthesis. Plant Physiol. Biochem. 46, 340-355.

STÖCKIGT, J., PANJIKAR, S., RUPPERT, M., BARLEBEN, L., MA, X. LORIS, E., HILL, M. (2007). The molecular architecture of major enzymes from ajmaline biosynthetic pathway. Phytochem. Rev. 6, 15-34.

STÖCKIGT, J., PANJIKAR, S. (2007). Structural Biology in Plant Natural Product Biosynthesis-Architecture of Enzymes from Monoterpenoid Indole and Tropane Alkaloid Biosynthesis. Nat. Prod. Rep. 24, 1382-1400.

STÖCKIGT, J., RUPPERT, M. (1999). Strictosidine – The Biosynthetic Key to Monoterpenoid Indole Alkaloids in Comprehensive Natural Products Chemistry (Barton, D. H. R., Nakanishi, K., Eds.) Elsevier Science, Oxford Vol. 4, 109 – 138.

STÖCKIGT, J., ZENK, M. H. (1977a). Strictosidine (Isovincoside): the Key Intermediate in the Biosynthesis of Monoterpenoid Indole Alkaloids. J. Chem. Soc. Chem. Comm., 646-648.

STÖCKIGT, J., ZENK, M. H. (1977b). Isovincoside (Strictosidine), the Key Intermediate in the Enzymatic Formation of Indole Alkaloids. FEBS Letters 79, 233-237.

STORK, G., NIU, D., FUJIMOTO, A., KOFT, E. R., BALKOVEC, J. M., TATA, J. R., GREGORY R. DAKE, G. R. (2001). The First Stereoselective Total Synthesis of Quinine. J. Am. Chem. Soc. 123, 3239 -3242.

STORK, G., TANG, C. P., CASEY, M., GOODMAN, B., TOYOTA, M. (2005). Regiospecific and Stereo-selective Syntheses of (±)-Reserpine and (-)-Reserpine. J. Am. Chem. Soc. 127, 16255 -16262.

SUN, L., RUPPERT, M., SHELUDKO, Y., WARZECHA, H., ZHAO, Y., STÖCKIGT, J. (2008). Purification, Cloning, Functional Expression and Characterization of Perakine Reductase – the First Example from the AKR Enzyme Family Specifically Extending the Alkaloidal Network of the Plant *Rauvolfia*. Plant Mol. Biol. 67, 455-467.

SVOBODA, G. H., BLAKE, D. A. (1975). The phytochemistry and pharmacology of Catharanthus roseus (L.) Don. In: The Catharanthus alkaloids. W. I. Taylor, N. R. Farnsworth (Eds.). Marcel Dekker Inc. New York, 45-84.

TATUSOVA, T. A., MADDEN, T. L. (1999). BLAST 2 Sequences, a new tool for comparing protein and nucleotide sequences. FEMS Microbiol. Lett. 174, 247-50.

TREIMER, J. F., ZENK, M. H. (1979a). Purification Strictosidine synthase from cell cultures of Apocynaceae plants. FEBS Lett. 97, 159-162.

Treimer, J. F., Zenk, M. H. (1979b). Purification and properties of strictosidine synthase, the key enzyme in indole alkaloid formation. Eur. J. Biochem. 101, 225-233.

Ungemach, F., Cook, J. M. (1978). The spiroindolenine intermediate. A review . Heterocycles, 9, 1089-1119.

Vagin, A., Teplyakov, A. (1997). MOLREP: An automated program for molecular replacement. J. Appl. Cryst. 30, 1022-1025.

Verma, A., Hartonen, K., Riekkola, M. L. (2008). Optimization of Supercritical Fluid Extraction of Indole Alkaloids from *Catharanthus roseus* using Experimental Design Methodology – Comparison with other Extraction Techniques. Phytochem. Anal. 19, 52-63.

Verpoorte, R., van der Heijden, R., Schripsema, J. (1993). Plant Cell Biotechnology for the Production of Alkaloids: Present Status and Prospects. J. Nat. Prod. 56 186-207.

Verpoorte, R., van der Heijden, R., ten Hoopen, H. J. G., Memelink, J. (1999). Metabolic engineering of plant secondary metabolite pathways for the production of fine chemicals. Biotech. Lett. 21, 467-479.

Verpoorte, R., van der Heijden, R., Memelink, J. (2000). Engineering the plant cell factory for secondary metabolite production. Transgenic Res. 9, 323-343.

Vincze, T., Posfai, J., Roberts, R. J. (2003). NEBcutter: a program to cleave DNA with restriction enzymes. Nucleic Acids Res. 31, 3688-3691.

von Schumann, G., Gao, S., Stöckigt, J. (2002). Vomilenine Reductase – a Novel Enzyme Catalyzing a Crucial Step in the Biosynthesis of the Therapeutically Applied Antiarrhythmic Alkaloid Ajmaline. Bioorg. Med. Chem. 10, 1913-1918.

Warzecha, H., Gerasimenko, I., Kutchan, Toni M. and Stöckigt, J. (2000). Molecular cloning and functional bacterial expression of a plant glucosidase specifically involved in alkaloid biosynthesis. Phytochemistry 54, 657-666.

Warzecha, H., Obitz, P., Stöckigt, J. (1999). Purification, partial amino acid sequence and structure of the product of raucaffricine-O-ß-D-glucosidase from plant cell cultures of *Rauwolfia serpentina*. Phytochemistry 50, 1099 -1109.

Wang-Hong, Chen-Rong, Chen-Min, Sun-Min, Liao-Zhi-Hua. (2006). Cloning and analysis of strictosidine synthase in *Rauvolfia verticillata*. Xibei Zhiwu Xuebao 26, 900-905.

Weinreb, S. M. (2001). Chemistry: Synthetic lessons from quinine. Nature 411, 429-431.

Willfinger, W. W., Mackey, K., Chomcynski, P. (1997). Effect of pH and ionic strength on the spectrophotometric assessment of nucleic acid purity. Biotechniques 22, 474-476.

WICHTL, M. (2002). Teedrogen und Phytopharmaka; 4th edition, Wissenschaftliche Verlagsgesellschaft mbH (WVG), Stuttgart.

WONG, M. (1976). La médicine chinois par les plantes. Edition Tchou, Paris.

WOODWARD, R. B., DOERING, W. E. (1944) The Total Synthesis of Quinine. J. Am. Chem. Soc. 66, 849-849.

WOODWARD, R. B., DOERING, W. E. (1945) The Total Synthesis of Quinine. J. Am. Chem. Soc. 67, 860-874;

YAMAZAKI, Y., SUDO, H., YAMAZAKI, M., AIMI, N., SAITO, K. (2003a). Camptothecin biosynthetic genes in hairy roots of *Ophiorrhiza pumila*: cloning, characterization and differential expression in tissues and by stress compounds. Plant Cell Physiol. 44, 395-403.

YAMAZAKI, Y., URANO, A., SUDO, H., KITAJIMA, M., TAKAYAMA, H., YAMAZAKI, M., AIMI, N., SAITO, K. (2003b). Metabolite profiling of alkaloids and strictosidine synthase activity in camptothecin producing plants. Phytochemistry 62, 461-470.

YERKES, N., WU, J. X., MCCOY, E., GALAN, M. C., CHEN, S., O'CONNOR, S. E. (2008). Substrate specificity and diastereoselectivity of strictosidine glucosidase, a key enzyme in monoterpene indole alkaloid biosynthesis. Bioorg. Med. Chem. Lett. 18, 3095-3098.

YOKOSHIMA, S., UEDA, T., KOBAYASHI, S., SATO, A., KUBOYAMA, T., TOKUYAMA, H., FUKUYAMA, T. (2002). Stereocontrolled total synthesis of (+)-vinblastine. J. Am. Chem. Soc. 124, 2137-2139.

ZENK, M. H. (1980). Enzymatic Synthesis of Ajmalicine and Related Indole Alkaloids. J. Nat. Prod. 43, 438-451.

ZENK, M. H., JUENGER M. (2007). Evolution and current status of the phytochemistry of nitrogenous compounds. Phytochemistry 68, 2757-2772.

Parts of the current work have been published:

Original Articles:

MA X. Y., PANJIKAR S., KOEPKE J., **LORIS E.**, STÖCKIGT J. (2006). The structure of *Rauvolfia serpentina* strictosidine synthase is a novel six-bladed beta-propeller fold in plant proteins. Plant Cell 18, 907-920.

STÖCKIGT J., PANJIKAR S., RUPPERT M., BARLEBEN L., MA X., **LORIS E.**, HILL M. (2007). The molecular architecture of major enzymes from ajmaline biosynthetic pathway. Phytochem. Rev. 6, 15-34.

LORIS E. A., PANJIKAR S., RUPPERT M., BARLEBEN L., UNGER M., SCHÜBEL H., STÖCKIGT J. (2007). Structure based engineering of Strictosidine Synthase – Auxiliary for new Alkaloid Libraries, Chem. Biol. 14, 979-985.

MARESH J. J., GIDDINGS L. A., FRIEDRICH A., **LORIS E. A.**, PANJIKAR S., TROUT B. L., STÖCKIGT J., PETERS B., O'CONNOR S. E. (2008). Strictosidine synthase: mechanism of a Pictet-Spengler catalyzing enzyme. J. Am. Chem. Soc. 130, 710-723.

STÖCKIGT J., BARLEBEN L., PANJIKAR S., **LORIS E. A.** (2008). 3D-Structure and Function of Strictosidine Synthase – the Key Enzyme of Monoterpenoid Indole Alkaloid Biosynthesis. Plant Physiol. Biochem. 46, 340-355.

Poster Presentations:

MA, X., PANJIKAR, S., KOEPKE, J., **LORIS, E. A.**, STÖCKIGT, J. (2005). Crystal Structure of Strictosidine Synthase. The Annual meeting of the German Pharmaceutical Society, October 5 – 8, 2005 in Mainz, Germany.

LORIS, E. A., MA, X., PANJIKAR, S., STÖCKIGT, J. (2005). Molecular analysis of strictosidine synthase – the biosynthetic entry to the monoterpenoid indole alkaloid family. Biotechnology Conference "Biothailand 2005", November 2 – 3, 2005 in Bangkok, Thailand.

LORIS, E. A., PANJIKAR, S., STÖCKIGT, J. (2007) Structure-based Engineering of Strictosidine Synthase. EMBO-Workshop on integrated approaches in Structural Enzymology", June 20 – 22, 2007 in Hamburg, Germany.

Oral Presentations:

LORIS, E. A., PANJIKAR, S., STÖCKIGT, J. (2006). Structural analysis of Strictosidine Synthase. The 49th Annual meeting of the Phytochemical Society of Europe, April 25 – 29, 2006 in Belek, Turkey.
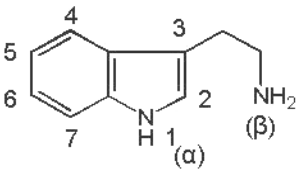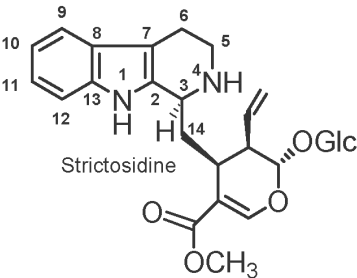
LORIS, E. A., PANJIKAR, S., STÖCKIGT, J. (2007). Structure-based Re-engineering of Strictosidine Synthase (Erweiterung der Substrat-Spezifität durch rationales Enzym-Design). The Annual meeting of the German Pharmaceutical Society, October 10 – 13, 2007 in Erlangen, Germany.

LORIS, E. A., PANJIKAR, S., STÖCKIGT, J. (2008). Strictosidine Synthase: Breaking new ground through Structure-based Re-engineering. Banff Conference on Plant Metabolism, July 30 - August 03, 2008 in Banff, Alberta, Canada (Lecture Award: Best graduate student oral presentation).

IX. Appendix

IX.1 Retention times

Table A 1. The retention times of selected tryptamine analogues and the (expected) retention times of respective enzymatic products are listed. A variation was observed in a range of ± 0.1 – 0.2 min (depended on temperature).

Substrates	Retention time (min)	Products	Retention time (min)
		Strictosidine	
Tryptamine	4.9	Strictosidine	8.0
5-Fluoro-tryptamine	5.8	10-Fluoro-strictosidine	8.7
6-Fluoro-tryptamine	5.9	11-Fluoro-strictosidine	8.7
5-Hydroxy-tryptamine (Serotonin)	2.7	10-Hydroxy-strictosidine	6.0
5-Methyl-tryptamine	6.6	10-Methyl-strictosidine	9.2
6-Methyl-tryptamine	6.7	11-Methyl-strictosidine	9,2
7-Methyl-tryptamine	6.7	12-Methyl-strictosidine	9.1
5-Methoxy-tryptamine	5.4	10-Methoxy-strictosidine	8.0
6-Methoxy-tryptamine	5.5	11-Methoxy-strictosidine	8.2
2-Methyl-5-hydroxy-tryptamine	3.1	n. d.	
N(α)-Methyl-tryptamine	5.6	n. d.	
N(α)-Acetyl-5-hydroxy-tryptamine	5.8	1- N-acetyl-10-hydroxystrictosidine	8.4
N(β)-Methyltryptamine	5.0	n. d.	

IX.2   STR1 Sequence

Protein sequence   1   MAKLSDSQTMALFTVFLLFLSSSLALSSPILKEILIEAPSYAPNSFTFD

Nucleotide sequence   1   agactgtcaagctagtcctctttcgcttcatagataggcttgcattatg
                             tcatcacactcttcttttttccctctcccttaatttacccaccactcta
                             gcatttgatgagcccccttccctgctcctacgagtgtgttctcctccccc

Protein sequence   50   STNKGFYTSVQDGRVIKYEGPNSGFVDFAYASPYWNKAFCENSTDAEKR

Nucleotide sequence   148 taaagttatgcggcgaatggcatgtggtgtgtcttaagttgaaagggaa
                             ccaagtacctaaggttaaagcacgttatcacccagaactgaagcacaag
                             accagcccccatcatcgcaaccctcccctatccgcagctgccatagaa

Protein sequence   99   PLCGRTYDISYNLQNNQLYIVDCYYHLSVVGSEGGHATQLATSVDGVPF

Nucleotide sequence   295 cttgaatgattatcaacctaggtttcctgggtgggcgaccgaagggct
                             ctgggcaatcaataaaatattagaaatcttgcaggaccatccgtagtct
                             cgtggatttatcgaccgtctttcttttgtttatgttcaccccttagac

Protein sequence   148 KWLYAVTVDQRTGIVYFTDVSTLYDDRGVQQIMDTSDKTGRLIKYDPST

Nucleotide sequence   442 atctggaggcaagagttaggaattggaggccaagaagaagacaatgcta
                             agtactctaagcgttatcatgctaaaggtaattacgaacggttaaaccc
                             ggctaaattgatgttcccttccattcatcaatgtactaaaaaagttccc

Protein sequence   197 KETTLLLKELHVPGGAEVSADSSFVLVAEFLSHQIVKYWLEGPKKGTAE

Nucleotide sequence   589 agaacctagccgcggggggaggattgcgggttaccagattcggcaagagg
                             aacctttaatatcggcatgcagcttttcattgaattaagtagcaagcca
                             aaaaaggagactatgaactatcctttgtgtgctatcatgaagtggctgg

Protein sequence   246 VLVKIPNPGNIKRNADGHFWVSSSEELDGNMHGRVDPKGIKFDEFGNIL

Nucleotide sequence   736 gtgaacacgaaaaagggcttgttaggtggaacgaggcagaatggtgaac
                             tttatcacgatagacagatgtccgaatagataggtacagtataatgatt
                             tagacacaataggcttattgtcataaatatgcaatttaaaattgtgctt

Protein sequence   295 EVIPLPPPFAGEHFEQIQEHDGLLYIGTLFHGSVGILVYDKKGNSFVSS

Nucleotide sequence   883 ggaccccctgggctgcacgcggtctagactcgtggatgtgaagattgta
                             attctccctcgaataataaaagttatgcttagctgtttaaaagacttcg
                             atcacaaatataccaatagtttggctacgctctgcaaattggattttat

Protein sequence   344 H
Nucleotide sequence   1030 c
                             a
                             t

174

IX.3 Sequence Alignment of STR1 from *Rauvolfia serpentina* with orthologous enzymes from different plant species[11].

STR_RS = STR from *R. serpentina* (CAA68725); STR_RV = *R. verticillata* (AAY81922); STR_RM = *R. mannii* (CAA45025); STR_CA = *C. roseus* (CAA43936); STR_OP = *Ophiorrhiza pumila* (BAB47180).

```
              1         10        20        30        40
STR_RS   MAKLSDSQTMA--LFTVFLLFLSSSLALSS--PILKEILIEAPSYA
STR_RV   MAKLSDSQTMA--LFTVFLLFLSSSLALSS--PILKEILIEAPSYA
STR_RM   --KLSDSQTMA--LFTVFLLFLSSSLALSS--PILKEILIEAPSYA
STR_CA   MANFSESKSMMAVFFMFFLLLLSSSSSSSSSPILKKIFIESPSYA
STR_OP   ---MHSSEAMV--VSILCALFLSSLSLVSS--SPEFFEFIEAPSYG

                   50        60        70        80
STR_RS   PNSFTFDSTNKGFYTSVQDGRVIKYEGPNSGFVDFAYASPYWNKAF
STR_RV   PNSFTFDSTNKGFYTSVQDGRVIKYEGPNSGFVDFAYASPYWNKAF
STR_RM   PNSFTFDSTNKGFYTSVQDGRVIKYEGPNSGFVDFAYASPYWNKAF
STR_CA   PNAFTFDSTDKGFYTSVQDGRVIKYEGPNSGFTDFAYASPFWNKAF
STR_OP   PNAYAFDSDGE-LYASVEDGRIIKYDKPSNKFLTHAVASPIWNNAL

              90        100       110       120       130
STR_RS   CENSTDAEKRPLCGRTYDISYNLQNNQLYIVDCYYHLSVVGSEGGH
STR_RV   CENSTDAEKRPLCGRTYDISYNLQNNQLYIVDCYYHLSVVGSEGGH
STR_RM   CENSTDAEKRPLCGRTYDISYNLQNNQLYIVDCYYHLSVVGSEGGH
STR_CA   CENSTDPEKRPLCGRTYDISYDYKNSQMYIVDGHYHLCVVGKEGGY
STR_OP   CENNTNQDLKPLCGRVYDFGFHYETQRLYIADCYFGLGFVGPDGGH

                   140       150       160       170
STR_RS   ATQLATSVDGVPFKWLYAVTVDQRTGIVYFTDVSTLYDD--RGVQQ
STR_RV   ATQLATSVDGVPFKWLYAVTVDQRTGIVYFTDVSTLYDD--RGVQQ
STR_RM   ATQLATSVDGVPFKWLYAVTVDQRTGIVYFTDVSTLYDD--RGVQQ
STR_CA   ATQLATSVQGVPFKWLYAVTVDQRTGIVYFTDVSSIHDDSPEGVEE
STR_OP   AIQLATSGDGVEFKWLYALAIDQQAGFVYVTDVSTKYDD--RGVQD

              180       190       200       210       220
STR_RS   IMDTSDKTGRLIKYDPSTKETTLLLKELHVPGGAEVSADSSFVLVA
STR_RV   IMDTSDKTGRLIKYDPSTKETTLLLKELHVPGGAEVSADSSFVLVA
STR_RM   IMDTSDKTGRLIKYDPSTKETTLLLKELHVPGGAEVSADSSFVLVA
STR_CA   IMNTSDRTGRLMKYDPSTKETTLLLKELHVPGGAEISADGSFVVVA
STR_OP   IIRINDTTGRLIKYDPSTEEVTVLMKGLNIPGGTEVSKDGSFVLVG

                   230       240       250       260    269
STR_RS   EFLSHQIVKYWLEGPKKGTAEVLVKIPNPGNIKRNADGHFWVSSSE
STR_RV   EFLSHQIVKYWLEGPKKGTAEVLVKIPNPGNIKRNADGHFWVSSSE
STR_RM   EFLSHQIVKYWLEGPKKGTAEVLVKIPNPGNIKRNADGHFWVSSSE
STR_CA   EFLSNRIVKYWLEGPKKGSAEFLVTIPNPGNIKRNSDGHFWVSSSE
STR_OP   EFASHRILKYWLKGPKANTSEFLLKVRGPGNIKRTKDGDFWVASSD

                   280       290       300       310
STR_RS   ELDGNMHGRVDPKGIKFDEFGNILEVIPLPPPFAGEHFEQIQEHDG
STR_RV   ELDGNMHGRVDPKGIKFDEFGNILEVIPLPPPFAGEHFEQIQEHDG
STR_RM   ELDGNMHGRVDPKGIKFDEFGNILEVIPLPPPFAGEHFEQIQEHDG
STR_CA   ELDGGQHGRVVSRGIKFDGFGNILQVIPLPPPYEGEHFEQIQEHDG
STR_OP   --NNGIT--VTPRGIRFDEFGNILEVVAIPLPYKGEHIEQVQEHDG

              320       330                   340
STR_RS   LLYIGTLFHGSVGILVYD-------KKGNS--------FVSSH
STR_RV   LLYIGTLFHGSVGILVYD-------KKGNS--------FVSSH
STR_RM   LLYIGTLFHGSVGILVYD-------KKGNS--------FVSSH
STR_CA   LLYIGSLFHSSVGILVYDD----HDNKGNS--------YVSS-
STR_OP   ALFVGSLFHEFVGILHNYKSSVDHHQEKNSGGLNASFKEFSSF
```

---

[11] The program ALSCRIPT (Barton, G. J. (1993), ALSRIPT – A Tool to Format Multiple Alignments, Prot. Eng., 6, 37-40) was used for sequence alignment. Residue numbering corresponds to the STR_RS sequence

IX.4 PCR Protocols

IX.4.1 W149A

(A) Composition of PCR reaction mixture

str1-pQE2 (ca. 10 ng/ml)	5.0 µl
Primer W149A-for (10 pM)	1.0 µl
Primer W149A-rev (10 pM)	1.0 µl
5xPhusion Control buffer	10.0 µl
dNTPs (20 mM)	2.5 µl
Phusion™ Polymerase (2U/µl)	1.0 µl
Ampuwa water	ad 50.0 µl

(B) PCR cycler program

Temperature (°C)	Time (min)	Cycles
95	2	1
95	0.5	
58	1	26
72	4	
72	10	1

IX.4.2 V167A

(A) Composition of PCR reaction mixture

str1-pQE2 (ca. 10 ng/ml)	3.0 µl
Primer V167A-for (10 pM)	1.0 µl
Primer V167A-rev (10 pM)	1.0 µl
5xPhusion Control buffer	10.0 µl
dNTPs (20 mM)	2.5 µl
Phusion™ Polymerase (2U/µl)	1.0 µl
Ampuwa water	ad 50.0 µl
Hotstart	

(B) PCR cycler program

Temperature (°C)	Time (min)	Cycles
95	2	1
95	0.5	
60.5	1	30
72	4	
72	10	1

IX.4.3 V167G

(A) Composition of PCR reaction mixture

str1-pQE2 (ca. 10 ng/ml)	3.0 µl
Primer V167G-for (10 pM)	1.0 µl
Primer V167G-rev (10 pM)	1.0 µl
5xPhusion Control buffer	10.0 µl
dNTPs (20 mM)	2.5 µl
Phusion™ Polymerase (2U/µl)	1.0 µl
Ampuwa water	ad 50.0 µl
Hotstart	

(B) PCR cycler program

Temperature (°C)	Time (min)	Cycles
95	2	1
95	0.5	
60.5	1	30
72	4	
72	10	1

IX.4.4 V208A

(A) Composition of PCR reaction mixture

str1_E205V/V208A-pQE2 (ca. 10 ng/ml)	2.0 µl
Primer V208A-for (10 pM)	1.0 µl
Primer V208A-rev2 (10 pM)	1.0 µl
5xPhusion Control buffer	10.0 µl
dNTPs (20 mM)	2.5 µl
Phusion™ Polymerase (2U/µl)	1.0 µl
Ampuwa water	ad 50.0 µl

(B) PCR cycler program

Temperature (°C)	Time (min)	Cycles
95	2	1
95	0.5	
58	1	28
72	4	
72	10	1

IX.4.5 V208G

(A) Composition of PCR reaction mixture

str1-pQE2 (ca. 10 ng/ml)	3.0 µl
Primer V208G-for (10 pM)	1.0 µl
Primer V208G-rev (10 pM)	1.0 µl
10xPfu buffer	5.0 µl
dNTPs (20 mM)	2.5 µl
PfuPlus! Polymerase (5 U/µl)	1.0 µl
Ampuwa water	ad 50.0 µl
Hotstart	

(B) PCR cycler program

Temperature (°C)	Time (min)	Cycles
95	2	1
95	0.5	
60	1	30
72	4	
72	10	1

IX.4.6 E205V/V208A

(A) Composition of PCR reaction mixture

str1-pQE2 (ca. 10 ng/ml)	2.0 µl
Primer V208A-for (10 pM)	1.0 µl
Primer V208A-rev1 (10 pM)	1.0 µl
5xPhusion Control buffer	10.0 µl
dNTPs (20 mM)	2.5 µl
Phusion™ Polymerase (2U/µl)	1.0 µl
Ampuwa water	ad 50.0 µl

(B) PCR cycler program

Temperature (°C)	Time (min)	Cycles
95	2	1
95	0.5	
58	1	26
72	4	
72	10	1

IX.4.7 V167G/V208A

(A) Composition of PCR reaction mixture	
str1_V208A-pQE2 (ca. 10 ng/ml)	3.0 µl
Primer V167G-for (10 pM)	1.0 µl
Primer V167G-rev (10 pM)	1.0 µl
10xPfu buffer	5.0 µl
dNTPs (20 mM)	2.5 µl
PfuPlus! Polymerase (5 U/µl)	1.0 µl
Ampuwa water	ad 50.0 µl
Hotstart	

(B) PCR cycler program

Temperature (ºC)	Time (min)	Cycles
95	2	1
95	0.5	
60	1	30
72	4	
72	10	1

IX.5   Sequencing Results

```
STR1         MAKLSDSQTMALFTVFLLFLSSSLALSSPILKEILIEAPSYAPNSFTFDSTNKGFYTSVQ 60
V208A        ----------------------HAGAPILKEILIEAPSYAPNSFTFDSTNKGFYTSVQ
V208G        -----------------HHHHHHAGAPILKEILIEAPSYAPNSFTFDSTNKGFYTSVQ
E205V/V208A  ------------------------------------------------------------
V167A        ---------------HHHHHHHMHAGAPILKEILIEAPSYAPNSFTFDSTNKGFYTSVQ
V167G        ---------------HHHHHHHMHAGAPILKEILIEAPSYAPNSFTFDSTNKGFYTSVQ
W149A        --------------------------ILKEILIEAPSYAPNSFTFDSTNKGFYTSVQ
E309D        ------------------------------------------------------------


STR1         DGRVIKYEGPNSGFVDFAYASPYWNKAFCENSTDAEKRPLCGRTYDISYNLQNNQLYIVD 120
V208A        DGRVIQYEGPNSGFVDFAYASPYWNKAFCENSTDAEKRPLCGRTYDISYNLQNNQLYIVD
V208G        DGRVIQYEGPNSGFVDFAYASPYWNKAFCENSTDAEKRPLCGRTYDISYNLQNNQLYIVD
E205V/V208A  ----------------------------------------------------------YIVD
V167A        DGRVIKYEGPNSGFVDFAYASPYWNKAFCENSTDAEKRPLCGRTYDISYNLQNNQLYIVD
V167G        DGRVIKYEGPNSGFVDFAYASPYWNKAFCENSTDAEKRPLCGRTYDISYNLQNNQLYIVD
W149A        DGRVIKYEGPNSGFVDFAYASPYWNKAFCENSTDAEKRPLCGRTYDISYNLQNNQLYIVD
E309D        ----------------------------------------------------------YIVD
                                                                       * * * *


                                            149                167
STR1         CYYHLSVVGSEGGHATQLATSVDGVPFKWLYAVTVDQRTGIVYFTDVSTLYDDRGVQQIM 180
V208A        CYYHLSVVGSEGGHATQLATSVDGVPFKWLYAVTVDQRTGIVYFTDVSTLYDDRGVQQIM
V208G        CYYHLSVVGSEGGHATQLATSVDGVPFKWLYAVTVDQRTGIVYFTDVSTLYDDRGVQQIM
E205V/V208A  CYYHLSVVGSEGGHATQLATSVDGVPFKWLYAVTVDQRTGIVYFTDVSTLYDDRGVQQIM
V167A        CYYHLSVVGSEGGHATQLATSVDGVPFKWLYAVTVDQRTGIVYFTDASTLYDDRGVQQIM
V167G        CYYHLSVVGSEGGHATQLATSVDGVPFKWLYAVTVDQRTGIVYFTDGSTLYDDRGVQQIM
W149A        CYYHLSVVGSEGGHATQLATSVDGVPFKALYAVTVDQRTGIVYFTDVSTLYDDRGVQQIM
E309         CYYHLSVVGSEGGHATQLATSVDGVPFKWLYAVTVDQRTGIVYFTDVSTLYDDRGVQQIM
             ***************************** ***************** *************


                                      205 208
STR1         DTSDKTGRLIKYDPSTKETTLLLKELHVPGGAEVSADSSFVLVAEFLSHQIVKYWLEGPK 240
V208A        DTSDKTGRLIKYDPSTKETTLLLKELHAPGGAEVSADSSFVLVAEFLSHQIVKYWLEGPK
V208G        DTSDKTGRLIKYDPSTKETTLLLKELHGPGGAEVSADSSFVLVAEFLSHQIVKYWLEGPK
E205V/V208A  DTSDKTGRLIKYDPSTKETTLLLKVLHAPGGAEVSADSSFVLVAEFLSHQIVKYWLEGPK
V167A        DTSDKTGRLIKYDPSTKETTLLLKELHVPGGAEVSADSSFVLVAEFLSHQIVKYWLEGPK
V167G        DTSDKTGRLIKYDPSTKETTLLLKELHVPGGAEVSADSSFVLVAEFLSHQIVKYWLEGPK
W149A        DTSDKTGRLIKYDPSTKETTLLLKELHVPGGAEVSADSSFVLVAEFLSHQIVKYWLEGPK
E309D        DTSDKTGRLIKYDPSTKETTLLLKELHVPGGAEVSADSSFVLVAEFLSHQIVKYWLEGPK
             *********************** ** ********************************


STR1         KGTAEVLVKIPNPGNIKRNADGHFWVSSSEELDGNMHGRVDPKGIKFDEFGNILEVIPLP 300
V208A        KGTAEVLVKIPNPGNIKRNADGHFWVSSSEELDGNMHGRVDPKGIKFDEFGNILEVIPLP
V208G        KGTAEVLVKIPNPGNIKRNADGHFWVSSSEELDGNMHGRVDPKGIKFDEFGNILEVIPLP
E205V/V208A  KGTAEVLVKIPNPGNIKRNADGHFWVSSSEELDGNMHGRVDPKGIKFDEFGNILEVIPLP
V167A        KGTAEVLVKIPNPGNIKRNADGHFWVSSSEELDGNMHGRVDPKGIKFDEFGNILEVIPLP
V167G        KGTAEVLVKIPNPGNIKRNADGHFWVSSSEELDGNMHGRVDPKGIKFDEFGNILEVIPLP
W149A        KGTAEVLVKIPNPGNIKRNADGHFWVSSSEELDGNMHGRVDPKGIKFDEFGNILEVIPLP
E309D        KGTAEVLVKIPNPGNIKRNADGHFWVSSSEELDGNMHGRVDPKGIKFDEFGNILEVIPLP
             ************************************************************


                     309
STR1         PPFAGEHFEQIQEHDGLLYIGTLFHGSVGILVYDKKGNSFVSSH 344
V208A        PPFAGEHFEQIQEHDGLLYIGTLFHGSVGILVYDKKGNSFVSSH
V208G        PPFAGEHFEQIQEHDGLLYIGTLFHGSVGILVYDKKGNSFVSSH
E205V/V208A  PPFAGEHFEQIQEHDGLLYIGTLFHGSVGILVYDKKGNSFVSSH
V167A        PPFAGEHFEQIQEHDGLLYIGTLFHGSVGILVYDKKGNSFVSSH
V167G        PPFAGEHFEQIQEHDGLLYIGTLFHGSVGILVYDKKGNSFVSSH
W149A        PPFAGEHFEQIQEHDGLLYIGTLFHGSVGILVYDKKGNSFVSSH
E309         PPFAGEHFDQIQEHDGLLYIGTLFHGSVGILVYDKKGNSFVSSH
             ******** ***********************************
```

IX.6   Ramachandran plots

IX.6.1 Proline plot STR1-strictosidine complex

IX.6.2 Proline plot STR1-inhibitor complex

IX.7 Index of Figures

IX.8 Index of Tables

X. Acknowledgements

XI. Curriculum vitae